

Analysis of the functional roles of the RTR complex partners TOP3 $\alpha$  and  
RMI1 in *Solanum lycopersicum* in relation to DNA repair and meiotic  
pathways

Zur Erlangung des akademischen Grades einer

DOKTORIN DER NATURWISSENSCHAFTEN

(Dr. rer. nat.)

von der KIT-Fakultät für Chemie und Biowissenschaften

des Karlsruher Instituts für Technologie (KIT)

genehmigte

DISSERTATION

von

Amy Leanne Whitbread M.Res

1. Referent: Prof. Dr. Holger Puchta

2. Referent: Prof. Dr. Peter Nick

Tag der mündlichen Prüfung: 15.12.2022

## **Acknowledgements**

This section should be called ‘gratitude list’ because I do not just want to acknowledge these people but sincerely express my utmost gratitude towards them. I am grateful for everyone who has been a part of this journey and still is today.

First and foremost, I must express my heartfelt gratitude to Prof. Dr. Holger Puchta for allowing me to be a part of the Puchta lab and his research team and for providing me with a fantastic project, publication opportunity, and helping me with my development as a researcher. I would also like to say thank you, not just for being a great supervisor but for also supporting me throughout everything.

I would also like to thank Dr. Annika Dorn for being the best supervisor and a great person, for all of the corrections, support, and for listening to me when I needed someone to talk to. Annika was a great source of inspiration for me, not only as a scientific researcher but also as an individual. Thank you for reading and correcting this thesis and everything else that I have written beforehand.

Thank you also to Prof. Dr. Peter Nick for his interest in me and my work, and for agreeing to be co-reviewer.

The Puchta lab. I have seen many people come and go during my time in the lab, and I want to thank everyone in the group who made me feel welcome from day one, supported me, and aided me with my PhD journey.

I want to thank Dr. Janine Pietralla for being such an amazing colleague and friend, supporting me during the times I needed it, and constantly reaching out to me. Thank you. Also, thank you to Dr. Natalja Beying, who was also a great colleague and remains a close friend.

I would also like to thank all of the technicians and trainees who helped me with my project and generally just around the lab. But I would like to give a huge thank you to Carina Jülch and Julia Kahles for going above and beyond and for really helping me out with my PhD experimental work. Also, a big thank you to Maren Scheidle for being a brilliant technician, helping me out, and being someone that I could talk to. Of course, I have to express my gratitude to the gardeners at the botanical gardens, particularly Herr Siegfried Bendel and Herr Joachim Daumann, whom I highly appreciate for all the hard work and support with the greenhouse work and looking after the tomato plants.

Thank you to everyone within the COMREC ITN for all the support, laughs, friendship, and of course, the scientific expertise shared and the collaborations.

I also want to thank my family, my parents in particular, for their constant love and support, despite everything, and for my partner Manuel and his family. And thank you to everyone else who was there for me during the “dark times”.

And finally, an enormous thank you to Seline Zschach. You were a gift to me in more ways than you can imagine.

*“Success is not final, failure is not fatal:  
it is the courage to continue that counts.”*

- Winston Churchill

## Publications

Most of the following has been published in:

**Whitbread, A.L.**, Dorn, A., Röhrig, S. & Puchta, H. (2021) Different functional roles of RTR complex factors in DNA repair and meiosis in *Arabidopsis* and tomato. *The Plant Journal* 106(4), p. 965. DOI:10.1111/tpj.15211.

### Other publications:

Lambing, C.; Kuo, P.; Kim, J.; Osman, K.; **Whitbread, A.L.**; Yang, J.; Choi, K.; Franklin, F.C.H. & Henderson, I.R. (2022) Differentiated function and localisation of SPO11-1 and PRD3 on the chromosome axis during meiotic DSB formation in *Arabidopsis thaliana*. *PLoS Genet* 18(7), e1010298. DOI: 10.1371/journal.pgen.1010298.

Vesty, E.F.; **Whitbread, A.L.**; Needs, S.; Tanko, W.; Jones, K.; Halliday, N. *et al.* (2020) Cross-kingdom signalling regulates spore germination in the moss *Physcomitrella patens*. *Scientific reports* 10(1), p. 2614. DOI: 10.1038/s41598-020-59467-5.

Vesty, E.F.; Saidi, Y.; Moody, L.A.; Holloway, D.; **Whitbread, A.**; Needs, S. *et al.* (2016) The decision to germinate is regulated by divergent molecular networks in spores and seeds. *The New phytologist* 211(3), pp. 952–966. DOI: 10.1111/nph.14018.

**Table of contents**

|  |     |
|--|-----|
| Table of contents .....                                  | I   |
| List of figures .....                                    | III |
| List of tables .....                                     | IV  |
| Abbreviations .....                                      | VI  |
| 1. Introduction .....                                    | 1   |
| 1.1 DNA damage and repair .....                          | 2   |
| 1.1.1 DNA damage .....                                   | 2   |
| 1.1.2 Ultraviolet-induced DNA damage .....               | 3   |
| 1.1.3 DNA repair mechanisms .....                        | 3   |
| 1.1.4 Nucleotide excision repair .....                   | 4   |
| 1.1.5 Base excision repair .....                         | 5   |
| 1.1.6 Mismatch repair .....                              | 7   |
| 1.1.7 DNA Damage Tolerance .....                         | 8   |
| 1.2 Double-strand breaks .....                           | 9   |
| 1.2.1 DSB repair .....                                   | 10  |
| 1.2.2 Non-Homologous End Joining .....                   | 11  |
| 1.2.3 Homologous Recombination .....                     | 13  |
| 1.3 The RTR complex .....                                | 17  |
| 1.3.1 RecQ helicase .....                                | 18  |
| 1.3.2 The structural protein Rmi1 .....                  | 20  |
| 1.3.3 Type 1A topoisomerase .....                        | 22  |
| 1.4 Meiosis .....  | 24  |
| 1.4.1 Meiotic recombination .....                        | 27  |
| 1.4.2 Roles of the RTR complex partners in meiosis ..... | 32  |
| 1.5 From Arabidopsis to crops .....                      | 33  |
| 1.6 Tomato as a model crop plant .....                   | 35  |
| 1.7 Aim and objectives .....                             | 36  |
| 2. Materials and Methods .....                           | 37  |
| 2.1 Materials .....                                      | 37  |
| 2.1.1 Chemicals .....                                    | 37  |
| 2.1.2 Enzymes .....                                      | 37  |
| 2.1.3 Genotoxins and antibiotics .....                   | 38  |
| 2.1.4 Instruments .....                                  | 39  |

---

|        |   |     |
|--------|---|-----|
| 2.1.5  | Kits and consumables .....  | 41  |
| 2.1.6  | Media, buffers and solutions .....  | 41  |
| 2.1.7  | Organisms.....  | 43  |
| 2.1.8  | Software and databases .....  | 43  |
| 2.1.9  | Oligonucleotides.....   | 44  |
| 2.1.10 | Plasmids .....  | 44  |
| 2.2    | Methods.....  | 45  |
| 2.2.1  | Molecular biology techniques .....  | 45  |
| 2.2.2  | Microbiology techniques.....  | 49  |
| 2.2.3  | Plant biology techniques .....  | 50  |
| 3.     | Results.....  | 58  |
| 3.1    | Characterisation of TOP3 $\alpha$ and RMI1 tomato homologues.....           | 58  |
| 3.2    | Identification of the RMI1 tomato homologue .....                           | 58  |
| 3.2.1  | Cas9-mediated mutagenesis of <i>SIRMI1</i> .....                            | 59  |
| 3.2.2  | Characterisation of <i>slrmi1</i> mutant lines .....                        | 62  |
| 3.3    | Identification of the TOP3 $\alpha$ tomato homologue .....                  | 77  |
| 3.3.1  | Cas9-mediated mutagenesis of <i>SITOP3<math>\alpha</math></i> .....         | 78  |
| 3.3.2  | Characterisation of <i>sltop3<math>\alpha</math></i> mutant lines.....      | 82  |
| 4.     | Discussion .....  | 90  |
| 4.1    | Characterisation of TOP3 $\alpha$ and RMI1 tomato homologues.....           | 90  |
| 4.1.1  | Identification of the RMI1 and TOP3 $\alpha$ tomato homologues .....        | 91  |
| 4.1.2  | Cas9-mediated mutagenesis of RMI1 and TOP3 $\alpha$ tomato homologues ..... | 93  |
| 4.1.3  | Characterisation of the functional role of RMI1 in tomato.....              | 95  |
| 4.1.4  | Characterisation of the functional role of TOP3 $\alpha$ in tomato.....     | 101 |
| 4.1.5  | The RTR-complex and dissolution pathway in tomato.....                      | 104 |
| 4.1.6  | Hypothesised model for the dissolution pathway in tomato .....              | 106 |
| 4.1.7  | The importance of translational studies in crop plants.....                 | 109 |
| 5.     | Summary .....   | 112 |
| 6.     | References .....  | 113 |
| 7.     | Supplementary.....  | 138 |
|        | Curriculum vitae.....   | 150 |
|        | Affidavit .....   | 151 |

## List of figures

|  |     |
|--|-----|
| Figure 1.1. Schematic diagram illustrating the canonical non-homologous end joining pathway and the factors involved. ....   | 12  |
| Figure 1.2. Schematic diagram illustrating the dissolution pathway of homologous recombination.....  | 17  |
| Figure 1.3. Overview of meiosis in plants. ....  | 26  |
| Figure 1.4. Schematic diagram illustrating meiotic recombination pathways. ....  | 28  |
| Figure 3.1. SIRMI1 protein domain structure and comparison and SIRMI1 gene structure....   | 60  |
| Figure 3.2. cDNA sequence alignment of SIRMI1 to confirm mutations on an mRNA level.   | 62  |
| Figure 3.3. <i>slrmi1-1</i> and <i>slrmi1-2</i> homozygous mutant plants compared to wild type.....  | 63  |
| Figure 3.4. Average number of seeds per fruit of <i>slrmi1-1</i> and <i>slrmi1-2</i> homozygous mutant plant lines compared to wild type. ....   | 64  |
| Figure 3.5. Average percentage of viable pollen for both <i>slrmi1-1</i> and <i>slrmi1-2</i> homozygous mutant plants compared to wild type. ....  | 66  |
| Figure 3.6. DAPI-stained chromatin spreads of pollen mother cells from wild-type tomato and the mutant lines <i>rmi1-1</i> and <i>rmi1-2</i> .....   | 68  |
| Figure 3.7. Genotoxin sensitivity analysis of <i>slrmi1-1</i> and <i>slrmi1-2</i> homozygous mutant lines compared to wild type, with the genotoxic agents <i>cis</i> -Platin and CPT.....                                     | 71  |
| Figure 3.8. Genotoxin sensitivity analysis of <i>slrmi1-1</i> and <i>slrmi1-2</i> homozygous mutant lines compared to wild type, with the genotoxic agents MMS and MMC. ....   | 73  |
| Figure 3.9. Root length analysis of the <i>rmi1</i> tomato mutant lines <i>rmi1-1</i> and <i>rmi1-2</i> .....  | 75  |
| Figure 3.10. Meristematic root cell viability analysis in <i>rmi1</i> tomato mutant lines. ....  | 76  |
| Figure 3.11. SITOP3 $\alpha$ protein domain structure, and comparison and SITOP3 $\alpha$ gene structure. ....   | 78  |
| Figure 3.12. cDNA sequence alignment of SITOP3 $\alpha$ to confirm mutations on an mRNA level. ....  | 80  |
| Figure 3.13. <i>sltop3<math>\alpha</math>-1</i> and <i>sltop3<math>\alpha</math>-2</i> heterozygous mutant plants compared to wild type. ....  | 82  |
| Figure 3.14. Relative percentage of regular (> 1 mm) seed number from <i>sltop3<math>\alpha</math>-1</i> and <i>sltop3<math>\alpha</math>-2</i> heterozygous mutant plants compared to wild type. ....                         | 83  |
| Figure 3.15. Fruit analysis of <i>sltop3<math>\alpha</math>-1</i> and <i>sltop3<math>\alpha</math>-2</i> heterozygous mutant plants compared to wild type.....   | 85  |
| Figure 3.16. Average percentage of viable pollen for both <i>sltop3<math>\alpha</math>-1</i> and <i>sltop3<math>\alpha</math>-2</i> heterozygous mutant plants compared to wild type. ....                                     | 86  |
| Figure 3.17. Analysis of <i>sltop3<math>\alpha</math>-1</i> and <i>sltop3<math>\alpha</math>-2</i> heterozygous mutant lines compared to a wild type control line.....   | 88  |
| Figure 4.1. Hypothesised model for the meiotic dissolution pathway in <i>Solanum lycopersicum</i> , compared to the known pathway in Arabidopsis. ....   | 108 |
| Figure 7.1. Standard curve for the calibration of the absorbance and the uptake of Evan's blue dye in $\mu\text{g/ml}$ , at various concentrations for calculating the uptake by the roots in the cell viability analysis..... | 146 |
| Figure 7.2. OsMEICA1/AtFLIP phylogenetic analysis and domain structure comparison...   | 148 |

## List of tables

|   |     |
|---|-----|
| Table 2.1. Overview of antibiotics .....  | 38  |
| Table 2.2. Overview of the concentrations of the genotoxin solutions used in the sensitivity assays.....  | 56  |
| Table 3.1. The number and percentage of heterozygous, homozygous mutant plants and wild type plants, identified from the progeny of the two heterozygous <i>top3α</i> mutant lines, <i>top3α-1</i> and <i>top3α-2</i> . ..... | 81  |
| Table 3.2. Percentage of regular and small seeds in both of the <i>top3α</i> heterozygous lines, compared to the expected. ....   | 89  |
| Table 7.1. Oligonucleotides and sequences used for amplification of <i>TOP3α</i> and <i>RM11</i> genomic DNA (gDNA) and copy DNA (cDNA) within the genome of <i>Solanum lycopersicum</i> . .....                              | 138 |
| Table 7.2. Oligonucleotides used for analysis of loci targeted during Cas9-mediated mutagenesis, via Sanger sequencing. ....  | 139 |
| Table 7.3. Oligonucleotides used for High Resolution Melting analysis.....  | 139 |
| Table 7.4. Oligonucleotides used for cloning the CRISPR/Cas9 constructs used for Cas9-mediated mutagenesis of both <i>TOP3α</i> and <i>RM11</i> in tomato.....  | 140 |
| Table 7.5. Number of seeds per fruit of <i>slrmil-1</i> and <i>slrmil-2</i> homozygous mutant plant lines compared to wild type. ....   | 141 |
| Table 7.6. Percentage of viable pollen for both <i>slrmil-1</i> and <i>slrmil-2</i> homozygous mutant plants compared to wild type. ....  | 141 |
| Table 7.7. Raw data for the genotoxin sensitivity analysis of <i>slrmil-1</i> and <i>slrmil-2</i> homozygous mutant lines compared to wild type, with the genotoxic agent <i>cis</i> -Platin.....                             | 142 |
| Table 7.8. Raw data for the genotoxin sensitivity analysis of <i>slrmil-1</i> and <i>slrmil-2</i> homozygous mutant lines compared to wild type, with the genotoxic agent CPT.....  | 143 |
| Table 7.9. Raw data for the genotoxin sensitivity analysis of <i>slrmil-1</i> and <i>slrmil-2</i> homozygous mutant lines compared to wild type, with the genotoxic agent MMS.....  | 144 |
| Table 7.10. Raw data for the genotoxin sensitivity analysis of <i>slrmil-1</i> and <i>slrmil-2</i> homozygous mutant lines compared to wild type, with the genotoxic agent MMC.....   | 145 |
| Table 7.11. Average root lengths of <i>slrmil-1</i> and <i>slrmil-2</i> homozygous mutant plant lines compared to wild type .....   | 146 |
| Table 7.12 Raw data for the meristematic root cell viability analysis in <i>rmi1</i> tomato mutant lines. ....  | 146 |
| Table 7.13. Raw data for the fruit diameter and seed counts of both the regular (> 1 mm) seed number from <i>sstop3α-1</i> and <i>sstop3α-2</i> heterozygous mutant plants compared to wild type..                            | 147 |
| Table 7.14. Raw data for the average percentage of viable pollen for both <i>sstop3α-1</i> and <i>sstop3α-2</i> heterozygous mutant plants compared to wild type.....   | 148 |

**Abbreviations**

|                    |   |
|--------------------|---|
| aa                 | Amino Acid  |
| bp                 | Base pair   |
| BER                | Base excision repair                                      |
| BIR                | Break-induced replication                                 |
| BLM                | Bloom's syndrome  |
| bNHEJ              | Backup non-homologous end joining                         |
| Cas                | CRISPR-associated   |
| cNHEJ              | Canonical non-homologous end joining                      |
| cDNA               | Complementary DNA   |
| <i>cis</i> -Platin | <i>cis</i> -diamminedichloroplatinum (II)                 |
| CL                 | Crosslink   |
| CO                 | Crossover   |
| CPD                | Cyclobutane pyrimidine dimers                             |
| CPT                | Camptothecin  |
| CRISPR             | Clustered regularly interspaced short palindromic repeats |
| C-Terminus         | Carboxy-Terminus  |
| DAPI               | 4',6-diamidino-2-phenylindole                             |
| D-loop             | Displacement loop   |
| DDR                | DNA damage response                                       |
| DDT                | DNA damage tolerance                                      |
| dHJ                | double Holliday junction                                  |
| DPC                | DNA-protein crosslink                                     |
| DSB                | Double-strand break                                       |
| DSBR               | Double-strand break repair                                |
| FDA                | Fluorescein diacetate                                     |
| gDNA               | Genomic DNA   |
| GM                 | Germination medium  |
| HR                 | Homologous recombination                                  |
| HRM                | High resolution melting                                   |
| INDELs             | Insertions and deletions                                  |
| MMC                | Mitomycin C   |
| MMEJ               | Microhomology-mediated end joining                        |
| MMR                | Mismatch repair   |
| MMS                | Methyl methanesulfonate                                   |
| MRN                | MRE11/RAD50/NBS1  |
| mRNA               | Messenger RNA   |
| NCO                | Non-crossover   |
| NcNHEJ             | Non-canonical non-homologous end joining                  |
| NER                | Nucleotide excision repair                                |
| NHEJ               | Non-homologous end joining                                |
| N-Terminus         | Amino-Terminus  |
| nt                 | Nucleotide  |
| OB                 | Oligonucleotide/oligosaccharide binding                   |

|       |                                      |
|-------|--------------------------------------|
| PAM   | Protospacer adjacent motif           |
| RMI1  | RECQ-mediated genome instability 1   |
| rpm   | Revolutions per minute               |
| RTR   | RECQ/TOP3/RMI1                       |
| SC    | Synaptonemal complex                 |
| SCJ   | Sister chromatid junction            |
| SDSA  | Synthesis-dependent strand annealing |
| sgRNA | Single guide RNA                     |
| SSB   | Single-strand break                  |
| ssDNA | Single-stranded DNA                  |
| T     | Transformation generation            |
| T-DNA | Transfer-DNA                         |
| TLS   | Translesion synthesis                |
| TOP3  | Topoisomerase 3                      |
| UV    | Ultraviolet                          |
| WT    | Wild type                            |
| ZDF   | Zinc-finger domain                   |

## 1. Introduction

The integrity of genomes is constantly at risk by both endogenous and exogenous sources that can ultimately lead to DNA damage, as well as errors that arise during DNA replication. Therefore, the ability to protect and thus ensure genome integrity is fundamental for all organisms. Defects that occur during DNA replication and chromosome segregation can lead to mutations and, more detrimentally, to potential cell death and lethality. As a result, it is not surprising that many essential repair mechanisms are apparent throughout all kingdoms that have evolved, to prevent such adverse defects from occurring during cellular processes.

Much knowledge has been gained regarding the mechanisms of these extensive DNA repair pathways on a molecular level (Cadet and Wagner, 2013). The vastness of this insight comes from studies performed in bacteria, yeast, and mammalian systems. The incentive behind understanding the underlying principles of DNA repair pathways is predominantly to increase our knowledge on the diseases caused as a result of DNA repair defects, particularly in humans, to potentially aid with possible preventative and treatment measures. Furthermore, DNA repair pathways and the factors involved are also of great interest in terms of genome editing techniques and generating means of establishing permanent changes within genomes (overview in Yeh *et al.*, 2019). Incidentally, such genome editing techniques would also benefit the treatment and prevention of said DNA repair disorders.

DNA repair pathways have also been extensively studied within plants, particularly the model plant species *Arabidopsis thaliana*. Plants are notably quite different from other higher eukaryotic organisms, such as mammals, because they are sessile and unable to move away from danger such as environmental stresses, they are phototrophic, and they also do not possess a reserve germline. As a result of studies being performed in plants, it is becoming increasingly evident that although DNA repair pathways and the factors involved are highly conserved across eukaryotic kingdoms, there are apparent differences between kingdoms that are being elucidated, owing to the differences between plants and other systems (overview in Spampinato, 2017).

*Arabidopsis* as a model system for functional studies is advantageous for several reasons, mainly due to its small size, short generation time, and the increasing number of genetic resources available, including genomic information and mutant lines. In addition, *Arabidopsis* is amenable to most molecular techniques for conducting experiments. The transformation of plants is relatively easy and not so time-consuming, owing to several reporter systems that are available for aiding with investigations.

The incentive to expand our knowledge on DNA repair and the factors involved in plants is not only due to the transferability of such knowledge to other systems, and the advantages of working with plants, but also due to the increasing pressures as a result of the global population growth and climate change. With DNA repair mechanisms at the forefront of genome editing techniques, understanding such mechanisms in plants, and more so in crop plants, is a prerequisite for establishing strategies to generate improved crop varieties and classical breeding approaches.

With the global population expected to reach 9.7 billion by 2050 (Roser *et al.*, 2013), in conjunction with the projected (and present) negative adverse effects as a result of climate change, it is more timely than ever that knowledge previously obtained from studies carried out in *A. thaliana* is translated to crop species to help aid with efforts to ensure food security.

This thesis presents such a translation whereby an insight into the DNA repair mechanisms in the crop plant tomato is conveyed.

## **1.1 DNA damage and repair**

### **1.1.1 DNA damage**

The preservation of genomic integrity and sequence information is crucial for maintaining life on earth. Mutagenesis can be beneficial, to a certain extent, in terms of it being necessary for adaptation, and consequently evolution. Genomic sequence information is comprised of DNA, the basic unit of inheritance. DNA molecules are notably reactive and thus highly susceptible to modifications via endogenous and exogenous sources. Such modifications lead to what is known as DNA damage; that is, a modification in DNA structure by physical or chemical means that leads to an altered DNA molecule that differs in terms of its chemical, structural, or physical properties from the original DNA molecule (as defined by Chakarov *et al.*, 2014). DNA damage can arise due to several factors, including those of exogenous and endogenous origins. Exogenous sources occur outside of the cell itself, such as environmental agents, whereby endogenous factors arise within the cell, such as harmful by-products produced through standard cellular metabolism mechanisms. Agents that are capable of inducing DNA damage are known as genotoxic agents. Some genotoxic agents generate damage due to their chemical nature, while others cause damage through their physical properties. Examples of chemical DNA damaging agents include oxidising agents, alkylating agents, and chemicals that induce DNA-DNA or DNA-protein crosslinks. These agents can either directly disrupt the DNA chemical structure, such as base modifying agents, or induce physical, structural changes that can increase the risk of further DNA damage, such as introducing strand breaks, or causing

bulky adducts. DNA damaging agents that induce damage via their physical properties include radiation, such as ionising radiation, and in some cases, low-energy electromagnetic waves, such as microwave, radio, and infrared radiation (Deshmukh *et al.*, 2013; Harper *et al.*, 2010).

### **1.1.2 Ultraviolet-induced DNA damage**

Ultraviolet (UV) radiation is a physical genotoxic agent that damages DNA molecules due to the short-wavelength electromagnetic energy. UV radiation poses a particular threat to plants throughout their life cycles; with plants being both phototrophic and sessile organisms, they are at particular risk of DNA damage via UV radiation emitted from the sun. Plants, as phototrophic organisms, utilise blue and red light as a source of energy for photosynthesis. Nevertheless, alongside the photosynthetically active radiation, harmful UV radiation is also continuously emitted from the sun. Despite the ozone layer providing a layer of protection against the harmful types of UV radiation, a small yet still consequential fraction of both UV-A spectrum (from 315 to 400 nm) and UV-B (from 280 to 315 nm) radiation can be detected at sea level (Dag Brune *et al.*, 2013). DNA, via its nucleotides, absorbs UV radiation as a chromophore, with peak absorption occurring at around 260 nm, within the UV-C range. However, as UV radiation with a wavelength of less than 280 nm is not significant at the earth's surface level, DNA damage to living organisms is predominantly from UV-B and, more so, UV-A radiation (Britt, 1996). Exposure to UV radiation for plants and animals, therefore, results in DNA damage in the form of various types of DNA lesions. The most common of these lesions are pyrimidine dimers such as CPDs (cyclobutane pyrimidine dimers). Additionally, 6-4 PPs (pyrimidine (6-4) pyrimidone photoproducts) can also arise, which can isomerise into Dewar photoproducts. Moreover, 8-oxo-dG (8-oxo-7,8-dihydro-2'-deoxyguanosine), FapyAde (e.g., 4,6-diamino-5-formamidopyrimidine), uracil, SSBs (single-strand breaks), and DSBs (double-strand breaks) can also be formed as a result of UV radiation (Dany and Tissier, 2001; Doetsch *et al.*, 1995; Douki and Cadet, 2001; Douki and Sage, 2016; Peak and Peak, 1990; Kielbassa, 1997; Peng and Shaw, 1996).

### **1.1.3 DNA repair mechanisms**

Plant cells can effectively repair certain types of UV-induced DNA lesions via a process called photoreactivation. This repair system is limited to the repair of Dewar photoproducts, 6-4 PPs, and CPDs (Ai *et al.*, 2011; Banaś *et al.*, 2020; Sancar, 2003). Enzymes known as photolyases act within photoreactivation to use blue and UV-A light energy to reverse the formation of pyrimidine dimers (Britt, 1996). However, although present across most eukaryotic and

prokaryotic kingdoms, these photolyases are not found within placental mammals. Moreover, photoreactivation is shown as key in maintaining genome stability within plants, and this reaction is not always adequate in repairing the damage caused by UV radiation (Dany and Tissier, 2001). First off, this process is light-dependent and is therefore ineffective when there is a lack of light sources.

Furthermore, the photolyases cannot repair particular DNA lesions, such as SSBs and DSBs, that are formed indirectly by UV radiation. Therefore, alternative repair mechanisms exist and must be employed to ensure genome integrity in these circumstances. These alternative DNA repair pathways include NER (nucleotide excision repair), BER (base excision repair), MMR (mismatch repair), TLS (translesion synthesis), NHEJ (non-homologous end joining), and HR (homologous recombination).

#### **1.1.4 Nucleotide excision repair**

NER is a DNA repair pathway that takes over the repair of pyrimidine dimers when it cannot be carried out by photoreactivation due to deficiencies in light, therefore highlighting the ability of the NER pathway to recognise and repair DNA lesions such as CPDs and 6-4 PPs, which is notably how these structures are repaired in mammalian systems which lack photoreactivation (Gillet and Schärer, 2006). Most of our knowledge on NER is based primarily on studies from yeast, animal, and human models. There are two apparent sub-pathways of NER; GGR (global genome repair) and TCR (transcription-coupled repair). GGR acts on the entire genome, as the name implies, whereas TCR only operates on transcriptionally active regions. The GGR pathway in humans is based on a protein complex called XPC-HR23-CEN2, which is comprised of XPC (*Xeroderma pigmentosum*, complementation group C), CEN2 (centrin 2), and either HR23A or HR23B (UV excision repair protein RAD23 homologue A or B) (Araki *et al.*, 2001; Masutani *et al.*, 1994). The XPC-HR23-CEN2 complex can recognise a vast array of bulky DNA lesions, including 6-4 PPs, postulated to result from these lesions' secondary DNA structure (Batty *et al.*, 2000; Sugasawa *et al.*, 2002; Sugasawa *et al.*, 2001). However, CPDs, the most commonly occurring UV-induced DNA lesions, are not recognised by the XPC-HR23-CEN2 complex, despite the complex's ability to bind to various substrates. CPDs are thought to be repaired via the action of the heterodimeric UV-DDB (UV-damaged DNA-binding) complex (Fujiwara *et al.*, 1999). TFIIH (transcription factor II H) is another indispensable component of the NER DNA repair pathway, which is a ssDNA (single-stranded DNA) binding complex. Interaction of XPC with part of the core sub-complex of TFIIH was shown to be required to successfully recruit TFIIH complex to the area of the DNA damage to

be repaired (Yokoi *et al.*, 2000). Components of the core complex of TFIIH, XPB and XPD are proteins with helicase activity that unwind the DNA in an ATPase-dependent manner (Compe and Egly, 2016). This activity is subsequently regulated by a protein called XPA, which inhibits the translocation of the TFIIH core complex along the DNA strand upon detection of a DNA lesion, while promoting the helicase activity within undamaged areas (Kokic *et al.*, 2019). In contrast to GGR, DNA damage recognition during TCR differs slightly, with the detection of DNA lesions within transcribed DNA strands being carried out by RNAPII (RNA polymerase II) (Xu *et al.*, 2017). When stalled at a DNA lesion, RNAPII acts as a signal, recruiting additional DNA repair factors, ultimately leading to the recruitment of TFIIH (overview in Nakazawa *et al.*, 2020). Despite alternative factors being required for TCR, compared to GGR, following TFIIH recruitment to the DNA lesion, the subsequent mechanisms for both sub-pathways proceed in a similar manner (Okuda *et al.*, 2017). Although homologues of most of the NER repair factors have been identified within plants (Kimura and Sakaguchi, 2006; Kunz *et al.*, 2005), a homologue of the key NER protein in yeast and humans, XPA, has yet to be identified, providing speculation that an alternative protein is responsible for TFIIH regulation and the detection of lesions in plants. However, multiple studies have shown that NER is a key DNA repair pathway in plants, particularly for UV-induced DNA damage (Al Khateeb and Schroeder, 2009; Castells *et al.*, 2011; Koga *et al.*, 2006; Molinier *et al.*, 2008; Molinier *et al.*, 2004), with both the GGR and TCR sub-pathways being present (Fidantsef and Britt, 2012).

### 1.1.5 Base excision repair

The BER pathway is a mechanism that can remove certain types of modified lesions that may arise as a result of UV radiation, such as deaminated or oxidised bases (Cooke *et al.*, 2000; Peng and Shaw, 1996). This DNA repair mechanism is based on the activity of a DNA glycosylase in eukaryotes, whereby the glycosylase can detect damaged bases (Dalhus *et al.*, 2009). Due to the differential specificity of DNA glycosylases and their catalytic function, they can act on many different types of base lesions (O'Brien and Ellenberger, 2004; Stivers and Jiang, 2003), either acting as a monofunctional enzyme or a bifunctional one (Fortini and Dogliotti, 2007). Monofunctional DNA glycosylases act by cleaving the N-glycosidic bond, which releases the defective base, while leaving the sugar-phosphate backbone intact, via the formation of an AP (apurinic/apyrimidinic) site (Krokan and Bjørås, 2013). With this, an AP endonuclease is then able to cleave the backbone at an abasic site via the 5' end, leaving a free 3'-OH (3'-hydroxyl) and 5' deoxyribose 5-phosphate termini. On the other hand, when a

bifunctional DNA glycosylase, which carries additional AP lyase activity (Fortini and Dogliotti, 2007), recognises a DNA lesion, internal AP lyase activity can cleave the DNA backbone. In both instances, either with the monofunctional or bifunctional DNA glycosylases, the result is relatively similar, the DNA lesion is excised from the DNA strand generating single-strand breaks with a 3'-OH' end and either 5'-deoxyribose 5-phosphate or 5'-phosphate termini, for monofunctional or bifunctional enzymes, respectively (Hegde *et al.*, 2008; Roldán-Arjona *et al.*, 2019). The subsequent stages of the BER pathway involve filling the gap generated as a result of the excision of the DNA lesion. Two sub-pathways are essential for this process; the short patch (SP) and long patch (LP) pathways (Frosina *et al.*, 1996). SP operates when a free 5'-phosphate is present, with DNA polymerase  $\beta$  (Pol  $\beta$ ) acting to convert non-functional BER intermediates to functional ones, via its 5'-deoxyribose 5-phosphate lyase activity (Allinson *et al.*, 2001; Srivastava *et al.*, 1998). For both SP and LP BER, Pol  $\beta$  can fill in one nucleotide within the gap (Podlutzky *et al.*, 2001). However, in SP, the XRCC1-LIG3a (DNA ligase 3a) complex carries out the subsequent ligation of the gap (Dianov *et al.*, 1992; Nash *et al.*, 1997), whereas, in LP, replicative pol  $\delta$  and pol  $\epsilon$  are employed for DNA strand elongation, following the formation of a Schiff base. During LP BER, a flap structure is formed as a result of the action of pol  $\delta$  and pol  $\epsilon$ , which is subsequently digested by flap endonuclease 1 (FEN1), which enables the successful ligation of the new DNA fragment with the repaired DNA strand by LIG1 (Roldán-Arjona *et al.*, 2019). PCNA, a pol  $\delta$  processivity factor, has also been shown as indispensable for LP BER as a coordinator of DNA synthesis, flap removal, and ligation (Strzalka and Ziemienowicz, 2011). Although most of our understanding of the BER pathway comes from studies carried out in yeast and animal models, studies in plants have revealed that homologues of BER factors are present, and that BER is not only limited to nuclear DNA but also acts to repair lesions within plant chloroplast and mitochondrial DNA (Boesch *et al.*, 2009; Cooke *et al.*, 2000; Gutman and Niyogi, 2009). *In vitro* studies investigating potential nuclear DNA glycosylases in Arabidopsis provide evidence that suggest that factors such as AtMMH (MutM homologue) (Ohtsubo *et al.*, 1998), AtOGG1 (N-glycosylase/DNA lyase OGG1) (Dany and Tissier, 2001; García-Ortiz *et al.*, 2001), and AtFPG1 (formamidopyrimidine-DNA glycosylase) (Gao and Murphy, 2001), may play functional roles in BER as glycosylases due to their ability to repair 8-oxo-dG (8-oxo-7,8-dihydro-2'-deoxyguanosine) products, which represent DNA damage induced by oxidation by UV radiation (Córdoba-Cañero *et al.*, 2014). Moreover, DNA pols, AtLIG1, AtPCNA1, AtPCNA2, and AtFEN1 (Roldán-Arjona *et al.*, 2019; Strzalka and Ziemienowicz, 2011) have also been identified in plants, which are other essential factors of BER pathways, besides DNA glycosylases and AP endonucleases. Despite

this, plants are deficient in homologues of human Pol  $\beta$  and LIG3a. AtPOL $\lambda$  is a factor postulated to function in a pol  $\beta$ -like manner within the BER pathway, due to the 5'-deoxyribose phosphate demonstrated in *in vitro* analyses (Uchiyama *et al.*, 2004). However, it has been shown that both the SP and LP BER pathways are present and active within plants (Córdoba-Cañero *et al.*, 2014).

### 1.1.6 Mismatch repair

Genome integrity and replication fidelity are ensured by the evolutionarily conserved mismatch repair (MMR) pathway (Kunkel and Erie, 2005). This type of DNA repair pathway is key for correcting errors generated during replication processes, such as insertion-deletion mismatches (IDLs) and base substitution mismatches. Propagation of such mismatched nucleotides can lead to severe defects within cellular functions, mainly due to mismatched bases being unable to form correct hydrogen bonds between the complementary DNA strands. The detection of mismatches and their subsequent repair via the MMR pathway is carried out by the MutS $\alpha$  or MutS $\beta$  complex in humans. The MutS $\alpha$  complex comprises of the MSH2 (MutS homologue 2) and MSH6 proteins. These proteins act in a clamp-like manner to detect binding of mismatched bases, with the complex being able to identify and recognise one or two unpaired bases. The MutS $\beta$  complex, on the other hand, can detect DNA with 3'-single-stranded overhangs and insertion-deletion loops of up to 15 nucleotides, and consists of the MSH2 and MSH3 proteins (Pećina-Šlaus *et al.*, 2020). Most of the aforementioned mammalian factors involved in the MMR pathway have been identified in plants. In Arabidopsis, the heterodimers MutS $\alpha$ , MutS $\beta$  and MutS $\gamma$  are formed due to AtMSH2 binding with AtMSH6, AtMSH3, or AtMSH7, respectively. These heterodimers all differ to one another in terms of their affinity to particular DNA substrates, with MutS $\alpha$  and MutS $\beta$  preferring the same substrates as the homologues within mammalian systems. Notably, MSH7 is a unique MMR protein specific to plants, in addition to the MutS $\gamma$  complex that is formed when MSH7 binds with MSH2 (Culligan and Hays, 2000). The fact that plants harbour three MutS complexes, rather than the two in other eukaryotic systems, enables plants to recognise and repair a more comprehensive array of mismatches (Culligan and Hays, 2000; Wu *et al.*, 2003). Studies in Arabidopsis have also suggested the involvement of the MMR factors AtMSH2, AtMSH6, and AtMSH7 in the repair of CPDs in response to UV, with T-DNA mutant lines deficient in all three found to have higher levels of CPDs when compared to WT plants, following irradiation with UV-B and UV-A (Lario *et al.*, 2015; Lario *et al.*, 2011).

### 1.1.7 DNA Damage Tolerance

In eukaryotes, DNA replication is mediated by the replicative polymerase complex, comprised of the primase Pol  $\alpha$  and two replicases, Pol  $\delta$  and Pol  $\epsilon$ . When bound to DNA within the nucleus, this complex, alongside the supportive roles of numerous specialised proteins making up the replication machinery, generates a replication fork that allows for the synthesis of new DNA strands and permits the replication of DNA (Leman and Noguchi, 2013). Unrepaired DNA lesions can block the movement of the replicative polymerase complex along DNA strands during replication. DNA lesions such as pyrimidine dimers may cause stalling of the replication fork, thus blocking DNA synthesis (Mirkin Ekaterina V. and Mirkin Sergei M., 2007; Pedroza-Garcia *et al.*, 2019; Tourrière and Pasero, 2007). Stalled replication forks can be detrimental to the cell, due to the possibility of DSB formation. As a result, to overcome such obstacles during DNA replication, a DNA damage tolerance (DDT) pathway may be initiated, enabling the completion of replication (Mirkin Ekaterina V. and Mirkin Sergei M., 2007). There are two pathways of DDT: the translesion synthesis (TLS) pathway and the template-switching pathway (Giannattasio *et al.*, 2014; Hoege *et al.*, 2002; Stelter and Ulrich, 2003; Tourrière and Pasero, 2007). The decision as to which of the two pathways is carried out has been shown in yeast to be made following the detection of the DNA damage via ubiquitination of PCNA (proliferating cell nuclear antigen) (Hoege *et al.*, 2002). PCNA is considered a regulatory cofactor for DNA polymerases, during DNA replication. Acting in a sliding clamp manner, the homotrimer PCNA forms a ring, with one surface interacting with and therefore stabilising DNA polymerases, thus securing them to the DNA (Leman and Noguchi, 2013). When a DNA lesion blocks the replicative polymerase complex, monoubiquitination of PCNA acts to recruit TLS polymerase. Studies in yeast have indicated that this ubiquitination of PCNA is mediated by RAD18 (E3 ubiquitin-protein ligase RAD18) and RAD6 (ubiquitin-conjugating enzyme E2) proteins (Brown *et al.*, 2009; Hendel *et al.*, 2011; Hoege *et al.*, 2002; Kannouche *et al.*, 2004; Stelter and Ulrich, 2003). This recruitment of the TLS polymerases to the DNA replication machinery at the stalled replication fork permits the replacement of the replicative polymerases for the TLS ones (Vaisman and Woodgate, 2017). The TLS polymerases then incorporate nucleotides on the opposing strand of the lesion. In some cases, incorrect nucleotides can be incorporated, owing to the possible error-prone nature of the TLS pathway. Such errors occur due to the lack of proof-reading ability of TLS polymerases, in conjunction with their flexible active centre (Bi, 2015). When such errors occur, the incorrect bases are removed by MMR or by the replicative polymerases via their exonucleolytic activity. However, when TLS-mediated errors occur and are not resolved, the incorporated nucleotides persist as mutations within the

DNA (Sakamoto, 2019). The fidelity of TLS is dependent upon the TLS polymerases recruited, which in turn depends on the type of DNA lesion blocking the replicative polymerase complex. In Arabidopsis, AtREV1, a TLS polymerase, is preferentially recruited in response to CPD DNA lesions. AtREV1 subsequently recruits additional polymerases such as AtPOL $\zeta$ ; however, this mechanism is error-prone. On the other hand, when 6-4 PP DNA lesions are responsible for the stalled replication fork, AtPOL $\eta$  is recruited instead, which leads to error-free DNA synthesis across the lesion.

Template switching (TS), the second DDT pathway, is entirely error-free. The stalled nascent strand switches to the newly synthesised sister strand with no DNA damage, to enable replication to continue over the lesion temporarily. Strand invasion then enables the two newly synthesised DNA strands to pair, forming a sister chromatid junction (SCJ) structure, once the undamaged sister strand has served as a template to fill in the gap. This resultant SCJ structure is resolved, leading to the recombination of two duplex DNA strands (Giannattasio *et al.*, 2014). Whereas TLS is initiated following monoubiquitination of PCNA, the error-free TS pathway is activated following polyubiquitination of PCNA via RAD5 (DNA repair protein RAD5) (Hoege *et al.*, 2002). TS is therefore also referred to as both the error-free DDT pathway and the RAD5-dependent DDT pathway. Both DDT pathways, TS and TLS, are present and active in plants, as shown by studies in Arabidopsis (Wang *et al.*, 2011). Regulation of DDT, regarding which of the two pathways are employed due to DNA damage, is postulated to be regulated by specific ubiquitination of PCNA, as discussed. This conclusion came to fruition when it was shown that AtPCNA1 and AtPCNA2 in Arabidopsis can be ubiquitinated (mono- or poly-) in a RAD5A-dependent manner (Strzalka *et al.*, 2013).

## 1.2 Double-strand breaks

As mentioned previously, DNA breaks, both SSBs and DSBs, are a form of DNA damage that can arise (Lindahl, 1993). SSBs can be generated as a result of UV-induced ROS (reactive oxygen species) or from other exogenous sources (Thompson, 2012; Ward, 1994), during BER of damaged bases (Caldecott, 2008), or directly as a consequence of the disintegration of oxidized sugar within the sugar-phosphate DNA backbone. SSBs are a discontinuation within one strand of the DNA double helix. Within proliferating cells, unrepaired SSBs that result in stalled DNA replication forks can cause the formation of more severe damage in the form of a DSB (Kuzminov, 2001). DNA DSBs arise when the backbones of two complementary strands of DNA are both broken simultaneously. Besides arising as a result of unrepaired SSBs during replication, two nicks within both strands of a DNA molecule can also occur, due to high levels

of irradiation (Milligan *et al.*, 1995). Due to their severity, DSBs are considered one of the most detrimental forms of DNA lesion that can occur, making them highly deleterious and a threat to genomic stability (Mehta and Haber, 2014).

### 1.2.1 DSB repair

Due to the severity of DNA DSBs and the threat that they pose to genome stability and survival, it is not surprising that there are various mechanisms in place that are carried out in order to prevent DSB accumulation, and eliminate them prior to replication of the genome (Puchta, 2004; Puchta and Fauser, 2014; Wang and Xu, 2017). The DNA damage response (DDR) is a comprehensive and complex signal transduction pathway involved in the detection of DNA damage. It is responsible for initiating subsequent repair mechanisms to repair such damage. DSBs are one of the types of DNA damage in which the DDR pathway and all the machinery involved can detect and thus repair, through the action of signalling cascades. Within DDR, three kinases have been identified to act as the primary detectors and subsequent signal transducers of DSBs: ATM (ataxia-telangiectasia mutated), ATR (ATM- and Rad3-related), and DNA-PKcs (DNA dependent protein kinase catalytic subunit). The MRN-complex, comprised of the three proteins: MRE11, RAD50, and NBS1 (Nijmegen breakage syndrome 1), is responsible for the recruitment of ATM to the DSB sites. Meanwhile, ATR is recruited by ATRIP to RPA-coated ssDNA, and DNA-PKcs is activated by Ku70/Ku80- bound DSB ends. Once activated and recruited, all three kinases are then able to phosphorylate downstream signal transducers, regulators, and effectors involved in further DNA damage repair pathways (Blackford and Jackson, 2017). Histone H2AX is one such factor that is phosphorylated in response to kinase signal transduction (Blackford and Jackson, 2017), with phosphorylated H2AX ( $\gamma$ -H2AX) often being used as an indication and thus a marker of DSBs (Mah *et al.*, 2010; Maréchal and Zou, 2013). However, studies have shown that  $\gamma$ -H2AX may also be associated with other types of DNA damage besides DSBs; therefore DSB frequency may be overrepresented in these circumstances (Löbrich *et al.*, 2010; Soutoglou and Misteli, 2008; Valdiglesias *et al.*, 2013).  $\gamma$ -H2AX acts to recruit and allow for the accumulation of DNA repair proteins to the DSB sites (Fillingham *et al.*, 2006). In addition to the three kinases, ATM, ATR, and DNA-PKcs, additional factors also play key roles in the regulation of DSB repair pathways, such as MDC1 (mediator of DNA-damage checkpoint protein 1) and 53BP1 (p53-binding protein 1) (Blackford and Jackson, 2017; Ruff *et al.*, 2020; Sancar *et al.*, 2004). Studies in *Arabidopsis* have identified homologues of ATM and ATR in plants, which are thought to be involved in DNA repair processes; however biochemical analyses of these kinases have yet to

be carried out (Culligan *et al.*, 2004; Garcia *et al.*, 2003; Jia *et al.*, 2013). Repair of DNA DSBs is achieved by mechanisms that are broadly grouped into two main pathways: non-homologous end joining (NHEJ) and homologous recombination (HR).

### 1.2.2 Non-Homologous End Joining

The NHEJ pathway is the predominant and preferential repair pathway of DSBs in higher eukaryotic somatic cells (Chang *et al.*, 2017; Puchta and Fauser, 2014), since this pathway can be carried out independently of any or extensive (< ~10 bp) homology acting to guide repair. This pathway involves the apposition, processing, and direct re-ligation of DNA ends, following the occurrence of a DSB (Chang *et al.*, 2017). NHEJ is prevalent throughout the entire cell cycle, as it is not reliant on the presence of homologous chromosomes to take place (Lieber, 2010); however, it has been shown to play a particularly key role during G1, which is lacking in a homologous chromosome (Chang *et al.*, 2017). Although the most predominant pathway, NHEJ is notably error-prone, in contrast to HR, with the introduction of mutations, such as nucleotide insertions and deletions (INDELS), which are commonly observed at the DSB cleavage site (Shrivastav *et al.*, 2008) (see Figure 1.1). Therefore, it is not surprising that there are apparent control mechanisms that are key in regulating the repair of DSBs, in a manner that ensures that the error rate, and thus the loss of genetic information, does not pose a significant threat to genomic stability (Shrivastav *et al.*, 2008).

NHEJ is divided into two sub-pathways: canonical NHEJ (cNHEJ) and non-canonical NHEJ (ncNHEJ) pathways. cNHEJ depends on the Ku70/80 (ATP-dependent DNA helicase Ku70/80) heterodimer (Walker *et al.*, 2001) (Figure 1.1). This complex is responsible for the initial recognition and binding of DSBs, and the subsequent recruitment of further key factors, such as DNA-PKcs, XRCC4 (x-ray cross complementing protein 4), XLF (XRCC4-like factor), and LIG4 (DNA ligase 4). The Ku70/80 complex bound to the DNA termini stimulates the kinase DNA-PKcs, which is then required to regulate the recruitment of additional factors needed to repair the cleavage site. The broken DNA ends are initially bridged together via filament formation, mediated by XRCC4 and XLF proteins. In conjunction with DNA-PKcs and Ku70/80, this filament is postulated to generate a complex that acts to protect the DNA termini. The specific proteins involved in the subsequent repair steps are dependent on the complexity and nature of the DSBs. Numerous DNA end processing factors act to process DSBs in order to generate ligatable DNA ends, such as the enzymes PNKP, APTX (aprataxin), APLF (aprataxin and PNKP-like factor), TDT (terminal deoxynucleotidyl transferase), and Artemis

nuclease (Figure 1.1). Recruitment of these specific proteins is determined by a scaffold structure generated via the XRCC4 protein.

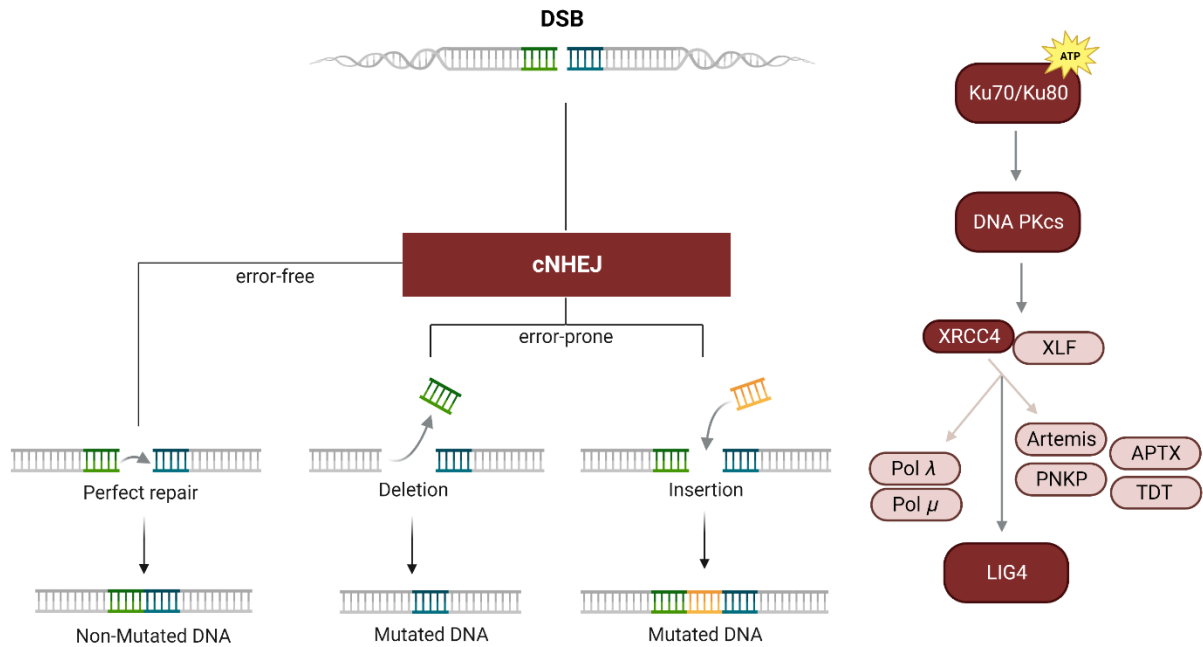


**Figure 1.1. Schematic diagram illustrating the canonical non-homologous end joining pathway and the factors involved.**

The non-homologous end joining pathway (NHEJ) is the preferential pathway for double-strand break (DSB) repair in eukaryotes, with the canonical NHEJ (cNHEJ) representing one of the sub-pathways of the repair pathway. Following a DNA DSB, the Ku70/Ku80 heterodimer acts in an ATP-dependent manner to recruit, recognise and bind to the break site, recruiting the kinase DNA PKcs, which in turn acts to recruit additional factors to the break site. XRCC4 and XLF mediate the formation of a filament, acting to protect the DNA ends, together as part of a complex comprising Ku70/Ku80 and DNA PKcs. XRCC4 then recruits additional factors, depending on the complexity of the break (light red), which generate ligatable ends. As NHEJ repair pathways are error-prone, the incorporation of nucleotide insertions or deletions (INDELS) can occur that, following ligation by Ligase 4 (LIG4), are present within the repaired DNA molecule. Alternatively, when the DSB ends do not require processing prior to ligation, an error-free route of perfect repair is carried out, leading to a non-mutated DNA molecule. Figure created with BioRender.com.

In mammals, the Werner (WNR) protein was identified to not only act alongside the XRCC4-LIG4 complex in the processing of DNA ends (Kusumoto *et al.*, 2008), but also have some regulatory functions with both promoting cNHEJ and inhibiting alternative NHEJ sub-pathways from being initiated (Shamanna *et al.*, 2016). For more complex DSBs, Pol  $\lambda$  or Pol  $\mu$  are employed to fill the gap between the broken DNA ends, prior to ligation. LIG4, mediated by XRCC4, is responsible for ligating the DNA ends, which is the final stage of cNHEJ. cNHEJ is a highly conserved and essential DNA repair pathway. Despite the possible formation of minor mutations with this error-prone pathway, cNHEJ is fundamental in ensuring

genome integrity with the loss of cNHEJ via protein deficiencies being strongly deleterious, owing to growth defects and even lethality as a result of the persistent lethal DSB intermediates (discussed in Chiruvella *et al.*, 2013). Besides cNHEJ, which is dependent on the Ku70/80 complex, additional sub-pathways of NHEJ are prevalent, which are not dependent on Ku70/80, termed non-canonical NHEJ. These alternative ncNHEJ (alt-NHEJ) sub-pathways include microhomology-mediated end joining (MMEJ), which requires microhomology (< ~10 bp) between the DSB junction sites (Sfeir and Symington, 2015; Wang and Xu, 2017), and backup NHEJ (bNHEJ). For MMEJ and bNHEJ, instead of the initial recognition and binding of DSBs by Ku70/80, this is carried out by PARP1.

NHEJ repair mechanisms are thought to be similar in plants as they are in mammals, with the presence of both cNHEJ and the alternative NHEJ pathways, bNHEJ and MMEJ (García-Medel *et al.*, 2019; Osakabe *et al.*, 2010). Homologues of the known cNHEJ proteins Ku70, Ku80, XRCC4, and LIG4 have been reported in the model plant species *Arabidopsis* and other plant species (reviewed in Manova and Gruszka, 2015). *Arabidopsis* plants deficient in AtKu80 and AtLIG4 were shown to be more sensitive to DSB-inducing agents (van Attikum *et al.*, 2003; West *et al.*, 2002), with the presence of DSB-inducing agents leading to an increase in the up-regulation of *AtKu70* and *AtLIG4* expression, as well as for *AtKu80*, *AtXRCC4*, and *AtLIG1* (Tamura *et al.*, 2002; West *et al.*, 2000). Moreover, in *Arabidopsis*, besides AtLIG1 also being shown to play a role in the repair of both SSBs and DSBs (Waterworth *et al.*, 2009), AtKu70 was also demonstrated to interact with AtWEX (a Werner syndrome-like endonuclease) via *in vitro* analysis, highlighting AtWEX as another critical factor within the repair of DSBs (Li *et al.*, 2005; Waterworth *et al.*, 2009). AtXRCC1 is an additional factor identified in *Arabidopsis*, which was shown to act in an AtKu80-dependent manner to repair DSBs, thus playing a role within NHEJ (Charbonnel *et al.*, 2010). However, there have been no apparent homologues in plants identified for some of the other known key players of mammalian cNHEJ, such as DNA PKcs, XLF, pol  $\mu$ , APLF, PNKP, or TDT.

### 1.2.3 Homologous Recombination

The repair of DNA DSBs and replicative DNA damage may also be carried out via the HR pathway, instead of NHEJ. In comparison to NHEJ, HR is notably an error-free pathway that does not constitute any loss of genetic information during the repair process and is therefore integral for ensuring and maintaining genomic stability. Unlike NHEJ, HR comprises extensive DNA-end processing mechanisms and is dependent on homologous DNA sequences to the broken DSB ends that can serve as a template for accurate DNA-synthesis repair (Huertas,

2010). However, it is the use of such a template that allows for HR to precisely repair damaged genomic loci following a DSB. In most cases, the sister chromatid predominantly serves as a template instead of the homologous chromosome (Johnson and Jasin, 2000). The process of which template is to be used is a tightly regulated mechanism, whereby HR is even inhibited when a sister chromatid is absent during G1 of the cell cycle (Hustedt and Durocher, 2017). The initiation of HR begins within the initial steps of cNHEJ itself, with characteristics of the newly replicated chromatin being shown to act to promote the initial steps of HR (Nakamura *et al.*, 2019; Pellegrino *et al.*, 2017; Saredi *et al.*, 2016). It is postulated that the successful removal of the Ku70/80 complex from the DSB ends acts to stimulate further HR steps. HR proceeds with 5' to 3' resection of the DNA strand at the DSB, which various factors carry out, including nucleases and multiple accessory proteins. The result of this strand resection is to generate a 3' ssDNA molecule (Huertas, 2010; Symington, 2014), and act as a determining factor for the subsequent HR pathway employed, that will determine the outcome of the DSB repair. In humans, a replication checkpoint protein known as RAD17 is responsible for the early recruitment of the MRN complex to the DSB (Wang *et al.*, 2014). The MRN complex bound to the DSB ensures phosphorylation of the histone H2AX via ATM, subsequently activating chromatin modifications that permit the onset of strand resection of the 5' DSB ends. Short strand resection, mediated by MRN, BRCA1 (breast cancer type 1 susceptibility protein), and CtIP (C-terminal binding protein 1 (CtBP1) interacting protein), allows for the generation of 3' ssDNA overhangs. The subsequent HR step involves stretching the 3' ssDNA molecule previously generated as a result of strand resection, to enable it to be used for template search and recombination mechanisms. This step in humans is promoted by the BLM (Bloom's syndrome) helicase and either EXO1 or the DNA2 (the DNA replication helicase/nuclease 2) nuclease, which are recruited to the 3' overhangs and responsible for generating 3' protruding ends. RPA then rapidly coats the newly generated 3' protruding ends to eliminate secondary structures in the ssDNA (Nimonkar *et al.*, 2011), which is then replaced by RAD51. Within this process, RAD51 heptamers are firstly disassembled via the action of the BRCA1-PALB2-(a partner and localizer of BRCA2)-BRCA2 complex, which then allows for RAD51 monomers to load onto the ssDNA, forming RAD51 filaments (Trenner and Sartori, 2019). The process mentioned above involving processing the DNA damage, including strand resection and the generation of the RAD51 filament, is also referred to as the presynaptic stage of HR.

The subsequent HR stage is conceptually termed synapsis, whereby the RAD51 filament is involved in a homology search, and a displacement loop (D-loop) is formed due to DNA-strand

invasion (Heyer *et al.*, 2006). The D-loop joint molecule enables DNA repair synthesis to proceed and acts as the branching point from which the latter stages of HR can be carried out. In order to successfully repair the DSB or replicative DNA damage via HR, several varying mechanisms as part of the post-synapsis stage can be utilised in eukaryotic systems, including BIR (break-induced replication), SDSA (synthesis-dependent strand annealing), or DSBR (double-strand break repair) (Heyer *et al.*, 2010). Additionally, SSA (single-strand annealing) can be carried out, which is considered a non-conservative HR pathway and the most straightforward mechanism of HR. SSA takes place at the sites in which DSBs have occurred and between sequence repeats, during which deletions of intervening sequences and one of the repeats occurs between the homologous sequences. This sub-pathway involves annealing complementary ssDNA, following 5' resection by EXO1 and RAD52. The XPF-ERCC1 nuclease complex then removes the resultant non-homologous 3' overhangs, the gap is filled, and the DNA ends are successfully ligated (discussed in Puchta, 2004; Steinert *et al.*, 2016; Sun *et al.*, 2020). BIR, the non-canonical sub-pathway of HR, involves long-range conservative DNA synthesis from the invading DSB end of the D-loop molecule. The second end of the D-loop is not successfully engaged; hence BIR has also been termed one-ended DSB repair. With BIR, the D-loop, in the absence of a second-end, is essentially processed to become a replication fork that can be used for further replication processes. Although ultimately restoring genomic integrity, BIR can lead to loss of heterozygosity of the genetic information that is distal to the DSB site, via the formation of genomic rearrangements and point mutations (Chandramouly *et al.*, 2013).

On the other hand, the SDSA and DSBR pathways are two-ended DSB HR repair mechanisms, otherwise known as canonical pathways, due to their apparent high fidelity. SDSA and DSBR are distinguished, on the most part, by their propensity to cause genetic exchanges as repair outcomes, or not (Moynahan and Jasin, 1997). In both somatic and meiotic cells, reproductive outcomes of HR sub-pathways are either a non-crossover (NCO) or a crossover (CO) product, with COs representing the exchange of genetic information. Concerning the reciprocal exchange of genetic information between homologous chromosomes, and thus the induction of heterozygosity, COs can be harmful; however, when the sister chromatid is used as a donor instead, the CO is rendered genetically silent (Kadyk and Hartwell, 1992; Soutoglou and Misteli, 2008). As a result, various regulatory mechanisms are employed that aim to limit CO formation (reviewed in Elbakry and Löbrich, 2021). SDSA is thought to be the most predominant HR sub-pathway and notably does not result in the formation of CO products, with HR intermediates being processed to generate NCOs instead. During SDSA, in the presence of

a second end, the extended D-loop is reversed, resulting in the newly synthesised strand and the resected strand of the second end annealing to one another, generating a NCO product (Pâques and Haber, 1999).

The dHJ sub-pathway of HR refers to an alternative mechanism involving the formation of a double Holliday junction (dHJ) joint molecule from the D-loop recombination intermediate, resulting in either a NCO or CO product. Via a second-end capture step, the non-invading end can anneal with the displaced strand of the D-loop, leading to the formation of the dHJ, following end-filling and ligation. This HR intermediate may also be generated when two resected ends simultaneously invade the donor and are subsequently extended. The dHJ joint molecule is then either resolved by endonucleases to give rise to CO or NCO products, or dissolved via the dissolution pathway resulting, in the formation of a NCO product (West, 2003; Wu and Hickson, 2003).

#### **1.2.3.1 The dissolution pathway**

The formation of dHJs during homologous recombination, as a result of the interactions between homologous chromosomes, occurs to facilitate DNA repair. However, when unprocessed, these four-way intermediate structures are potentially toxic, with a single unresolved dHJ molecule resulting in severe defects such as chromosome nondisjunction and aneuploidy (Matos and West, 2014). Therefore, pathways that act to resolve dHJ intermediates are integral for cell survival and are highly conserved throughout all eukaryotic kingdoms. The dissolution pathway is one such mechanism that acts to entangle dHJs, separating the recombining molecules, resulting exclusively in NCO products; that is, without the occurrence of genetic exchanges (Knoll *et al.*, 2014; Wu and Hickson, 2003) (see Figure 1.2). As a result, the dissolution pathway contributes to the numerous factors employed to avoid and therefore regulate the formation of COs, ensuring genome integrity (Dayani *et al.*, 2011; Wechsler *et al.*, 2011; Wu and Hickson, 2003). The dissolution pathway is mediated by the activity of a dissolvasome complex, known as the RTR complex (Knoll *et al.*, 2014; Wu and Hickson, 2003).

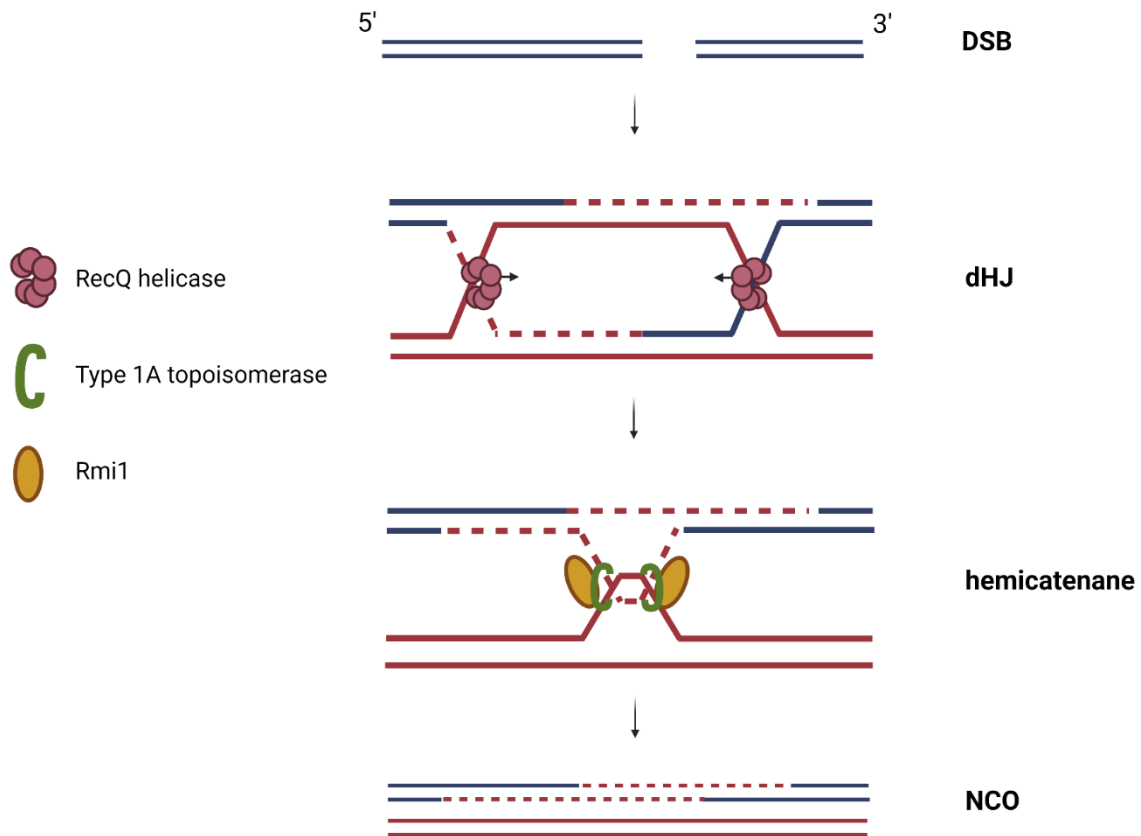


**Figure 1.2. Schematic diagram illustrating the dissolution pathway of homologous recombination.**

Following a DSB, the dissolution pathway represents one of the pathways that acts to repair the break, leading to the generation of a non-crossover (NCO) product. The double-Holliday junction (dHJ) joint molecule, is processed ensuring disentanglement of the chromosomes by the concerted action of the RTR complex partners. The RecQ helicase pushes the dHJ junctions closer to one another, via its branch migration activity, forming a hemicatenane intermediate. The type 1A topoisomerase, stabilised by the structural protein Rmi1, then acts to cleave the junction points of the hemicatenane, resulting in the formation of a NCO product, via dissolution. Figure created with BioRender.com.

### 1.3 The RTR complex

The RTR (RecQ/Top3/Rmi1) complex comprises of at least a RecQ helicase, a type 1A topoisomerase, and the structural protein Rmi1 (RecQ-mediated genome instability). This multi-subunit complex, otherwise referred to as the dissolvasome, has been shown to be involved in the dissolution pathway of HJ (Holliday junction) processing during HR for various organisms within all eukaryotes (Bizard and Hickson, 2014; Wyatt and West, 2014). During the dissolution pathway, the concerted action of the factors of the RTR complex act to process dHJ intermediates, generating a NCO product (Figure 1.2).

Firstly, via helicase branch migration activity, the RecQ helicase mediates the convergent migration of two HJ molecules. With this migration action, the junctions of the dHJ are brought within close proximity to one another, enabling the formation of a hemicatenane intermediate. The decatenase action of the topoisomerase within the RTR complex subsequently ensures the dissociation of the hemicatenane intermediate structure, via cleavage of the joints. This activity, stabilised by Rmi1, enables the unlinking of the DNA molecules, leading to the formation of a NCO product (Yang *et al.*, 2010).

With the unprecedented importance and fundamental role of the RTR complex in maintaining and ensuring genome stability, it comes as no surprise that the complex is highly conserved throughout all eukaryotic kingdoms, from yeast to humans. In yeast *Saccharomyces cerevisiae*, the interacting complex partners of the RTR complex are the RecQ helicase Sgs1, topoisomerase 3 (Top3), and Rmi1. The RTR complex in humans is known as the BTR complex, which comprises of four subunits, as opposed to the three observed in yeast. These factors are the BLM helicase, the TOP3 $\alpha$  topoisomerase, and RMI1 and RMI2 (Chaganti *et al.*, 1974; Ellis *et al.*, 1995; German, 1993; Wu and Hickson, 2003). In the model plant species *Arabidopsis thaliana*, the RTR complex comprises of four proteins, including RMI2, similar to that of the BTR complex in humans (Röhrig *et al.*, 2016). However, RECQ4A was demonstrated as the functional homologue of ScSgs1 and HsBLM in plants, owing to the complex being termed the RTR (RECQ4A/TOP3 $\alpha$ /RMI1/2) complex (Hartung *et al.*, 2000). Across all kingdoms, all factors of the RTR complex have been shown to play further, partly distinct roles in both DNA repair and homologous recombination. Disruption of the complex via one or more of the complex partners has been shown to result in severe, characteristic phenotypes related to the functions of the RTR complex and its factors (Onoda *et al.*, 2000).

### 1.3.1 RecQ helicase

One of the integral components of the RTR complex and, therefore, the effective dissolution of dHJ intermediates, is a RecQ helicase. This RecQ-family DNA motor protein is necessary for the migration of the two junctions of dHJs, enabling the formation of the hemicatenane structure required for subsequent cleavage by the topoisomerase 3 cofactor of the RTR complex (Wu and Hickson, 2003). Helicases, including RecQ helicases, act in an ATP-dependent manner to catalyse the unwinding of double-stranded DNA, RNA, and DNA-RNA duplexes. Necessary for a wide array of processes involved in DNA and RNA metabolism, such as DNA replication, transcription, DNA repair, and recombination, DNA helicases are highly conserved and apparent within all kingdoms of life. RecQ helicases, with their 3' to 5' directionality, can act

on and unwind several DNA molecules, including forked DNA duplexes, D-loops, DNA junctions, and G-quadruplexes (Croteau *et al.*, 2014), in addition to promoting branch migration of HJs and annealing of complementary ssDNAs. RecQ helicases are indispensable for ensuring genomic stability (Bohr, 2008; Croteau *et al.*, 2014; Urban *et al.*, 2017), owing to the presence of at least one functional homologue apparent in each organism, from prokaryotes to more complex eukaryotic organisms such as humans. Interestingly, the number of RecQ homologues has been found to differ between organisms, correlating with the complexity of the genome (reviewed in Dorn and Puchta, 2019). RecQ helicases are distinguishable by the highly conserved core helicase domain that they all share, the DEAD/DEAH box, and the helicase conserved C-terminal domain. In budding yeast, two RecQ helicases have been identified, Sgs1 and Hrq1, with Sgs1 being the RecQ helicase factor of the RTR complex (Bochman *et al.*, 2014; Choi *et al.*, 2013; Rogers *et al.*, 2017; Watt *et al.*, 1996). In humans, however, there are five different RecQ helicases: RECQL1, BLM, Werner syndrome helicase (WRN), RECQL4, and RECQL5, with BLM being the functional homologue of ScSgs1 (Bohr, 2008; Croteau *et al.*, 2014; Hickson, 2003). All of the human RecQ helicases have been found to play distinct functions within most DNA repair mechanisms, including DSB repair pathways. Defects in RecQ helicases in humans have been shown to result in several human genetic disorders, carcinogenesis, and premature aging, all of which are speculated to arise as a result of defective DSB repair (Datta *et al.*, 2021; Oshima *et al.*, 2018). Defects in the BLM helicase, the RTR complex partner in humans, are associated with the hereditary disease known as Bloom's Syndrome. This genetic disorder is characterised by growth retardation and increased susceptibility to cancer (Cunniff *et al.*, 2017; de Renty and Ellis, 2017), due to genomic instability. This instability results from enhanced sister chromatid exchanges due to an elevated HR rate (Chaganti *et al.*, 1974; Ellis *et al.*, 1995; German, 1993). Genetic mutations disrupting the yeast *Sgs1* gene were also shown to result in yeast cells exhibiting a hyperrecombination phenotype and hypersensitivity against genotoxic agents (Onoda *et al.*, 2000). These phenotypes of elevated recombination frequencies alongside increased genotoxin sensitivities were identified as the predominant one's characteristic for mutants lacking the RecQ helicase factor of the RTR complex. The characteristic phenotypes of yeast and human cells lacking *Sgs1* and *BLM*, respectively, can be attributed to the multifaceted role that RecQ helicases play during multiple DNA repair pathways, but more so during HR. BLM was identified as indispensable for both the early phase of HR, involving strand resection, and the later steps involving the dissolution of HJs during the dissolution pathway (Croteau *et al.*, 2014). This involvement was identified as a result of GFP-tagged BLM being shown to accumulate to DSB

sites within a few seconds following DSB induction, and remain for several hours (Karmakar *et al.*, 2006; Singh *et al.*, 2010). In terms of the early steps of HR, BLM was found to bind to 3' ssDNA and unwind the dsDNA in order to facilitate the endonucleolytic activity of DNA2, enabling further strand resection and therefore the generation of the extended 3' ssDNA (Gravel *et al.*, 2008; Nimonkar *et al.*, 2011). In doing this, BLM was also shown to interact with other factors, including RPA and CtIP (Brosh *et al.*, 2000; Daley *et al.*, 2017; Doherty *et al.*, 2005; Li and Comai, 2000; Nimonkar *et al.*, 2011; Qin *et al.*, 2020; Soniat *et al.*, 2019), and also promote the nuclease activity of EXO1 on dsDNA (Nimonkar *et al.*, 2008). Within strand invasion, BLM can act to disrupt the RAD51-ssDNA filaments, displacing the invading strand from the D-loop intermediate, acting in an anti-recombinase-like manner (Bachrati *et al.*, 2006; Bugreev *et al.*, 2009; Bugreev *et al.*, 2007; Kikuchi *et al.*, 2009; Manthei and Keck, 2013; van Brabant *et al.*, 2000; Wu *et al.*, 2001; Xue *et al.*, 2019). The latter involvement of BLM in HR is its instrumental role in the dissolution of HJs during the dissolution pathway, alongside the other RTR complex partners, the type1A topoisomerase and the structural proteins RMI1 and RMI2.

In plants, via studies in the model plant species *A. thaliana*, the functional homologue of HsBLM and ScSgs1 was identified as AtRECQ4A (Dorn and Puchta, 2019). Arabidopsis, a member of the *Brassicaceae* plant family, harbours two RecQ4 homologues, RECQ4A and RECQ4B, which possess high sequence similarity and demonstrate highly conserved domain structures (Hartung *et al.*, 2007a). However, only RECQ4A was shown to act as an actual functional homologue of HsBLM, due to the sub-functionalisation of the two plant paralogues. RECQ4A was demonstrated as integral for somatic DNA repair in Arabidopsis, with deficiencies leading to elevated HR and hypersensitivity to genotoxins; the characteristic phenotypes of mutants of the RTR complex partners (Bagherieh-Najjar *et al.*, 2005; Hartung *et al.*, 2000; Knoll and Puchta, 2011; Mannuss *et al.*, 2010; Schröpfer *et al.*, 2014). Whereas AtRECQ4A was found to be involved in numerous aspects of DNA repair and HR, similarly to BLM (Higgins *et al.*, 2011), AtRECQ4B was not found to play a role in somatic DNA repair. However, a role in promoting CO formation during meiosis has been speculated (Séguéla-Arnaud *et al.*, 2015).

### 1.3.2 The structural protein Rmi1

Rmi1, although lacking its own catalytic function, is an important factor and interacting partner of the RTR complex. Within the RTR complex, the role of Rmi1 is to essentially stimulate dHJ dissolution during the final decatenation step, acting as a 'scaffolding' protein (Cejka *et al.*,

2010). Rmi1 stabilises the hemicatenane molecule formed during the dissolution pathway, and consequently stimulates the activity of the Type 1 topoisomerase; enabling cleavage of the joint molecules and the subsequent formation of a NCO product (Yang *et al.*, 2010). As with all of the RTR complex partners, Rmi1 is highly conserved with homologues present across all eukaryotic kingdoms; owing to its fundamental role in genome stability maintenance (Bussen *et al.*, 2007; Chang *et al.*, 2005; Chen and Brill, 2007; Mullen *et al.*, 2005; Raynard *et al.*, 2006; Wu *et al.*, 2006; Yin *et al.*, 2005). In yeast, ScRmi1 is composed of an N-terminal domain of unknown function 1767 (DUF1767; pfam08585) and an oligonucleotide/oligosaccharide binding-fold (OB-fold) domain (OB1) (Xu *et al.*, 2008). Yeast cells lacking Rmi1 demonstrate growth defects, hypersensitivity to genotoxins, elevated HR and increased sister-chromatid exchange rates; notably the characteristic phenotypes of the RTR complex partner mutants (Chang *et al.*, 2005). Intriguingly, ScRmi1 is considerably shorter than the homologous protein identified in mammals, known as BLAP75 (for Blooms associated protein 75kd), with ScRmi1 lacking the second OB-fold domain (OB2), which is present at the C-terminal end of the mammalian homologue. OB-fold domains were initially thought to mediate protein-ssDNA interactions (reviewed in Flynn and Zou, 2010), however, studies have demonstrated that the OB1 domain of the human RMI1 homologue does not mediate such interactions, with the domain not having any DNA binding activity at all (Cejka *et al.*, 2010; Raynard *et al.*, 2006; Wu *et al.*, 2006). In fact, it has become increasingly apparent that the OB1 domain actually enables protein-protein interactions between RMI1 and the other RTR complex partners, TOP3 $\alpha$  and BLM, as part of its role for being essential for the dissolution of dHJs (Bussen *et al.*, 2007; Raynard *et al.*, 2006). Moreover, the second OB-fold domain, OB2, that is not present in yeast Rmi1, enables the interaction of HsRMI1 with an additional RTR complex partner, RMI2 (Singh *et al.*, 2008; Xu *et al.*, 2008). Despite no homologue in yeast, RMI2 has been found to be the fourth RTR complex partner in animals and *C. elegans* (Singh *et al.*, 2008; Velkova *et al.*, 2021). RMI1 and RMI2 were found to interact with one another via their OB-2 and OB-3 domains, respectively (Xu *et al.*, 2008), and in a similar manner as RMI1, RMI2 is necessary for stabilisation of the RTR complex, whilst also functioning in the mediation of post-translational modifications of its RTR cofactors (Singh *et al.*, 2008). As mentioned previously, this fourth additional RTR complex partner, RMI2, is also present in plants, and as observed in mammals and more recently in *C. elegans*, it is also an integral factor of the complex and thus the dissolution pathway of homologous recombination (Röhrig *et al.*, 2016). In Arabidopsis, plants deficient in either one of the RMI proteins, RMI1 or RMI2, demonstrate the characteristic phenotypes similar to those observed for plants deficient in RECQ4A (Bonnet

*et al.*, 2013; Hartung *et al.*, 2008). For both *Atrmi1* and *Atrmi2* mutants, plants exhibit the characteristic phenotype of the RTR complex with both mutants showing increased homologous recombination rates, and *Atrmi1* mutants also demonstrating hypersensitivity to genotoxins (Bonnet *et al.*, 2013; Hartung *et al.*, 2008; Röhrig *et al.*, 2016). Therefore, both RMI1 and RMI2 are integral components of not just the RTR complex, but for DNA repair in plants itself.

### 1.3.3 Type 1A topoisomerase

The RTR complex and its essential function in dissolving recombination intermediates and generating NCO products is dependent upon the activity of a type 1A topoisomerase. Acting as a single-stranded decatenase (Champoux, 2001; Seol and Neuman, 2016), the type 1A topoisomerase is crucial in the processing of the hemicatenane structure, formed as a result of the previous branch migration action of the RecQ helicase (Chen *et al.*, 2014). Hemicatenane structures are essentially two dsDNA molecules linked by a single-stranded crossover, and hence also referred to as entanglements. Such entanglements of DNA molecules arising during genetic processes like DNA repair, exert torsional stress on the DNA, which leads to local changes in the topology of the DNA. In order to relieve such torsional stress, key enzymes known as topoisomerases play pivotal roles in regulating the topological state of DNA and thus disentangling DNA strands that are entwined with one another (Champoux, 2001; Seol and Neuman, 2016). Due to the requisite function of topoisomerases, it is not surprising that they are present and conserved throughout all domains of life (Forterre and Gadelle, 2009), with different types carrying out distinct and specific actions (discussed in Spakman *et al.*, 2021). All topoisomerases act by changing the topology of DNA via the induction of transient breaks in the DNA phosphate backbone of DNA, via a transesterification reaction (Chen and Wang, 1998; Cheng *et al.*, 2008). Type 1 and Type 2 topoisomerases differ in whether they cleave one or both of the entwined DNA molecule backbones. Acting in an ATP-independent manner, Type 2 topoisomerases classically cleave both DNA strands, whereas Type 1 topoisomerases only cleave one of the DNA phosphate backbones (Forterre and Gadelle, 2009). Moreover, Type 1 topoisomerases can be further classified into sub-families dependent on the structure of the enzyme and the mechanism in which they conduct the transesterification reaction (Baker *et al.*, 2009; Forterre and Gadelle, 2009). Type 1A topoisomerases utilise a mechanism involving an enzyme-bridged strand-passage, enabling the decatenation of the DNA. Type 1B topoisomerases, on the other hand, induce topological changes in DNA by a swivel mechanism that allows the relaxation of DNA supercoiling (Koster *et al.*, 2005; Stivers *et al.*, 1997; Taneja

*et al.*, 2007). Prevalent in nearly all living organisms (Forterre and Gadelle, 2009), partly due to their key RNA topoisomerase activity (Wang *et al.*, 1996) and speculated role in evolution itself, Type 1A topoisomerases are distinct from other topoisomerase enzymes in that their catalytic activity requires single-stranded DNA or RNA as the substrate (DiGate and Marians, 1988; Kirkegaard and Wang, 1985).

Within the RTR complex in eukaryotes, the Type 1A topoisomerase component is a member of the TopoIII sub-group, in which is characterised by its increased efficiency at decatenating DNA (DiGate and Marians, 1988; Terekhova *et al.*, 2014). Due to their prevalence throughout all domains of life, TopoIII enzymes have been extensively studied in terms of their structure and functions. Interestingly, these studies have demonstrated remarkably differing phenotypes for *Top3* mutants within different organisms. In baker's yeast, cells deficient in Top3 grow significantly slower than wild-type yeast cells with a functional Top3 enzyme. Furthermore, *top3* yeast mutants additionally exhibit sporulation defects, whilst still remaining viable. This differs to *top3* mutants in fission yeast in which are not viable, thus demonstrating the differences between TopoIII mutant phenotypes even between types of unicellular eukaryotic organisms (Gangloff *et al.*, 1994). In yeast, as with other eukaryotic organisms, TopoIII is part of the RTR complex acting in a concerted manner with the other two RTR-complex partners, the RecQ-helicase and Rmi1. In higher eukaryotes, however, there are two TopoIII homologues present, TopoIII $\alpha$  and TopoIII $\beta$ , with only TopoIII $\alpha$  acting as part of the RTR complex, as the true homologue of ScTop3 (Xu *et al.*, 2013). TopoIII $\alpha$ , otherwise referred to as TOP3 $\alpha$ , has been shown as essential in *Drosophila melanogaster*, *Caenorhabditis elegans* and mammals. Mutant phenotypes of TOP3 $\alpha$  intriguingly differ in severity within these higher eukaryotes, with phenotypes ranging from complete embryo lethality to premature death occurring during early developmental stages (Kim *et al.*, 2000; Li and Wang, 1998; Plank *et al.*, 2005).

In plants, the phenotype of *top3a* mutants was interestingly not clear for over a period of ten years (Hartung *et al.*, 2008; Hartung, *et al.*, 2007a). This uncertainty arose as a result of the confusion surrounding two distinct T-DNA mutant lines in the model plant species *Arabidopsis*. Both of these T-DNA mutant lines displayed different phenotypes to one another, making it unclear as to which of the two phenotypes was indeed the true null mutant phenotype. With the breakthrough advancements regarding gene-editing and the application of CRISPR/Cas9 technology in eukaryotes, this issue was only recently resolved. CRISPR/Cas9-mediated mutagenesis generating a complete knockout of the *TOP3a* gene in *Arabidopsis*, surprisingly confirmed a viable mutant phenotype (Dorn *et al.*, 2018). This finding was unforeseen due to the severity of the mutant phenotypes in mammals and other eukaryotic organisms, that had

previously been demonstrated, whereby TOP3 $\alpha$  is regarded as essential. In plants however, *top3 $\alpha$*  mutants are viable, although displaying somatic defects highlighting the significant role that TOP3 $\alpha$  conducts within plants as part of DNA repair mechanisms. The somatic defects displayed include the characteristic RTR mutant phenotypes of hypersensitivity to genotoxins and increased HR, in addition to other defects such as fasciated organs, dwarfism, and replication-associated DNA damages, demonstrated via increased cell-death within the root meristem (Dorn *et al.*, 2018). The differences in phenotypes between kingdoms for mutants of TOP3 $\alpha$  elucidates slightly varying roles of the RTR-complex partner in terms of its importance within DNA repair and other integral biological processes. Furthermore, studies in plants also highlighted an entirely unique role for TOP3 $\alpha$  that had not been observed for other eukaryotic organisms before. Arabidopsis *top3 $\alpha$*  mutant plants, although viable, are actually rendered sterile due to severe defects during the process of meiosis; which was also the case for *rml1* mutant plants (Dorn *et al.*, 2018; Hartung *et al.*, 2008).

#### 1.4 Meiosis

Meiosis is a specialised form of cell division that forms the basis of sexual reproduction, within most sexually reproducing eukaryotic organisms. Meiosis is comprised of a single round of DNA replication, followed by two sequential nuclear divisions known as meiosis I and meiosis II. Meiosis I and meiosis II, otherwise referred to as the reductional and equational divisions, respectively, allow for the formation of four haploid gametes. Meiosis is therefore essential in ensuring genomic stability via the restoration of chromosome number, and permitting stable chromosome complements across generations (Gray and Cohen, 2016; Mercier *et al.*, 2015). Both meiosis I and meiosis II are divided into four cytogenetically distinct stages – prophase, metaphase, anaphase and telophase, which can be distinguished as belonging to either meiosis I or meiosis II, via the structure and number of the chromatin that can be observed (see Figure 1.3). Typical of meiosis I, within prophase I, the nuclear envelope of the meiocytes begins to break down, whilst condensation of the chromatin takes place. The resultant homologous chromosomes visible as bivalent structures, align on the equatorial plane in the middle of the meiocyte, during metaphase I, in preparation for subsequent steps. In anaphase I, the homologous chromosomes are then separated from one another and begin migrating towards opposite ends of the cell. With each individual chromosome from each homologous chromosome pair now at opposite poles of the meiocyte, telophase I involves the decondensing of the chromosomes, and the formation of a nuclear envelope to generate two diploid daughter cells. A distinctive event that occurs during meiosis I, is that of homologous

recombination between the two homologous chromosomes, during early prophase I (Figure 1.3). This event involves the reciprocal exchange of genetic material between the homologous chromosomes, resulting in genetically recombined chromosome pairs that subsequently lead to the formation of genetically recombined chromosomes within the two daughter cells at the end of meiosis I. This recombination event, otherwise known as a crossover event, can be visualised cytogenetically as a result of the chiasmata that is physically manifested during the process. Despite no recombination taking place during meiosis II, the process is analogous to that of meiosis I, with the four distinct phases (Figure 1.3), differing only in that no crossovers are formed and that the sister chromatids are separated from one another, as opposed to the chromosomes being separated, as occurs during meiosis I. With the successful completion of telophase II, during meiosis II, four haploid gametes are generated, that are then available for possible fertilisation, whereby the ploidy level is restored, with the zygote harbouring genetic information from both parents, in which their gametes were the products of meiosis (Figure 1.3).

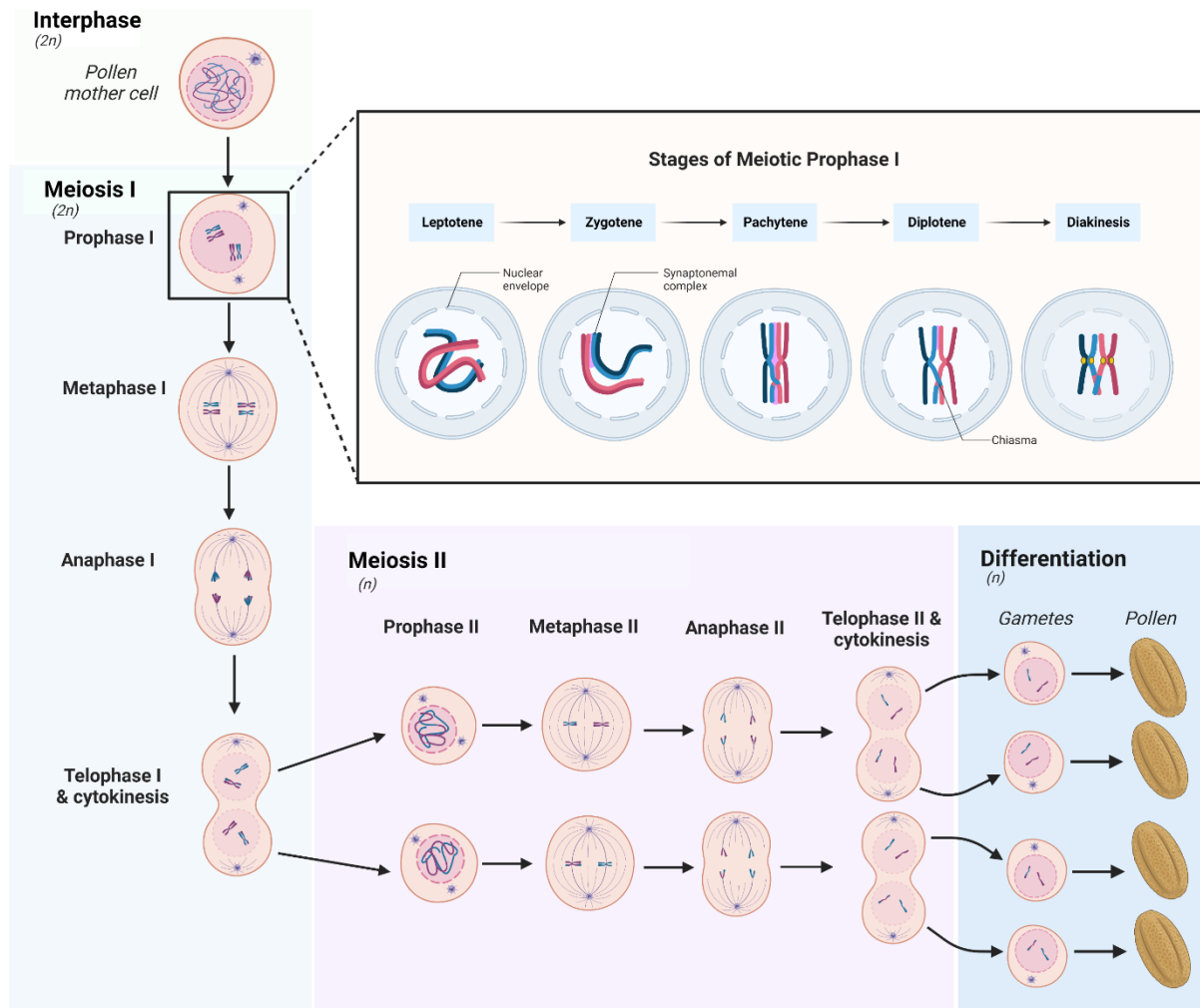


**Figure 1.3. Overview of male meiosis in plants.**

Prior to meiosis, interphase occurs comprising of a round of DNA replication resulting in a diploid cell, with double the genetic content ( $2n$ ). Meiosis is divided into meiosis I and meiosis II (highlighted in light blue and purple, respectively), which are both comprised of four analogous stages: prophase, metaphase, anaphase and telophase. Meiosis I begins with prophase I (highlighted in the yellow call-out box), which is further sub-divided into five cytologically distinct sub-stages: leptotene, zygotene, pachytene, diplotene and diakinesis. During leptotene, the nuclear envelope forms and meiotic recombination is initiated. Zygotene involves the formation of the synaptonemal complex (SC) (shown in pink), and thus synapsis of the homologous chromosomes. By the completion of pachytene, synapsis is complete. The SC begins to dissociate during diplotene, and the homologous chromosomes are connected by chiasma, physical manifestations of where crossovers (COs) have taken place during recombination. During diakinesis, the chromosomes begin to condense, forming bivalents that can be distinguished cytologically. At the end of prophase I, the nuclear envelope breaks down. The bivalents align along the metaphase plate during metaphase I, and the chromosomes migrate to opposite ends of the cell in anaphase I. Telophase I is when two diploid nuclei are present as dyads. Meiosis II begins with the decondensing of the chromosomes during prophase II. In metaphase II, the chromosomes align along the metaphase plate and the sister chromatids separate during anaphase II. Four nuclei form during telophase II, with the formation of four genetically distinct haploid ( $n$ ) gametes at the end of meiosis II. These gametes then give rise to pollen spores, the product of male meiosis in plants. Figure created with BioRender.com.

Meiosis I involves the pairing, recombining and separation of homologous chromosome pairs, thereby halving the chromosome number. Prophase I of meiosis I, is further sub-divided into five cytologically prominent sub-stages – leptotene, zygotene, pachytene, diplotene and

diakinesis (see Figure 1.3). During prophase I, numerous DSBs are formed in which are repaired via homologous recombination, whereby the reciprocal exchange of genetic information between the two homologous chromosomes takes place. During each of the stages of prophase I, individual steps of meiotic recombination can be determined visually. During leptotene, the initial stage of prophase I, meiotic recombination is initiated following the induction of DSBs. This is when the condensation of the chromatin takes place. In zygotene, formation of the synaptonemal complex (SC) occurs, with the proteinaceous axis bringing the homologous chromosomes into close proximity to one another via synapsis, to enable subsequent steps. Synapsis of the homologous chromosomes is completed during pachytene, which allows for recombination between the homologous chromosomes to proceed, and thus the formation of a CO event. Diplotene involves the dissolution of the SC, with the homologous chromosomes remaining physically connected to one another via the chiasmata, that indicate the location of CO events. During the final stage of prophase I, diakinesis, further condensation of the chromosomes takes place, generating the characteristic bivalent structures that are further separated during the ongoing stages of meiosis I (Armstrong and Jones, 2003; Armstrong and Jones, 2001; Ross *et al.*, 1996). Subsequently, meiosis II consists of the separation of the sister chromatids, which leads to the formation of genetically distinct, recombined haploid gametes and thus new combinations of alleles, which contribute to the generation of genetic diversity (Mercier *et al.*, 2015; Osman *et al.*, 2011).

#### 1.4.1 Meiotic recombination

Meiotic recombination is the homologous recombination that takes place during meiosis, assuring genetic variation via the regulated genetic exchange between homologous chromosomes. The generation of genetic variation as a result of both meiotic recombination and the random chromosome segregation that occurs during meiosis, is the fundamental basis upon which selection can act, whether that be natural via evolutionary processes, or artificial during classical breeding (Lambing and Heckmann, 2018).

Similarly with homologous recombination, meiotic recombination involves the repair of DSBs and the subsequent formation of either a CO or NCO product (see Figure 1.4). During meiosis, the formation of CO products assures accurate chromosome segregation during meiosis I, and therefore viable gametes by the end of meiosis II. As a result, CO formation during meiosis is a tightly-controlled process, with numerous molecular mechanisms employed to ensure regulation in terms of the frequency and distribution of CO products (Mercier *et al.*, 2015; Osman *et al.*, 2011; Wang *et al.*, 2021).

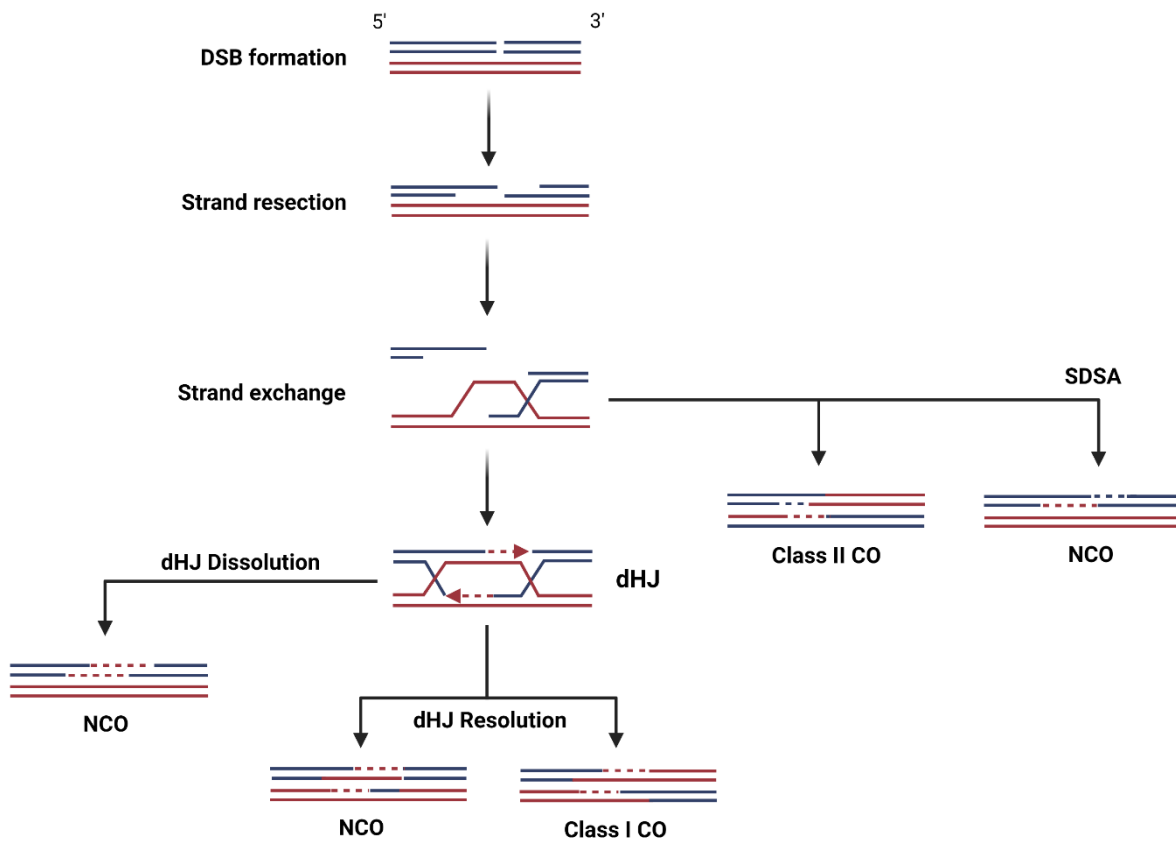


**Figure 1.4. Schematic diagram illustrating meiotic recombination pathways.**

Processing of programmed DNA double-strand breaks (DSBs) begins with strand resection of the 5'-ends. Strand invasion and exchange takes place leading to the formation of a displacement-loop (D-loop) structure. A portion of these structures are processed to generate a Class II crossover (CO), or lead to the generation of a non-CO (NCO) product, via the synthesis-dependent strand annealing (SDSA) pathway. Second-end capture of the invading strand of the D-loop, and subsequent synthesis and ligation, leads to the formation of a double Holliday junction (dHJ) intermediate. These structures can either be resolved by endonucleases leading to a Class I CO, or a NCO, or the dHJ structure can be resolved via the dissolution pathway, mediated by the RTR complex, generating a NCO product. Figure created with BioRender.com.

#### 1.4.1.1 Meiotic DNA Double-Strand Break Formation

Meiotic recombination is initiated upon the induction of programmed DNA DSBs (see Figure 1.4), generated by the type II topoisomerase-like SPO11 family of proteins (Bergerat *et al.*, 1997; Keeney *et al.*, 1997). The key protein, SPO11, is highly conserved across all eukaryotes, with homologues present in fungi, animals and plants; however, the number of homologues present has been found to differ between kingdoms. In plants, for example, studies in *Arabidopsis* revealed the presence of three SPO11 homologues, AtSPO11-1, AtSPO11-2 and AtSPO11-3. However, only AtSPO11-1 and AtSPO11-2 were found to be involved in meiotic DSB formation, acting in concert as part of a heterodimer with one another. AtSPO11-3, despite no apparent role in meiosis, was found to be involved in endo-reduplication with *Atspo11-3* mutants demonstrating somatic cell defects suggestive of such a role (Hartung *et al.*, 2007b;

Hartung and Puchta, 2001; Hartung and Puchta, 2000). In plants, another of the key factors involved in the formation of DSBs, forming a catalytic complex with the SPO11 homologues, is MTOPVIB. With mutants deficient in MTOPVIB showing no meiotic recombination initiation, MTOPVIB was postulated to mediate the formation of a bridge between SPO11-1 and SPO11-2, thus owing to the formation of the SPO11 heterodimer complex and the initiation of meiotic recombination (Vrielynck *et al.*, 2016). In addition to SPO11-1, SPO11-2 and MTOPVIB, additional factors have also been found to play important roles within meiotic DSB formation. In Arabidopsis, these co-factors include PRD1, PRD2, PRD3, DFO and CRC1 (De Muyt *et al.*, 2007; Miao *et al.*, 2013; De Muyt *et al.*, 2009; Nonomura *et al.*, 2004; Zhang *et al.*, 2012), with each playing distinct roles within DSB formation (discussed in Mercier *et al.*, 2015). Although SPO11 is highly conserved, the array of accessory proteins required for meiotic DSB formation has been shown to differ across kingdoms, with either sequence or functional divergences observed. For instance, in *S. cerevisiae*, nine additional proteins act in conjunction with Spo11 (Rad50, Mre11, Xrs2, Rec102, Rec104, Rec114, Ski8, Mer2 and Mei4), all of which are required for the induction of meiotic DSBs (de Massy, 2013), whereas orthologues of some of these are not required for DSB formation in plants (reviewed in Mercier *et al.*, 2015). Therefore, despite the highly conserved SPO11-complex and SPO11-programmed DSBs being essential for meiotic recombination initiation, the DSB machinery and factors involved varies amongst kingdoms, and even species.

#### 1.4.1.2 Meiotic DSB processing

Following meiotic DSB formation, meiotic recombination is initiated, which essentially acts to repair the induced breaks within the DNA. After cleavage, in yeast and mammals, Spo11 remains covalently attached to the 5'-DNA ends on either side of the DSB. Processing of the DSB is then initiated with the recruitment and subsequent nucleolytic activity of the MRX/MRN complex (Mre11-Rad50-Xrs2/NBS1), facilitated by the phosphorylation of the histone variant, H2AX, over the surrounding regions of the break site. In conjunction with Com1/Sae2, Spo11 is removed and the 5'-end is resected, forming 3'-ssDNA overhangs (Figure 1.4) (Neale *et al.*, 2006). Analyses in plants determined orthologous genes for *MRE11*, *RAD50* and *COM1*, with the respective proteins carrying out similar roles as in yeast and mammals during the early steps of processing DNA DSBs (Puizina *et al.*, 2004; Uanschou *et al.*, 2007).

### 1.4.1.3 Meiotic strand invasion and exchange

With the generation of 3' ssDNA, similar to events occurring in homologous recombination during somatic DNA repair, the RecA-related recombinases, Rad51 and Dmc1, are recruited (Bishop *et al.*, 1992; Shinohara *et al.*, 1992). Mediated by Brca2 and 3'-end coating with Rpa, the recruitment and loading of both Rad51 and Dmc1 onto the 3' ssDNA, facilitates the onset of meiotic recombination, via strand invasion and exchange, and therefore the formation of nucleofilaments necessary for homology search (Figure 1.4). Following homology searches, single-end invasion takes place, in which results in the generation of a heteroduplex molecule, known as a joint molecule, that is then implemented as part of the initiation of strand exchange (Brown and Bishop, 2014). An orthologue of Dmc1 was identified in plants, from analyses conducted in *A. thaliana*. Moreover, six paralogues of Rad51 were identified, with only three been shown as essential for meiotic recombination; AtRAD51, AtRAD51C and AtXRRC3 (Doutriaux *et al.*, 1998; Pradillo *et al.*, 2014). Arabidopsis plants lacking AtRAD51 were shown to be infertile, highlighting the importance of this factor in SPO11-induced DSB repair, alongside its role within somatic DNA repair; with AtRAD51 being shown to be important in the repair of DSBs using the sister chromatid as a template (Li *et al.*, 2004). On the other hand, AtDMC1 acts exclusively during meiotic recombination, and is crucial for the promotion and thus assurance of CO formation as part of inter-homologous (IH) biased DNA repair, therefore acting to ensure genetic variation (Couteau *et al.*, 1999). In both yeast and Arabidopsis, RAD51 was elucidated as an accessory factor to DMC1 for CO formation during meiosis, with DMC1-mediated IH DNA repair acting as the predominant pathway in wild-type meiosis (Cloud *et al.*, 2012; Da Ines *et al.*, 2013). *AtDmc1* plants were shown to lack inter-homologue recombination with mutants demonstrating random segregation of univalents at anaphase I, with AtRAD51 being shown to act as a back-up pathway ensuring correct DNA repair (Kurzbaue *et al.*, 2012). When both RAD51 and DMC1 are present, regulatory mechanisms are employed in order to suppress the function of RAD51, thereby promoting IH repair with the homologous chromosome, and the formation of COs (Uanschou *et al.*, 2013).

### 1.4.1.4 Pathways to meiotic CO formation

Regulatory mechanisms underpin both the frequency and distribution of CO formation during meiotic recombination, initiated with the decision of whether recombination intermediates should be resolved to give rise to a CO or to a NCO product. During meiosis, at least one meiotic CO is required per homologous chromosome pair in order to assure proper chromosome segregation and successful meiotic progression, known as the 'obligate' CO (Martini *et al.*,

2006). Despite the IH bias of DSB repair apparent during meiotic recombination, in addition to CO assurance leading to obligate crossover formation, a large proportion of the IH invasion molecules result in a NCO event, with only a subset maturing into CO products (Martini *et al.*, 2006; Osman *et al.*, 2011). The decision of whether a recombination molecule, and even an individual DSB, is going to form a NCO or CO product, is thought to be made early on during prophase I of meiosis (Allers and Lichten, 2001).

In the majority of eukaryotes, two alternative pathways co-exist that lead to the formation of COs (Figure 1.4). The first pathway is the major pathway, and leads exclusively to the formation of class I COs, mediated by a series of recombination proteins, referred to collectively as ZMMs (the zipper proteins: Zip1, Zip2, Zip3 and Zip4, Mer3 (Meiotic Recombination 3) and the MutS homologues: Msh4 and Msh5) (Börner *et al.*, 2004). Furthermore, despite the class I CO pathway also being termed the ZMM pathway, two additional conserved proteins, Mlh1 and Mlh3, have functional roles within the pathway. Msh4 and Msh5 act as a dimer and promote CO formation by binding and stabilising single-end invasion molecules, via a sliding clamp mechanism (Nishant *et al.*, 2010; Snowden *et al.*, 2004). In doing this, the conversion of recombination intermediates into dHJs, and subsequent resolution of these by nucleases giving rise to COs, is promoted. In yeast, no apparent dHJs or COs were observed in cells lacking Msh5, providing evidence for the fundamental role in CO formation for this protein (Nishant *et al.*, 2010). The ZMM proteins within the class I pathway are therefore thought to promote CO formation, by protecting joint molecule recombination intermediates (Börner *et al.*, 2004). In Arabidopsis, the class I pathway is the major pathway, accounting for approximately 85 - 90 % of total CO events, despite class I COs being subject to CO interference which influences CO distribution (Osman *et al.*, 2011). Functional homologues of the ZMM proteins in Arabidopsis include AtHEI10, AtSHOC1, AtZIP4, AtMSH4/5, AtMER3, AtPTD, and AtMLH1/3; mutants of which all show reduced CO formation, although not completely eliminated, even in combination mutants where more than one protein is knocked out (reviewed in Mercier *et al.*, 2015). This observed residual CO number is due to the class II CO pathway, accounting for 5 - 10 % of COs in *A. thaliana*. Independent of the ZMM proteins, this pathway is not subjected to CO interference, resulting in an uneven distribution of COs along the chromosome arms, and requires the activity of structure-specific endonucleases, including MUS81 (methyl methanesulfonate and ultraviolet-sensitive gene clone 81) (Berchowitz *et al.*, 2007; Higgins *et al.*, 2008), or FANCD2 (Fanconi anemia D2) (Kurzbaue *et al.*, 2018).

Nevertheless, despite both class I and class II CO pathways acting to promote CO formation, the majority of meiotic DSBs are actually repaired to form NCO products, with multiple factors

having been identified that actively limit CO formation (Mercier *et al.*, 2015). One such anti-CO factor identified in *Arabidopsis* is the FANCM helicase, acting via the synthesis-dependent strand annealing (SDSA) pathway of meiotic recombination (see Figure 1.4), in conjunction with the two co-factors MHF1 and MHF2 (Crismani *et al.*, 2012; Girard *et al.*, 2014; Li *et al.*, 2021). In this anti-CO pathway, NCO products are generated with the single-end invasion intermediate molecule being repaired by annealing to the other end of the DSB of the same DNA molecule (Crismani *et al.*, 2012). An alternative anti-CO pathway leading to NCO products in plants, involves the unfoldase FIGL1 (Girard *et al.*, 2015), and its partner FLIP (Fernandes *et al.*, 2018a). AtFIGL1 acts to limit CO formation by interacting directly with RAD51 and DMC1, regulating their dynamics and thus limiting single-end invasion, and subsequent CO number (Fernandes *et al.*, 2018a; Girard *et al.*, 2015). Moreover, additional anti-CO pathways acting to limit CO formation in *A. thaliana* involve the RTR complex partners, AtTOP3 $\alpha$ , AtRMI1 and AtRECQ4A (Séguéla-Arnaud *et al.*, 2015).

#### 1.4.2 Roles of the RTR complex partners in meiosis

The RTR complex during meiotic recombination, analogous to its role in somatic DNA repair, acts to generate NCO products, via the dissolution pathway, with the unwinding of D-loop structures (Figure 1.4) (Knoll *et al.*, 2014). Besides acting as part of the RTR complex during the dissolution pathway, the RECQ4A helicase was found to exhibit anti-CO roles in plants, in conjunction with its paralogue RECQ4B, with double mutants in *Arabidopsis* showing a six-fold increase in CO frequency, compared to that of wild-type plants (Séguéla-Arnaud *et al.*, 2015). RECQ4A and RECQ4B are thought to limit CO formation, by directing recombination intermediates towards the SDSA pathway instead, leading to the formation of NCO products (Séguéla-Arnaud *et al.*, 2015; Serra *et al.*, 2018).

Surprisingly, TOP3 $\alpha$  and RMI1, were both found to be indispensable for proper meiotic progression in plants, a dual role for both RTR complex partners in which is not common throughout all eukaryotic organisms. Acting as a sub-complex, AtTOP3 $\alpha$  and AtRMI1, were found to be essential for meiosis, with mutants showing severe meiotic defects and sterility (Chelysheva *et al.*, 2008; Dorn *et al.*, 2018; Hartung *et al.*, 2008; Séguéla-Arnaud *et al.*, 2017). Similar mutant phenotypes have only been described for *S. cerevisiae* and *C. elegans* (Gangloff *et al.*, 1999; Goodwin *et al.*, 1999; Wicky Collaud *et al.*, 2004), owing to the intriguing aspect of these findings as being previously unforeseen in plants. *Arabidopsis* mutant lines of both TOP3 $\alpha$  and RMI1 displayed detrimental meiotic defects, with homologous chromosomes remaining connected during metaphase I, by links that are independent of ZMM proteins but

dependant on SPO11, resulting in extensive chromosome fragmentation and chromatin bridges during anaphase I. The result of such catastrophic defects is ultimately meiotic arrest prior to the onset of meiosis II. The extent of the meiotic damage observed for both *Attop3α* and *Atrmil* mutant lines is postulated to be due to the build-up of unresolved recombination intermediates, in which require single-strand topoisomerase activity for resolution as a NCO product. Therefore, the TOP3α-RMI1 sub-complex is speculated to be necessary for the resolution of these recombination intermediates, as part of an essential role in ensuring proper entanglement and segregation of chromosomes during meiotic recombination (Chelysheva *et al.*, 2008; Dorn *et al.*, 2018; Hartung *et al.*, 2008). Furthermore, this sub-complex was also found to act in an anti-CO manner in Arabidopsis, suppressing the formation of COs during meiosis (Séguéla-Arnaud *et al.*, 2017).

### **1.5 From Arabidopsis to crops**

Much of the current understanding of the molecular mechanisms underpinning both DNA repair and meiosis in plants have been deciphered since the late 1990s utilising *Arabidopsis thaliana* as a model species (Hays, 2002; Mercier *et al.*, 2015). *A. thaliana*, a member of the *Brassicaceae* plant family, emerged as a model plant species over 25 years ago owing to its numerous beneficial characteristics including its small size, relatively short life cycle and the vast array of genomic resources available (Provart *et al.*, 2016). With the sequencing of its genome (The Arabidopsis Genome Initiative, 2000), in conjunction with its amenability to both cytogenetic analyses and transformation methods, *Arabidopsis thaliana* enabled plant biologists to combine cytogenetic, genetic and molecular approaches, proving invaluable in understanding the molecular mechanisms of many biological processes in plants. Since its emergence as the model plant species, Arabidopsis has been the fundamental feature for most plant studies, allowing for the formulation of an abundant collection of mutant lines, extensive bioinformatics resources, and much of our current understanding within plant biology (Hays, 2002; Provart *et al.*, 2016). Up until recently, *A. thaliana* was the species of choice for plant biologists and considered the “gold standard”, with much of the insights obtained through studies with this dicotyledonous plant species seen as the ground truth and therefore representative of all plant species. However, more recently, an increasing number of studies have been conducted using *Oryza sativa*, considered an alternative model plant species representative of monocotyledonous plants and cereals (Goff *et al.*, 2002). Such analyses in rice have allowed for the characterisation of DNA repair mechanisms and meiotic pathways in other plant species, besides Arabidopsis.

Over recent years, studies predominantly conducted in Arabidopsis and now in rice, have led to the current extensive knowledge of plant molecular mechanisms, including DNA repair and meiosis. Nevertheless, analyses in rice have not only increased our insights but also highlighted the extent of the gaps in our knowledge when it comes to understanding such mechanisms in plants other than Arabidopsis, such as non-model and crop plants. Through translational studies, the factors involved and mechanisms employed in both DNA repair and meiosis have been shown to differ slightly in rice, compared to that already known for Arabidopsis (Manova and Gruszka, 2015; Mercier *et al.*, 2015). These differences highlight the need to utilise alternative plant species, whereby our knowledge is evidently far more limited.

The need for understanding DNA repair and meiotic mechanisms in crop plants is timelier than ever. With the exponentially increasing human population, in addition to the adverse effects associated with climate change, it is more important than ever to accelerate our current efforts towards ensuring food security.

In light of relieving agricultural constraints, the ability to generate improved and sustainable crop varieties, offering advantageous traits and enhanced productivity, is the basis behind the majority of studies conducted in plants, including those analysing DNA repair and meiosis. Increasing our understanding of DNA repair mechanisms in plants, and ultimately in crop species, is crucial in aiding with the development of mechanisms aimed at maintaining genome integrity in plants, despite the exogenous and endogenous factors constantly challenging genomic integrity. Moreover, insights into DNA repair, particularly homologous recombination, have been at the forefront of much of the recent advancements in genome modification and gene editing approaches, in which offer much potential in accelerating crop improvement approaches (Schmidt *et al.*, 2019; Zaidi *et al.*, 2019). Additionally, understanding meiosis and meiotic recombination in plants offers plant biologists the insights to generate strategies in order to potentially manipulate the process, in order to increase genetic variation available to plant breeders, as a way to develop improved crop varieties (Lambing and Heckmann, 2018). Therefore, it is evident that our current understanding of both DNA repair and meiotic recombination in plants needs to be translated from Arabidopsis to crops, in an attempt to increase our knowledge of the processes in plant species with more practical impact. The rapid and ongoing advancements in genome editing technology and the increasing analyses portraying the ease, accuracy and speed at which techniques such as CRISPR/Cas9 (Jinek *et al.*, 2012) can be applied to non-model crop plants, have provided the means to make such a translation from Arabidopsis to crops far less challenging than was previously conceived (Georges and Ray, 2017).

## 1.6 Tomato as a model crop plant

Tomato, otherwise known as *Solanum lycopersicum*, is an agronomically important crop plant, being one of the most cultivated fresh-market vegetable crops to date, with its nutrient dense fruit being a fundamental global food source. Belonging to the *Solanaceae* family, tomato is a member of the same family as some other economically important plants including tobacco, potato and pepper. With being the most extensively and intensively analysed member of the *Solanaceae* family, tomato has emerged as the model system representative of all other species (Barone *et al.*, 2008; Kimura and Sinha, 2008). The increasing use of tomato as a model system is mainly a result of characteristic features that make it amenable to all fundamental analyses including genetics, cytogenetics, proteomics and molecular studies. Tomato has a short generation time, in comparison to other Solanaceous family members and other crop plants, is diploid, has a vast array of genetic resources available, and can be genetically transformed easily compared to other crops. With the sequencing of the whole tomato genome being completed over a decade ago (Sato *et al.*, 2012), a substantial collection of bioinformatic resources have also been accumulated to date, in which act to increase the attractiveness of using *S. lycopersicum* as a model crop plant. With both current plant model systems, Arabidopsis and rice, not being fruit-bearing plants, this feature makes tomato an even more popular research material for plant studies, when looking into fruit-development processes and fruit-related research (Kimura and Sinha, 2008). Furthermore, the increasing use of tomato as an alternative model system for plant research led to the development of varieties and cultivars that aid with functional genomic approaches, and thus accelerate such research. One example of these varieties is Micro-Tom (Shikata and Ezura, 2016), a dwarf tomato cultivar that has been recognised as a model system for tomato research, resulting from its notable features that make it advantageous for genomic approaches, such as its small size, ability to grow under fluorescent lights at high density, short life cycle, and efficient transformation method. Furthermore, with such beneficial characteristics, comparable to those for Arabidopsis, a large collection of mutant lines has been generated, aiding with research capabilities of the cultivar. Micro-Tom is therefore an attractive model cultivar for tomato research, in which knowledge obtained via research can be translated to tomato, and moreover to other members of the *Solanaceae* plant family (Shikata and Ezura, 2016).

## 1.7 Aim and objectives

The RTR complex has been elucidated as indispensable for ensuring genomic stability in eukaryotic organisms, with complex partners having partly distinct roles within homologous recombination and DNA repair, related to their role in the dissolution of recombination intermediate structures. Studies in *Arabidopsis* revealed a surprising dual role for both TOP3 $\alpha$  and RMI1 in plants, with both factors harbouring functional roles in DNA repair and meiosis. This revelation was surprising as such a role in both meiosis and somatic DNA repair is not observed across all eukaryotes. Therefore, it is interesting to see whether these differences between the functions of the RTR complex are specific to plants, with such knowledge being beneficial for translational studies of crop plants.

This thesis aims to gain an understanding of DNA repair mechanisms and meiotic recombination in crops, using tomato as a model system. These two processes will be analysed particularly with respect to the involvement of the RTR complex partners, TOP3 $\alpha$  and RMI1, both of which were shown to harbour surprising dual somatic and meiotic roles in *Arabidopsis*. Subsequently, Cas9-mediated mutagenesis will be carried out to establish tomato mutant lines deficient in both TOP3 $\alpha$  and RMI1, and a multidisciplinary approach will be conducted to ascertain the meiotic and somatic phenotypes of the resultant mutant lines. A plethora of techniques will thus be utilised to decipher the individual roles that these RTR complex factors play in specific processes, such as crosslink repair, replication-dependent DNA repair and meiotic recombination, therefore providing insights into the DNA repair and meiotic mechanisms in tomato. Consequently, the functional roles of the RTR complex partners within tomato will be elucidated, increasing current understanding of somatic DNA repair and meiosis in crop plants. The model tomato cultivar Micro-Tom will be used throughout this thesis due to its small size and the vast array of functional genomic resources available.

## 2. Materials and Methods

### 2.1 Materials

#### 2.1.1 Chemicals

Unless stated otherwise, the chemicals used for the experimental procedures were of *p.a.* quality and obtained from AppliChem (Darmstadt), Duchefa Biochemie (Haarlem, The Netherlands), Fluka (Buchs), Carl Roth (Karlsruhe), Merck (Darmstadt), Serva Elektrophoresis (Heidelberg), Roche Diagnostics (Mannheim) and VWR International (Darmstadt).

- Acetosyringone (Sigma-Aldrich Chemie GmbH, Taufkirchen)
- Agarose SeaKem® LE Agarose (Lonza Group Ltd., Basel, Switzerland)
- Beef Extract (GERBU Biotechnik GmbH, Wieblingen)
- dNTP Mix (10 mM) (Thermo Fisher Scientific, Braunschweig)
- Evans blue (Alfa Aesar, VWR Internration, Darmstadt)
- GeneRuler™ 1 kb DNA Ladder (Thermo Fisher Scientific, Braunschweig)
- GeneRuler™ Low Range DNA Ladder (Thermo Fisher Scientific, Braunschweig)
- Indole-3-butyric acid (IBA) (Duchefa Biochemie, Haarlem, The Netherlands)
- Micro agar (Duchefa Biochemie, Haarlem, The Netherlands)
- Murashige & Skoog (Jones 256) ready-to-use medium including Nitsch vitamins (Duchefa Biochemie, Haarlem, The Netherlands)
- Murashige & Skoog (MS-B 222) ready-to-use medium including vitamins (Duchefa Biochemie, Haarlem, The Netherlands)
- Nitsch 224 (Duchefa Biochemie, Haarlem, The Netherlands)
- Plant agar (Duchefa Biochemie, Haarlem, The Netherlands)
- Vectashield antifade mounting medium with DAPI (4',6-diamidino-2-phenylindole) (Vector Laboratories, Burlingame, USA)
- VERTIMEC PRO (Syngenta Agro GmbH, Maintal, Hesse, Germany).
- Zeatin-riboside (Duchefa Biochemie, Haarlem, The Netherlands)
- Zeatin (Duchefa Biochemie, Haarlem, The Netherlands)

#### 2.1.2 Enzymes

##### Polymerases

- DreamTaq™ DNA polymerase (Thermo Fisher Scientific, Braunschweig)

### Restriction enzymes

- AflII, BbsI, NheI (New England Biolabs, Frankfurt am Main)
- HindIII (Thermo Fisher Scientific, Braunschweig)

### Additional enzymes

- Cellulase from *Trichoderma sp.* C1794 (Sigma-Aldrich, Munich)
- DNaseI, RNase free (Qiagen, Hilden)
- Gateway LR clonase II (Thermo Fisher Scientific, Braunschweig)
- KAPA HRM FAST master mix (Kapa Biosystems, Basel, Switzerland)
- Pectolyase from *Aspergillus japonicus* P5936 (Merck, Darmstadt)
- Proteinase K (Thermo Fisher Scientific, Braunschweig)
- T4 DNA-ligase (Thermo Fisher Scientific, Braunschweig)

### 2.1.3 Genotoxins and antibiotics

#### Genotoxins

- Camptothecin (CPT) (Merck, Darmstadt)
- *cis*-Platin (*cis*-diamminedichloroplatinum (II)) (Merck, Darmstadt)
- Methyl methanesulfonate (MMS) (Sigma-Aldrich, Munich)
- Mitomycin C (MMC) (Duchefa Biochemie, Haarlem, The Netherlands)

#### Antibiotics

An overview of the antibiotics used and their concentrations within media are shown in Table 2.1.

**Table 2.1. Overview of antibiotics**

Antibiotics used, the solvents used for dissolving and the concentrations of the stock solutions, and the final concentrations used in media for the cultivation of *E. coli*, *A. tumefaciens* and *S. lycopersicum*.

| Antibiotic | Solvent          | Stock solution | <i>E. coli</i> | <i>A. tumefaciens</i> | <i>S. lycopersicum</i> |
|------------|------------------|----------------|----------------|-----------------------|------------------------|
| Ampicillin | H <sub>2</sub> O | 100 mg/ml      | 100 mg/l       |                       |                        |
| Gentamycin | H <sub>2</sub> O | 100 mg/ml      |                |                       |                        |
| Kanamycin  | H <sub>2</sub> O | 100 mg/ml      |                | 20 mg/l               | 50 mg/l                |
| Rifampicin | DMSO             | 100 mg/ml      |                | 100 mg/l              |                        |

|  |                  |           |          |          |   |
|--|------------------|-----------|----------|----------|---|
| <b>Spectinomycin</b>   | H <sub>2</sub> O | 100 mg/ml | 100 mg/l | 100 mg/l |   |
| <b>Ticarcillin disodium</b>  | H <sub>2</sub> O | 100 mg/ml |          |          | * |
| <b>Timentin<br/>(ticarcillin disodium /<br/>cluvulanate potassium<br/>mixture)</b> | H <sub>2</sub> O | 100 mg/ml |          |          | * |

\* Concentration varies, see Section 2.1.6.

## 2.1.4 Instruments

### Balances

- OHAUS PA214 (OHAUS, Parsippany, USA)
- Precision balance 440-47 (Kern & Sohn, Balingen)
- Precision balance AB104-S (Mettler-Toledo, Gießen)

### Centrifuges

- Centrifuge types Z 216 M, Z 383 K, Z 233 MK-2, Z 233 M-2 (Hermle, Wehingen)
- CM-70 M.07 (neoLab Migge Laborbedarf, Heidelberg)
- MiniSpin® (Eppendorf, Hamburg)

### DNA gel imaging and documentation

- Gel iX Imager gel documentation system (Intas Scienc Imaging Instruments, GmbH, Göttingen)

### Heating blocks, shakers, stirrers and incubators

- Digital hotplate stirrer (Benchmark Scientific, Edison, USA)
- Drying cabinet types BE 400, UE 500 and UL 50 (Mettmert, Schwabach)
- Growth cabinet CU-36L/4 (Percival Scientific, Perry, USA)
- Incubation shaker 3032 (Gesellschaft für Labortechnik (GFL) GmbH, Burgwede)
- Magnetic stirrer Hei-Mix S (Heidolph Instruments, Schwabach)
- Magnetic stirrer IKAMAG REC-G (IKA-Werke GmbH & Co. KG, Staufen)
- Magnetic stirrer yellow MAG HS7 (IKA-Werke GmbH & Co. KG, Staufen)
- Revolver rotator model D-6050 (neoLab Migge GmbH, Heidelberg)
- Thermoblock TDB-120 (lab4you, Berlin)
- Thermomixers comfort, compact and C with 1.5 ml block (Eppendorf, Hamburg)

### Microscopes

- Binocular Stemi DV4 (Carl Zeiss, Jena)
- Binocular SZB300 (VWR International, Darmstadt)
- Confocal laser scanning microscope (LSM) 700 with Zeiss AxioCam HRm (Carl Zeiss, Jena), filter set 43 Cy 3 shift free, filter set 49 DAPI shift free, objective lens Plan-Apochromat 20x/0.8 M27, objective lens Pan-Apochromat 100x/1.4 Oil DIC M27
- Fluorescence binocular SZX-ILL-B2-220 with Camera ColourView II (Olympus, Tokyo, Japan)

### Sterile benches and safety cabinets

- 1300 Series Class II, Type A2 Biological Safety Cabinet (Thermo Fisher Scientific GmbH, Braunschweig)
- MaxiSafe 2020 1.5 Class II Biological Safety Cabinet (Thermo Fisher Scientific, Braunschweig)
- Safety cabinet NU-480-500E (NuAire, Plymouth, USA)
- Safety cabinet et130V (Ehret, Emmendingen)
- Sterile bench Type HF (BDK Luft- und Reinraumtechnik, Sonnenbühl-Genking)
- Sterile bench Uniflow UVU 700 (UniEquip, Planegg)
- Vertical flow sterile bench Type KVF (Weiss Pharmatechnik, Sonnenbühl-Genkingen)

### Thermal cyclers

- Labcycler 48 (SensoQuest, Göttingen)
- LightCycler 480 (Roche Diagnostics GmbH, Mannheim)
- MyCycler™ (Bio-Rad Laboratories, Munich)
- SimpliAmp (Thermo Fisher Scientific, Braunschweig)
- Tpersonal thermal cycler (Analytik Jena, Jena)
- T100 thermal cycler (Bio-Rad Laboratories, Munich)

### Additional instruments

- Autoclave model 3870 ELV-D (Tuttnauer Europe B.V., Breda, The Netherlands)
- Electroporation machine Gene Pulser II (Bio-Rad Laboratories, Munich)
- NanoDrop™ Lite spectrophotometer (Thermo Fisher Scientific, Braunschweig)
- TKA high purity water system (Thermo Fisher Scientific, Braunschweig)

- Ultrapure water unit PURELAB Classic (ELGA LabWater, Celle)
- Photometer Ultrospec 1000 (Amersham Pharmacie Biotech, München)

### 2.1.5 Kits and consumables

- ECO2Box/green filter (Duchefa Biochemie, Haarlem, The Netherlands)
- Electroporation cuvette 2 mm electrode distance (VWR International, Darmstadt)
- KAPA HRM FAST qPCR Mastermix (VWR International, Darmstadt)
- PCR-Cycle Pure Kit (VWR International, Darmstadt)
- peqGOLD Plasmid Miniprep Kit (VWR International, Darmstadt)
- qScript cDNA Synthesis Kit (VWR International, Darmstadt)
- RNeasy Plant Mini Kit (Qiagen, Hilden)
- TC-plates 100, standard (Sarstedt, Nümbrecht)

### 2.1.6 Media, buffers and solutions

All media used for experimental procedures was prepared using double deionized H<sub>2</sub>O. The pH of the media was adjusted to the required value and all media was sterilised via autoclaving at 121 °C for 20 min. Antibiotics, hormones and other heat-susceptible components were added under sterile conditions once the media had cooled to 50 °C.

#### Media for bacterial culture

- LB medium (Lysogeny Broth medium for *E. coli*): 10 g/l tryptone; 5 g/l yeast extract; 5 g/l NaCl; 17.5 g/l plant agar for solid medium
- YEB medium (Yeast Extract Broth medium for *A. tumefaciens*): 5 g/l beef extract; 5 g/l peptone; 1 g/l yeast extract; 5 g/l sucrose; 493 mg/l MgSO<sub>4</sub>; 12 g/l plant agar for solid medium

#### Media for *in vitro* cultivation and transformation of *S. lycopersicum* cv. Micro-Tom

- GM-Tom (Germination medium for Micro-Tom): 2.17 g/l Nitsch 224 (Nitsch including vitamins); 20 g/l sucrose; 9 g/l micro agar for solid medium; pH 5.8 with NaOH
- PIM (Pre-Inoculation Medium): 4.4 g/l MS-B 222 (MS including vitamins); 30 g/l sucrose; 9 g/l micro agar; pH 5.8 with NaOH; 1 ml/l acetosyringone (100 mM); sterile filter paper was placed on the surface of the medium and plates were kept in the dark
- Liquid Jones medium: 4.4 g/l Jones 256; 30 g/l sucrose; pH 5.2 or 5.8 with NaOH

- Sel.I (Selection I medium): 4.4 g/l Jones 256; 30 g/l sucrose; pH 5.8 with NaOH; 9 g/l micro agar; 4 ml/l ticarcillin disodium (100 mg/ml) or 2 ml/l timentin (100 mg/ml); 500 µl/l kanamycin (100 mg/ml); 1 ml/l zeatin (1 mg/ml)
- Sel.II (Selection II medium): 4.4 g/l Jones 256; 30 g/l sucrose; pH 5.8 with NaOH; 9 g/l micro agar; 2.5 ml/l ticarcillin disodium (100 mg/ml) or 2 ml/l timentin (100 mg/ml); 500 µl/l kanamycin (100 mg/ml); 500 µl/l zeatin (1 mg/ml); 500 µl/l zeatin riboside (1 mg/ml)
- Sel.III (Selection III medium): 4.4 g/l Jones 256; 30 g/l sucrose; pH 5.8 with NaOH; 9 g/l micro agar; 2.5 ml/l ticarcillin disodium (100 mg/ml) or 2 ml/l timentin (100 mg/ml); 500 µl/l kanamycin (100 mg/ml); 200 µl/l zeatin (1 mg/ml)
- RM (Root Medium): 2.2 g/l Nitsch 224 (Nitsch including vitamins); 20 g/l sucrose; pH 5.8 with NaOH; 9 g/l micro agar; 1.5 ml/l ticarcillin disodium (100 mg/ml) or 2 ml/l timentin (100 mg/ml); 500 µl/l kanamycin; 1 ml/l indole-3-butyric acid (IBA) (2 mg/ml)

#### **Buffers for DNA extraction from plant material**

- DNA extraction buffer: 0.2 M Tris-HCl (pH 9.0); 0.4 M LiCl; 25 mM EDTA; 1 % SDS
- TE buffer (Tris-EDTA buffer): 0.01 M Tris-HCl (pH 8.0); 1 mM EDTA

#### **Buffers and solutions for agarose gel electrophoresis**

- 6x loading buffer: 0.2 % Orange G; 0.05 % xylene cyanol; 10 % glycerol; 60 mM EDTA
- 20x SB buffer: 8 g/l NaOH; 47 g/l boric acid; pH 8.0
- 0.9 % SB agarose gel: 0.9 % agarose; 400 ml 1x SB buffer; 15 µl 1 % ethidium bromide
- 50x TAE buffer (Tris Acetate EDTA- buffer): 224 g/L Tris; 57.1 ml/l glacial acetic acid; 0.5 M EDTA; pH 8.0
- 0.9 % TAE agarose gel: 0.9 % agarose; 400 ml 1x TAE buffer; 15 µl 1 % ethidium bromide

#### **Buffer and solutions for chromatin preparations**

- 0.01 M citrate buffer: 4.45 ml 0.1 M sodium citrate; 5.55 ml 0.1 M citric acid; total volume of 100 ml with ddH<sub>2</sub>O; pH 4.5
- Fixing solution: 75 % absolute ethanol; 25 % glacial acetic acid
- Digestion solution: 1 % cellulase; 1 % pectolyase in 0.01 M citrate buffer; stored at -20 °C

### Buffer and solutions for FDA fertility analyses

- FDA stock solution: 2 mg/ml FDA in acetone
- FDA working solution: stock solution diluted to 100 µg/ml using 7 % sucrose in water (w/v) solution.

### 2.1.7 Organisms

#### *Agrobacterium tumefaciens*

For the stable transformation of *Solanum lycopersicum*, competent *Agrobacterium tumefaciens* cells of the strain GV3101::pMP90 (Koncz *et al.*, 1984) were used. This strain has chromosomally-encoded rifampicin resistance and the modified Ti plasmid pTiC58ΔT-DNA which contains a gentamycin resistance cassette.

#### *Escherichia coli*

Competent *E. coli* cells were used for transformation of plasmid DNA for propagation; strains used were either NEB5α (New England Biolabs, Frankfurt) or DB3.1 (Bernard and Couturier, 1992) when ccdB resistance was required.

#### *Solanum lycopersicum*

The *S. lycopersicum* cultivar Micro-Tom ecotype Wildtype –BDX (WT-BDX) (Rothan, C., INRA, France) was used for all experimental procedures.

### 2.1.8 Software and databases

- ApE – A plasmid Editor (M. Wayne Davis, Salt Lake City, USA)
- EMBL-EBI Clustal Omega (Sievers *et al.*, 2011)
- EMBL-EBI InterProScan 5 (Madeira *et al.*, 2019)
- EnsemblPlants (<https://plants.ensembl.org/>)
- Image J 1.48v (National Institutes of Health, USA)
- iTOL v5 (Letunic and Bork, 2019) (<https://itol.embl.de/>)
- LightCycler480 Gene Scanning Software 1.5.1 (Roche Diagnostics, Mannheim)
- LightCycler480 Software 1.5.1 (Roche Diagnostics, Mannheim)
- National Center for Biotechnology Information (NCBI) (<http://www.ncbi.nlm.nih.gov/>)
  - BLAST (Basic Local Alignment Search Tool) (<http://blast.ncbi.nlm.nih.gov/Blast.cgi>)

- Nucleotide BLAST  
([https://blast.ncbi.nlm.nih.gov/Blast.cgi?PAGE\\_TYPE=BlastSearch](https://blast.ncbi.nlm.nih.gov/Blast.cgi?PAGE_TYPE=BlastSearch))
- Primer BLAST (<https://www.ncbi.nlm.nih.gov/tools/primer-blast/>)
- Poly Peak Parser (Hill *et al.*, 2014)
- R studio (<https://www.rstudio.com/>)
- SmartRoot4.1 Plugin for Image J (Lobet *et al.*, 2011)
- Sol Genomics Network (<https://solgenomics.net/>)
- TAIR – The *Arabidopsis* Information Resource (<http://www.arabidopsis.org/>)
- ZEN black 2012, ZEN blue 2012 (Carl Zeiss, Jena)

All stated websites were last accessed on: 14.09.2022.

### 2.1.9 Oligonucleotides

The oligonucleotides used are listed as part of the supplemental data in the appendix in Section 7.1. The oligonucleotides were used for carrying out standard PCR and ordered desalted from Eurofins Genomics (Ebersberg).

### 2.1.10 Plasmids

#### **pEn-Chimera plasmid**

The pEn-Chimera plasmid pEn-Spy-Chimera (Fauser *et al.*, 2014) was used as entry vector for the gateway cloning to generate the CRISPR/Cas9 destination vector to be used for Cas9-mediated mutagenesis. The pEn-Chimera plasmid was linearised using BbsI and a DNA sequence termed the spacer sequence was incorporated into the plasmid. The pEn-Chimera plasmid has an ampicillin resistance cassette for bacterial selection following transformation in *E. coli*.

The following plasmids were generated via spacer sequence integration into pEn-Chimera:

- **pEn-Spy-Chimera-RMI1**
- **pEn-Spy-Chimera-TOP3 $\alpha$**

#### **pDe-CAS9 Plasmid**

The pDe-Cas9 plasmid was the destination vector used for the gateway cloning procedure to generate the final CRISPR/Cas9 vectors for induced mutagenesis within the target loci. This

vector contains a Cas9 expression cassette and enable the expression of the spacer sequence as part of the single guide RNA (sgRNA). The plasmid harbours a spectinomycin resistance cassette for selection in bacteria. The pDe-Spy-Cas9 plasmid (Fauser *et al.*, 2014) has a phosphinothricin (PPT) resistance cassette as a herbicide for plant selection use.

The following plasmids were generated following Gateway Cloning of the aforementioned pEn-Chimera plasmid into the pDe-Cas9 destination vector:

- **pDe-Spy-Cas9-RMI1**
- **pDe-Spy-Cas9- TOP3 $\alpha$**

## **2.2 Methods**

### **2.2.1 Molecular biology techniques**

#### **2.2.1.1 DNA extraction from plant material**

For the isolation of genomic DNA in a timely and efficient manner from plant material, the following protocol was carried out. Plant material, typically a small (~ 1 cm) portion of a leaf, was homogenised in a 1.5 ml tube with a micro pestle. 500  $\mu$ l DNA extraction buffer was added and the material was homogenised completely, briefly vortexed and centrifuged for 5 min at 12,000 rpm (revolutions per minute). For precipitation of the DNA, 400  $\mu$ l of the resultant supernatant was transferred to a new 1.5 ml tube containing 400  $\mu$ l isopropanol, mixed by inversion and left at room temperature for 2 min. The precipitated DNA was pelleted by centrifugation for 10 min at 14,000 rpm and the supernatant discarded. The DNA pellet was dried O/N at room temperature and re-suspended in 50 – 100  $\mu$ l TE buffer, dependent on the desired DNA concentration.

#### **2.2.1.2 RNA extraction from plant material**

For RNA isolation, 100 mg of plant material was harvested and placed in a 1.5 ml tube and immediately frozen using liquid nitrogen. The RNeasy Plant Mini Kit was subsequently used for RNA extraction according to the manufacturer's instructions.

#### **2.2.1.3 cDNA synthesis**

cDNA synthesis was carried out using 1  $\mu$ g extracted RNA from plant material. The qScript cDNA Synthesis Kit was used according to the manufacturer's guidelines. The synthesised

cDNA was diluted with 180 µl TE buffer. Analysis of the quality of the obtained cDNA was performed via PCR whereby primers for the tomato *Actin* (*Solyc03g078400.2.1*) were used to check for gDNA contamination. The primers were designed to amplify both gDNA and cDNA, thus providing a larger fragment of PCR product when the sample contained gDNA and was therefore comprised of introns. The primers used for the quality analysis of cDNA can be found in Table 7.1 (Supplementary data).

#### 2.2.1.4 PCR

The polymerase chain reaction (PCR) was performed for the amplification of nucleic acids. The reaction is comprised of three steps: denaturation, annealing and elongation. The total reaction volume was either 25 µl for PCR-based genotyping or 50 µl for colony PCR. Oligonucleotide design was completed using either NCBI primer blast (Ye *et al.*, 2012) or manually taking the following factors into consideration: primer length was between 18 and 24 nucleotide bases, G/C content was > 50 %, the melting temperature ( $T_m$ ) was 50 – 60 °C, the  $T_m$  for primer pairs was relatively similar and the primer pairs were not complementary to one another and the primers were not compatible with themselves. In order to calculate the  $T_m$  for oligonucleotide design, the following formula was used:

$$T_m [^{\circ}\text{C}] = 4 \times (\text{G} + \text{C}) + 2 \times (\text{A} + \text{T})$$

The elongation time used for reactions varied depending on the length of the PCR product being amplified and the capabilities of the polymerase used.

#### Colony PCR

During cloning procedures, colony PCRs were conducted to confirm the successful integration of the desired recombinant plasmid DNA into *E. coli* following transformation. Primers were designed to amplify a region spanning across the inserted fragment and vector backbone boundary, therefore producing a PCR product when the recombinant plasmid is present harbouring both vector and insert. A single transformed *E. coli* colony was used as template for the PCR reaction. Thus, once positive colonies have been identified, they can be used to set up liquid cultures for the subsequent isolation of the plasmid DNA or for storage as a glycerol stock.

### **Sequencing-based genotyping**

Mutant lines in which only had a small deletion or insertion, such as one or two nucleotides (nts), following Cas9-mediated mutagenesis, sequencing-based genotyping was performed. In this case, a PCR was carried out to amplify the genomic region harbouring the mutation. The resultant PCR product was subsequently purified using the PCR cycle Pure Kit according to the manufacturer's guidelines and the purified product was sequenced via Sanger sequencing. The sequence information and chromatograms obtained were used in order to determine whether the plant from which the gDNA was isolated from was WT, heterozygously mutated or homozygously mutated. The online tool Poly Peak Parser (Hill *et al.*, 2014) was used for analysis of chromatograms.

The primer combinations and sequences used are listed in Table 7.2 (Supplementary data).

### **High Resolution Melting Analysis**

High resolution melting (HRM) analyses were carried out in order to identify individual plants harbouring mutations following Cas9-mediated mutagenesis. Oligonucleotide primers were designed for this in which produced an amplicon of approximately 150 bp in length with the target cutting site for the Cas9 nuclease being amplified as well. Genomic DNA extracted from plants that had been subjected to Cas9-mediated mutagenesis, was used as the template for HRM analysis. The KAPA HRM FAST master mix was used according to the manufacturer's guidelines. The master mix contains a dye in which integrates into amplifying dsDNA. The generated amplicons are subsequently denatured during the high-resolution melting process. PCR products from potential mutant plants, in which harbour mutations, have differing melting properties to those generated from WT plants. Therefore, curves generated that differ to those of the known WT control templates, can be distinguished and thus considered as those from the gDNA of potential mutant plants that can be further analysed. The primers used for HRM analysis are listed in Table 7.3 (Supplementary data).

#### **2.2.1.5 Gateway Cloning**

Gateway cloning was carried out as part of the cloning of the CRISPR constructs to be used for Cas9-mediated mutagenesis. Gateway cloning was used for the integration of customised sgRNA expression cassettes into the Cas9 expression vectors in order to generate the plasmids to be used for plant transformation. Firstly, the sgRNA expression cassettes were customised by integration of protospacer sequences to target the Cas9 nuclease to the cutting site within the target loci. A 20 nt long sequence was identified within the target loci, which had a protospacer

adjacent motif (PAM) sequence at the 3' distal end. For cloning of *S. pyogenes* Cas9 expression constructs, this PAM was NGG. 20 nt long oligonucleotides were synthesised with a 5'-ATTG overhang in front of the protospacer sequence and a second with a 5' AAAC overhang prior to the reverse-complement of the protospacer sequence. These oligonucleotides were subsequently hybridized via denaturation at 95 °C for 5 min, and then annealed for 20 min at room temperature. The entry vector for gateway cloning, pEn-Spy-Chimera, in which had previously been linearized via BbsI digestion to create complementary sticky ends to the oligonucleotide overhangs, was used for ligation of the annealed oligonucleotides. Gateway cloning was carried out to integrate the DNA of the sgRNA cassette into the plant expression vector, pDe-Spy-Cas9. The gateway reaction was performed using the LR Clonase II mix according to the manufacturer's instructions. Oligonucleotides used for cloning of the CRISPR constructs are listed in Table 7.4 in the appendix.

#### **2.2.1.6 Restriction digest of plasmid DNA**

To determine whether integration of inserts into vector backbones was successful during cloning procedures, control restriction digests were performed. Plasmid DNA was linearised by digestion via restriction enzymes, and the resultant fragment sizes were analysed by DNA agarose gel electrophoresis. The restriction enzymes were used according to the manufacturer's instructions. Digestion was carried out at 37 °C for 1.5 h. The reaction was loaded onto a 0.9 % TAE agarose gel and the separated DNA fragments were visualised using a gel documentation system. The fragment sizes were compared to those expected as previously determined by *in silico* sequence analysis using the known restriction enzyme cutting sites within the desired recombinant plasmid DNA.

#### **2.2.1.7 Ligation**

For the ligation of DNA fragments into vector backbones with complementary sticky-ends, T4 DNA Ligase was used according to the manufacturer's guidelines.

#### **2.2.1.8 Sequencing**

DNA sequence analysis was carried out using Sanger sequencing performed by the company GATC Biotech (Konstanz). The obtained sequence data was subsequently analysed by the plasmid editor program ApE.

## 2.2.2 Microbiology techniques

### 2.2.2.1 Transformation and culture of *E. coli*

*E. coli* cells were made chemically competent via the calcium chloride method as per the protocol described by (Hanahan, 1983). The cells were stored at -80 °C and sufficiently thawed on ice for 10 - 30 min prior to transformation by the heat shock method (Hanahan, 1983). 200 ng of plasmid DNA or 2 – 5 µl of a ligation reaction was added to a 100 µl aliquot of thawed competent *E. coli* cells and incubated on ice for 20 min. Heat shock was performed at 42 °C for 90 s, with immediate transfer to ice for 2 min. 500 µl of preheated liquid LB medium was added to the cells which were then incubated for 1 h at 37 °C with shaking at 650 rpm, for cell recovery. 100 – 200 µl of the transformation mixture was then plated on solid LB medium with the antibiotic required for selection of transformed cells. The plates were incubated O/N at 37 °C.

For liquid culture of *E. coli* cells, 5 ml liquid LB medium with the desired antibiotic selection was inoculated with a single colony or directly from a glycerol stock and incubated at 37 °C O/N with shaking at 200 rpm. Glycerol stocks of cultures were prepared by gently mixing 700 µl of liquid culture with 300 µl sterile glycerol and freezing with liquid nitrogen for long-term storage at -80 °C.

### 2.2.2.2 Extraction and purification of plasmid DNA from *E. coli*

Plasmid DNA extraction was carried out using 4 ml of liquid culture using the peqGOLD Plasmid Miniprep Kit as specified by the manufacturer's guidelines. The isolated plasmid DNA was eluted using 50 µl ddH<sub>2</sub>O.

### 2.2.2.3 Transformation and culture of *A. tumefaciens*

Electrocompetent *Agrobacterium tumefaciens* cells of the strain GV3101::pMP90 were stored at -80 °C until needed. For transformation of plasmid DNA, a 50 µl aliquot of cells was thawed on ice for 20 min and gently mixed with 1 µl plasmid DNA. Following transfer to a cooled cuvette, electroporation was carried out with a Gene Pulser II at 2500 V, 25 µF and 200 Ω for 5 ms. The cell and plasmid DNA solution was added to 500 µl preheated YEB liquid medium and incubated at 28 °C for 1 h with shaking at 650 rpm. 100 µl of recovered cells were spread onto a YEB solid medium plate with the appropriate antibiotics for selection of transformed *Agrobacterium* with the plasmid. The plates were incubated at 28 °C for 48 h. Liquid cultures

of *Agrobacteria* were set up by inoculation of 5 ml liquid YEB medium with antibiotic selection, and incubation at 28 °C with shaking at 200 rpm until an optical density (OD) of 0.8 at 600 nm was obtained. Glycerol stocks were set up the same way as previously mentioned for *E. coli* in Section 2.2.2.1.

### 2.2.3 Plant biology techniques

#### 2.2.3.1 Cultivation and growth of *S. lycopersicum* cv. Micro-Tom

*Solanum lycopersicum* cultivar Micro-Tom plants were grown in the greenhouse on substrate containing 1:1 mixture of Floraton 3 (Floragard, Oldenburg, Germany) and vermiculite (2 - 3 mm, Deutsche Vermiculite Dämmstoff, Sprockhövel, Germany), with alternating 16 h light and 8 h darkness, at 24 °C during the day and 20 °C at night. For *in vitro* cultivation, plants were grown in a growth room under axenic conditions in an ECO2BOX with green filter, containing GM-Tom. Plants were subjected to 14 h light and 10 h darkness and a temperature of 24 °C.

#### Seed collection and storage

Harvested fruits were opened and the flesh and seeds were extracted. Seeds were obtained via collection in a sieve with 1 mm openings and washed several times to remove pulp. The washed seeds were then spread out on a flat surface and dried for a minimum of 24 h at room temperature. Dried seeds were stored in a cool, dry and dark place in a paper envelope.

#### 2.2.3.2 Sterilisation and sowing of Micro-Tom seeds

For *in vitro* cultivation of Micro-Tom plants, seeds were surface sterilised prior to sowing. Dry seeds were placed into a 50 ml falcon tube and filled up with 70 % ethanol. The tube was then slowly inverted on a rotator for 3 min. The ethanol was discarded, including any seeds that had floated to the surface, which were deemed inviable. 50 ml 3 % sodium hypochlorite with 0.1 % Tween-20 (Polysorbate-20) was added to the seeds and the falcon was rotated for 14 min. The sterilised seeds were then transferred to a sterile sieve with 1 mm openings and washed with 2.5 l (5 x 500 ml bottles) sterile ddH<sub>2</sub>O. The seeds were then transferred from the sieve to a sterile glass petri dish and a small amount of sterile ddH<sub>2</sub>O was added. The seeds were then left at room temperature in the ddH<sub>2</sub>O for 2 h for synchronisation of germination.

Following the 2 h incubation, the sterile seeds were gently transferred to solid GM-Tom media within an ECO2BOX with green filter, using sterile forceps.

### 2.2.3.3 *Agrobacterium*-mediated transformation of Micro-Tom

For stable transformation, Micro-Tom cotyledons were transformed using the *Agrobacterium* strain GV3101, as described in Meissner *et al.*, (1997), with the same modifications as discussed in (Dahan-Meir *et al.*, 2018). The following was all conducted under sterile conditions. 7-10 days after sowing, just as the first leaf is just starting to appear, Micro-Tom plantlets were removed from the media and placed into a large sterile glass petri dish containing Liquid Jones media at pH 5.8. Using a sterile blade, both cotyledons from each plantlet were cut at each distal end and placed on the filter paper covered PIM with the abaxial side facing upwards. The PIM plates were wrapped in aluminium foil for dark conditions and kept at room temperature for 2 days.

For transfection, GV3101 *Agrobacterium* liquid cultures were set up with the *Agrobacterium* harbouring the desired construct for transformation. 50 ml YEB liquid medium, with the appropriate selection antibiotics, was added to a sterile 100 ml conical flask. The medium was inoculated with the *Agrobacterium* using thawed glycerol stock. The liquid culture was then incubated at 28 °C with 200 rpm until an OD<sub>600</sub> of 0.8 was obtained. The culture was then transferred to sterile 50 ml falcon tubes and centrifuged for 10 min at 6,000 rpm and 4 °C. The pellet was then re-suspended in Liquid Jones media with pH 5.2 to obtain a final OD<sub>600</sub> of 0.4. 100mM acetosyringone was added to a final concentration of 100 µM.

The cut cotyledons that had been incubated in the dark on PIM for 2 nights, were added to the *Agrobacterium* suspension medium and inverted on a falcon rotator slowly for 20 min. The cotyledons were then transferred to sterile filter paper to absorb any excess liquid and then placed on filter paper on the surface of PIM, abaxial side upwards and flat. The plates were sealed with parafilm and kept in the dark for 2 days at room temperature.

The cotyledons were then transferred to Sel.I plates, abaxial side facing down with the surface and cut ends in direct contact with the medium. The plates were then sealed with parafilm and placed at low light (~ 10 PPF (photosynthetic photon flux)), within a growth room for 12 - 14 days. The cotyledons were then transferred to Sel.II plates, abaxial side in contact with the medium. The plates were sealed with parafilm and placed in normal light conditions within a growth room. After 14 days, calli were excised from the dying explants and transferred to new Sel.II plates. Throughout the regeneration process, dead tissue and brown callus was removed and the explants were transferred onto fresh Sel.II plates at least every two weeks. Shoots formed from calli were excised and placed onto Sel.III medium within taller plates (TC-plates). Regenerated shoots were transferred to fresh Sel.III medium every two weeks. Large shoots were transferred to RM within an ECO2BOX with green filter. Rooted regenerated

plants were transferred to soil and acclimatised to greenhouse conditions. Plants were kept in high humidity for 2 - 5 days using a plastic covering. Acclimatised regenerated plants were grown in the greenhouse until maturity.

#### **2.2.3.4 Cas9-mediated mutant line establishment**

In order to establish mutant lines, Cas9-mediated mutagenesis was carried out. The aim of this was to generate homozygous mutant lines harbouring frameshift mutations within the target loci and lines in which were transgene-free, whereby the CRISPR constructs have been segregated out via Mendelian segregation.

#### **Identification of individual mutant plants (T1-Generation)**

Following *Agrobacterium*-mediated transformation of Micro-Tom wild type (WT) cotyledon explants, the regenerated T0 plants transformed with the T-DNA were continuously selected for kanamycin resistance which was conferred by the resistance cassette within the integrated T-DNA (CRISPR/Cas9 constructs). Regenerated transgenic plantlets were propagated in the greenhouse to full maturity. Approximately 50 seeds obtained from each plant were surface-sterilised and sown onto GM-Tom. Individual mutant plants within these lines were identified following gDNA extraction from leaf material of the seedlings to be used for subsequent HRM analyses and Sanger sequencing. With HRM analyses, a potential mutant candidate was identified when a melting curve was generated that deviated from that of the wild-type curve. Sanger sequencing was then carried out to determine the type of the mutation on a sequence level. The zygosity of the mutation was also determined via analysis of the chromatogram data from the Sanger sequencing. Plants harbouring desirable frameshift mutations were further cultivated in the greenhouse to maturity.

#### **Identification of *single-locus* mutant lines (T2-Generation)**

Single-locus lines are those in which the T-DNA was integrated into the genome at only one location. Such lines segregate according to Mendelian segregation during meiosis meaning that a ratio of 1:2:1 is obtained of homozygous: heterozygous: wild type, respectively. Therefore, 25 % of the progeny of a segregating line would be wild type, whereby the T-DNA has segregated out (transgene-free). As a result, the progeny of T1 mutant plants (T2 generation) were propagated under axenic conditions and PCR genotype screening was performed to determine the presence or absence of the T-DNA for approximately 50 of the plants within each line. Two PCRs were used, one to amplify a portion of the kanamycin resistance cassette and a

second to amplify a fragment of the respective Cas9 used. A plant line was confirmed as single locus when 75 % of the screened plants contained the T-DNA and therefore produced a PCR product for both PCRs, and 25 % did not. This was confirmed statistically using the  $\chi^2$  test. Plants of single locus lines were further analysed to determine the zygosity of the previously identified Cas9-induced mutation, via HRM analysis and subsequent Sanger sequencing. In the case of large insertions or deletions, a PCR-based genotyping screen was carried out as previously discussed in Section 2.2.1.4. Heterozygous and homozygous mutant plants of single locus lines were then further propagated, self-pollinated and grown to maturity. According to Mendelian segregation, 25 % of the progeny of a self-pollinated heterozygous mutant plant will be homozygous for the mutation.

### **Identification of transgene-free homozygous mutant lines (T3-Generation)**

Seeds obtained from the T2 generation were sown onto GM-Medium. DNA was extracted from the leaves of a sample of seedlings, as previously carried out for the T2 generation, whereby PCRs were conducted to determine whether the line was transgene-free or not. Lines were deemed transgene-free when a PCR product for the Cas9 or kanamycin resistance cassette was not obtained for any of the analysed plants. Lines in which were still found to carry the transgene in a segregating manner, were further propagated in the greenhouse to obtain the T4 generation. The extracted DNA from T3 generation plants was also used in order to determine the homozygous individual mutant plants from previously identified heterozygous mutant lines. Transgene-free mutant plants were desired for phenotypical analysis, therefore identified homozygous plants from transgene-free lines were also further propagated via selfing, until a sufficient number of seeds could be obtained. Lines of further generations were always analysed and screened using the techniques previously mentioned, in order to confirm mutations prior to use in experimental analyses.

### **2.2.3.5 Chromosome spreading and visualisation of male meiocytes**

For chromosome structural and behavioural analysis during meiosis, chromatin preparations of male meiocytes were carried out based on the technique described by (Armstrong *et al.*, 2009), with minor modifications. Primary inflorescences from plants of approximately 6 weeks old were excised and fixed in freshly prepared fixative solution, and kept on ice. The fixative solution was changed following 2 - 3 hours of incubation on ice or at 4 °C. The inflorescences were transferred to fresh fixing solution until the plant material was completely white and the solution was no longer green in colour. Fixed material was stored for a maximum of 6 months

at -20 ° C. For chromatin preparations, inflorescences were transferred to a black watch glass containing fresh fixative solution. Individual buds were excised using watchmaker's forceps and a mounted needle, ensuring they remain in the fixative solution at all times. Buds between 2 - 3 mm in length were used. The selected buds were washed twice with -0.01 M citrate buffer and incubated in a humidified atmosphere at 37 °C for 4 hours immersed in 1 ml digestion solution (333 µl stock digestion solution completed with 667 µl 0.01 M citrate buffer). Following this, the digestion was stopped by removal of the digestion solution and immersion of the buds in ice cold ddH<sub>2</sub>O. The sepals were carefully removed from the buds using a dissecting microscope and the buds were arranged according to size. For the preparation of microscope slides, one bud was carefully transferred to a slide with a small volume of ddH<sub>2</sub>O. Using a mounted needle, the bud was macerated until completely homogenised. This was carried out quickly in order to avoid the bud from drying out. 7 µl of 60 % acetic acid was added to the homogenate and mixed, ensuring the material did not exceed an area greater than that of a cover slip. The slide was placed on a hot block at 45 °C for 30 s. The material was then washed using 1 ml of fixative solution, whereby the solution was dispensed around the perimeter of the visible circle. The slide was then held down and an additional 1 ml of fixative solution was rinsed across the surface of the slide. A commercial hair dryer was then used to dry the slide by directing the heat to the rear of the slide. 12 µl of DAPI was added to the centre of the fixed material on the slide, in order to stain the chromatin. A cover slip was then carefully placed on top and the prepared slides were stored at 4 ° C in the dark for a minimum of 12 h. Fluorescence microscopy using the LSM 700 microscope was then performed to visualise and analyse the DAPI-stained chromatin.

### **2.2.3.6 Root length analysis**

For measurement of root lengths, Micro-Tom seeds were sterilised and sown onto GM-Tom. Following 12 days in the growth chamber, the plantlets were gently placed onto a black piece of card. The plants were flattened by gentle pressure using a clear plastic tray, ensuring that the roots remained relatively straight. Photographs were taken and analysed using the SmartRoot Plug-in of ImageJ (Lobet *et al.*, 2011) to determine root length. Five roots were analysed for each biological replicate, of which three were performed for each line to be analysed for comparison.

### 2.2.3.7 Cell viability quantification

The viability of cells was determined and quantified by the use of the Evan's Blue staining procedure as described by (NV *et al.*, 2017). This procedure was carried out within the roots of Micro-Tom plants. Seeds were surface sterilised and sown onto GM-Tom and grown under sterile conditions. Following 9 days of maturation, the plantlets were carefully removed from the medium and 1 cm of the root, including the tips, were gently excised and transferred to a tube. This was carried out with the roots of five plants, for each independent line, for one biological replicate. 0.25 % solution of Evan's Blue was added to the tube with the excised roots, and incubated at room temperature for a period of 20 minutes with continual shaking at 300 rpm. The stained roots were then washed three times using distilled water and a micro-pestle was used to homogenise the material completely in 1 ml 1 % sodium dodecyl sulphate (SDS). The tubes were then centrifuged at 12,000 g for 5 minutes and the resultant supernatant was transferred to a new tube. The optical density (OD) of the supernatant was then measured using a spectrometer, at 600 nm. A calibration curve was generated whereby the OD of solutions containing various known concentrations of Evan's blue were measured. The absorbance values obtained from the supernatant solutions were then used to determine the concentration of Evan's blue, using the calibration curve. The concentration of Evan's blue within the solutions indicated the amount in which had previously been taken up by the roots during the staining procedure. The amount of Evan's blue taken up by the root cells was an indication of the amount of non-viable cells within the roots, as the dye is able to penetrate the damaged cell membranes. The standard curve was generated by measuring the absorbance at 600 nm of various different concentrations of Evan's blue solutions, ranging from 1 – 30 µg/ml.

### 2.2.3.8 Sensitivity assays

As a means to investigate the potential functions of proteins within somatic DNA repair, sensitivity assays were carried out similarly to the methods described by (Hartung *et al.*, 2007a), with a few modifications for tomato. These were performed with the mutant lines lacking the proteins to be analysed in comparison to WT plants. The growth of seedlings following treatment with genotoxins was analysed via measurement of the fresh and dry weight. The seeds of the lines were surface-sterilised and sown onto GM-Tom solid medium. The plants were grown for 9 days under sterile conditions, in the growth room. Five plantlets were transferred into one well of a 6-well plate containing 4 ml liquid GM. Following one day of growth in a CU-36L4 growth cabinet, with 16 h light at 22 °C and 8 h dark at 20 °C, 1 ml of genotoxin solution was added to each well to achieve the necessary concentration within the total volume

of solution. Each 6-well plate (one for each line) had two wells whereby 1 ml of liquid GM was added, as opposed to genotoxin solution. These wells were the untreated controls, used as references for the normal growth of each line. After six days of further growth in the growth cabinet, the fresh weight of the plants in each well was measured. The mean fresh weight of the plants within the two untreated control wells was used to calculate the relative fresh weight for each plant line after genotoxin treatment. The genotoxins and concentrations used are shown in Table 2.2.

**Table 2.2. Overview of the concentrations of the genotoxin solutions used in the sensitivity assays.**

The genotoxins and concentrations of the stock solutions and the final concentrations used, and the units are listed.

| Genotoxin          | Stock solution | Final concentrations |     |     |     | Unit       |
|--------------------|----------------|----------------------|-----|-----|-----|------------|
| CPT                | 10 $\mu$ M     | 50                   | 100 | 150 | 300 | nM         |
| <i>cis</i> -Platin | 1 mM           | 1.5                  | 2.5 | 5   | 10  | $\mu$ M    |
| MMC                | 1 mg/ml        | 10                   | 20  | 30  | 35  | $\mu$ g/ml |
| MMS                | 10 %           | 25                   | 40  | 60  | 100 | PPM        |

### 2.2.3.9 Fertility analysis

Fertility analysis of plants was via quantification of seeds per ripe fruit, whereby fully ripe fruits from plants of the same age for each line, were harvested and the visible seeds were counted. Five plants per line were analysed, and 10 fruits per plant were used for seed quantification. The number of fruits per plant was also measured as an indication of fertility. The number of fully ripe (dark red) fruits were counted from five plants for each line of the same age. Additionally, fruit diameter was taken into consideration. Hereby, fully ripe fruits were measured along their diameter using a standard ruler. A plastic tray was placed at 0 on the ruler and the fruits were placed between this and a second plastic tray for measurement.

### 2.2.3.10 Pollen viability analysis

The viability of pollen was ascertained via the Fluorescein diacetate (FDA) staining method as described by (Heslop-Harrison and Heslop-Harrison, 1970). 350 ml of working FDA staining solution was then transferred to a tube and mature flower buds were added. The tube was then vortexed for 5 min. Following this, the flowers were removed using forceps, and the solution was centrifuged for 5 min at 9,000 rpm. The resultant pellet of stained pollen was then washed with 7 % sucrose in distilled water and a drop of this was added to a microscope slide. The slide

was kept in the dark for 10 min and then the stained pollen was visualised using a fluorescence binocular microscope.

### 3. Results

#### 3.1 Characterisation of TOP3 $\alpha$ and RMI1 tomato homologues

For this work, the homologous RTR complex partner proteins TOP3 $\alpha$  and RMI1 from *Solanum lycopersicum* cv. Micro-Tom were functionally characterised for the first time. Due to both of these proteins harbouring surprising dual roles in both meiosis and DNA repair in *Arabidopsis thaliana*, the tomato homologues were analysed in order to elucidate whether this is also the case in other dicotyledonous plant species. A multidisciplinary approach involving a number of analytical techniques was conducted utilising single mutant lines generated that were deficient in each of the RTR complex partners, TOP3 $\alpha$  and RMI1, to investigate meiotic recombination and DNA repair. The dwarf tomato cultivar was used throughout as a model tomato system due to its numerous advantageous characteristics such as small size, short regeneration time and relative amenability for transformation.

#### 3.2 Identification of the RMI1 tomato homologue

In order to generate a tomato mutant of the RTR complex partner, RMI1, the homologous factor had to first be identified. To do this, the sequence data of the corresponding factor from *A. thaliana* was utilised. Firstly, the Arabidopsis gene homologue *AtRMII* (AT5G63540) was used. Therefore, the genomic sequence data was obtained using TAIR. The nucleotide sequence of *AtRMII* then served as the input for a query search to obtain potential homologues within the *S. lycopersicum* genome using NCBI BLAST and EnsemblPlants. Based on sequence similarity, the gene *Solyc12g005900.2* (locus identifier within the current Tomato Genome version SL4.0 available from The Sol Genomics Network (SGN)) was identified as a potential homologue of *RMII* in tomato, with 49.26 % sequence identity to *AtRMII*. The gene *Solyc12g005900.2*, herein referred to as *SIRMII*, is located on chromosome 12, is 2389 bp in length, and comprises eight exons (Figure 3.1). EMBL-EBI InterProScan 5 was used to analyse the domain structure of the protein which is encoded for by *SIRMII*. The protein, which is 659 aa in length, was found to harbour both the DUF1767 functional domain and the OB-fold domain 1, which were both found to be important domains for the functional roles of RMI1 in Arabidopsis and other eukaryotic organisms. In addition to this, *SIRMII* also has the lysine that is conserved in both Arabidopsis and human RMI1 orthologues (Figure 3.1). Furthermore, the presence of *RMII2* was also confirmed within tomato, with the gene *Solyc11g066690.2* on chromosome 11 being identified as the homologue of *AtRMII2* (*At1g08390*), with the homologous protein's amino acid sequence being 56 % identical to that of *AtRMII2*.

### 3.2.1 Cas9-mediated mutagenesis of *SIRMI1*

For the characterisation of *RMI1* in tomato, mutants were established. This was performed using targeted mutagenesis via the CRISPR/Cas9 system in Micro-Tom. With this system, the Cas9 nuclease is used to introduce a DSB within a specified target locus of the genome. From studies previously carried out in *Arabidopsis*, the error-prone pathway of NHEJ is known to be responsible for the repair of the majority of DSBs. Repair via the NHEJ pathway incorporates mutations such as insertions and deletions, in which can ultimately lead to a frameshift within the coding region of a gene (see Section 1.2.2).

To generate the *RMI1* mutant lines that were characterised in this study, Cas9-mediated mutagenesis using the Cas9 orthologue from *S. pyogenes* (Fauser *et al.*, 2014) was used. Therefore, the expression vector pDe-Spy-Cas9 was used. However, the resistance cassette was exchanged from PPT to kanamycin to aid transgenic selection during the transformation and regeneration procedure. A target sequence within the first exon of *SIRMI1* (*SIRMI1* Protospacer 5'-TTCGGATTGTGGTATTGGTC-3'), was identified, and the spacer sequence corresponding to this was cloned into the pDe-Spy-Cas9 destination vector via gateway cloning (see Section 2.2.1.5). This spacer sequence enables targeting and binding of the Cas9 nuclease to the predetermined loci. The loci in exon 1 being within the coding region for the DUF1767 domain of the protein (Figure 3.1). The final CRISPR/Cas9 expression construct was integrated into the genome of wild-type Micro-Tom tomato plants via *Agrobacterium tumefaciens*-mediated transformation, using the cotyledon leaf disc method. Following transformation, the transformed cotyledons, now known as explants, were selected for using kanamycin. Transgenic explants were resistant to kanamycin as a result of the resistance cassette within the CRISPR/Cas9 destination vector. This selection was consistently carried out through the regeneration tissue culture process whereby calli gave rise to shoots, in which eventually formed roots. Transgenic regenerated plantlets (T0 generation) with sufficient roots and shoot height were matured in soil in the greenhouse. The seeds harvested from these individual transgenic lines (T1 generation) were subsequently screened for potential induced mutations using HRM analysis, and single-locus lines were identified (see Section 2.2.1.4). The Cas9-mediated mutagenesis described above resulted in the successful induction of DSBs within the target loci for both expression vectors used, leading to induced mutations via NHEJ.

Consequently, the following two *SIRMI1* tomato mutant lines were generated: *slrmi1-1* and *slrmi1-2*. The precise mutations induced within the two aforementioned *rmi1* mutant lines were determined using Sanger sequencing. For *slrmi1-1*, the mutation was an insertion of one base

pair, resulting in a frameshift mutation and a subsequent premature stop codon, which leads to a truncated functionally redundant protein being encoded for. The second mutant line, *slrmi1-2*, was found to have a deletion of four base pairs, which also led to a frameshift, inducing a premature stop codon.

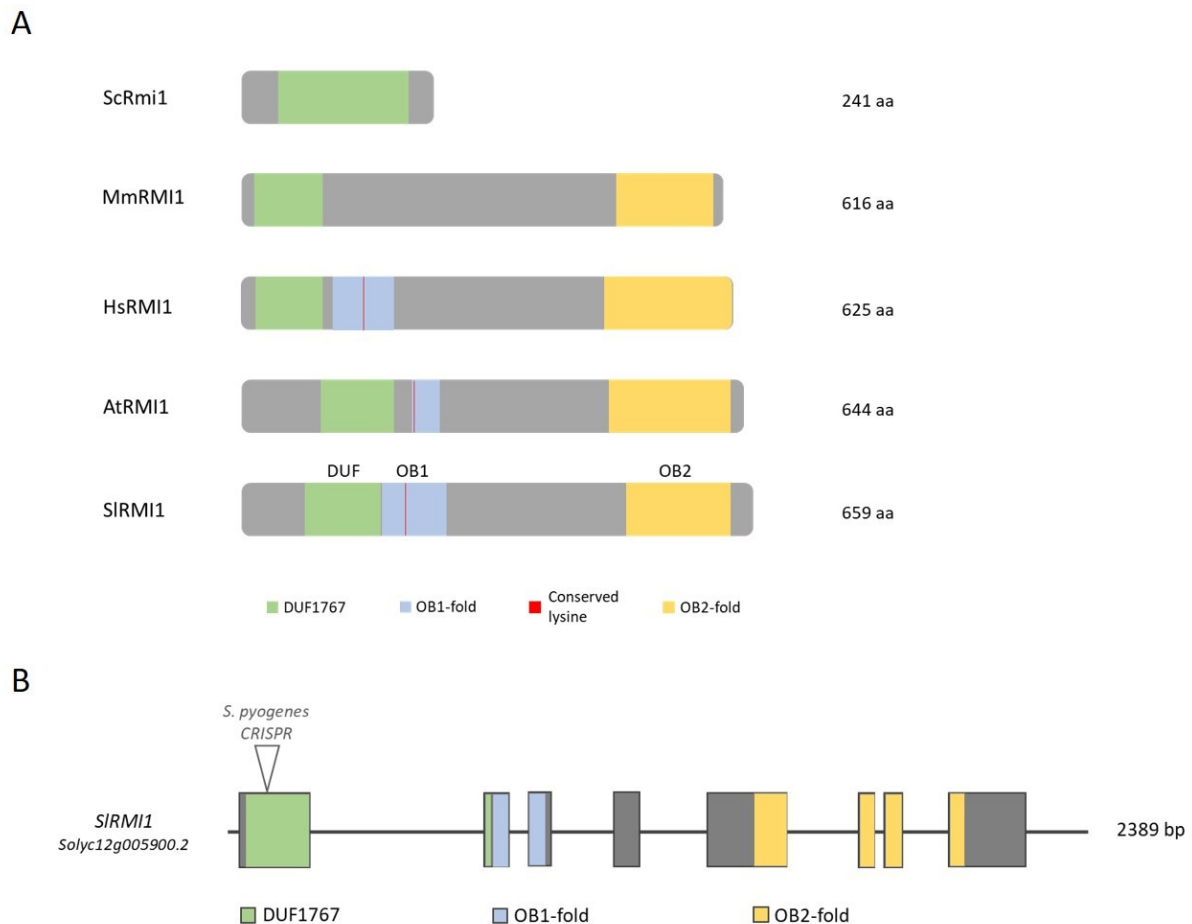


**Figure 3.1. SIRM1 protein domain structure and comparison, and *SIRM1* gene structure.**

Schematic diagram illustrating the protein domain structure of the tomato RMI1 orthologue with homologues from other eukaryotes and the gene structure of *SIRM1*.

- (A) Schematic diagram depicting the conserved protein domains in RMI1 orthologues from *Saccharomyces cerevisiae* (Sc, baker's yeast), *Mus musculus* (Mm, mouse), *Homo sapiens* (Hs, human), *Arabidopsis thaliana* (At, Arabidopsis) and the identified orthologue in *Solanum lycopersicum* (Sl, tomato). The tomato RMI1 protein is 659 amino acids (aa) in length and contains the three domains known to be important for the function of RMI1 in *A. thaliana* (Bonnet *et al.*, 2013): (DUF: aa 83–177; OB1: aa 175–260; OB2: aa 496–638). The red line indicates the conserved lysine that is a known essential aa for the interaction of RMI1 with TOP3 $\alpha$  (K220 in *S. lycopersicum*).
- (B) *SIRM1* gene structure indicating exons (boxes), domain structure within these and untranslated regions including introns as a line. *RMI1* gene in tomato is comprised of eight exons and is 2389 bp in length. The site within exon one is indicated by the arrow, where Cas9 was targeted to via the spacer sequence for induced mutagenesis.

For both of the generated mutant lines, the zygosity of the mutations was determined using both HRM analysis and Sanger sequencing, whereby it was shown that both harboured the mutations in a heterozygous manner. Thus, the lines had to be further propagated to obtain the next generation (T2), whereby homozygous mutant plants should be present according to Mendelian segregation. In addition to analysis of the zygosity of the mutations, the lines were also screened to determine the presence of the Cas9 expression cassette, which would also be segregating according to Mendel's laws of segregation in single-locus lines. The objective was to ultimately establish homozygous mutant lines in which were free of the Cas9 transgene. This was achieved for both of the *slrmi1* mutant lines. Each were further propagated until this was the case and until sufficient seeds for each of the lines had been harvested to enable analyses to be carried out for characterisation of RMI1 in tomato. The mutations for each of the mutant lines were also confirmed on an mRNA level. In doing this, the total RNA was extracted from each of the lines, converted to cDNA via reverse-transcription and the cDNA was amplified and sequenced using Sanger sequencing. From this, the mutations of both mutant lines were successfully confirmed within the cDNA and therefore on an mRNA level (Figure 3.2).

|               |   |     |
|---------------|---|-----|
| WT            | AAAACCAATAAAATTCCTAAATTCGCCGGCGAAGAAATGCGTAGACGGCGCCTGCAAC                          | 120 |
| <i>rmi1-1</i> | AAAACCAATAAAATTCCTAAATTCGCCGGCGAAGAAATGCGTAGACGGCGCCTGCAAC                          | 120 |
| <i>rmi1-2</i> | AAAACCAATAAAATTCCTAAATTCGCCGGCGAAGAAATGCGTAGACGGCGCCTGCAAC<br>*****                 | 120 |
| WT            | TCCGGTACTCTCCGACGAAGAAGAAGAAGATGAAACTGGAACAAGCGGAGTTGGTGATT                         | 180 |
| <i>rmi1-1</i> | TCCGGTACTCTCCGACGAAGAAGAAGAAGATGAAACTGGAACAAGCGGAGTTGGTGATT                         | 180 |
| <i>rmi1-2</i> | TCCGGTACTCTCCGACGAAGAAGAAGAAGATGAAACTGGAACAAGCGGAGTTGGTGATT<br>*****                | 180 |
| WT            | CTGTTCCAGAGCTTTGGTATTG-CCTTCATCTATAACAACCGGAAACCTCAGTATCGTCGAAT                     | 239 |
| <i>rmi1-1</i> | CTGTTCCAGAGCTTTGGTATTGCTTTCATCTATAACAACCGGAAACCTCAGTATCGTCGAAT                      | 240 |
| <i>rmi1-2</i> | CTGTTCCAGAGCTTTGG----GCTTCATCTATAACAACCGGAAACCTCAGTATCGTCGAAT<br>*****              | 235 |
| WT            | TCTAACCCCTAATCCCGGTGAGAGAATCGCTATATCGGAAGTTGAGATTATCGACGTTTTT                       | 299 |
| <i>rmi1-1</i> | TCTAACCCCTAATCCCGGTGAGAGAATCGCTATATCGGAAGTTGAGATTATCGACGTTTTT                       | 300 |
| <i>rmi1-2</i> | TCTAACCCCTAATCCCGGTGAGAGAATCGCTATATCGGAAGTTGAGATTATCGACGTTTTT<br>*****              | 295 |
| WT            | GGTAATCCCCAGCCTACACCGCCGGATTCTAGTATTCTACACCGTATCCGGTTTATCCG                         | 359 |
| <i>rmi1-1</i> | GGTAATCCCCAGCCTACACCGCCGGATTCTAGTATTCTACACCGTATCCGGTTTATCCG                         | 360 |
| <i>rmi1-2</i> | GGTAATCCCCAGCCTACACCGCCGGATTCTAGTATTCTACACCGTATCCGGTTTATCCG<br>*****                | 355 |
| WT            | TCCGAGTCAGTGAGCGGCAATGACTATGAATCGCCGATCAGTGAGGTTCTTTCTCGAATG                        | 419 |
| <i>rmi1-1</i> | TCCGAGTCAGTGAGCGGCAATGACTATGAATCGCCGATCAGTGAGGTTCTTTCTCGAATG                        | 420 |
| <i>rmi1-2</i> | TCCGAGTCAGTGA <del>TC</del> CGGCAATGACTATGAATCGCCGATCAGTGAGGTTCTTTCTCGAATG<br>***** | 415 |

**Figure 3.2. cDNA sequence alignment of *SIRMI1* to confirm mutations on an mRNA level.**

Aligned sequences of wild type (WT) cDNA and the cDNA of the two *rmi1* tomato mutant lines, *rmi1-1* and *rmi1-2*. Sequences obtained by amplification via PCR and Sanger Sequencing. Asterisks indicate aligned nucleotides. The numbers on the right side inform the position within the cDNA sequence of *SIRMI1*. The green box highlights the start codon (ATG) and the start of the open reading frame (ORF). The yellow line shows the position of the induced mutations confirmed on an mRNA level in both *rmi1* mutant lines. When aligned to the cDNA of WT, the 1 bp insertion (T) and 4 bp deletion (TATT) can be seen for *rmi1-1* and *rmi1-2*, respectively. Red boxes show the position of the premature stop codons that result from the frameshifts.

### 3.2.2 Characterisation of *slrmi1* mutant lines

The two mutant lines for RMI1, *slrmi1-1* and *slrmi1-2*, generated via Cas9-mediated mutagenesis, were cultivated together with WT plants, initially in the growth chamber and subsequently transferred to the greenhouse. In order to compare the mutant lines in terms of their growth phenotype, to that of WT plants, the mutant and WT lines to be analysed were sown on the same day and subjected to the same growth and handling conditions throughout development. The growth and development of the mutant lines from seedling through to mature plant with flowers and ripe fruits for both *rmi1-1* and *rmi1-2* were phenotypically indistinguishable from WT plants (Figure 3.3).

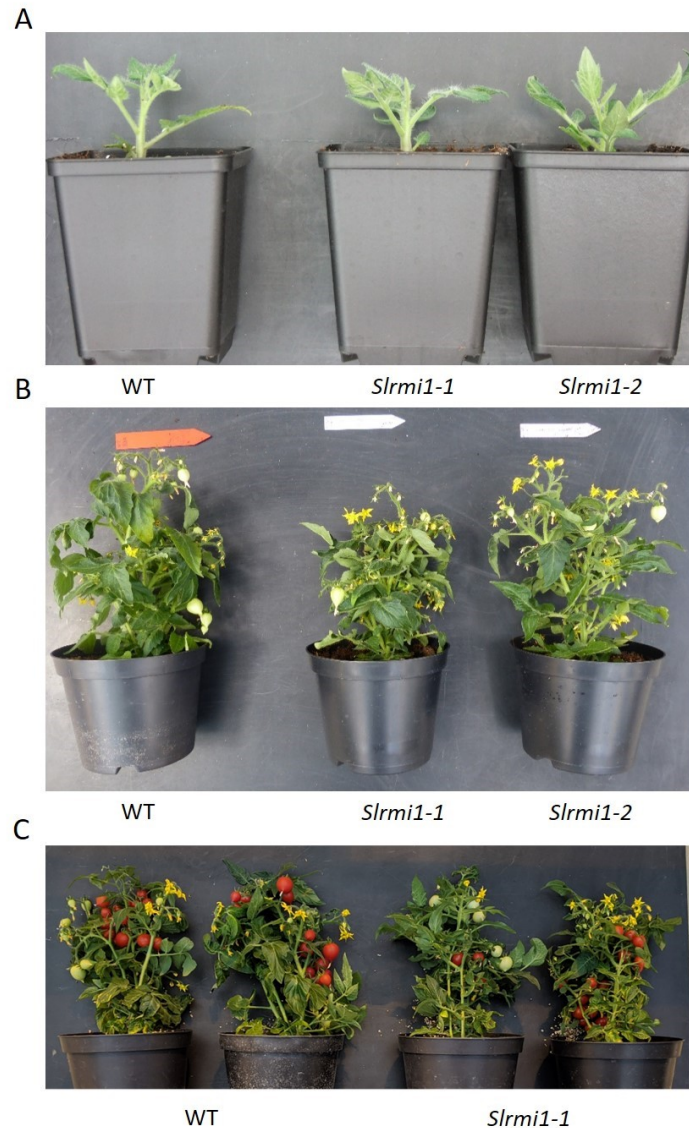


**Figure 3.3. *slrmi1-1* and *slrmi1-2* homozygous mutant plants compared to wild type (WT).**

- A) Three-week-old plants from both *rmi1* mutant lines, *rmi1-1* and *rmi1-2*, with a wild type control plant. Both mutant plants are indistinguishable to WT with respect to their growth and height.
- B) 2-month-old plants from both *rmi1* mutant lines, *rmi1-1* and *rmi1-2*, with a wild type control plant. Mutants appear the same as WT phenotypically, with a similar height and no abnormal flower development or reduced number of maturing fruits.
- C) 3-month-old *rmi1-1* mutant plants with control WT plants. *rmi1-1* plants do not appear different to the WT control plants as there are no apparent defects in growth and flower and fruit development or maturation to fully ripe.

The initial characterisation of the RTR-complex partner tomato mutant lines, deficient in the structural protein RMI1, involved analysing the fertility of the plants. Fertility analyses provide key information regarding potential defects within meiosis and meiotic recombination. When fertility is affected, whether that be to a degree or completely abolished leading to sterility, it provides an insight into whether the protein being investigated plays a functional role within meiosis. Therefore, to elucidate whether the RMI1 tomato homologue may play a role in

meiosis, the fertility of the two mutant lines were analysed. The lines, *slrmi1-1* and *slrmi1-2*, were cultivated in conjunction with wild-type plants, initially within a growth chamber and later on in the greenhouse. Once plants had grown to full maturity, all ripe fruits were harvested from at least five plants for each genotype. The ripe fruits were dissected and every seed within each fruit was counted to determine the average number of seeds per fruit for each of the lines analysed. The calculated mean values are shown in Figure 3.4, as a box plot.

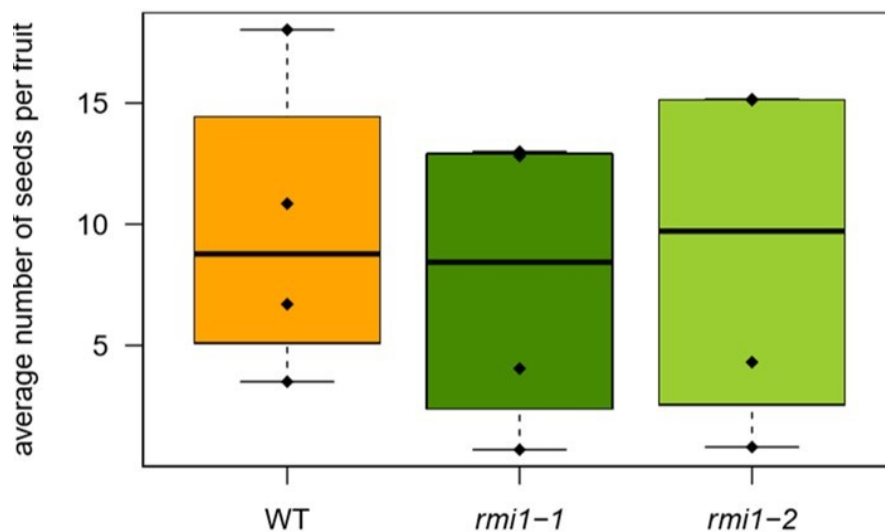


**Figure 3.4. Average number of seeds per fruit of *slrmi1-1* and *slrmi1-2* homozygous mutant plant lines compared to wild type (WT).**

Boxplot illustrating the average number of seeds per ripe fruit from mature *rmi1-1* and *rmi1-2* mutant plants, compared with wild-type (WT) plants of the same age, determined from four independent assays with > 10 fruits analysed from five plants, for each line. Median for the WT line and two *rmi1* mutant lines, indicated by the black lines, and interquartile range as shown by the coloured boxes, are similar for each line, indicating that there is no reduction in the seed number per fruit for both mutant lines, *rmi1-1* and *rmi1-2*, compared with WT. *P*-values were calculated according to the Mann–Whitney *U*-test, which confirmed that there was no statistical difference between the lines. Individual data points for the assays are shown as black diamonds.

Interestingly, the first notable result, as apparent in Figure 3.4, is that both of the *rmi1* tomato mutant lines are in fact fertile and not sterile, as fruits contained seeds. A mean number of seeds per fruit of 9 could be quantified in wild-type plants. The analysed *rmi1-1* and *rmi1-2* mutant lines did not differ significantly from that of the WT line, with average seed counts per fruit being 7 and 8 for *rmi1-1* and *rmi1-2*, respectively. Moreover, there is no significant difference between the average number of seeds per fruit between the two mutant lines themselves. Despite the number of seeds being one or two less per fruit on average for the mutant lines, compared to WT, this reduction was not significant and does not suggest any fertility defects

for both of the *rmi1* mutant lines. The raw data of the seed count fertility analysis can be found in the appendix (Table 7.5).

In order to further clarify the fertility of the *rmi1* mutant lines, the viability of the pollen was determined, compared to that of WT plants. As the resultant product of meiosis, the presence and subsequent viability of pollen is a credible indication of fertility and thus normal meiosis. To analyse the viability of the pollen, the fluorescein diacetate (FDA) staining method, as described by (Heslop-Harrison and Heslop-Harrison, 1970), was performed. This technique is based on the fluorochromatic reaction which involves testing membrane integrity and enzyme activity. FDA, a non-fluorescent polar dye, is able to pass through intact semi-permeable membranes. The hydrolyzation of FDA by intracellular non-specific esterases enables the fluorescein to accumulate within the cell cytoplasm, which is visible as fluorescent green. Fluorescing pollen are therefore deemed viable. On the other hand, pollen grains that are not fluorescent are considered metabolically inactive and thus non-viable. To ascertain pollen viability for the mutant lines *rmi1-1* and *rmi1-2*, the fluorescent and non-fluorescent pollen were quantified, and the percentage of viable pollen grains for both lines were compared to that of the WT control line (see Figure 3.5).

For this, both mutant lines, *slrmi1-1* and *slrmi1-2*, were grown to full maturity under the same conditions as wild-type plants that would act as a control for comparison. All lines were initially cultivated within a growth chamber, until adequate shoot and root growth had taken place. Subsequently, all lines were simultaneously transferred for further growth in soil within the greenhouse. Once a sufficient number of flower buds were present on all lines, a single bud for analysis of the pollen spores to deduce their viability. The FDA staining method was carried out for three independent assays to determine the mean percentage of viable pollen for each line analysed, as depicted in Figure 3.5. The raw data of the pollen viability fertility analysis can be found in the appendix (Table 7.6).

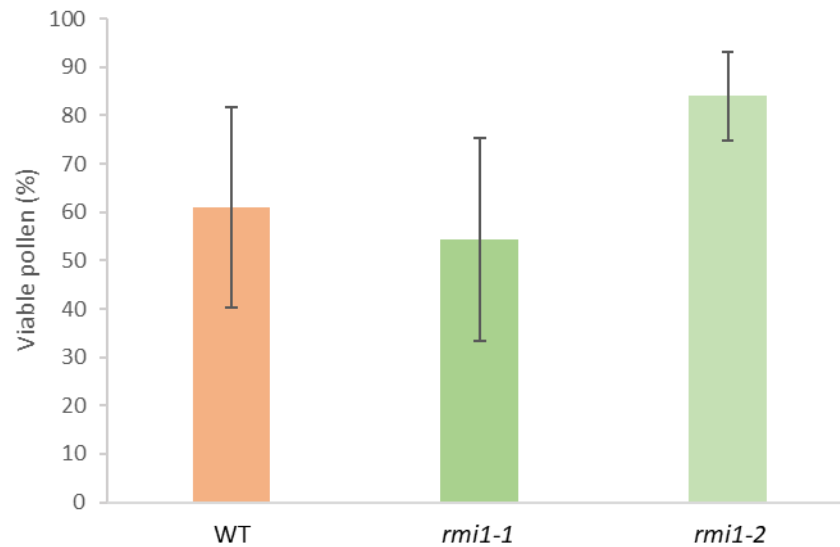


**Figure 3.5. Average percentage of viable pollen for both *slrmi1-1* and *slrmi1-2* homozygous mutant plants compared to wild type (WT).**

Average percentage of viable pollen grains from the flower buds of *rmi1-1* and *rmi1-2* mutant plants, compared with wild-type (WT) plants, grown under the same conditions for the same duration of time. Viable pollen was visualised and quantified via fluorescein diacetate staining of pollen spores from three independent assays with one flower bud analysed for each plant, for each line. Viable pollen numbers were calculated as a percentage of the total number of pollen spores. Standard deviation of the mean was determined, as shown with the error bars, and statistical analysis was conducted using a two-tailed *t*-test with unequal variances. There is no statistically significant difference between the percentage of viable pollen between the two *rmi1* mutant lines and the WT control line.

The mean percentage of viable pollen for *rmi1-1* and *rmi1-2* were 54 % and 84 %, respectively, whereby the percentage for the WT control line was 64 %. With one of the *rmi1* mutant lines displaying a lower mean percentage to that of WT, and the second showing a mean value of 20 % higher, it appears that there is not a reduced pollen spore viability for *rmi1* mutant lines compared to that of a wild-type line. This was confirmed following statistical analysis of the data obtained, whereby no statistically significant difference in the mean percentage of viable pollen between all the two mutant lines and WT could be observed. As a result, owing to the fact that there was no significant difference between both *rmi1* mutant lines, *slrmi1-1* and *slrmi2*, and WT, it can be deduced that the knockout of RMI1 in tomato does not lead to reduced pollen spore viability. Consequently, this data in conjunction with the seed count analysis as seen in Figure 3.4, further hint to no apparent reduced fertility in tomato *rmi1* mutants.

To further investigate the fertility of *rmi1* tomato mutant lines and clarify that tomato RMI1 mutants are indeed fully fertile, meiosis was analysed to get further insights into the structure and behaviour of the chromosomes. Chromatin preparations of pollen mother cells were carried out to investigate the meiotic progression of both of the *rmi1* mutant lines, in comparison to

that of wild type. The *slrmil-1* and *slrmil-2* plants to be analysed were grown alongside WT control plants, under the same conditions, firstly in a growth chamber on medium, and then in the greenhouse. Following six weeks of growth since the seeds initially been sown on media, the primary inflorescences from plants of the mutant lines and WT line, were excised, fixed and later the buds were further dissected and digested in order to stain the meiocytes and therefore the chromatin within, utilising DAPI staining. Fluorescent microscopy was then used in order to visualise the DAPI stained chromatin during all stages of meiosis, to analyse meiotic progression within the two *rmil* tomato mutant lines, and compare it to that of wild-type meiosis. Analysis of all individual stages of meiosis, through both meiosis I and meiosis II, to the formation of haploid pollen spores, was carried out as a way to determine whether lack of RMI1 in tomato leads to any visible meiotic defects or not (see Figure 3.6).

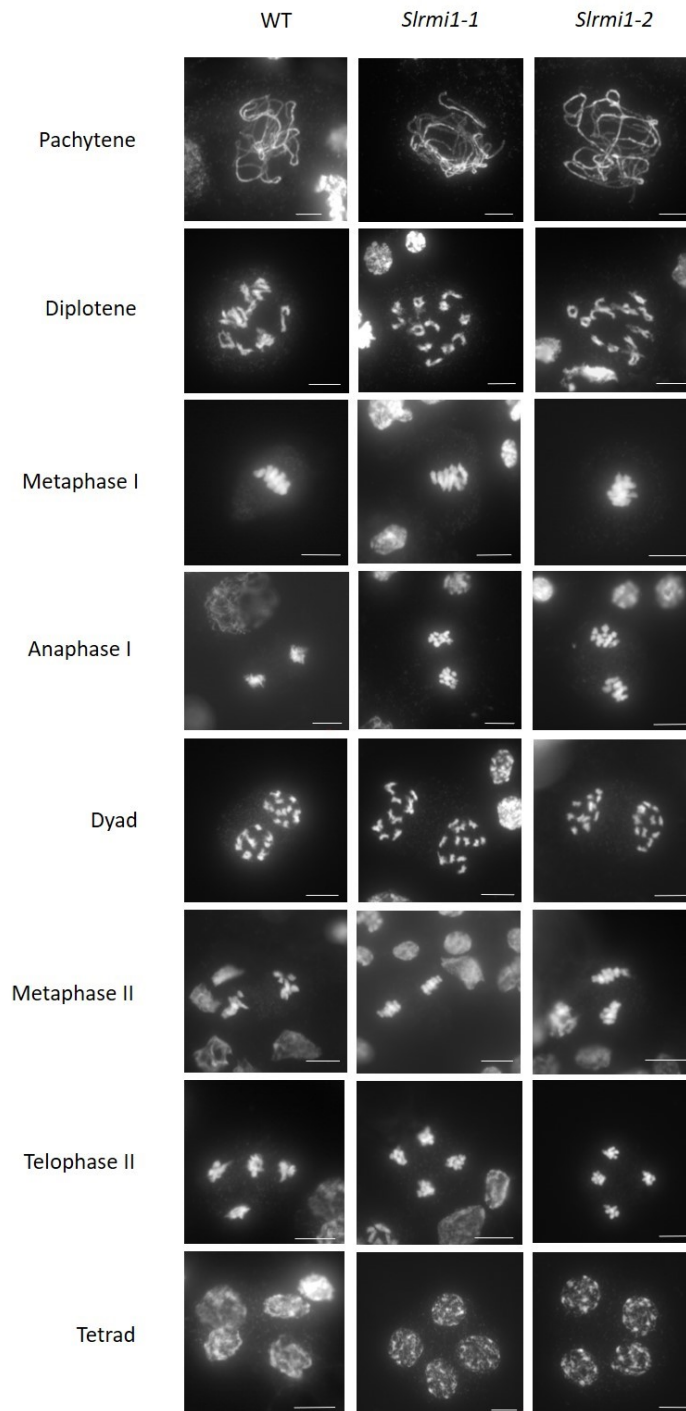


**Figure 3.6. DAPI-stained chromatin spreads of pollen mother cells from wild-type tomato and the mutant lines *rmi1-1* and *rmi1-2*.**

Observation of meiosis and chromosome structure and behaviour at various meiotic stages, via DAPI staining of pollen mother cells, for both homozygous *rmi1* mutant lines, *rmi1-1* and *rmi1-2*, and WT as a control. No apparent increased number of defects could be observed for either of the two *rmi1* mutant lines, when compared to WT. Full synapsis of homologous chromosomes occurred during pachytene, and the expected 12 bivalent structures can be recognised at diplotene. During anaphase I, no defects can be seen during separation of the homologous chromosomes, in terms of chromosomal fragmentation or chromatin bridges. Both *rmi1* homozygous mutant lines show balanced dyad formation, with each harbouring 12 chromosomes, as expected, showing normal progression of meiosis I. Meiosis II also appeared indistinguishable from that of WT, for both *rmi1-1* and *rmi1-2*, with the proper formation of clear tetrads containing the separated sister chromatids. Scale bars represent 10  $\mu\text{m}$ .

DAPI-staining of the chromatin for both the *rmi1* homozygous mutant lines, *rmi1-1* and *rmi1-2*, validated that meiotic progression proceeds in a normal manner when RMI1 is absent, as an increased number of defects was not observed compared to that of WT (Figure 3.6). For both of the *rmi1* mutant lines, meiosis I took place as in WT, with the correct formation of balanced dyads, each containing the expected 12 chromosomes. Subsequently, the sister chromatids of these chromosomes were then separated successfully during meiosis II, leading to the correct formation of tetrads, in a manner comparable to that of WT. As a result, lack of RMI1 in tomato does not seem to have an effect to any degree on meiosis, in terms of chromosome structure and behaviour, and the progression of meiosis itself, which further corroborates earlier findings that *rmi1* null mutants are fully fertile.

With the initial observation that tomato plants deficient in RMI1 produce fruits with seeds and are actually fertile, it was at least assumed that the level of fertility would be reduced to some extent compared to that of WT. However, taking into account the fact that seed count is not decreased in *rmi1* mutants (Figure 3.4) and neither is the percentage of viable pollen spores (Figure 3.5), in addition to no meiotic defects during either meiosis I nor meiosis II (Figure 3.6), it can be deduced that *rmi1* null mutants in tomato are indeed fully fertile. Therefore, following fertility analyses with both of the *rmi1* mutant lines, it can be assumed that RMI1 may not have an essential role within meiotic recombination in tomato.

With no evident role in meiosis in tomato, further characterisation of SIRMI1 involved investigating whether this RTR complex partner shows an involvement in somatic DNA repair. For this, the *rmi1* null mutant lines *slrmi1-1* and *slrmi1-2*, were subjected to various genotoxic agents in order to investigate the capacity of their DNA repair mechanisms, and thus elucidate potential roles for SIRMI1 within these.

Seeds of both the *rmi1-1* null mutant lines and WT acting as a control, were initially sown on media and grown for nine days in a growth chamber, under the same axenic conditions. Five nine-day-old seedlings were then transferred to one well of a 6-well plate containing liquid medium, in which genotoxic DNA damaging agents were added to include analysis of a range of concentrations, as described by (Hartung, *et al.*, 2007a). An untreated control was also performed whereby five seedlings, for each line including WT, were not subjected to any genotoxic agents. Following six days in a growth chamber, the fresh weight of the seedlings within each well was measured, and the measurements were normalised to that of the respective untreated control as a way to obtain the relative fresh weight (see Section 2.2.3.8). Firstly, in order to determine whether SIRMI1 has a putative role in the repair of DNA-protein crosslinks

(DPCs) and DNA-DNA crosslinks (CLs), sensitivity assays with the genotoxic DNA damaging agents *cis*-Platin and camptothecin (CPT) were carried out. *Cis*-Platin is a crosslinking genotoxic agent in which acts to induce both non-enzymatic DPCs by cross-linking DNA with DNA-associated proteins, and DNA-DNA crosslinks, with intrastrand CLs being the main DNA damage lesion generated by the genotoxin. CPT, on the other hand, is a topoisomerase 1 inhibitor and induces enzymatic DPCs in the form of topoisomerase I-DNA-cleavage complexes (Top1ccs). Following the treatment of the nine-day-old seedlings to both *cis*-Platin and CPT for a total of six days, fresh weight was measured, and normalised relative to that of an untreated control. The mean values of the relative fresh weights for both *cis*-Platin and CPT sensitivity assays are depicted as bar charts in Figures 3.7.A and 3.7.B, respectively. The raw data of the sensitivity assays with *cis*-Platin and CPT can be found in the appendix (Table 7.7; Table 7.8).

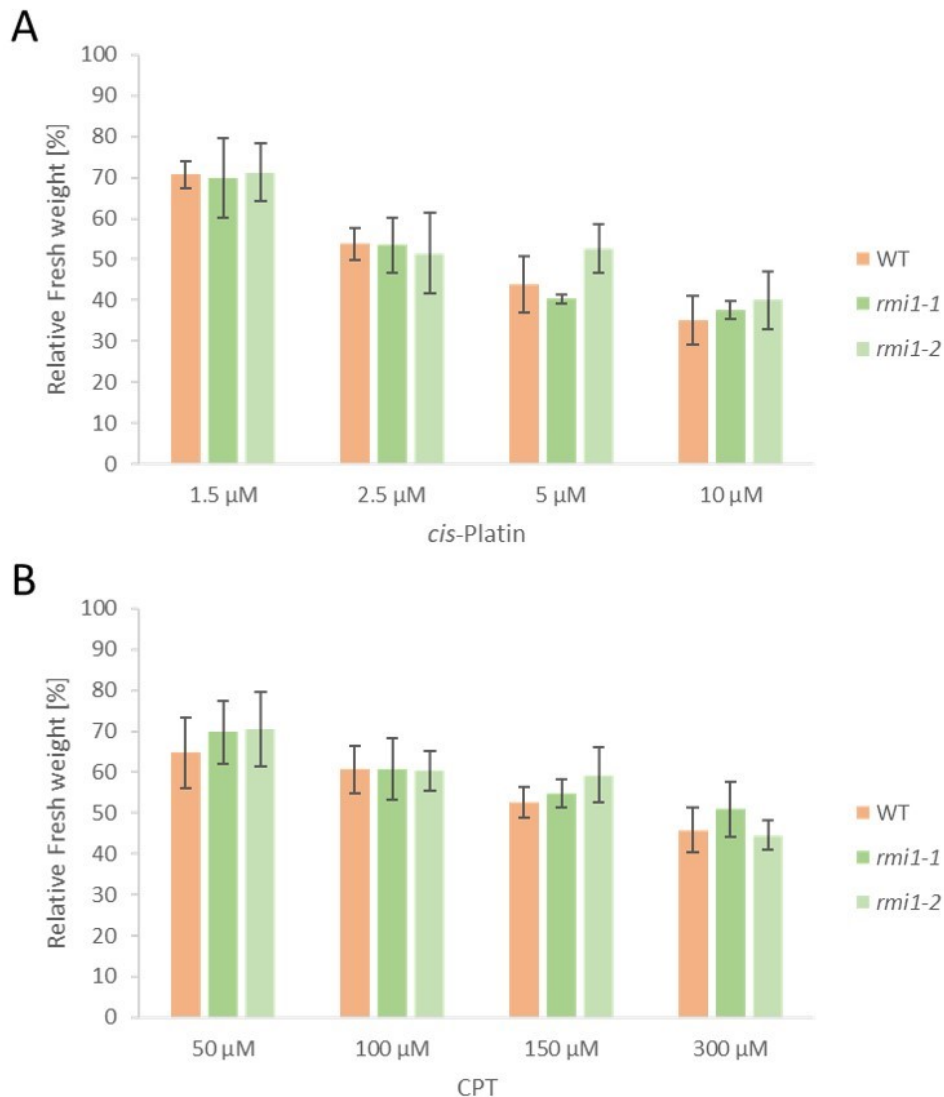


**Figure 3.7. Genotoxin sensitivity analysis of *slrmi1-1* and *slrmi1-2* homozygous mutant lines compared to wild type (WT), with the genotoxic agents *cis*-Platin and CPT.**

The mean fresh weight values of the tomato *rmi1* mutant lines, *rmi1-1* and *rmi1-2*, and WT, normalised relative to an untreated control, following treatment with crosslink-inducing genotoxic agents. Three independent assays were conducted for each analysis to calculate the mean fresh weight values. The standard deviation of the mean values was calculated and is shown as error bars. Statistical analysis was performed using a two-tailed t-test with unequal variances.

- Mean relative fresh weight of seedlings following treatment with 1.5, 2.5, 5 and 10 µM *cis*-Platin for three independent assays. Neither *rmi1-1* nor *rmi1-2* mutant lines displayed reduced relative fresh weight compared with WT, at any of the concentrations used of *cis*-Platin, indicating no increased sensitivity.
- Mean relative fresh weight of seedlings following treatment with 50, 100, 150 and 300 µM camptothecin (CPT) for four independent assays. Neither *rmi1-1* nor *rmi1-2* mutant lines displayed reduced relative fresh weight compared with WT, at any of the concentrations used of CPT, indicating no increased sensitivity.

Sensitivity analysis of both the *rmi1* tomato mutant lines, *rmi1-1* and *rmi1-2*, showed no reduced growth demonstrating increased sensitivities when treated with either the crosslinking agent *cis*-Platin or the topoisomerase 1 inhibitor CPT (Figure 3.7). For all four of the

concentrations of *cis*-Platin analysed, the mean relative fresh weight of the five seedlings measured were not significantly different to that measured for WT. When treated with a concentration of 1.5  $\mu$ M *cis*-Platin, for example, the mean relative fresh weight for WT was 82 %, which was no different to the 80 % and 81 % measured for *rmil-1* and *rmil-2*, respectively. Even at the highest concentration of *cis*-Platin analysed in the sensitivity assays, which was 10  $\mu$ M, the mean relative fresh weight for the *rmil* mutant lines was no different to that measured for the WT control (Figure 3.7.A). Therefore, both *rmil* homozygous lines did not show any increased sensitivity to the crosslinking genotoxic agent *cis*-Platin. Furthermore, no increased sensitivities were observed for either *rmil-1* or *rmil-2*, when treated with CPT at all four of the concentrations used, when compared to WT (Figure 3.7.B). The mean relative fresh weight for both *rmil* mutant lines was indifferent to those obtained for WT, following statistical analysis. When CPT was added at a concentration of 50  $\mu$ M, the lowest analysed, the mean relative fresh weight for *rmil-1* and *rmil-2* were 81 % and 84 %, respectively, whereas WT was 79 %. Consequently, treatment with CPT did not result show any increased sensitivities for seedlings lacking RMI1, when compared to WT.

To further characterise RMI1 in tomato and decipher a putative role within somatic DNA repair, sensitivity assays were also performed using the alkylating agent methylmethane sulfonate (MMS) and the crosslinker mitomycin C (MMC) (Figure 3.8). The raw data of the sensitivity assays with MMS and MMC can be found in the appendix (Table 7.9; Table 7.10).

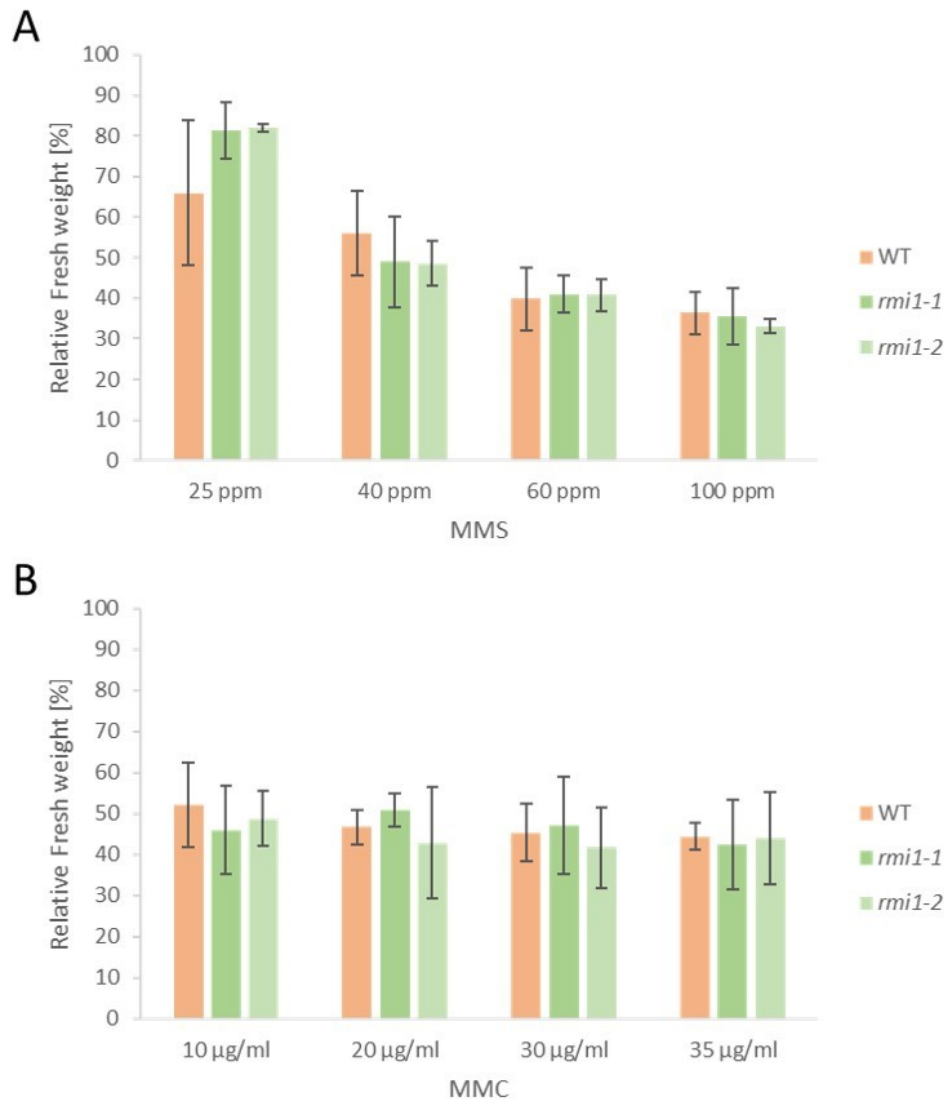


**Figure 3.8. Genotoxin sensitivity analysis of *slrmi1-1* and *slrmi1-2* homozygous mutant lines compared to wild type (WT), with the genotoxic agents MMS and MMC.**

The mean fresh weight measurements of the homozygous mutant lines *slrmi1-1* and *slrmi1-2*, following treatment with the genotoxic agents MMS and MMC, compared to those for WT. Mean fresh weight values were normalized to those of the respective untreated control. The mean values were calculated from the individual values obtained from three independent assays, and the standard deviation was determined and is shown as error bars. A two-tailed *t*-test with unequal variances was conducted for statistical analysis.

- Mean relative fresh weight of seedlings following treatment with 25 parts per million (ppm), 40, 60 and 100 ppm methylmethane sulfonate (MMS) for three independent assays. Neither *rmi1-1* nor *rmi1-2* mutant lines displayed reduced relative fresh weight compared with WT, at any of the concentrations used of MMS, indicating no increased sensitivity.
- Mean relative fresh weight of seedlings following treatment with 10, 20, 30 and 35 µg ml/ml mitomycin C (MMC) for three independent assays. Neither *rmi1-1* nor *rmi1-2* mutant lines displayed reduced relative fresh weight compared with WT, at any of the concentrations used of MMC, indicating no increased sensitivity.

Evidently, neither of the two *rmi1* homozygous mutant lines, *rmi1-1* nor *rmi1-2*, showed increased sensitivities when treated with either MMS or MMC, when compared to the WT

control. When subjected to both MMS, the two *rmi1* mutant lines had mean relative fresh weight values, comparable to those obtained for WT, and not different on a statistical level (Figure 3.8.A). MMS at a concentration of 25 ppm, the lowest concentration used in the sensitivity assay, the mean relative fresh weight for the WT control was 66 %, whereas for the *rmi1-1* mutant lines, the mean relative fresh weights were 81 % and 82 %, for *rmi1-1* and *rmi1-2*, respectively. This indifference between the mean relative and fresh weights, and therefore deemed sensitivities, was also apparent across all concentrations of MMS analysed, providing evidence that *rmi1* tomato mutants do not exhibit increased sensitivity to the alkylating agent MMS. In addition to this, seedlings deficient in RMI1 also did not show any increased sensitivity to the crosslinker MMC, compared to WT (Figure 3.8.B). The mean relative fresh weight measured for WT was similar to that measured for both *rmi1-1* and *rmi1-2*, when exposed to MMC at all four of the concentrations used.

In consideration of all of the sensitivity assays performed with the four genotoxic agents, *cis*-Platin, CPT, MMS and MMC, as shown in Figures 3.7 and 3.8, it seems that *rmi1* tomato mutant plants do not have increased sensitivity to genotoxins, when compared to WT. Accordingly, RMI1 in tomato does not seem to have a role in somatic DNA repair following genotoxin-induced DNA damage.

In an attempt to further investigate a possible role for the tomato homologue of RMI1 within somatic DNA repair, further analyses were carried out in order to see whether SIRMI1 could be involved in replication-associated repair mechanisms. Analysis of root length of both of the tomato homozygous mutant lines, *rmi1-1* and *rmi1-2*, were firstly analysed and compared to that of WT (Figure 3.9). Root length analyses represents a way in which replication-associated repair can be investigated, owing to the prolific cell division taking place within the dividing tissues of the root meristem. When replication-associated damage occurs within the root meristem that is not sufficiently repaired, the subsequent accumulation of such spontaneous DNA damage can result in damage within the dividing cells, and even cell death, in which ultimately leads to a decrease in the length of the roots, of which can of course be measured in a quantitative manner (Beemster and Baskin, 1998). Therefore, measurement and analysis of root lengths in mutant lines, is one such way in which an insight can be obtained regarding the possible involvement of factors within replication-associated DNA repair mechanisms. Root length analysis was conducted on 12-day-old plantlets, that had been grown in the growth chamber. Root lengths were measured using the ImageJ Plugin SmartRoot, for both of the *rmi1* tomato mutant lines, *rmi1-1* and *rmi1-2*, and compared to that of a WT control line that had

been grown under the same conditions for the same number of days. The mean root lengths for the two *rmi1* mutant lines and the respective WT control line are shown as a bar chart in Figure 3.9, with the raw data available in the appendix (Table 7.11).

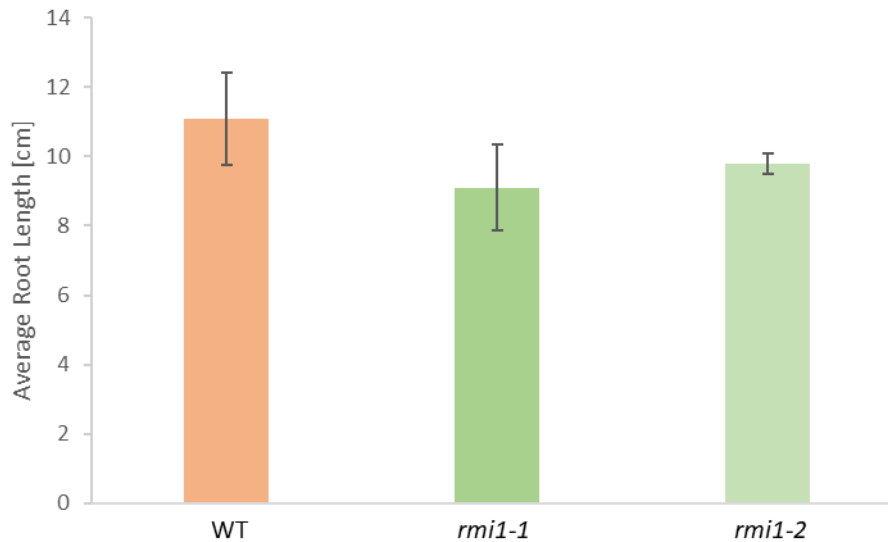


**Figure 3.9. Root length analysis of the *rmi1* tomato mutant lines *rmi1-1* and *rmi1-2*.**

The average root length measurements calculated from five 12-day-old tomato seedlings of both *slrmi1-1* and *slrmi1-2* mutant lines, compared to those obtained for respective wild-type (WT) seedlings. Measurements shown are the average root lengths from three independent assays, with the error bars corresponding to the standard deviation of the values from the three assays. A two-tailed *t*-test with unequal variances was carried for statistical analysis. Average root length measured for the two *rmi1* mutant lines was comparable to that of the WT control.

Analysis of the root lengths of the two *rmi1* tomato mutant lines showed no difference in length to those obtained for WT (Figure 3.9). The average root length for WT was 11 cm, whereas for the two *rmi1* mutant lines, the average lengths were 9 cm and 9.1 cm, for *rmi1-1* and *rmi1-2*, respectively. Although the average root lengths of the plantlets lacking RMI1 were comparatively smaller than those for WT, this difference is not statistically significant and therefore does not conclude a decreased root length for *rmi1* mutants. Thus, tomato plants deficient in RMI1 do not show any apparent defects in root growth, compared to WT.

Further investigation into possible roles for the RMI1 tomato homologue in replication-associated repair processes involved analysis of cell viability within the root meristem. During cell division, a buildup of DNA damage that is not adequately repaired can ultimately lead to cell death (Beemster and Baskin, 1998). With the cells in root meristems of plants being ones in which undergo numerous cellular divisions, any defect in repair of replication-associated DNA damage, would result in an increased number of non-viable cells,

as a result of cell death. Consequently, analysis of the viability of the cells within root meristems is another way in which the potential involvement of factors within replication-associated DNA repair processes can be determined. In order to analyse and quantify cell viability within the roots of the tomato *rmi1* mutant line, the azo dye Evan's blue was used. Evan's blue is a dye that is able to penetrate the membranes of damaged cells, leading to staining of the whole cell. With the uptake of the dye only being possible for non-viable cells, analysis of the uptake and the resultant stained cells, allows for cell viability to be measured in a quantitative manner (NV *et al.*, 2017). For this analysis, 1 cm of root tip dissected from nine-day-old plantlets were subjected to the Evan's blue dye, washed, and the uptake of the dye by the non-viable cells was measured, corresponding to the calculated amount of Evan's blue dye extracted from the root material and measured via absorbance in the solution. The root tips of three plantlets from each of the two tomato *rmi1* mutant lines, *rmi1-1* and *rmi1-2*, were used for analysis with Evan's blue staining, and the uptake of Evan's blue was compared to that of WT plants, acting as a control (Figure 3.10). The raw data of the Evan's blue analysis can be found in the appendix (Figure 7.1 and Table 7.6).

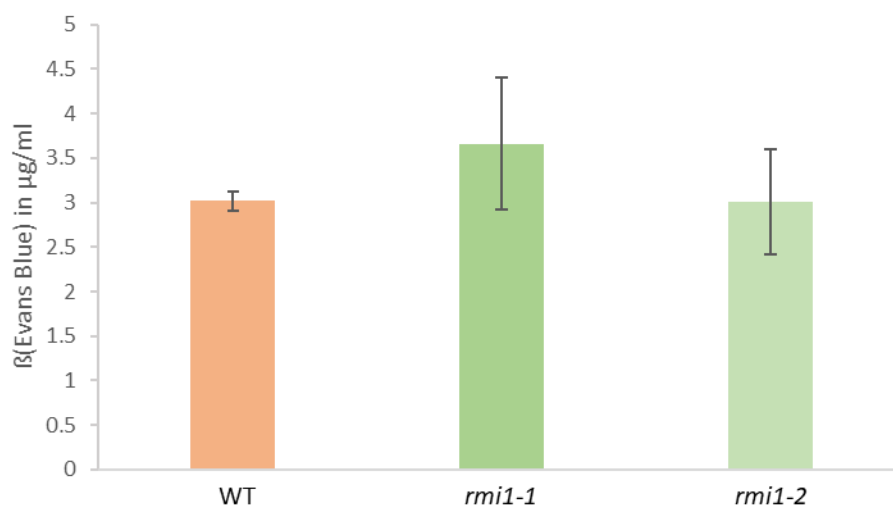


**Figure 3.10. Meristematic root cell viability analysis in *rmi1* tomato mutant lines.**

The mean measurement of Evan's blue dye uptake ( $\mu\text{g/ml}$ ) from three roots of nine-day-old plantlets for *slrmi1-1* and *slrmi1-2* mutant lines, compared with WT. Mean measurements were calculated from three independent assays and standard deviation is shown as error bars. Statistical analysis was determined using a two-tailed *t*-test with unequal variances. Evan's blue uptake was similar for all lines, suggesting no difference in cell viability between the two *rmi1* mutant lines and the WT control.

There were no differences between the uptake of Evan's blue for either of the two *rmi1* mutant lines, compared to that for the WT control (Figure 3.10). For WT, the uptake of Evan's blue was  $3 \mu\text{g/ml}$ , with the uptake for the *rmi1* mutant lines, *rmi1-1* and *rmi1-2*, was  $3.7 \mu\text{g/ml}$  and

3 µg/ml, respectively. With no significant difference between the uptake for the mutant lines, compared to WT, it seems that plants lacking RMI1 do not have an increased number of non-viable cells within their root meristems and therefore RMI1 is not involved in the repair of replication-associated DNA damage in tomato.

Overall, taking into account the analyses of the tomato null mutants deficient in RMI1, there is evidence to support that RMI1 is not required for somatic DNA repair processes in tomato. Together with the previous fertility analyses, the tomato RMI1 homologue does not appear to have a functional role in meiotic recombination, fertility in general, or in somatic DNA repair.

### 3.3 Identification of the TOP3α tomato homologue

For identification of the *TOP3α* orthologous gene within the tomato genome, the known Arabidopsis genomic sequence of *AtTOP3α* (*At5g63920*) was used in order to conduct homology searches, which was retrieved from the *Arabidopsis thaliana* database TAIR. The nucleotide sequence of *AtTOP3α* was then used to search potential homologues within the *S. lycopersicum* genome using NCBI BLAST and EnsemblPlants, as the input query. The potential homologous gene in tomato was identified as *Solyc05g014720.3.1* (locus identifier within the current Tomato Genome version SL4.0 available from The Sol Genomics Network (SGN)), which was termed *SITOP3α*. Located on chromosome 5 of the tomato genome, *SITOP3α* is 3564 bp in length, comprised of 24 exons (Figure 3.11) and 68.43 % identical in sequence to *AtTOP3α*. The protein encoded by the identified *TOP3α* orthologue in tomato, is 915 amino acids in length, of which 70.04 % are identical to those in *AtTOP3α*. The domain structure of *SITOP3α* was analysed using EMBL-EBI InterProScan 5, which revealed that the tomato homologue has the conserved domains, TOPRIM domain and central domain with the catalytic tyrosine residue, in which have been identified as essential for the function of the orthologous topoisomerases in plants, and other eukaryotic organisms (Dorn *et al.*, 2018) (Figure 3.11).

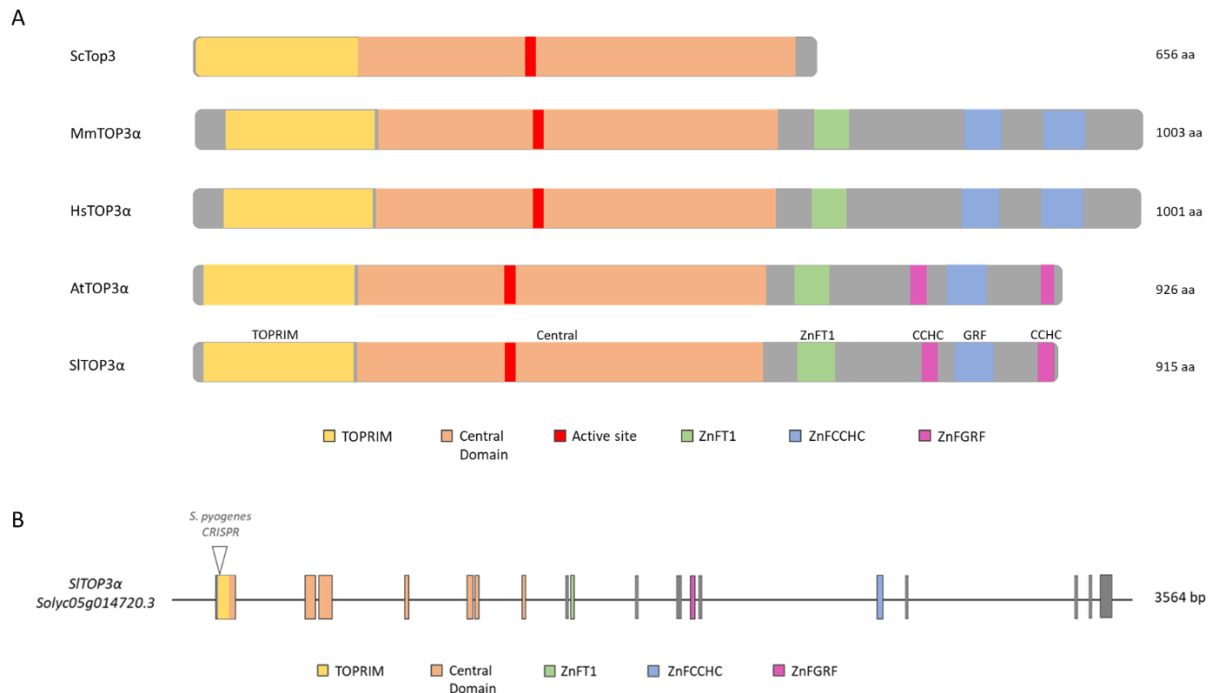


**Figure 3.11. SITOP3 $\alpha$  protein domain structure and comparison and SITOP3 $\alpha$  gene structure.**

Schematic diagram illustrating the protein domain structure of the tomato TOP3 $\alpha$  orthologue with homologues from other eukaryotes and the gene structure of SITOP3 $\alpha$ .

- (A) Schematic diagram showing the conserved protein domains in TOP3 $\alpha$  orthologues from *Saccharomyces cerevisiae* (Sc, baker's yeast), *Mus musculus* (Mm, mouse), *Homo sapiens* (Hs, human), *Arabidopsis thaliana* (At, Arabidopsis) and the identified orthologue in *Solanum lycopersicum* (Sl, tomato). The tomato TOP3 $\alpha$  protein is 915 amino acids (aa) in length and contains the domains known to be integral for the function of TOP3 $\alpha$  in *A. thaliana* (Dorn *et al.*, 2018); N-terminal TOPRIM domain, central domain with the active site, as indicated by the red line, and C-terminal zinc (Zn) zinc domains T1, two CCHC-type and GRF-type, the same as with Arabidopsis.
- (B) SITOP3 $\alpha$  gene structure indicating exons (boxes), domain structure within these and untranslated regions including introns as a line. TOP3 $\alpha$  gene in tomato is comprised of 24 exons and is 3564 bp in length. The location of the cutting site is indicated by the arrow, where Cas9 was targeted to via the spacer sequence for induced mutagenesis.

### 3.3.1 Cas9-mediated mutagenesis of SITOP3 $\alpha$

In order to generate mutants of TOP3 $\alpha$  in tomato, targeted mutagenesis was carried out to induce mutations within SITOP3 $\alpha$ , using CRISPR/Cas9. Mutagenesis was performed using the tomato cultivar Micro-Tom as a model system for tomato plants. As with the mutagenesis of SIRMII (described in Section 3.2.1), the Cas9 nuclease of the CRISPR/Cas9 system was used to generate a targeted DSB within a pre-determined locus of the genome, within the target gene, which in this case was SITOP3 $\alpha$ . With repair of DSBs predominantly being repaired via the error-prone NHEJ pathway, repair would likely introduce mutations at the break site, in which could lead to a frameshift within the coding sequence of the gene, and therefore generate a complete knockout of the protein encoded for by the target gene. Cas9-mediated mutagenesis

using the Cas9 orthologue from *S. pyogenes* (Fauser *et al.*, 2014) was used in this study, in order to generate the TOP3 $\alpha$  mutants in tomato. The CRISPR/Cas9 constructs as discussed in (Fauser *et al.*, 2014) were used, with the Cas9 from *S. pyogenes* as part of the destination vector pDe-Spy-Cas9. The resistance cassette was changed from a phosphinothricin cassette to a kanamycin one, in order to conduct selection of transgenic plants, during the transformation and regeneration process. A specific target sequence within the first exon of *SITOP3 $\alpha$*  (*SITOP3 $\alpha$*  Protospacer 5'-GATGCTGTTACATCTGTCA-3') was identified, and this spacer sequence was then incorporated into the CRISPR/Cas9 expression cassette by gateway cloning methods (see Section 2.2.1.5). The spacer sequence enabled the subsequent targeting and binding of the Cas9 nuclease, to the corresponding loci within the tomato genome, which for this case, was within exon 1 of *SITOP3 $\alpha$* , at the beginning of the coding sequence for the TOPRIM domain of the protein (Figure 3.11).

*Agrobacterium tumefaciens*-mediated transformation and the cotyledon leaf disc method was used to integrate the final CRISPR/Cas9 expression constructs into the genome of wild-type Micro-Tom plants, as was described for the generation of the *slrmi1* mutant lines (see Section 3.2.1). The seeds of the regenerated transgenic plants were harvested (T1 generation), and extracted DNA from the seedlings was screened using HRM analysis and Sanger sequencing to identify plants harbouring a mutation at the targeted sequence within TOP3 $\alpha$  (see Section 2.2.3.4). The independent transgenic lines were also screened to ensure that they had only a single-locus of the T-DNA. As a result of this, the two different, independent mutant lines with heterozygous mutations were identified within the T1 generation: *sttop3 $\alpha$ -1* and *sttop3 $\alpha$ -2*. Sanger sequencing of these *top3 $\alpha$*  mutant plants determined the exact mutation that had been induced during Cas9-mediated mutagenesis. The first heterozygous mutant line, *sttop3 $\alpha$ -1*, was identified within the T1 generation and harboured a mutation of a one base pair insertion. The second mutant line, *sttop3 $\alpha$ -2*, was found to have a one base pair deletion. The mutations within both of the two heterozygous mutant lines, led to a frameshift and therefore a premature stop codon in which could lead to the formation of a truncated and functionally redundant protein from the gene. The mutations for each of the mutant lines were also confirmed on an mRNA level. In doing this, the total RNA was extracted from each of the lines, converted to cDNA via reverse-transcription and the cDNA was amplified and sequenced using Sanger sequencing. From this, the mutations of both mutant lines were successfully confirmed within the cDNA and therefore on an mRNA level (Figure 3.12).

|         |  |     |
|---------|--|-----|
| WT      | GCGACGATATAAGAAAGGGGCATTCCGGCAACCGTTTCGTCTGGGAAAATG          | 480 |
| top3A-1 | GCGACGATATAAGAAAGGGGCATTCCGGCAACCGTTTCGTCTGGGAAAATG          | 480 |
| top3A-2 | GCGACGATATAAGAAAGGGGCATTCCGGCAACCGTTTCGTCTGGGAAAATG          | 480 |
| *****   |  |     |
| WT      | GAGGGCGGGTGATAAGGGTACTTAATGTGGCTGAAAAGCCGTGCGTGGCCAAAGCAGTGT | 540 |
| top3A-1 | GAGGGCGGGTGATAAGGGTACTTAATGTGGCTGAAAAGCCGTGCGTGGCCAAAGCAGTGT | 540 |
| top3A-2 | GAGGGCGGGTGATAAGGGTACTTAATGTGGCTGAAAAGCCGTGCGTGGCCAAAGCAGTGT | 540 |
| *****   |  |     |
| WT      | CGGGGATACTATCGAAGAACCACCAGGTGGCATTAGAGTAAGAGACGGACGTTCCAGGT  | 600 |
| top3A-1 | CGGGGATACTATCGAAGAACCACCAGGTGGCATTAGAGTAAGAGACGGACGTTCCAGGT  | 600 |
| top3A-2 | CGGGGATACTATCGAAGAACCACCAGGTGGCATTAGAGTAAGAGACGGACGTTCCAGGT  | 600 |
| *****   |  |     |
| WT      | ACAACAAAATCTTTGAGTTCACTACACCATTTCGGAACCGCCTTGCCAGATGCTGTTCA  | 660 |
| top3A-1 | ACAACAAAATCTTTGAGTTCACTACACCATTTCGGAACCGCCTTGCCAGATGCTGTTCA  | 660 |
| top3A-2 | ACAACAAAATCTTTGAGTTCACTACACCATTTCGGAACCGCCTTGCCAGATGCTGTTCA  | 660 |
| *****   |  |     |
| WT      | CATCTG-TCACGGGACATCTCATGGAGATTGAGTTTCACGAGCGTTACCGGAAATGGCAC | 719 |
| top3A-1 | CATCTGATCACGGGACATCTCATGGAGATTGAGTTTCACGAGCGTTACCGGAAATGGCAC | 720 |
| top3A-2 | CATCT--GCACGGGACATCTCATGGAGATTGAGTTTCACGAGCGTTACCGGAAATGGCAC | 718 |
| *****   |  |     |
| WT      | TCGTGTGACCCGCTCGACCTCTATAATGCGCCTATTCGGAAGTTTGTCCCTGAGGATAAG | 779 |
| top3A-1 | TCGTGTGACCCGCTCGACCTCTATAATGCGCCTATTCGGAAGTTTGTCCCTGAGGATAAG | 780 |
| top3A-2 | TCGTGTGACCCGCTCGACCTCTATAATGCGCCTATTCGGAAGTTTGTCCCTGAGGATAAG | 778 |
| *****   |  |     |
| WT      | TTGGATATCAAAGGACACTGGAGGCAGAAGCCAGAAGTTGTCAAGTGGATTATATTGTGG | 839 |
| top3A-1 | TTGGATATCAAAGGACACTGGAGGCAGAAGCCAGAAGTTGTCAAGTGGATTATATTGTGG | 840 |
| top3A-2 | TTGGATATCAAAGGACACTGGAGGCAGAAGCCAGAAGTTGTCAAGTGGATTATATTGTGG | 838 |
| *****   |  |     |
| WT      | CTCGATTGTGATAGAGAAGGAGAAAAATTTGCATTTGAAGTGTGGATGTATGTAGACAA  | 899 |
| top3A-1 | CTCGATTGTGATAGAGAAGGAGAAAAATTTGCATTTGAAGTGTGGATGTATGTAGACAA  | 900 |
| top3A-2 | CTCGATTGTGATAGAGAAGGAGAAAAATTTGCATTTGAAGTGTGGATGTATGTAGACAA  | 898 |
| *****   |  |     |
| WT      | GCGAATCATAACCTTACTGTGTGGAGAGCTCGGTTCTCTGCC TTAATTGACAGGAAATT | 959 |
| top3A-1 | GCGAATCATAACCTTACTGTGTGGAGAGCTCGGTTCTCTGCC TTAATTGACAGGAAATT | 960 |
| top3A-2 | GCGAATCATAACCTTACTGTGTGGAGAGCTCGGTTCTCTGCC TTAATTGACAGGAAATT | 958 |
| *****   |  |     |

**Figure 3.12. cDNA sequence alignment of *SITOP3a* to confirm mutations on an mRNA level.**

Aligned sequences of wild type (WT) cDNA and the cDNA of the two *top3a* tomato mutant lines, *top3a-1* and *top3a-2*. Sequences obtained by amplification via PCR and Sanger Sequencing. Asterisks indicate aligned nucleotides. The numbers on the right side inform the position within the cDNA sequence of *SITOP3a*. The green box highlights the start codon (ATG) and the start of the open reading frame (ORF). The yellow line shows the position of the induced mutations confirmed on an mRNA level in both *top3a* mutant lines. When aligned to the cDNA of WT, the 1 bp insertion (A) and 1 bp deletion (T) can be seen for *top3a-1* and *top3a-2*, respectively. Red boxes show the position of the premature stop codons that result from the frameshifts.

For both *sitop3a-1* and *sitop3a-2* mutant lines, the zygosity of the mutations was analysed using both HRM analysis and Sanger sequencing, which showed that the mutations for both independent T1 lines, were heterozygous, meaning only one of the two alleles harboured the mutation. Therefore, both lines were further propagated to obtain the seeds of the next generation (T2), to obtain homozygous mutant lines. The seeds of the T2 generation, were collected using a 1 mm mesh sieve, sterilised and sown on germination medium. After two

weeks of growth in a growth chamber, DNA was extracted from the seedlings and used for HRM and Sanger sequencing once again to determine the zygosity of the plants. Interestingly, for both independent mutant lines, *top3α-1* and *top3α-2*, no homozygous plants were identified, at all within the T2 generation. According Mendelian segregation in genetics, 25 % of the progeny from a self-pollinated heterozygous plant should be homozygous. Nevertheless, from all of the plants analysed, for both *top3α-1* and *top3α-2*, no homozygous plants were identified with around a third of the plants for each line being WT, and the remaining two-thirds being heterozygous (Table 3.1).

**Table 3.1.** The number and percentage of heterozygous, homozygous mutant plants and wild type (WT) plants, identified from the progeny of the two heterozygous *top3α* mutant lines, *top3α-1* and *top3α-2*.

| Line                   | No. plants | Wild type (+/+) | Heterozygous (+/-) | Homozygous (-/-) | 1:2:1 Mendelian segregation $\chi^2 < 5.99$ | 1:2 Mendelian segregation $\chi^2 < 3.84$ |
|------------------------|------------|-----------------|--------------------|------------------|---|---|
| <i>sltop3α-1</i> (+/-) | 48         | 17 (35.4 %)     | 31 (64.6 %)        | 0                | 16.1  | 2.78                                      |
| <i>sltop3α-2</i> (+/-) | 59         | 19 (32.2 %)     | 40 (67.8 %)        | 0                | 19.7  | 1.63                                      |

As can be seen from Table 3.1, for both *top3α-1* and *top3α-2* heterozygous lines, the numbers of WT and heterozygous progeny observed corresponded to around one third being WT and two-thirds being heterozygous, which would imply 1:2 Mendelian segregation, as opposed to the normal, expected 1:2:1 segregation in which would result in homozygous plants. Chi-squared ( $\chi^2$ ) statistical analysis was used in order to confirm that the segregation observed was indeed 1:2, rather than 1:2:1 and therefore it was very unlikely that homozygous plants would be obtained from the *top3α* heterozygous mutant lines. As a result of no homozygous plants being identified for either of the two *top3α* mutant lines analysed, it seemed that a homozygous mutation within the *TOP3α* gene of tomato, leads to plants in which are not viable. Therefore, the two heterozygous lines *top3α-1* and *top3α-2*, were further propagated to obtain plants free of the Cas9-transgene and sufficient seeds in order to perform analysis for the characterisation of *TOP3α* in tomato.

### 3.3.2 Characterisation of *stop3a* mutant lines

Owing to the fact that no homozygous *stop3a* mutant lines were identified within the T1 generation during Cas9-mediated mutagenesis (see Section 3.3.1), or subsequent generations propagated from the T1 heterozygous mutant lines, it seemed reasonable to speculate that complete knockout of TOP3 $\alpha$  in tomato may lead to non-viable plants. Consequently, analysis was conducted on the established heterozygous *top3a* mutant lines, *top3a-1* and *top3a-2*, in order to gain further insights into the apparent essential role of TOP3 $\alpha$  in tomato.

Firstly, both heterozygous *top3a* mutant lines appeared as WT, with no differences in growth or any other noticeable phenotype (Figure 3.13), when grown under the same conditions and for the same length of time.

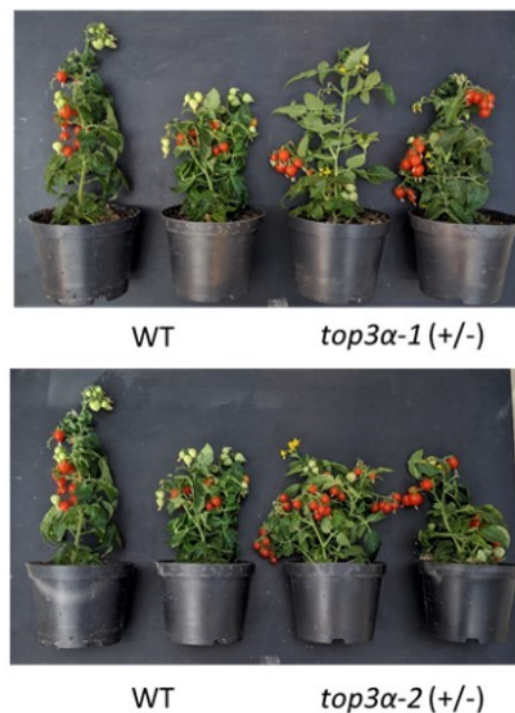


**Figure 3.13.** *stop3a-1* and *stop3a-2* heterozygous mutant plants compared to wild type (WT).

Photographs of mature plants with ripe fruits from *top3a* heterozygous lines (+/-), *top3a-1* and *top3a-2*, and WT plants as control. Both heterozygous mutant lines and WT plants were grown for under the same conditions, for the same period of time. The heterozygous lines both appear as WT, with no difference in growth or any other noticeable phenotype.

Due to the known functional role of TOP3 $\alpha$  in Arabidopsis, whereby the RTR complex partner constitutes an essential role in meiosis (Dorn *et al.*, 2018; Hartung *et al.*, 2008), fertility analyses were initially carried out to see if meiosis and therefore fertility is also affected within the *top3a* heterozygous tomato mutant lines, *top3a-1* and *top3a-2*. To do this, a seed count analysis was conducted. For each line, the two heterozygous mutant lines and a WT line, a minimum of 10

ripe fruits were harvested from a single plant and all were seeds extracted and collected using a 1 mm sieve. The seeds obtained within the sieve were then counted to determine the total seed count for each plant. A total of five plants were analysed for each line, to determine the average seed count, with three independent assays being carried out in total. The mean number of seeds for each independent assay were normalized, relative to WT and the mean relative percentage seed number was calculated (Figure 3.14). The raw data of the seed count analysis can be found in the appendix (Table 7.13).

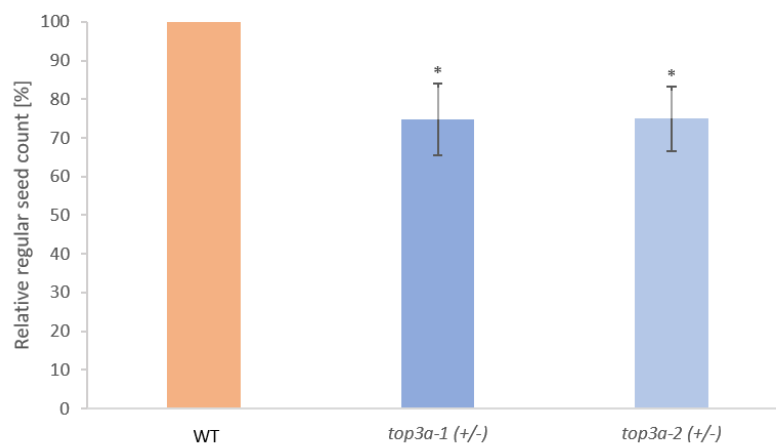


**Figure 3.14. Relative percentage of regular (> 1 mm) seed number from *stop3a-1* and *stop3a-2* heterozygous mutant plants compared to wild type (WT).**

The relative percentage of regular seeds from *top3a-1* and *top3a-2* heterozygous (+/-) mutant lines, and the respective WT control plants. Seeds were extracted and collected using a 1 mm sieve. Seeds from > 10 ripe fruits were counted from five plants, for each independent assay. Mean values were calculated from three independent assays, as shown by the columns. Seed numbers were normalized to those for the WT control line, and are shown as a relative percentage. Standard deviation is represented by the error bars. Statistical analysis was calculated using a two-tailed *t*-test with unequal variances: \* $P < 0.05$ . Both of the heterozygous mutant lines, *top3a-1* and *top3a-2*, show a significantly reduced number of regular seeds, compared to WT.

In doing this, both *stop3a-1* and *stop3a-2* heterozygous mutant lines showed a significantly reduced number of seeds compared to WT (Figure 3.14). The heterozygous mutant lines *stop3a-1* and *stop3a-2* had a regular seed count of 74.8 % and 75.0 %, respectively, relative to that for the WT control line. Noticeably, with both heterozygous mutant lines showing 75 % of the regular seeds counted for WT, there is not only a significant reduction in the number of seeds for the mutant lines, but this reduction amounts to 25 % less than WT.

Further characterisation of *stop3a-1* and *stop3a-2*, involved investigating the fertility of the *top3a* heterozygous tomato mutant lines by analysis of the fruits, via two methods. The first being measuring the diameter of ripe fruits, and the second being counting ripe fruits on mature

plants at a given time point (Figure 3.15). For analysis of fruit diameter and therefore size, the diameter of the largest part (latitudinal diameter) of ripe fruits that were dark red in colour, were measured using a ruler. More than 10 ripe fruits were measured from a total of five plants for each line, with three independent assays being conducted in total. The resultant mean fruit diameter for each line was calculated, and statistical analysis was performed. The mean fruit diameter for both the *top3a* heterozygous tomato mutant lines, *sltop3a-1* and *sltop3a-2*, were compared to that of the respective WT control line (Figure 3.15.A). The second method employed was determining the average number of fruits per plants. All ripe fruits were harvested from a mature plant at a given time point, and the number of fruits were counted. Fruits were considered ripe when red in colour, as opposed to orange, yellow or green. All ripe fruits were counted for a total of 10 plants for each line analysed, and the mean number of fruits per plant was calculated using the data from three independent assays. The mean number of fruits per plant was measured for both of the *top3a* heterozygous tomato mutant lines, *sltop3a-1* and *sltop3a-2*, and compared to that of WT (Figure 3.15.B). All plants analysed in each assay were of the same age and had been grown under the same conditions to one another. The raw data of the fruit analysis can be found in the appendix in Table 7.13.

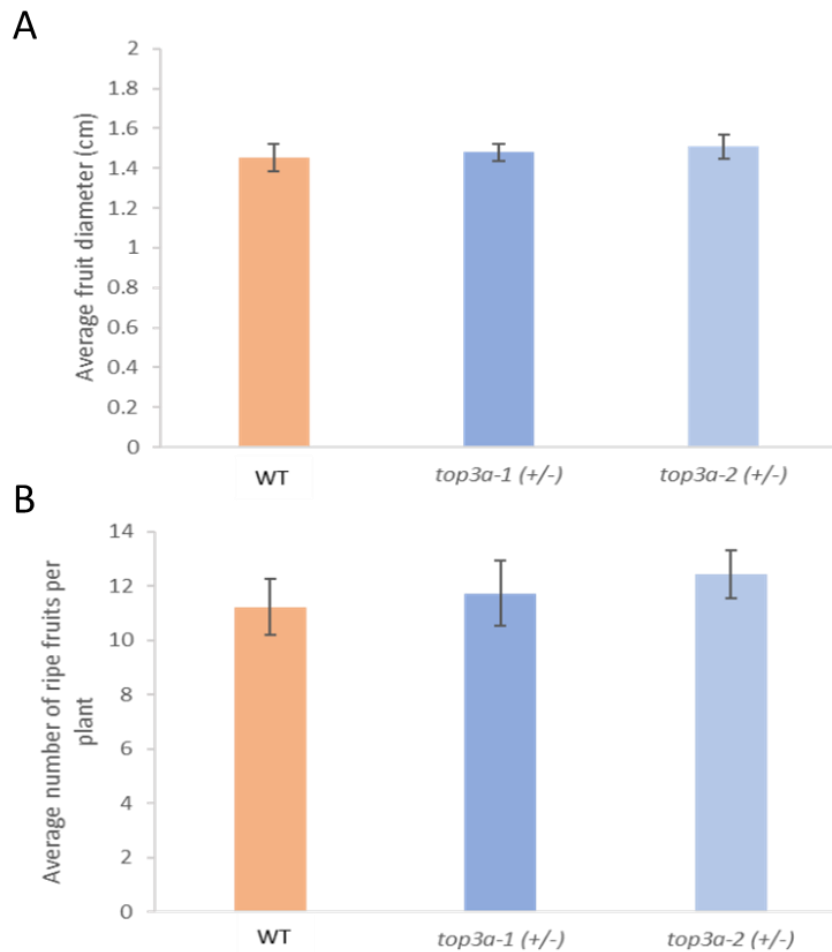


**Figure 3.15. Fruit analysis of *stop3a-1* and *stop3a-2* heterozygous mutant plants compared to wild type (WT).**

- A) Mean diameter of ripe fruits from both *top3a* heterozygous lines (+/-), *top3a-1* and *top3a-2*, and a wild type (WT) as control. More than 10 fruits from five plants for each line were measured. Three independent assays were conducted. The size of the fruits via their latitudinal diameter is similar for both heterozygous lines and WT. Error bars indicate standard deviation. Statistical analysis was calculated using a two-tailed *t*-test with unequal variances.
- B) Mean number of ripe fruits per plant from both *top3a* heterozygous lines (+/-), *top3a-1* and *top3a-2*, and a wild type (WT) as control. Data is from independent assays. All ripe fruits from five plants per line were harvested at the same time for quantification. Red fruits were considered ripe. The mean value and standard deviation (error bars) was determined and statistical analysis was calculated using a two-tailed *t*-test with unequal variances. Both heterozygous lines show no statistically significant difference in the number of ripe fruits per plant to WT.

The fruits of plants of the *top3a* heterozygous tomato mutant lines, *top3a-1* and *top3a-2*, did not differ to that of WT, in terms of either their size as measured by diameter, or in their number. The average diameter of the fruit harvested from both *top3a* heterozygous mutant lines, was not significantly different to that of the comparable WT control line (Figure 3.15.A), with the average fruit diameter being around 1.4 cm for both heterozygous mutant lines and the WT line. Moreover, there were no significant differences in terms of the mean number of fruits per plant

between the two heterozygous *top3α* mutant lines and WT, as can be seen from Figure 3.15.B. Taken together, the fruit analysis implies there are no differences between the two heterozygous mutant lines *sltop3α-1* and *sltop3α-2*, compared to WT.

To further analyse fertility of the heterozygous mutant lines, *sltop3α-1* and *sltop3α-2*, FDA staining was carried out to determine pollen viability, as described by (Heslop-Harrison and Heslop-Harrison, 1970). FDA staining is a technique used to determine membrane integrity and enzyme activity, with the polar dye being able to pass through intact semi-permeable membranes. Once within cells, FDA is hydrolysed by esterases which leads to the accumulation of fluorescein within the cytoplasm of the cell, causing the cells to fluoresce in green colour. Viable pollen will therefore fluoresce green and can be visibly distinguished from non-viable pollen (see Section 2.2.3.10). The viability of pollen from both *sltop3α-1* and *sltop3α-2*, was ascertained by quantifying the number of fluorescent pollen and non-fluorescent pollen, corresponding to the viable and non-viable pollen, respectively. The fluorescent pollen was then calculated as a percentage of the total number of pollen grains observed, and compared to that of the WT control line (Figure 3.16). The raw data of the pollen viability analysis can be found in the appendix in Table 7.14.

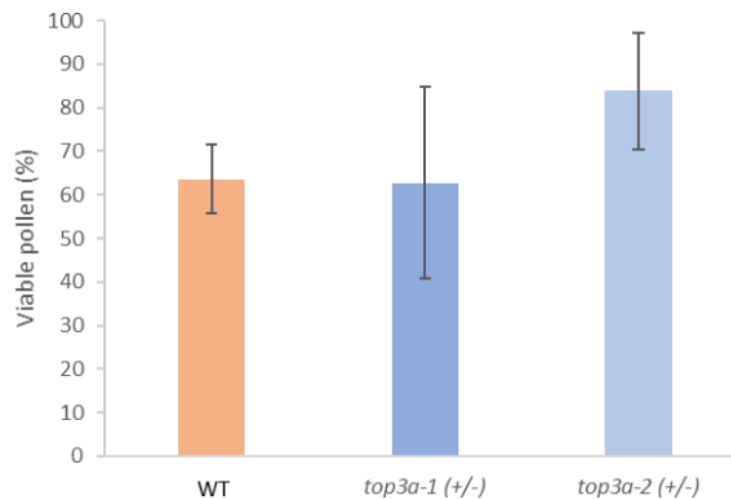


**Figure 3.16. Average percentage of viable pollen for both *sltop3α-1* and *sltop3α-2* heterozygous mutant plants compared to wild type (WT).**

Percentage of viable pollen determined via FDA staining of spores for both *top3α* heterozygous lines (+/-), *top3α-1* and *top3α-2*, and WT as control, from three independent assays. Pollen from one flower bud per line was used for each assay. The mean value and standard deviation (error bars) was determined and statistical analysis was calculated using a two-tailed t-test with unequal variances. Both heterozygous lines show no statistically significant difference in the percentage of viable pollen to WT.

As evident from Figure 3.16, there was no significant difference in the percentage of viable pollen between either of the *top3α* heterozygous lines, *top3α-1* and *top3α-2*, when compared to WT. Consequently, taking this result together with the previous analyses of fruit diameter and fruit size, it appears that besides the 25 % reduction in regular seeds relative to WT, that there are no other apparent defects regarding somatic growth or those affecting the fruits of the plants.

However, whilst dissecting the fruits from both of the *top3α* heterozygous lines for harvesting the seeds it became clear that in all fruits, there were a number of small seeds that seemed more numerous than for those usually observed in WT fruits (Figure 3.17.A). These smaller seeds had not been previously accounted for or taken into consideration as they had not been collected. The sieve used for collecting seeds was 1 mm sieve, meaning that the sieve openings were 1 mm in size. With these smaller seeds being smaller than 1 mm in size, they had fallen through these sieve openings along with other waste material. The abundance of these smaller seeds within both *top3α-1* and *top3α-2* led to the proposal that these small seeds (< 1 mm) could potentially account for the homozygous progeny, in which had been deemed non-viable. In the case that this hypothesis was to be correct, then these small seeds would account for one quarter of all of the seeds obtained from heterozygous plants, according to Mendelian segregation. Subsequently, in order to clarify whether this is the case, the number of all seeds were again quantified, but this time, the small seeds were also collected and included in the analysis. All seeds for both heterozygous mutant lines *top3α-1* and *top3α-2* were quantified, in addition to a transformed WT line of the same generation, as an appropriate control. All lines to be analysed were grown under the same conditions and for the same period of time. More than 10 fruits per plant were harvested for analysis, with five individual plants for each line being analysed, the heterozygous mutant lines *top3α-1* and *top3α-2* and the WT control line. All visible seeds from all of the fruits were counted, both < 1 mm and  $\geq$  1mm, as indicated by the arrows in Figure 3.17.A. The total number of all small seeds (< 1 mm) was determined from all five plants for each line, and the percentage of small seeds out of all the seeds was calculated for each line. With small seeds (< 1 mm) also being present within the WT control line, the percentages were normalised to that of the WT control line, in order to see any difference within the heterozygous mutant lines, in a relative manner. The seed count analysis was carried out for three independent assays in total, with the mean relative percentages of both the small (< 1 mm) and regular ( $\geq$  1 mm) seeds determined and shown as a bar chart in Figure 3.17.B. The raw data of the seed count analysis can be found in the appendix in Table 7.13.

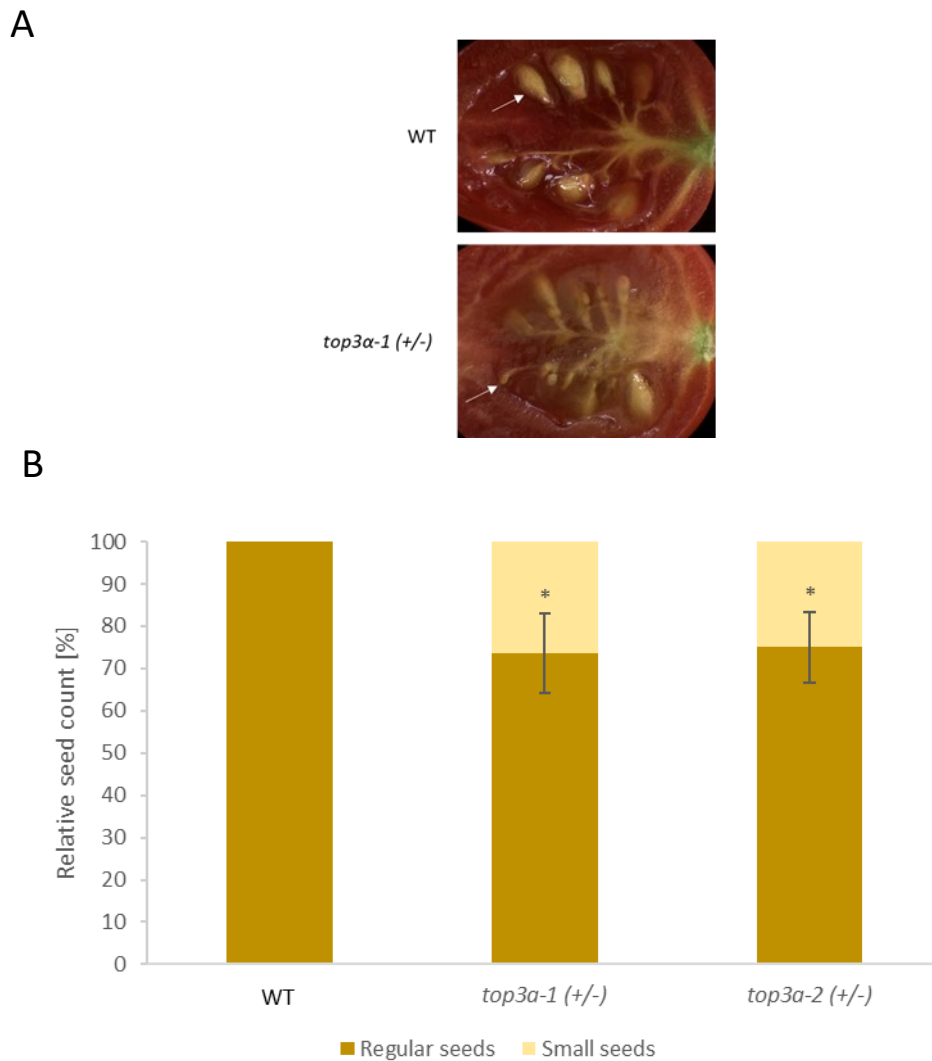


**Figure 3.17. Analysis of *stop3α-1* and *stop3α-2* heterozygous mutant lines compared to a wild type (WT) control line.**

- A) Photograph highlighting an exemplary regular seed (arrow) of > 1 mm in the WT control line and a small seed (arrow) of < 1 mm in size in the heterozygous ( $\pm$ ) tomato mutant line, *top3α-1*.
- B) The relative percentage of both the regular and small seeds from both the heterozygous ( $\pm$ ) tomato mutant lines, *top3α-1* and *top3α-2* and the corresponding WT control line. All seeds of more than 10 ripe fruits from five plants, for each line were counted. Three independent assays were conducted in total, with the means shown as columns and the error bars shown depicting the standard deviations of the mean. Statistical differences were calculated using a two-tailed *t*-test with unequal variances: \* $P < 0.05$ . The heterozygous ( $\pm$ ) tomato mutant lines, *top3α-1* and *top3α-2* had an increased number of small seeds, then for the WT control line, in which amounted to an increase of around 25 %.

As anticipated, in relation to the WT control line with 100 % regular seeds, both *stop3α-1* and *stop3α-2* heterozygous mutant lines did have an increased number of small (< 1 mm) seeds, and these seeds did account for approximately 25 % of the total number of seeds. The seeds within both of the heterozygous *top3α* mutant lines were therefore made up of around 75 % regular seeds, which were larger than 1 mm, and around 25 % small seeds that were smaller

than 1 mm in size (Figure 3.17.B). As a way to test the hypothesis that the percentage and therefore ratio of the small seeds corresponded to a quarter of all seeds, a chi-squared ( $\chi^2$ ) test was performed (Table 3.2).

**Table 3.2.** Percentage of regular and small seeds in both of the *top3a* heterozygous lines, compared to the expected when the small seeds correspond to the homozygous progeny and the regular seeds account for WT and heterozygous.

| Line                 | Regular seeds (%) | Small seeds (%) | 1:2 Mendelian segregation<br>$\chi^2 < 3.84$ |
|----------------------|-------------------|-----------------|--|
| Expected             | 75 %              | 25 %            |  |
| <i>sltop3a-1 +/-</i> | 73.6 %            | 26.4 %          | 0.74   |
| <i>sltop3a-2 +/-</i> | 75.0 %            | 25.0 %          | 1.00   |

In doing this, the hypothesis was verified as the results obtained from the seed count analysis corroborates with the expected of 75 % regular seeds and 25 % small seeds. As a result, the 75 % regular seeds would include the WT and heterozygous progeny, and the 25 % would be the homozygous progeny, as per Mendelian segregation. Therefore, as this was the case for both of the heterozygous mutant lines *top3a-1* and *top3a-2*, it was deemed that the small seeds (< 1 mm) may account for the null homozygous mutant progeny of the heterozygous lines. The small seeds and thus the homozygous mutant progeny was hence characterised as non-viable, as the small seeds were not able to germinate at all. The lack of ability to germinate could be realistically explained by the progeny having severe defects in embryonic development and therefore the null homozygous mutants being embryo lethal. This led to the plausible belief that, if these seeds were the actual homozygous *top3a* null mutants, then TOP3a could potentially have an essential role in tomato. Such a fundamental role was not postulated beforehand, due to the knowledge that homozygous *top3a* Arabidopsis mutants are viable (Dorn *et al.*, 2018), something that was previously considered to be conserved throughout all plants, as with most Arabidopsis findings.

## 4. Discussion

The RTR complex is an integral factor in ensuring genome stability in eukaryotes, with factors having roles in both DNA repair and homologous recombination, and being fundamental for the dissolution of double Holliday junction (dHJ) recombination intermediates. The factors of the RTR complex have been extensively studied across kingdoms, with mutants exhibiting characteristic phenotypes such as hyperrecombination and increased sensitivity to genotoxins. In animal models, TOP3 $\alpha$ , the type 1A topoisomerase RTR complex partner, was shown to be essential for viability, which was not the case when analysed in the plant model species *Arabidopsis*. In *Arabidopsis*, *top3a* mutants are viable with mutants showing extensive defects in DNA repair mechanisms, as is also the case with mutants deficient in RMI1 (Bonnet *et al.*, 2013; Dorn *et al.*, 2018). In contrast to other eukaryotes, both TOP3 $\alpha$  and RMI1 were also found to be fundamental for proper meiotic progression, with both proteins showing dual roles in DNA repair and meiosis (Chelysheva *et al.*, 2008; Hartung *et al.*, 2008). Not observed across all kingdoms, such a dual role for these two RTR complex partners is surprising. Therefore, it is interesting to decipher whether this is the case across all plants, and thus represents a plant-specific role, or not.

In this thesis, Cas9-based mutagenesis was used in order to generate mutants of both of the RTR complex partners, Topoisomerase 3 $\alpha$  (TOP3 $\alpha$ ) and RecQ-mediated genome instability protein 1 (RMI1), in tomato using Micro-Tom as a model system (Martí *et al.*, 2006). Through analyses and therefore characterisation of the mutants, an understanding of the functional roles of TOP3 $\alpha$  and RMI1 in tomato was deciphered for the first time, aiding with current understanding of the RTR complex and its factors during both DNA repair and meiosis in tomato.

### 4.1 Characterisation of TOP3 $\alpha$ and RMI1 tomato homologues

As part of the highly conserved RTR complex that is fundamental in maintaining genome stability, homologues of TOP3 $\alpha$  and RMI1 are prevalent throughout all eukaryotic kingdoms, with insights into their functional roles known in yeast, animals and plants (Wu and Hickson, 2003). All mutants of RTR complex partners exhibit characteristic phenotypes of hyperrecombination and sensitivity to genotoxins, which was notably the same as for the mutants analysed in plants, whereby *Arabidopsis thaliana* was used as the model plant system (Bonnet *et al.*, 2013; Dorn *et al.*, 2018; Hartung *et al.*, 2008; Chelysheva *et al.*, 2008; Röhrig *et al.*, 2016). However, mutants of both TOP3 $\alpha$  and RMI1 in *Arabidopsis* were also found to exhibit a surprising dual role, with both being indispensable for proper meiotic progression,

alongside being essential for the repair of DNA damage. Interestingly, such functional roles were not identified for the tomato homologues of TOP3 $\alpha$  and RMI1, with mutants displaying different phenotypes to those described for Arabidopsis mutants.

#### 4.1.1 Identification of the RMI1 and TOP3 $\alpha$ tomato homologues

Bioinformatic analyses were initially carried out in order to identify the putative homologues of both TOP3 $\alpha$  and RMI1 in tomato, using both the knowledge and sequence data of the Arabidopsis orthologous proteins. Homology searches using the genomic sequences of both *AtTOP3a* and *AtRMI1*, led to the identification of potential homologous genes within the genome of *Solanum lycopersicum*. It is not surprising that homologues of both RTR factors were identified within tomato, as the proteins functioning as part of the RTR complex are highly conserved across all kingdoms, owing to their fundamental roles within DNA repair pathways (Bizard and Hickson, 2014; Wyatt and West, 2014). Previous analyses investigating the RECQ helicase in tomato have already been conducted, whereby it was found that there is a single tomato RECQ4 homologue, functionally homologous to the RECQ4A paralogue in Arabidopsis, and to HsBLM, and ScSgs1 (Hartung *et al.*, 2008; Mieulet *et al.*, 2018; Schröpfer *et al.*, 2014), which is notably also the case for rice and the moss *Physcomitrella patens* (Hartung and Puchta, 2006). For TOP3 $\alpha$  and RMI1, single homologous genes were identified within tomato. The tomato homologous genes, termed *SITOP3 $\alpha$*  and *SIRMI1*, are around 68 % and 49 % identical in nucleotide sequence to the Arabidopsis homologues, respectively. This similarity stems mostly from the coding regions of the genes, in which encode for the highly conserved protein domains, that are fundamental for the functional roles of TOP3 $\alpha$  and RMI1 in all eukaryotic organisms. Using bioinformatics tools, the protein sequences and the protein domains were analysed for both *SITOP3 $\alpha$*  and *SIRMI1*. For RMI1, the putative tomato homologue consists of 659 aa and was found to harbour the N-terminal DUF1767 domain and the two oligonucleotide/oligosaccharide binding-fold domains, OB1 and OB2 (Figure 3.1), all three of which are apparent together in mammals and Arabidopsis (Bonnet *et al.*, 2013; Yin *et al.*, 2005). Both the DUF1767 domain and the OB1-fold domain were shown to be fundamental for the functional role of *AtRMI1* in DNA cross-link repair, in addition to the roles demonstrated within meiotic recombination (Bonnet *et al.*, 2013; Hartung *et al.*, 2008). Therefore, with the presence of these essential domains within the tomato RMI1 homologue, in addition to the known function of RMI1 in Arabidopsis, it was speculated that such roles within DNA repair and meiosis would also be observed in tomato. Moreover, with the tomato homologue also harbouring the second OB-fold domain, OB2, which was shown to allow for

the interaction with the fourth RTR complex partner RMI2 in mammals, *C. elegans* and more recently in Arabidopsis (Röhrig *et al.*, 2016; Singh *et al.*, 2008; Xu *et al.*, 2008), it was postulated that tomato would also have this fourth complex partner. Therefore, as was carried out for RMI1, bioinformatics tools were used to conduct homology searches using the Arabidopsis *RMI2* genomic sequence (Röhrig *et al.*, 2016). Consequently, a homologous gene was identified as a putative tomato RMI2 homologue, which was 56 % identical in nucleotide sequence to *AtRMI2*. With this, it could be proposed that as in Arabidopsis, RMI2 is a partner of the RTR complex in tomato, and may interact with RMI1 and have important roles in stabilising the RTR complex during the dissolution pathway of homologous recombination. However, confirmation of this should be conducted *in vivo* for further clarification. Within the OB1-fold domain of the RMI1 homologues in both humans and Arabidopsis, a conserved lysine was found to be an essential amino acid allowing for the interaction of RMI1 and TOP3 $\alpha$  (Bonnet *et al.*, 2013). This lysine amino acid was also observed in the tomato RMI1 homologue (Figure 3.1), and thus implies potential conservation of such an interaction between the two RTR complex partners in tomato.

The TOP3 $\alpha$  homologue in tomato consists of 915 aa and is comprised of six domains (Figure 3.11.A), similar to *AtTOP3 $\alpha$*  in which is 926 aa in length with the same six domains (Dorn *et al.*, 2018). On a protein level, *SITOP3 $\alpha$*  was found to be 70 % identical to *AtTOP3 $\alpha$* , in terms of amino acid sequence. As with all type IA and type II topoisomerases, in both eukaryotic and prokaryotic organisms, respectively, the N-terminus of *SITOP3 $\alpha$*  harbours a TOPRIM domain. Within the central domain of *SITOP3 $\alpha$* , the catalytic tyrosine residue was determined via amino acid sequence alignment, which has been deemed essential for the topoisomerase activity of TOP3 $\alpha$  and is conserved in all known eukaryotic type I topoisomerases (Shuman *et al.*, 1989). Both the TOPRIM and the active centre domains are known to be fundamental for the binding and breaking of DNA, in order to change the topological state of DNA molecules during DNA repair mechanisms. The C-terminus of the tomato TOP3 $\alpha$  homologue, consists of four zinc-finger domains (ZFDs), in which are all also present within *AtTOP3 $\alpha$*  (Dorn *et al.*, 2018). The first ZFD, T1, is conserved in all TOP3 $\alpha$  homologues across higher eukaryotes, and is typical for type IA topoisomerases. In Arabidopsis, in addition to the T1 and GRF ZFDs, two types of CCHC ZFDs (ZnFCCHC1/2) are also present, although only ZFD T1 was shown as essential for targeting and thus the resolution of HR intermediates in Arabidopsis, with no special role identified for GRF or ZnFCCHC1/2 (Dorn *et al.*, 2018). As demonstrated schematically in Figure 3.11.A, the arrangement and number of the ZFDs differs between species with the yeast TOP3 $\alpha$  homologue not possessing any ZFDs, and mammalian and human

TOP3 $\alpha$  differing to TOP3 $\alpha$  in Arabidopsis, with no CCHC ZFDs. From this, it seems that the tomato TOP3 $\alpha$  is similar to TOP3 $\alpha$  in Arabidopsis, and thus may also show similar functional roles to the model plant species, that has been shown to differ to those observed for other eukaryotic organisms (Dorn *et al.*, 2018; Hartung *et al.*, 2008).

As both of the putative RMI1 and TOP3 $\alpha$  tomato homologues identified were found to be comparable to those in Arabidopsis, following bioinformatical analyses, it was of interest to see whether the RTR complex partners in tomato would also demonstrate similar functions as identified for Arabidopsis, representing plant-specific functional roles for both DNA repair and meiosis. Consequently, mutants of both RMI1 and TOP3 $\alpha$  in tomato were generated in order to conduct functional analyses to investigate their roles further.

#### **4.1.2 Cas9-mediated mutagenesis of *RMI1* and *TOP3 $\alpha$* tomato homologues**

In order to analyse and therefore characterise RMI1 and TOP3 $\alpha$  in tomato, mutant lines for each factor were initially generated via a reverse genetics approach. For this, the CRISPR/Cas9 gene editing system was used (Jinek *et al.*, 2012). CRISPR/Cas9 is a site-specific nuclease technology, that allows for targeted gene editing, and therefore targeted mutagenesis. The Cas9 nuclease is directed to a specific target sequence by a programmable short synthetic gRNA sequence within a single guide RNA (sgRNA). Cas9 cleaves the target sequence, inducing a DSB 3-4 nucleotides upstream of the protospacer adjacent motif (PAM), a 5'-NGG located immediately after the target DNA sequence (Jinek *et al.*, 2012). In most instances, as the most prevalent repair mechanism of DSBs in somatic plant cells, these DSBs are then repaired by the NHEJ repair pathway. As a result of the error-prone nature of NHEJ, repair of the DSBs can lead to mutations in the form of insertions and deletions within the gene of interest. Such mutations ultimately cause a shift in the translational open reading frame (ORF) of the coding sequence, known as a frameshift. With this, a premature stop codon within the shifted ORF can arise which leads to an arrest in further protein translation, as long as no alternative start codon is within frame (Puchta and Fauser, 2014). The result is thus a functionally redundant, residual protein being translated, and a knock out of the target of interest.

Naturally functioning as part of a prokaryotic adaptive immune system against viral infections, the significant discovery of CRISPR and the associated *Cas* genes has revolutionised the field of genetic engineering, with biotechnological applications now being at the forefront of most pioneering work in both agriculture and medicine (Ishino *et al.*, 1987; Jinek *et al.*, 2012; Liu *et al.*, 2017; Mojica *et al.*, 2005), CRISPR/Cas9 techniques have since been used to edit the

genomes of a vast array of organisms, including a large number of plant species and more recently, an increasing number of crop plant species (reviewed in Jaganathan *et al.*, 2018).

For this thesis, the Cas9 orthologue from *Streptococcus pyogenes* was used as part of a plant-specific CRISPR/Cas9 expression system, as described by (Fauser *et al.*, 2014) (see Section 2.2.1.5), in order to perform Cas9-mediated mutagenesis of RMI1 and TOP3 $\alpha$  in the tomato cultivar Micro-Tom. For mutagenesis of *SIRMI1*, a CRISPR/Cas9 expression vector was generated that incorporated a spacer sequence targeting Cas9 to a specific region within the first exon of *SIRMI1* (see Figure 3.1.B). Targeting of this specific site within exon 1 was a strategic decision in order to ensure complete knockout of RMI1 via the formation of a residual, functionally redundant protein. The chosen locus was at the start of the coding region for the DUF1767 domain, assumed to be essential for the functional roles of RMI1 in plants, based on previous analyses conducted in Arabidopsis (Bonnet *et al.*, 2013; Hartung *et al.*, 2008). As a result of this approach, two acceptable mutant plants were identified within the T1 generation of the transgenic plants harbouring the CRISPR/Cas9 constructs, which were further propagated in order to establish mutant lines (see Section 2.2.3.4). The resultant mutant lines, *slrmi1-1* and *slrmi1-2*, had a 1 base pair insertion and 4 base pair deletion, respectively, at the beginning of the DUF1767 protein domain coding sequence.

A similar principle was applied for the mutagenesis of the second RTR complex partner, *SITOP3 $\alpha$* . As with the mutagenesis of *SIRMI1*, the same CRISPR/Cas9 expression constructs were used with the *S. pyogenes* Cas9 orthologue, but in this case, the spacer sequence was programmed to target the Cas9 to the beginning of the first exon within the *TOP3 $\alpha$*  genomic sequence (see Figure 3.11.B). In doing this, mutations were generated at the start of the coding sequence for the TOPRIM protein domain. Two *sltop3 $\alpha$*  mutant lines were therefore generated termed *sltop3 $\alpha$ -1* and *sltop3 $\alpha$ -2*, which had a 1 bp insertion and 1 bp deletion, respectively.

For confirmation of the deleterious effect of the induced mutations on the protein-coding sequence for both *SIRMI1* and *SITOP3 $\alpha$* , the mutations were analysed on an mRNA level. RNA was extracted from plants of the established mutant lines, and the cDNA was analysed via Sanger sequencing. When aligned with the cDNA sequence of the corresponding WT version of the sequence, the Cas9-induced mutations could be visualised and thus confirmed (Figure 3.2; Figure 3.12). From this, the mutations were seen to be preserved following splicing events and the premature stop codons within the shifted ORFs could be seen, highlighting the termination of translation, implying the formation of only a residual, functionally redundant protein for both *SIRMI1* and *SITOP3 $\alpha$* . Moreover, subsequent propagation of the mutant lines, and sequencing of the target genes confirmed inheritance of the mutations through the germline.

Subsequently, via Cas9-mediated mutagenesis of both RMI1 and TOP3 $\alpha$  homologues in tomato, and the resultant generation of mutant lines, functional characterisation of both of these RTR complex partners was conducted in tomato for the first time, providing insights into the mechanisms of both DNA repair and meiosis in tomato, and related crop species.

#### 4.1.3 Characterisation of the functional role of RMI1 in tomato

Following Cas9-mediated mutagenesis of the *RMI1* homologue in tomato, the two mutant lines *slrmi1-1* and *slrmi1-2* were identified within the T1 generation, which both originated from independent mutagenic events, and harboured a 1 bp insertion and 4 bp deletion mutation, respectively. Within the T1 generation, via HRM analysis and Sanger sequencing (described in Section 2.2.3.4), both of the mutant lines were identified as heterozygous, meaning that they each had one mutant allele harbouring their respective mutation, and one allele that corresponded to the WT version of RMI1. When propagated to obtain the T2 generation, as a result of Mendelian segregation, a quarter of the plants were identified as homozygous mutants, with both alleles of RMI1 harbouring the mutations. Consequently, the homozygous T2 mutant plants, for both *slrmi1-1* and *slrmi1-2* mutant lines were further propagated by selfing for analysis. From germination of the seeds and throughout the growth of the seedlings into fully mature plants with flowers and ripe fruits, all plants of the T3 generation for both mutant lines did not show any distinguishable growth phenotype, when compared to corresponding WT plants (Figure 3.3. *slrmi1-1* and *slrmi1-2* homozygous mutant plants compared to wild type (WT)). Therefore, in terms of vegetative growth, the two mutant lines *slrmi1-1* and *slrmi1-2*, did not appear to show any defects, even with regard to flower and fruit number and morphology. Arabidopsis *rmi1* mutant plants also do not show any defects in vegetative growth, with plants being comparable to WT, except for apparent shorter siliques which is a characteristic distinguishable feature of fertility issues. The reduced silique lengths of the null *rmi1* mutants in Arabidopsis are indeed indicative of the severe fertility defects that ultimately amount to sterility (Chelysheva *et al.*, 2008; Hartung *et al.*, 2008). Surprisingly, fruits from all homozygous plants of both *slrmi1-1* and *slrmi1-2* tomato mutant lines did harbour seeds. The fact that seeds were obtained from *rmi1* homozygous tomato mutant plants provided substantial evidence that *rmi1* tomato mutants are indeed not sterile. This initial result demonstrated that RMI1 may differ in its functional role in tomato, compared to that in Arabidopsis.

#### 4.1.3.1 Fertility analysis of *slrmi1* mutant lines

Given the fact that *rmi1* tomato mutants are fertile, further analyses were required to investigate the level of fertility. Consequently, following further propagation of the homozygous *rmi1* mutant lines, *slrmi1-1* and *slrmi1-2*, in order to obtain a sufficient seed number, subsequent analyses employing various techniques were carried out to investigate the fertility of the mutant lines. Firstly, the seed quantity per fruit was analysed. For this, ripe fruits from both of the two *rmi1* mutant lines and a corresponding WT line were harvested and the seeds within each fruit were counted. It must be clarified that throughout all analyses within this work whereby mutant lines were compared to WT in order to determine potential phenotypes, all plants were grown under the exact same conditions, from initial sowing of the seeds, transfer to soil and subsequent growth and maturity in the greenhouse. These conditions included the temperature, light, humidity and other external factors but also included the composition of the soil used and the volume and size of the pots that each plant were grown in. When conducting comparison studies, such considerations are crucial due to the potential effects certain external factors can have on both the vegetative growth and fertility of tomato plants, an example being that restrictive root growth using lower volume pots has been shown to increase fertility for some tomato cultivars at specific temperatures (Dominguez *et al.*, 2002). Therefore, when comparing the seed quantity per fruit between the *slrmi1-1* and *slrmi1-2* mutant lines and WT, it could be justified that any differences observed would be a result of the mutant plants being deficient in RMI1, and not because of any additional variables. However, the seed count analysis actually revealed that there are no differences between the two *rmi1* mutant lines and the WT line, with neither mutant line showing any significant reduction in the average number of seeds per fruit (Figure 3.4) compared to WT. This observation implies that the fertility of *rmi1* mutant plants is not reduced and corresponds to that of WT level, suggesting that *rmi1* tomato mutants are not just fertile, but fully fertile.

Due to the surprising nature of this revelation, an additional fertility analysis was conducted for confirmation. As a result, analysis of the pollen grains obtained from mature flowers was carried out via FDA staining and microscopy techniques. Both the presence and viability of pollen grains provides beneficial insights into the fertility of plants, due to pollen being the product of successful meiotic progression. FDA staining, as per the protocol described by Heslop-Harrison and Heslop-Harrison (1970), provides a method in which viable pollen spores can be distinguished from those that are non-viable, due to differential fluorescing of the spores with viable pollen fluorescing and non-viable ones not fluorescing. As a result, all visible pollen spores liberated from anthers of mature, open flowers for both of the mutant lines *rmi1-1* and

*rmi1-2* were quantified, and the percentage of viable pollen spores were compared to that of the WT control line. As illustrated in Figure 3.5, there was no significant difference in the mean percentage of viable pollen between the two *rmi1* tomato mutant lines and WT. Given that there was no difference between the average number of seeds per fruit between mutants and WT plants, implying full fertility of *rmi1* mutants, no reduction in pollen viability was expected, as viable pollen in which is metabolically active, is essential for proper pollen fertilisation and thus the generation of seeds. Nevertheless, neither result was actually expected for *rmi1* mutants prior to these fertility analyses being conducted, due to the sterility of *rmi1* mutants in *Arabidopsis* (Bonnet *et al.*, 2013; Chelysheva *et al.*, 2008; Hartung *et al.*, 2008).

Despite having not been observed for the vast majority of eukaryotic organisms, a lack of RMI1 in *Arabidopsis* was shown to render the plants sterile due to the catastrophic defects during meiosis, owing to the essential functional role of this RTR complex partner for normal meiotic progression (Chelysheva *et al.*, 2008; Hartung *et al.*, 2008). Similar roles for RMI1 homologues within meiotic recombination have only been described for *S. cerevisiae* and *C. elegans* (Gangloff *et al.*, 1999; Goodwin *et al.*, 1999; Wicky Collaud *et al.*, 2004), representing unique roles not conserved throughout all eukaryotes. As not observed for animals, this unforeseen fundamental role of RMI1 during the latter stages of meiotic recombination in *Arabidopsis* was postulated to be indicative of a plant-specific role (Chelysheva *et al.*, 2008; Hartung *et al.*, 2008). Therefore, despite the previous findings that *rmi1* tomato mutants seem to be fully fertile, DAPI-staining of chromatin was performed to ascertain whether meiosis is affected in any way by the absence of RMI1 in tomato. For this, chromosome-spreading techniques as described by Armstrong and Jones (2001), were performed for both *slrmi1-1* and *slrmi1-2* and the corresponding WT control line, and the cytologically distinct stages of meiosis were visualised using a fluorescent microscope, and compared to that of WT (see Section 1.4). In order to sufficiently compare meiosis within the mutant lines to that of WT, it was imperative that wild-type meiosis in tomatoes was fully understood, as a means to determine what is considered normal and what is not. Fortunately, due to the relatively large genome of tomato plants and therefore the resultant large chromosomes, tomato is particularly well-suited to cytogenetic analyses and was at the forefront of the field during its emergence, prior to use of *Arabidopsis thaliana* as the model plant species. Moreover, tomato was one of the initial species used for the early meiotic studies, which led to the basic understanding of meiosis and meiotic progression across all eukaryotic kingdoms (Lhuissier *et al.*, 2007; Lindstrom and Koos, 1931; Ramanna and Prakken, 1967; Sherman and Stack, 1995). In tomato, chromosome behaviour during meiosis is analogous to that of *A. thaliana*, with the same stages and events taking place

(Brukhin *et al.*, 2003). Prominently, much of our current knowledge and understanding of meiosis and meiotic recombination were deduced following extensive studies conducted using *A. thaliana*. With an abundant array of meiotic mutant lines and reporter lines, cytogenetic and immunocytological techniques were further improved using Arabidopsis, thus becoming the species of choice for most meiotic studies (Armstrong and Jones, 2003; Armstrong and Jones, 2001; Ross *et al.*, 1996). Tomato, importantly, has a larger genome than Arabidopsis, with 12 chromosomes in a diploid cell, compared to only five in Arabidopsis. Therefore, throughout diplotene and metaphase I, 12 bivalents comprised of two homologous chromosomes linked together by chiasmata, can be distinguished easily (see Figure 3.6). Analysis of all of the individual stages of meiosis through to the formation of haploid pollen spores was carried out as a way to determine whether lack of RMI1 in tomato leads to any visible meiotic defects or not. Astonishingly, as illustrated in Figure 3.6, DAPI-staining of the chromatin for both *rmi1* homozygous mutant lines confirmed that meiosis progresses normally in tomato in the absence of RMI1, with no increased number of defects observed, compared to WT. Both chromosome structure and behaviour were as expected for each of the various cytologically distinct stages of both meiosis I and meiosis II (see Section 1.4). During prophase I of meiosis I, both *slrmi1-1* and *slrmi1-2* showed full synapsis of the homologous chromosomes by completion of pachytene, with the expected 12 bivalent structures being prevalent at diplotene (Figure 3.6). As in WT meiosis, there were no apparent defects during anaphase I, with the separation of the homologous chromosomes. This differs drastically to the detrimental meiotic defects observed for *rmi1* mutants in Arabidopsis, in which chromosome entanglement during metaphase I leads to the formation of chromatin bridges and extensive chromosomal fragmentation in anaphase I, defects in which are so severe that meiotic arrest occurs resulting in no further progression to meiosis II (Chelysheva *et al.*, 2008; Hartung *et al.*, 2008). Nevertheless, this does not appear to be the case in tomato, with null *rmi1* mutants showing balanced dyad formation by the end of anaphase I, with each dyad harbouring 12 chromosomes, as in WT (Figure 3.6). Following the successful completion of meiosis I, the progression of meiosis II also appeared indistinguishable to WT, for both *rmi1-1* and *rmi1-2*, with no defects observed at any stage, including anaphase II, resulting in balanced tetrad formation and thus successful completion of meiosis. Consequently, in stark contrast to the meiotic phenotype in Arabidopsis (Chelysheva *et al.*, 2008; Hartung *et al.*, 2008), it could be deduced that lack of RMI1 in tomato does not seem to have an effect on meiosis, with meiotic progression taking place in a comparable manner to WT, for both of the null homozygous mutant lines. As a result, coinciding with the

previous findings, analysis of meiosis via DAPI-staining confirmed that *rmi1* null mutants are fully fertile, demonstrating that RMI1 does not have a fundamental role in meiosis in tomato. With limited studies on the role of RMI1 in other plant species besides *A. thaliana*, it cannot be deduced whether this difference in meiotic function of RMI1 between Arabidopsis and tomato is a phenomenon observed in other plant species as well. However, Li *et al.*, (2022) recently reported that for the dicotyledonous ornamental plant species *Gerbera hybrida*, a member of the *Asteraceae* plant family, the *RMI1* homologue has a higher expression level in flower buds than other tissues and stages, relative to a suitable reference gene. This significant differential expression in buds, the tissue in which meiosis takes place, implies that the RMI1 *G. hybrida* homologue possibly plays a functional role within meiotic recombination mechanisms. However, further analysis and functional characterisation are needed to ascertain whether this is the case or not. Nonetheless, this preliminary insight does present a case which differs to the one presented in this thesis, whereby RMI1 was not found to be involved in meiosis or meiotic recombination in tomato.

Considering all of the aforementioned results obtained from the fertility analyses of the null *rmi1* tomato mutant lines, it seems that tomato plants lacking the RTR complex partner RMI1 are fully fertile, with meiosis progressing as normal. Consequently, this provides the first inclination of a stark contrast between the functional role of RMI1 homologues between tomato and Arabidopsis, with RMI1 seemingly not having any role in meiosis, which is fundamentally different to the essential role for RMI1 in Arabidopsis.

#### **4.1.3.2 The role of SIRMI1 in somatic DNA repair mechanisms**

In Arabidopsis, RMI1 plays an integral role in somatic DNA repair, with mutants exhibiting hyperrecombination, and increased sensitivity to genotoxins, the characteristic phenotypes apparent for all RTR complex partners (Bonnet *et al.*, 2013; Hartung *et al.*, 2008). As the tomato RMI1 homologue was not found to have a role in meiosis, various analyses were conducted in this work to determine whether RMI1 at least plays a role in somatic DNA repair, as it does in Arabidopsis. In order to do this, the *rmi1* tomato mutant lines were subjected to treatment of various genotoxic agents to observe potential sensitivities. Therefore, seedlings of both of the homozygous mutant lines, *rmi1-1* and *rmi1-2*, were treated with genotoxic agents and the measurements of the fresh weight after a period of growth were analysed, and normalised to that of an untreated control, in order to establish whether the mutants showed any sensitivity to genotoxins, in relation to a WT control (Figure 3.7; Figure 3.8). Arabidopsis *rmi1* mutant plants were shown to exhibit increased sensitivity to both the crosslinking agent *cis*-Platin and the

methylating agent methylmethanesulfonate (MMS) (Hartung *et al.*, 2008), corroborating with the role of RMI1 being required for the repair of certain kinds of DNA damages, as part of its supportive role within the RTR complex. However, treatment of both tomato *rmi1* mutant lines with both *cis*-Platin and MMS, did not reveal any sensitivity to either of these genotoxic agents, with sensitivities being comparable to the level observed for WT (Figure 3.7; Figure 3.8). In addition to this, no increased sensitivities were observed for either *slrmi1-1* or *slrmi1-2* when treated with the topoisomerase 1 inhibitor, camptothecin (CPT), or the crosslinker mitomycin C (MMC), implying no functional role of RMI1 in tomato in the repair of interstrand crosslinks (CLs). The fact that tomato *rmi1* mutants did not show any increased sensitivities to either *cis*-Platin or MMS was definitely not anticipated, given that *rmi1* mutants in both Arabidopsis and yeast demonstrate increased sensitivities to both of these agents, owing to the role of RMI1 within the repair of intrastrand crosslinks and methylated DNA (Chang *et al.*, 2005; Hartung *et al.*, 2008). Moreover, expression analyses also confirmed that the expression of *SIRMII* is not induced following treatment with *cis*-Platin (Whitbread *et al.*, 2021), thus indicating that RMI1 in tomato is not a significant factor in the response mechanisms of genotoxin-induced DNA damage. Taken together, these results surprisingly imply that SIRMII does not possess a functional role within somatic DNA repair, at least for the repair of DNA damages induced by genotoxic agents.

Consequently, in a further attempt to elucidate a potential role for RMI1 within DNA repair, analyses were carried out in order to investigate cell division to analyse replication-associated repair. Utilising the highly replicative root meristem tissue in which the cells undergo multiple rounds of accelerated cell division, root length and cell viability analyses were conducted. In terms of the root length analyses, neither of the two homozygous *rmi1* mutant lines, *slrmi1-1* and *slrmi1-2*, showed any significantly decreased root lengths, compared to the WT control line (Figure 3.9). A decrease in root length occurs when there is an accumulation of spontaneous replication-associated DNA damage, leading to cell death and damage within the dividing cells of the root meristem, inhibiting normal root growth (Beemster and Baskin, 1998). Therefore, as the tomato *rmi1* mutants did not show any reduced root lengths, compared to WT, it seems that RMI1 in tomato is not involved in the repair mechanisms of such DNA damage. Analysis of cell viability within the root tips, using Evan's blue dye (see Section 2.2.3.7), also confirmed this, with no differences in the absorption of the azo dye for either of the two *rmi1* mutant lines compared to WT, indicating no differences in cell viability (Figure 3.10). Subsequently, RMI1 in tomato does not appear to be involved in the repair of replication-associated DNA damage. In humans, RMI1 was shown to play a role during replication stress, with mutant cells being

hypersensitive to the genotoxic agent hydroxyurea. Knockdown of RMI1 in human cells ultimately led to an accumulation of DNA damage, owing to the role of HsRMI1 in mediating the recovery and continuation of the cell cycle following spontaneous replication-associated DNA damage, acting to ensure loading of RAD51 onto the damaged sites (Xu *et al.*, 2017). However, the findings presented here do not portray such a similar functional role for RMI1 in tomato, whereby no functional role in the repair of any somatic DNA damage could be observed, for either replication-associated DNA damage or genotoxin-induced damage. Therefore, the RMI1 RTR complex partner in tomato does not seem to be involved in either meiotic mechanisms or somatic DNA repair processes, demonstrating surprising differences to the integral functional roles that the homologue plays in the model plant species *Arabidopsis* (Bonnet *et al.*, 2013; Chelysheva *et al.*, 2008; Hartung *et al.*, 2008).

#### 4.1.4 Characterisation of the functional role of TOP3 $\alpha$ in tomato

With the previously unforeseen knowledge that the role of RMI1 in tomato is fundamentally different to that observed for *Arabidopsis*, it was of interest to determine if this is also the case for additional factors of the RTR complex. Therefore, further analyses were conducted in order to try to characterise the TOP3 $\alpha$  homologue in tomato. Initial studies in *Arabidopsis* had previously led to some discrepancies in the mutant phenotype of *top3 $\alpha$* , with two T-DNA insertion mutant lines exhibiting distinctly differing phenotypes. The first mutant line *top3 $\alpha$ -1* exhibited a severe phenotype of non-viable plants (Hartung *et al.*, 2007a), comparable to that observed in other eukaryotes including *C. elegans*, *D. melanogaster*, and mice (Kim *et al.*, 2000; Li and Wang, 1998; Plank *et al.*, 2005), whereas the second mutant line *top3 $\alpha$ -2*, was viable due a less severe somatic phenotype (Hartung *et al.*, 2008). The second T-DNA mutant line was thus regarded as a hypomorph, with the *top3 $\alpha$ -1* phenotype postulated as that of the true null mutant. Nevertheless, this was recently revealed to not be the case following the generation of *top3 $\alpha$*  mutant lines via Cas9-mediated mutagenesis, whereby it was confirmed that *top3 $\alpha$*  null mutants in *Arabidopsis* are actually viable (Dorn *et al.*, 2018). Therefore, it was found that in contrast to the severe phenotype observed for other eukaryotic organisms, TOP3 $\alpha$  is not essential in plants as was first preconceived. In *Arabidopsis*, TOP3 $\alpha$  was found to still play significant roles in DNA repair mechanisms, with *top3 $\alpha$*  mutants harbouring somatic defects including increased sensitivity to genotoxins and enhanced HR, the characteristic phenotypes for mutants of the RTR complex partners. However, *Attop3 $\alpha$*  mutant plants were also shown to exhibit additional phenotypes including growth defects leading to dwarfism, fasciated organs and replication-associated DNA damage (Dorn *et al.*, 2018). Moreover, acting

as part of a sub-complex with RMI1, AtTOP3 $\alpha$  was demonstrated as essential for meiosis, with mutant plants being rendered sterile, despite their viability (Chelysheva *et al.*, 2008; Dorn *et al.*, 2018; Hartung *et al.*, 2008).

Prior to this current thesis, it was believed that this dual role for TOP3 $\alpha$  in Arabidopsis represents a plant-specific functional role, due to its lack of abundance throughout the majority of other eukaryotic kingdoms. The viability of *top3 $\alpha$*  mutants observed in Arabidopsis was also speculated to be representative of all plant species, as much of the insights from the model plant species are considered. Still, with the present understanding of the differences apparent between tomato and Arabidopsis for the functional roles of RMI1 (see Section 4.1.3), it was uncertain as to whether *top3 $\alpha$*  mutants in tomato would have the same mutant phenotypes as Arabidopsis. To investigate this, the two *top3 $\alpha$*  mutant plants identified following Cas-9-mediated mutagenesis in tomato (see Section 3.3.1), were used for further analysis. Both of the *top3 $\alpha$*  mutants, *sltop3 $\alpha$ -1* and *sltop3 $\alpha$ -2*, were identified as heterozygous mutants within the T1 generation, and were indistinguishable from WT, in terms of their somatic growth and morphology (Figure 3.13). For sufficient numbers of plants to conduct both somatic and fertility analyses, these lines were further cultivated within the greenhouse for propagation, to obtain the T2 generation. According to Mendelian segregation of genetics, the progeny obtained from a self-pollinated heterozygous plant should comprise of 25 % wild-type individuals, 25 % homozygous and 50 % heterozygous. Hence, it was unexpected when no homozygous plants were identified within the T2 generation for both independent mutant lines, *top3 $\alpha$ -1* and *top3 $\alpha$ -2*. In fact, DNA sequencing of a number of the plants from both lines confirmed that the proportion of the zygosity amounted to around two-thirds being WT, and the remaining one-third being heterozygous (Table 3.1). Statistical analysis confirmed that the Mendelian segregation was not the typical 1:2:1 segregation, as expected, but coincided with 1:2 segregation which implied that it would be highly unlikely to obtain homozygous mutant plants from the two *top3 $\alpha$*  heterozygous mutant lines. Consequently, at this point, it seemed plausible to speculate that homozygous mutations within TOP3 $\alpha$  in tomato may render the plants non-viable.

Although *top3 $\alpha$*  homozygous mutants could not be utilised, the heterozygous mutant lines were further investigated in an attempt to try to characterise the functional role of TOP3 $\alpha$  in tomato and gain insights into the detrimental somatic defects leading to non-viability. Interestingly, both *top3 $\alpha$ -1* and *top3 $\alpha$ -2* heterozygous lines showed a significantly reduced seed quantity, compared to that of a WT control line, with a reduction of approximately 25 % relative to WT (Figure 3.14). With the known meiotic defects and sterility of Arabidopsis *top3 $\alpha$*  homozygous

mutants, this was first believed to be a meiotic phenotype in tomato, with TOP3 $\alpha$  playing an essential role in meiosis, as in Arabidopsis (Chelysheva *et al.*, 2008; Dorn *et al.*, 2018; Hartung *et al.*, 2008). However, there were no associated reductions in either fruit set or fruit size that further suggested fertility defects of the TOP3 $\alpha$  heterozygous mutants (Figure 3.15). Pollen analysis via FDA staining (see Section 2.2.3.10) for both *top3 $\alpha$ -1* and *top3 $\alpha$ -2* also demonstrated no significant differences in the percentage of viable pollen grains for either of the two heterozygous mutant lines (Figure 3.16), further suggesting no fertility defects of heterozygous *sltop3 $\alpha$*  mutant plants.

Nonetheless, during dissection of fruits for seed collection in order to conduct the aforementioned analyses, it became increasingly apparent that a substantial number of small seeds were visible within the *top3 $\alpha$*  mutant lines (Figure 3.17.A). These small seeds had not been previously collected from fruits due to the use of a sieve in which had openings of 1 mm in width. Thus, any seeds less than 1 mm in size would not have been collected and would have been discarded along with the flesh and liquid components of the fruits. With the abundance of these smaller seeds within both *top3 $\alpha$ -1* and *top3 $\alpha$ -2*, it was hypothesised that they could potentially account for the homozygous progeny of the heterozygous mutant lines, in which had yet to be accounted for, although believed to be non-viable. Conscious collection and subsequent quantification of the small seeds (< 1 mm) did confirm this hypothesis, with the smaller seeds being representative of around 25 % of the total number of seeds for both heterozygous mutant lines, relative to a WT control line (Figure 3.17.B). The heterozygous mutant lines did, therefore, segregate according to the expected Mendelian segregation ratio of 1:2:1, as confirmed by statistical analysis (Table 3.2). The small seeds were thus deemed those of the homozygous *top3 $\alpha$*  mutant tomato plants. As the small seeds were unable to germinate, homozygous *top3 $\alpha$*  null mutants were once again found to be non-viable, with TOP3 $\alpha$  playing an essential role in tomato, with mutants likely being embryo lethal due to severe defects during embryonic development. These findings illustrate that TOP3 $\alpha$  differs in its role in tomato compared to that in Arabidopsis, with the topoisomerase playing a more fundamental role in tomato, reminiscent to that in mammals whereby mutant mice are also completely embryo-lethal (Li and Wang, 1998). This drastic phenotype in tomato is likely due to the accumulation of unresolved aberrant replication intermediates, given the known biochemical functions of TOP3 $\alpha$  in other organisms, which ultimately leads to cell death. TOP3 $\alpha$  is thus an indispensable factor of the RTR complex in tomato, with an essential role ensuring genomic stability, in contrast to the TOP3 $\alpha$  in Arabidopsis (Dorn *et al.*, 2018).

#### 4.1.5 The RTR-complex and dissolution pathway in tomato

In Arabidopsis, the RTR complex comprised of RECQ4A, TOP3 $\alpha$ , RMI1 and RMI2 (Chelysheva *et al.*, 2008; Dorn *et al.*, 2018; Hartung *et al.*, 2008, 2007; Röhrig *et al.*, 2016) was found to have the conserved role as observed across all kingdoms, with mutants of each complex partner exhibiting the characteristic phenotypes of hyperrecombination and hypersensitivity to genotoxins, owing to the integral function of the complex in the dissolution of recombination intermediates during HR. The RTR complex acts to dissolve recombination intermediates such as dHJs, generating a NCO product, therefore acting in an anti-CO promoting manner. During dissolution, RECQ4A causes the junctions of the dHJ molecule to move within close proximity to one another, via its branch migration activity, leading to the generation of a hemicatenane intermediate structure. AtTOP3 $\alpha$  subsequently cleaves the junctions of this molecule by its topoisomerase action, with both structural RMI proteins (RMI1 and RMI2) being essential for the stimulation and stabilisation of the complex (Bonnet *et al.*, 2013; Hartung *et al.*, 2008). Besides the aforementioned phenotypes of the RTR complex partners, AtTOP3 $\alpha$  and AtRMI1 were also shown to form a heterodimeric complex, indispensable for meiotic recombination, with mutants of each being rendered sterile as a result of the detrimental meiotic defects occurring during meiosis I (Chelysheva *et al.*, 2008; Hartung *et al.*, 2008). In Arabidopsis, this essential meiotic function of RMI1 involved in CO suppression, was shown to occur as a result of the N-terminus of the protein, with the C-terminal domain being responsible for the formation of the complex with AtTOP3 $\alpha$  (Bonnet *et al.*, 2013). Although maintaining a conserved role in Arabidopsis, some functional aspects of the RTR complex differ to that compared to in other eukaryotic organisms. TOP3 $\alpha$  was not found to be essential in Arabidopsis, for example, with mutants still remaining viable as opposed to the embryo lethality observed for mammals (Li and Wang, 1998). Moreover, the essential functions of both TOP3 $\alpha$  and RMI1 in meiotic recombination in Arabidopsis, is not apparent across all kingdoms and thus was speculated to be a plant-specific role.

Nevertheless, the findings of this current work proved otherwise and ultimately showed that the RTR complex partners, TOP3 $\alpha$  and RMI1, actually show differing roles in tomato compared to that in Arabidopsis, despite being similar on a sequence level. In tomato, using Micro-Tom as a model system, TOP3 $\alpha$  was found to be essential for maintaining genome stability with mutants thought to be embryo-lethal, in contrast to the viable mutant phenotype of *Attop3 $\alpha$*  mutant plants. Therefore, it seems that TOP3 $\alpha$  plays a more prominent role in tomato than in Arabidopsis, highlighting a different intensity of the role between both plant species. Furthermore, surprisingly, RMI1 was found to not be essential for meiotic recombination in

tomato, with mutant plants being fully fertile, with no meiotic defects at all suggestive of a role for this RTR complex partner in meiosis. RMI1 in tomato also does not appear to have a functional role in somatic DNA repair either, with mutant lines showing no defects in somatic DNA repair induced by genotoxins or in the repair of replication-associated DNA damage. From this, it seems that SIRMI1 does not demonstrate the conserved roles, as apparent in Arabidopsis and the majority of other eukaryotes, in terms of somatic DNA repair. With neither a somatic or meiotic role for SIRMI1 in DNA repair mechanisms, it can be assumed that RMI1 is not essential in its roles in stabilising and stimulating the RTR complex in tomato.

In yeast, the RMI1 homologue, Rmi1, was shown to mediate binding of Top3 to both dHJs and ssDNA, with biochemical studies suggesting that the structural protein mediates the opening and closing of the topoisomerase gate of Top3, thus regulating the decatenation activity of the protein (Bocquet *et al.*, 2014; Cejka *et al.*, 2012). However, with no somatic or meiotic defects in tomato plants lacking RMI1, it can be assumed that this regulation is either not required in tomato, or that the action of another factor comes into play either in the absence of RMI1, or even in its presence. As a homologue of RMI2 was identified in tomato, via bioinformatic analyses, it could be postulated that RMI2, as an additional partner of the RTR complex in plants, may account for the functional roles of RMI1 known in Arabidopsis. RMI2, conserved in mammals and plants, was found to be involved in the repair of intrastrand crosslinks and aberrant replication intermediates within the root meristem of Arabidopsis plants, although mutant phenotypes were not as prominent as those for the other RTR complex partners (Röhrig *et al.*, 2016). Previously, the role of RMI2 in Arabidopsis would have thought to have been conserved for all plants, however, with the knowledge of this current work and the differences observed in the functional roles of both RMI1 and TOP3 $\alpha$  in tomato, that assumption no longer holds ground. As a result, it would be interesting to elucidate the role of RMI2 in tomato, both in the presence and absence of the RMI1 homologue, with the generation of *rmi2* mutant lines and double mutant lines.

Although RMI2 is a possible candidate for taking over the functional roles of RMI1 in tomato, it could also be the case that neither of the RMI paralogues are required at all for the stabilisation of the RTR complex. RMI2 is not conserved in all eukaryotic organisms, with homologues only present in mammals, plants and *C. elegans* (Röhrig *et al.*, 2016; Singh *et al.*, 2008; Velkova *et al.*, 2021). In the insect *Drosophila melanogaster*, there is no RMI1 orthologue at all, with an insertion within the N-terminus of DmTOP3 $\alpha$  being shown to substitute the role of RMI1 (Chen *et al.*, 2012). Therefore, it is evident that the presence of RMI1 within the RTR complex is not conserved in all eukaryotes, and that genome stability is still ensured even in the absence of

RMI structural proteins. Despite RMI1 homologues demonstrated as essential in fission yeast and mice (Chang *et al.*, 2005; Guiraldelli *et al.*, 2013; Li and Wang, 1998), and known as a key component of the RTR complex, RMI1 has no catalytic activity itself, as shown by studies *in vitro*, and no biochemical properties accounting for its contribution in the dissolution of recombination intermediates, besides its role as a structural protein and ability to interact with both RECQ4A/BLM and TOP3 $\alpha$  (Wang *et al.*, 2010). As a result, the stabilisation and structural functions of SIRMI1 within the RTR complex could potentially be taken over by alternative factors in tomato.

#### 4.1.6 Hypothesised model for the dissolution pathway in tomato

Meiotic chromosome association 1 (MEICA1) is a protein that was recently identified in rice by Hu *et al.*, (2017), whilst performing a forward genetics screen to identify factors involved in meiosis. Due to the plants being sterile, a mutant line was found in which displayed aberrant chromosome interactions, with ectopic chromosomal associations during metaphase I, extensive chromosome bridges and fragmentation in anaphase I of meiosis I. The corresponding gene for these severe meiotic defects was deemed *MEICA1*, which encodes for a protein containing a DUF4487 domain, which has no clearly defined molecular function. Homology searches revealed that homologous proteins harbouring a DUF4487 domain are apparent throughout all eukaryotes and thus represents a highly conserved protein domain. The meiotic defects described for the sterile *meica1* mutants in rice, including chromosomal bridges and extensive fragmentation during anaphase I, are interestingly reminiscent to the severe meiotic defects of both *Arabidopsis top3 $\alpha$*  and *rmi1* mutants (Chelysheva *et al.*, 2008; Hartung *et al.*, 2008). Therefore, it was postulated as to whether MEICA1 could be a potential candidate as a replacement factor for the functional roles of RMI1. This speculation was further supported given the fact that MEICA1 was shown to be involved in recombination outcome determination, thought to act in the processing of recombination intermediates, and was demonstrated as indispensable for the later steps of meiotic recombination. Furthermore, OsMEICA1 was shown to interact with OsTOP3 $\alpha$ , functioning in an anti-CO manner (Hu *et al.*, 2017). Taking all of the information together on OsMEICA1, it seems that MEICA1 could potentially substitute RMI1 as the interactive partner involved in the dissolution of joint molecule intermediates during meiotic recombination, alongside TOP3 $\alpha$ .

An additional meiotic factor involved in rice meiosis is FIGNL1, which was shown to interact and form a complex with MEICA1 (Yang *et al.*, 2022). Acting in conjunction with MEICA1, FIGNL1 was found to inhibit meiotic COs with mutants exhibiting meiotic defects similar to

those of *meical*, including chromosome bridges and fragmentation during meiosis I (Hu *et al.*, 2017; Yang *et al.*, 2022). The MEICA1/FIGNL1 complex is highly conserved, with homologues of both factors identified in other plant species, including Arabidopsis. In Arabidopsis, the MEICA1 orthologue was recently identified, termed the FIDGETIN-LIKE-1 INTERACTION PROTEIN (FLIP) (Fernandes, *et al.*, 2018a), and was shown to form a complex with FIGETIN-LIKE 1 (FIGL1), the orthologue of OsFIGNL1, as with the rice orthologues (Hu *et al.*, 2017; Yang *et al.*, 2022). Both AtFLIP and AtFIGL1 were shown to function in the same anti-CO-limiting pathway as one another (Fernandes *et al.*, 2018a), as in rice, nonetheless, the mutant phenotypes of *Osmeical* and *Atflip* are drastically different to one another in their respective plant species. In comparison to the severe meiotic defects observed for rice *meical* mutants (Hu *et al.*, 2017), Arabidopsis *flip* mutants demonstrate a slight increase in the frequency of CO formation, however only minor meiotic defects are observed with both meiosis I and meiosis II progressing relatively normally (Fernandes *et al.*, 2018a).

A putative homologue of *AtFLIP/OsMEICA1* was identified within the genome of tomato, encoding for a protein harbouring the conserved DUF4487 domain. Phylogenetic analysis was conducted with the full-length amino acid sequence of the tomato MEICA1 homologue and those from a variety of plant species, demonstrating that it is related to the orthologues in rice and Arabidopsis, in evolutionary terms, and thus comparative in terms of its protein sequence and potential function (see Figure 7.2 in the appendix). However, with the strongly differing functions of MEICA1 between the orthologues in Arabidopsis and rice (Fernandes *et al.*, 2018a; Hu *et al.*, 2017), with an essential meiotic phenotype in rice, but not for Arabidopsis, assumptions on the functional role of the tomato MEICA1 homologue cannot be made with certain without proper experimental analyses being conducted. Nevertheless, with both the differing functions of MEICA1 between rice and Arabidopsis, and the differing functions for RMI1 between Arabidopsis and tomato, it can be hypothesised that the functions of these two proteins do differ between plant species. As both MEICA1 and RMI1 were shown to interact with TOP3 $\alpha$  and the mutant phenotypes of both demonstrated similar severe meiotic defects in at least one plant species, it can be assumed that both proteins are able to functionally replace one another, in stabilising the RTR complex. As no apparent functional role was identified for RMI1 in tomato, it may be the case that MEICA1 is interacting with TOP3 $\alpha$  and performing the structural roles during the dissolution pathway instead of RMI1. Therefore, a postulated model for the dissolution pathway in tomato for both somatic and meiotic homologous recombination is that MEICA1 is modulating the topoisomerase activity of TOP3 $\alpha$  and

therefore, ensuring successful cleavage of the hemicatenane intermediate, leading to the generation of NCO products (see Figure 4.1).

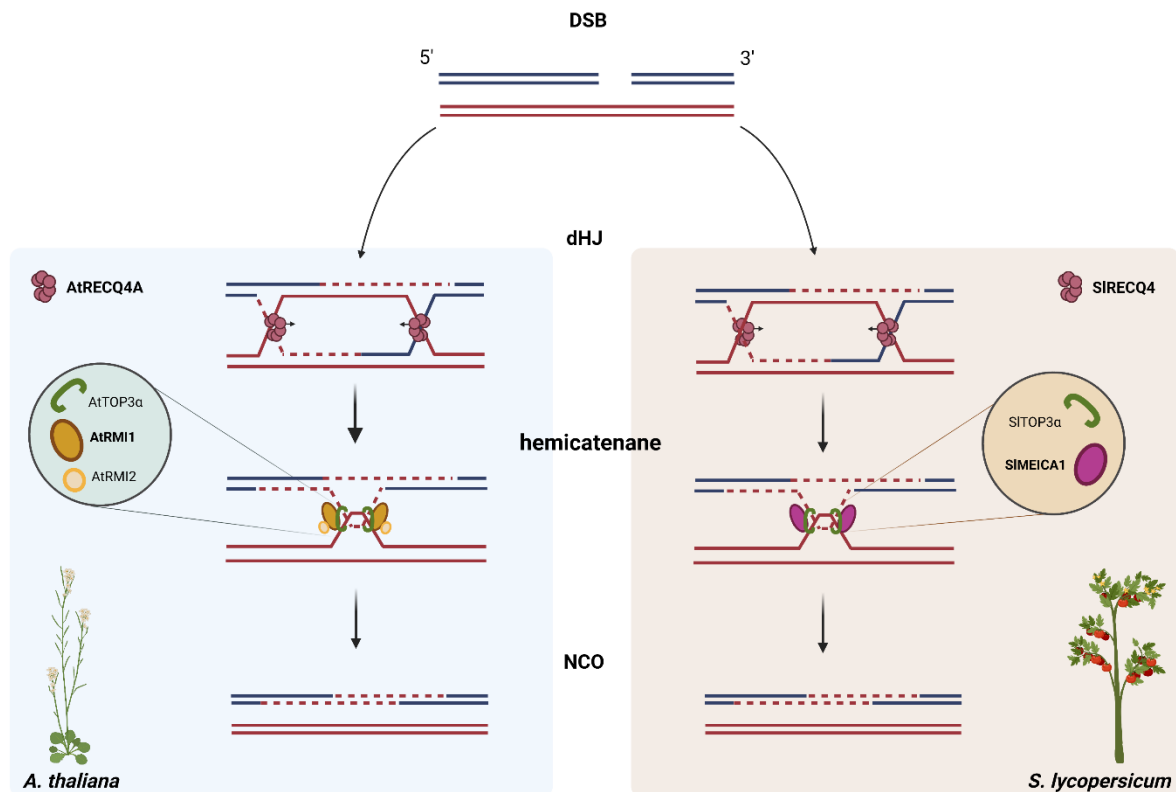


**Figure 4.1. Hypothesised model for the meiotic dissolution pathway in *Solanum lycopersicum*, compared to the known pathway in *Arabidopsis*.**

Schematic diagram illustrating the hypothesised model of the meiotic dissolution pathway in tomato, that is thought to differ to that of *Arabidopsis thaliana*. Homologous chromosomes are represented by the red and blue lines, with each colour depicting one chromosome. Following a programmed meiotic DSB, by the SPO11-complex, and the formation of a double Holliday Junction (dHJ) joint molecule, repair can be directed towards the dissolution pathway to generate a non-crossover (NCO) product (discussed in Mercier *et al.*, 2015). In both tomato and Arabidopsis, the RECQ helicase orthologues (AtRECQ4A in Arabidopsis and SIRECQ4 in tomato), act to migrate the junction points of the dHJ molecule, forming a hemicatenane intermediate. Cleavage of the hemicatenane is carried out by the activity of the TOP3 $\alpha$  topoisomerase orthologues. This cleavage activity of TOP3 $\alpha$  is supported by additional factors. In Arabidopsis, the AtRMI1 and AtRMI2 RTR complex partner structural proteins act to stabilise TOP3 $\alpha$ , enabling formation of a NCO product. In tomato, SIRMII was not found to have any role in meiotic recombination, and thus this supportive role during dissolution is postulated to be carried out by SIMEICA1 instead, based on the findings on the orthologous protein in rice, OsMEICA1 (Hu *et al.*, 2017). Figure created with BioRender.com.

With this hypothesised model, *meical* tomato mutants would exhibit the severe meiotic defects and somatic phenotypes as in rice, implying a functional role for MEICA1 in both meiotic recombination and somatic DNA repair in tomato, substituting the functional roles of RMI1. Analysis of both MEICA1 and RMI1 in tomato and rice, respectively, would therefore be of interest to confirm this suggestion, in order to elucidate the phenotypes of *meical* tomato

mutants and *rmi1* rice mutant plants. With RMI1 having not being analysed in other plant species, as of yet, besides Arabidopsis and tomato, the functional roles of RMI1 in certain plant species are not known, however, it may be that this model of dissolution involving MEICA1 instead of RMI1, is occurring in a number of plant species. As the roles of both RMI1 and MEICA1 have been shown to differ between plant species, it could be the case that these two proteins are of contrasting importance in different plant species, in terms of their interaction with TOP3 $\alpha$  and thus the stabilisation of the RTR complex. Furthermore, with the findings of this work indicating a more essential role of TOP3 $\alpha$  in tomato, compared to that in Arabidopsis, it could also be that the importance of TOP3 $\alpha$  also differs between plant species.

#### 4.1.7 The importance of translational studies in crop plants

The aim of this work was primarily to decipher the functional roles of both of the RTR complex partners, TOP3 $\alpha$  and RMI1 in tomato. Given the understanding of these proteins and their functions in Arabidopsis, it was thought that they would play similar roles in tomato. However, this was not found to be the case, with both TOP3 $\alpha$  and RMI1 demonstrating different roles in tomato than those observed in Arabidopsis, despite both plants being dicotyledonous species. Therefore, whilst providing knowledge into the RTR complex and dissolution pathway in tomato, this work also provides evidence that such differences between Arabidopsis and other plant species do exist. Interestingly, this is not the first case of such evidence being obtained. Over recent years, studies utilising non-model crop plant species have been increasingly carried out owing to the efforts to ensure food security, and the ease at which this can be carried out due to advancements in genome editing techniques. Such analyses have also showed that differences do exist between Arabidopsis and other plant species. One such example is that previously mentioned in which the homologues of OsMEICA1 and AtFLIP show different meiotic roles, with *meical* mutants in rice demonstrating more severe meiotic defects leading to sterility, as opposed to the relatively normal meiotic progression observed for the homologous *Atflip* mutants (Fernandes *et al.*, 2018a).

Much of the observed differences between Arabidopsis and crops have been identified via analyses of meiotic recombination and meiotic factors in various species. Understanding meiotic recombination is of great interest due to the potential to develop strategies to be able to manipulate recombination, and therefore increase genetic variation available to plant breeders, proving beneficial in the generation of sustainable crop varieties. The majority of our current understanding of meiotic recombination stems from analyses conducted using Arabidopsis, the model plant species, due to the numerous advantageous factors of working with such a small,

fast-growing and amenable plant for research purposes. However, with the increasing global population, in conjunction with adverse effects of climate change, translational studies are now being increasingly carried out in non-model crop plants. Previously, Arabidopsis was considered the “gold-standard” and representative of the entire plant kingdom, nevertheless, these translational studies are highlighting differences between plant species, as with the work presented in this thesis.

Meiotic studies in crops have now been conducted in a plethora of plant species, both monocotyledonous and dicotyledonous species, including rice, maize, wheat, barley, tomato and *Brassica* species, with insights into all stages of meiotic progression (reviewed in Wang *et al.*, 2021). Despite a number of conserved similarities between Arabidopsis and meiosis in other plant species, there are a number of differences that have been highlighted as well, throughout all of meiosis. For example, the cyclin protein SOLO DANCERS (SDS) was found to have differing roles between rice and Arabidopsis, with OsSDS being shown as essential for the formation of DSBs at the onset of meiotic recombination, whilst the Arabidopsis orthologue is not and is only required during further repair and processing of meiotic DSBs (De Muyt *et al.*, 2009; Wu *et al.*, 2015). Rice and maize are notably the most studied crop plants to date, accounting for the majority of known differences between Arabidopsis and crop plants. Both rice and maize are monocots, in contrast to Arabidopsis, which is a dicot plant species. Thus, these observed differences could be potentially attributed to these two species being more distantly related to Arabidopsis in terms of evolution. However, as illustrated in this work, differences between dicotyledonous plant species during meiosis have also been shown, particularly in studies with tomato.

Differences between tomato and Arabidopsis were demonstrated for the helicase RTR complex partner, RECQ4, with regards to its role as an anti-CO factor in meiosis. Double mutants lacking both *recq4a* and *recq4b*, in an Arabidopsis Col-0 background, showed a six-fold increase in meiotic COs (Fernandes *et al.*, 2018b). Despite also showing an increase in COs, analysis of ring bivalents in a biallelic *recq4* interspecific tomato mutant only demonstrated a 1.53-fold increase (de Maagd *et al.*, 2020), a drastically less increase than was observed for Arabidopsis. This difference in increase suggests that RECQ4 is less important, concerning the negative regulation of COs, in tomato than for Arabidopsis. Coinciding with the results of this current thesis highlighting the differences between TOP3 $\alpha$  and RMI1 homologues in Arabidopsis and tomato, the difference in the extent of the role of RECQ4 further supports that the factors of the RTR complex may differ in their roles between plant species. Differences between Arabidopsis and tomato are indicative of differences between two dicotyledonous plant species, showing

that this is a possible phenomenon, possibly owing to the differing physical genome and chromosome characteristics between the two species, despite the same ploidy level. Crop plants have much larger genomes than *Arabidopsis* in general, differing in their chromosome number and structure, and ploidy level. In meiosis, chromosome length has not been shown to affect the number of COs observed (Mercier *et al.*, 2015), indicating the importance of CO regulation mechanisms in crops with suppressing CO formation over large chromosomal regions. The complexity and diversity of genomes evident across crop species could therefore constitute to differences between molecular mechanisms, and the factors involved.

Collectively, these findings all emphasise the importance of analysing meiosis and other important biological processes in crop species, to determine the potential species-specific roles of certain factors. As a result, it may be the case that the establishment of strategies aiming to accelerate plant breeding efforts will need to be devised in a species-specific manner, accounting for such differences between plant species.

Consequently, it is timelier than ever to conduct translational studies in crop plants, gaining as much insight into each economically and agriculturally important crop species as possible, regarding the control of mechanisms underpinning important biological processes, such as DNA repair and meiosis. Fortunately, due to the revolutionary advancements in genome editing and genomic applications with technologies such as CRISPR/Cas9 (Jinek *et al.*, 2012) the use of non-model crop species is more accessible to researchers, with the generation of mutants being less challenging, less time consuming and less of a financial burden than before (Schindele *et al.*, 2020; Zhu *et al.*, 2020). However, translational studies from *Arabidopsis* to crops are still not going to be relatively straight forward. The differences observed between *Arabidopsis* and crop species mean that plant researchers should no longer regard knowledge from *Arabidopsis* as the “gold standard” and representative of the entire plant kingdom, as this is proving to not be true, as supported by the findings in this thesis.

## 5. Summary

The RTR complex is a highly conserved complex comprised of a RecQ helicase, type 1A topoisomerase and the structural protein Rmi1, and is essential for the dissolution of recombination intermediates, and thus fundamental for the maintenance of genomic stability. Analyses of the RTR complex partners have elucidated partly distinct roles in both homologous recombination and DNA repair, with mutants exhibiting characteristic phenotypes including hyperrecombination and increased sensitivity to genotoxins. RMI1 is important for somatic DNA repair, with mutants showing the characteristic phenotypes. In animals, the type 1A topoisomerase TOP3 $\alpha$  was demonstrated as essential, with mutants rendered embryo-lethal. Analyses in plants using the model plant species *Arabidopsis thaliana* showed a contrasting phenotype, with *top3 $\alpha$*  mutants remaining viable. Acting as a sub-complex, TOP3 $\alpha$  and RMI1 were also shown as essential for proper meiotic progression in plants, with mutants of one or the other demonstrating severe meiotic defects, leading to sterility. The dual role for both TOP3 $\alpha$  and RMI1 in DNA repair and meiosis is not conserved throughout all eukaryotic organisms, and thus was surprising when discovered in plants and postulated as a plant-specific role.

In this thesis, the tomato orthologues of TOP3 $\alpha$  and RMI1 were identified and mutant lines of both RTR complex partners were established using CRISPR/Cas9 technology, using Micro-Tom as a model system. Functional characterisation of these mutant lines revealed unexpected phenotypes for both TOP3 $\alpha$  and RMI1 in tomato, in stark contrast to those observed for *Arabidopsis*. Similar to animals, *top3 $\alpha$*  tomato mutants were non-viable due to embryo-lethality, implying an essential role for TOP3 $\alpha$  in tomato, drastically differing to the non-essential role elucidated in *Arabidopsis*. RMI1, on the other hand, was not found to play any functional roles in somatic DNA or meiosis in tomato, with plants lacking the complex partner showing no detectable phenotypes. Therefore, relevant differences exist between the functional roles for both TOP3 $\alpha$  and RMI1 in tomato, compared to those in *Arabidopsis*, providing evidence for differences between dicotyledonous plant species with regards to the RTR complex partners.

The work conducted in this thesis, not only provides insights into the functional roles of the RTR complex partners TOP3 $\alpha$  and RMI1, in tomato, but also provides necessary evidence to of the prevalence of such differences between *Arabidopsis* and crop species, that should be considered for future translational studies in plants.

## 6. References

- Ai, Y.-J., Liao, R.-Z., Chen, S.-L., Hua, W.-J., Fang, W.-H. and Luo, Y.** (2011) Repair of DNA Dewar Photoproduct to (6-4) Photoproduct in (6-4) Photolyase. *The Journal of Physical Chemistry B*, **115**, 10976–10982.
- Al Khateeb, W.M. and Schroeder, D.F.** (2009) Overexpression of Arabidopsis damaged DNA binding protein 1A (DDB1A) enhances UV tolerance. *Plant Molecular Biology*, **70**, 371–383.
- Allers, T. and Lichten, M.** (2001) Differential timing and control of noncrossover and crossover recombination during meiosis. *Cell*, **106**, 47–57.
- Allinson, S.L., Dianova, I.I. and Dianov, G.L.** (2001) DNA polymerase  $\beta$  is the major dRP lyase involved in repair of oxidative base lesions in DNA by mammalian cell extracts. *The EMBO Journal*, **20**, 6919–6926.
- Araki, M., Masutani, C., Takemura, M., Uchida, A., Sugasawa, K., Kondoh, J., Ohkuma, Y. and Hanaoka, F.** (2001) Centrosome protein centrin 2/caltractin 1 is part of the xeroderma pigmentosum group C complex that initiates global genome nucleotide excision repair. *J Biol Chem*, **276**, 18665–18672.
- Armstrong, S.J. and Jones, G.H.** (2001) Female meiosis in wild-type Arabidopsis thaliana and in two meiotic mutants. *Sex Plant Reprod*, **13**, 177–183.
- Armstrong, S.J. and Jones, G.H.** (2003) Meiotic cytology and chromosome behaviour in wild-type Arabidopsis thaliana. *Journal of Experimental Botany*, **54**, 1–10.
- Armstrong, S.J., Sanchez-Moran, E. and Franklin, F.C.H.** (2009) Cytological analysis of Arabidopsis thaliana meiotic chromosomes. *Methods in molecular biology (Clifton, N.J.)*, **558**, 131–145.
- Attikum, H. van, Bundock, P., Overmeer, R.M., Lee, L.-Y., Gelvin, S.B. and Hooykaas, P.J.J.** (2003) The Arabidopsis AtLIG4 gene is required for the repair of DNA damage, but not for the integration of Agrobacterium T-DNA. *Nucleic acids research*, **31**, 4247–4255.
- Bachrati, C.Z., Borts, R.H. and Hickson, I.D.** (2006) Mobile D-loops are a preferred substrate for the Bloom's syndrome helicase. *Nucleic Acids Res*, **34**, 2269–2279.
- Bagherieh-Najjar, M.B., Vries, O.M.H., Hille, J. and Dijkwel, P.P.** (2005) Arabidopsis RecQ14A suppresses homologous recombination and modulates DNA damage responses: Genome instability in RecQ14A mutants. *The Plant Journal*, **43**, 789–798.
- Baker, N.M., Rajan, R. and Mondragón, A.** (2009) Structural studies of type I topoisomerases. *Nucleic Acids Res*, **37**, 693–701.
- Banaś, A.K., Zglobicki, P., Kowalska, E., Bażant, A., Dziga, D. and Strzalka, W.** (2020) All You Need Is Light. Photorepair of UV-Induced Pyrimidine Dimers. *Genes*, **11**.
- Barone, A., Chiusano, M.L., Ercolano, M.R., Giuliano, G., Grandillo, S. and Frusciante, L.** (2008) Structural and Functional Genomics of Tomato. *International Journal of Plant Genomics*, **2008**, 1–12.

- Batty, D., Ropic'-Otrin, V., Levine, A.S. and Wood, R.D.** (2000) Stable binding of human XPC complex to irradiated DNA confers strong discrimination for damaged sites | Edited by M. Yaniv. *Journal of Molecular Biology*, **300**, 275–290.
- Beemster, G.T. and Baskin, T.I.** (1998) Analysis of cell division and elongation underlying the developmental acceleration of root growth in *Arabidopsis thaliana*. *Plant Physiol*, **116**, 1515–1526.
- Berchowitz, L.E., Francis, K.E., Bey, A.L. and Copenhaver, G.P.** (2007) The Role of AtMUS81 in Interference-Insensitive Crossovers in *A. thaliana*. *PLOS Genetics*, **3**, e132.
- Bergerat, A., Massy, B. de, Gabelle, D., Varoutas, P.-C., Nicolas, A. and Forterre, P.** (1997) An atypical topoisomerase II from archaea with implications for meiotic recombination. *Nature*, **386**, 414–417.
- Bi, X.** (2015) Mechanism of DNA damage tolerance. *World J Biol Chem*, **6**, 48–56.
- Bishop, D.K., Park, D., Xu, L. and Kleckner, N.** (1992) DMC1: A meiosis-specific yeast homolog of *E. coli* recA required for recombination, synaptonemal complex formation, and cell cycle progression. *Cell*, **69**, 439–456.
- Bizard, A.H. and Hickson, I.D.** (2014) The dissolution of double Holliday junctions. *Cold Spring Harbor Perspectives in Biology*, **6**, a016477.
- Blackford, A.N. and Jackson, S.P.** (2017) ATM, ATR, and DNA-PK: The Trinity at the Heart of the DNA Damage Response. *Molecular Cell*, **66**, 801–817.
- Bochman, M.L., Paeschke, K., Chan, A. and Zakian, V.A.** (2014) Hrq1, a homolog of the human RecQ4 helicase, acts catalytically and structurally to promote genome integrity. *Cell Rep*, **6**, 346–356.
- Bocquet, N., Bizard, A.H., Abdulrahman, W., et al.** (2014) Structural and mechanistic insight into Holliday-junction dissolution by Topoisomerase III $\alpha$  and RMI1. *Nat Struct Mol Biol*, **21**, 261–268.
- Boesch, P., Ibrahim, N., Paulus, F., Cosset, A., Tarasenko, V. and Dietrich, A.** (2009) Plant mitochondria possess a short-patch base excision DNA repair pathway. *Nucleic acids research*, **37**, 5690–5700.
- Bohr, V.A.** (2008) Rising from the RecQ-age: the role of human RecQ helicases in genome maintenance. *Trends in Biochemical Sciences*, **33**, 609–620.
- Bonnet, S., Knoll, A., Hartung, F. and Puchta, H.** (2013) Different functions for the domains of the *Arabidopsis thaliana* RMI1 protein in DNA cross-link repair, somatic and meiotic recombination. *Nucleic Acids Res*, **41**, 9349–9360.
- Börner, G.V., Kleckner, N. and Hunter, N.** (2004) Crossover/Noncrossover Differentiation, Synaptonemal Complex Formation, and Regulatory Surveillance at the Leptotene/Zygotene Transition of Meiosis. *Cell*, **117**, 29–45.

- Brabant, A.J. van, Ye, T., Sanz, M., German III, J.L., Ellis, N.A. and Holloman, W.K.** (2000) Binding and melting of D-loops by the Bloom syndrome helicase. *Biochemistry*, **39**, 14617–14625.
- Britt, A.B.** (1996) DNA DAMAGE AND REPAIR IN PLANTS. *Annu Rev Plant Physiol Plant Mol Biol*, **47**, 75–100.
- Brosh, R.M., Li, J.L., Kenny, M.K., Karow, J.K., Cooper, M.P., Kureekattil, R.P., Hickson, I.D. and Bohr, V.A.** (2000) Replication protein A physically interacts with the Bloom's syndrome protein and stimulates its helicase activity. *J Biol Chem*, **275**, 23500–23508.
- Brown, M.S. and Bishop, D.K.** (2014) DNA strand exchange and RecA homologs in meiosis. *Cold Spring Harb Perspect Biol*, **7**, a016659.
- Brown, S., Niimi, A. and Lehmann, A.R.** (2009) Ubiquitination and deubiquitination of PCNA in response to stalling of the replication fork. *Cell Cycle*, **8**, 689–692.
- Brukhin, V., Hernould, M., Gonzalez, N., Chevalier, C. and Mouras, A.** (2003) Flower development schedule in tomato *Lycopersicon esculentum* cv. sweet cherry. *Sex Plant Reprod*, **15**, 311–320.
- Bugreev, D.V., Mazina, O.M. and Mazin, A.V.** (2009) Bloom Syndrome Helicase Stimulates RAD51 DNA Strand Exchange Activity through a Novel Mechanism. *J Biol Chem*, **284**, 26349–26359.
- Bugreev, D.V., Yu, X., Egelman, E.H. and Mazin, A.V.** (2007) Novel pro- and anti-recombination activities of the Bloom's syndrome helicase. *Genes Dev*, **21**, 3085–3094.
- Bussen, W., Raynard, S., Busygina, V., Singh, A.K. and Sung, P.** (2007) Holliday Junction Processing Activity of the BLM-Topo III $\alpha$ -BLAP75 Complex \*. *Journal of Biological Chemistry*, **282**, 31484–31492.
- Cadet, J. and Wagner, J.R.** (2013) DNA Base Damage by Reactive Oxygen Species, Oxidizing Agents, and UV Radiation. *Cold Spring Harbor Perspectives in Biology*, **5**, a012559–a012559.
- Caldecott, K.W.** (2008) Single-strand break repair and genetic disease. *Nature Reviews Genetics*, **9**, 619–631.
- Castells, E., Molinier, J., Benvenuto, G., et al.** (2011) The conserved factor DE-ETIOLATED 1 cooperates with CUL4-DDB1DDB2 to maintain genome integrity upon UV stress. *The EMBO Journal*, **30**, 1162–1172.
- Cejka, P., Cannavo, E., Polaczek, P., Masuda-Sasa, T., Pokharel, S., Campbell, J.L. and Kowalczykowski, S.C.** (2010) DNA end resection by Dna2-Sgs1-RPA and its stimulation by Top3-Rmi1 and Mre11-Rad50-Xrs2. *Nature*, **467**, 112–116.
- Cejka, P., Plank, J.L., Dombrowski, C.C. and Kowalczykowski, S.C.** (2012) Decatenation of DNA by the *S. cerevisiae* Sgs1-Top3-Rmi1 and RPA complex: a mechanism for disentangling chromosomes. *Mol Cell*, **47**, 886–896.

- Chaganti, R.S., Schonberg, S. and German, J.** (1974) A manyfold increase in sister chromatid exchanges in Bloom's syndrome lymphocytes. *Proceedings of the National Academy of Sciences of the United States of America*, **71**, 4508–4512.
- Chakarov, S., Petkova, R., Russev, G. and Zhelev, N.** (2014) DNA damage and mutation. Types of DNA damage. *Biodiscovery*, **1**.
- Champoux, J.J.** (2001) DNA Topoisomerases: Structure, Function, and Mechanism. *Annual Review of Biochemistry*, **70**, 369–413.
- Chandramouly, G., Kwok, A., Huang, B., Willis, N.A., Xie, A. and Scully, R.** (2013) BRCA1 and CtIP suppress long-tract gene conversion between sister chromatids. *Nat Commun*, **4**, 1–12.
- Chang, H.H.Y., Pannunzio, N.R., Adachi, N. and Lieber, M.R.** (2017) Non-homologous DNA end joining and alternative pathways to double-strand break repair. *Nat Rev Mol Cell Biol*, **18**, 495–506.
- Chang, M., Bellaoui, M., Zhang, C., et al.** (2005) RMI1/NCE4, a suppressor of genome instability, encodes a member of the RecQ helicase/Topo III complex. *EMBO J*, **24**, 2024–2033.
- Charbonnel, C., Gallego, M.E. and White, C.I.** (2010) Xrcc1-dependent and Ku-dependent DNA double-strand break repair kinetics in Arabidopsis plants. *The Plant journal : for cell and molecular biology*, **64**, 280–290.
- Chelysheva, L., Vezon, D., Belcram, K., Gendrot, G. and Grelon, M.** (2008) The Arabidopsis BLAP75/Rmi1 Homologue Plays Crucial Roles in Meiotic Double-Strand Break Repair. *PLoS Genet*, **4**, e1000309.
- Chen, C.-F. and Brill, S.J.** (2007) Binding and activation of DNA topoisomerase III by the RMI1 subunit. *J Biol Chem*, **282**, 28971–28979.
- Chen, S.H., Plank, J.L., Willcox, S., Griffith, J.D. and Hsieh, T.** (2014) Top3 $\alpha$  is required during the convergent migration step of double Holliday junction dissolution. *PLoS One*, **9**, e83582.
- Chen, S.H., Wu, C.-H., Plank, J.L. and Hsieh, T.** (2012) Essential functions of C terminus of Drosophila Topoisomerase III $\alpha$  in double holliday junction dissolution. *J Biol Chem*, **287**, 19346–19353.
- Chen, S.J. and Wang, J.C.** (1998) Identification of active site residues in Escherichia coli DNA topoisomerase I. *J Biol Chem*, **273**, 6050–6056.
- Cheng, B., Sorokin, E.P. and Tse-Dinh, Y.-C.** (2008) Mutation adjacent to the active site tyrosine can enhance DNA cleavage and cell killing by the TOPRIM Gly to Ser mutant of bacterial topoisomerase I. *Nucleic Acids Research*, **36**, 1017–1025.
- Chiruvella, K.K., Liang, Z. and Wilson, T.E.** (2013) Repair of double-strand breaks by end joining. *Cold Spring Harbor Perspectives in Biology*, **5**, a012757.

- Choi, D.-H., Lee, R., Kwon, S.-H. and Bae, S.-H.** (2013) Hrq1 functions independently of Sgs1 to preserve genome integrity in *Saccharomyces cerevisiae*. *J Microbiol*, **51**, 105–112.
- Cloud, V., Chan, Y.-L., Grubb, J., Budke, B. and Bishop, D.K.** (2012) Rad51 is an accessory factor for Dmc1-mediated joint molecule formation during meiosis. *Science*, **337**, 1222–1225.
- Compe, E. and Egly, J.-M.** (2016) Nucleotide Excision Repair and Transcriptional Regulation: TFIIH and Beyond. *Annual Review of Biochemistry*, **85**, 265–290.
- Cooke, M.S., Mistry, N., Ladapo, A., Herbert, K.E. and Lunec, J.** (2000) Immunochemical quantitation of UV-induced oxidative and dimeric DNA damage to human keratinocytes. *Free Radical Research*, **33**, 369–381.
- Córdoba-Cañero, D., Roldán-Arjona, T. and Ariza, R.R.** (2014) Arabidopsis ZDP DNA 3'-phosphatase and ARP endonuclease function in 8-oxoG repair initiated by FPG and OGG1 DNA glycosylases. *The Plant journal : for cell and molecular biology*, **79**, 824–834.
- Couteau, F., Belzile, F., Horlow, C., Grandjean, O., Vezon, D. and Doutriaux, M.-P.** (1999) Random Chromosome Segregation without Meiotic Arrest in Both Male and Female Meocytes of a *dmc1* Mutant of Arabidopsis. *The Plant Cell*, **11**, 1623–1634.
- Crismani, W., Girard, C., Froger, N., Pradillo, M., Santos, J.L., Chelysheva, L., Copenhaver, G.P., Horlow, C. and Mercier, R.** (2012) FANCM limits meiotic crossovers. *Science*, **336**, 1588–1590.
- Croteau, D.L., Popuri, V., Opresko, P.L. and Bohr, V.A.** (2014) Human RecQ helicases in DNA repair, recombination, and replication. *Annu Rev Biochem*, **83**, 519–552.
- Culligan, K., Tissier, A. and Britt, A.** (2004) ATR regulates a G2-phase cell-cycle checkpoint in Arabidopsis thaliana. *The Plant cell*, **16**, 1091–1104.
- Culligan, K.M. and Hays, J.B.** (2000) Arabidopsis MutS homologs-AtMSH2, AtMSH3, AtMSH6, and a novel AtMSH7-form three distinct protein heterodimers with different specificities for mismatched DNA. *The Plant cell*, **12**, 991–1002.
- Cunniff, C., Bassetti, J.A. and Ellis, N.A.** (2017) Bloom's Syndrome: Clinical Spectrum, Molecular Pathogenesis, and Cancer Predisposition. *Mol Syndromol*, **8**, 4–23.
- Da Ines, O., Degroote, F., Goubely, C., Amiard, S., Gallego, M.E. and White, C.I.** (2013) Meiotic recombination in Arabidopsis is catalysed by DMC1, with RAD51 playing a supporting role. *PLoS Genet*, **9**, e1003787.
- Dag Brune, Ragnar Hellborg, Bertil R R Persson, and Rauno Pääkkönen** (2013) Radiation at Home, Outdoors and in the Workplace. *American Journal of Physics*, **82**.
- Dahan-Meir, T., Filler-Hayut, S., Melamed-Bessudo, C., Bocobza, S., Czosnek, H., Aharoni, A. and Levy, A.A.** (2018) Efficient in planta gene targeting in tomato using

- geminiviral replicons and the CRISPR/Cas9 system. *The Plant journal : for cell and molecular biology*, **95**, 5–16.
- Daley, J.M., Jimenez-Sainz, J., Wang, W., Miller, A.S., Xue, X., Nguyen, K.A., Jensen, R.B. and Sung, P.** (2017) Enhancement of BLM-DNA2-Mediated Long-Range DNA End Resection by CtIP. *Cell Rep*, **21**, 324–332.
- Dalhus, B., Laerdahl, J.K., Backe, P.H. and Bjørås, M.** (2009) DNA base repair – recognition and initiation of catalysis. *FEMS Microbiol Rev*, **33**, 1044–1078.
- Dany, A.L. and Tissier, A.** (2001) A functional OGG1 homologue from *Arabidopsis thaliana*. *Mol Gen Genomics*, **265**, 293–301.
- Datta, A., Dhar, S., Awate, S. and Brosh, R.M.** (2021) Synthetic Lethal Interactions of RECQ Helicases. *Trends in Cancer*, **7**, 146–161.
- Dayani, Y., Simchen, G. and Lichten, M.** (2011) Meiotic recombination intermediates are resolved with minimal crossover formation during return-to-growth, an analogue of the mitotic cell cycle. *PLoS genetics*, **7**, e1002083.
- De Maagd, R.A. de, Loonen, A., Chouaref, J., Pelé, A., Meijer-Dekens, F., Fransz, P. and Bai, Y.** (2020) CRISPR/Cas inactivation of RECQ4 increases homeologous crossovers in an interspecific tomato hybrid. *Plant Biotechnol J*, **18**, 805–813.
- De Muyt A.D., Vezon, D., Gendrot, G., Gallois, J.L., Stevens, R., Grelon, M.** (2007) AtPRD1 is required for meiotic double strand break formation in *Arabidopsis thaliana*. *EMBO J* **26**: 4126–4137.
- De Muyt, A.D., Pereira, L., Vezon, D., et al.** (2009) A High Throughput Genetic Screen Identifies New Early Meiotic Recombination Functions in *Arabidopsis thaliana*. *PLOS Genetics*, **5**, e1000654.
- Deshmukh, P.S., Megha, K., Banerjee, B.D., Ahmed, R.S., Chandna, S., Abegaonkar, M.P. and Tripathi, A.K.** (2013) Detection of Low Level Microwave Radiation Induced Deoxyribonucleic Acid Damage Vis-à-vis Genotoxicity in Brain of Fischer Rats. *Toxicol Int*, **20**, 19–24.
- Dianov G, Price A, and Lindahl T** (1992) Generation of single-nucleotide repair patches following excision of uracil residues from DNA. *Molecular and Cellular Biology*, **12**, 1605–1612.
- DiGate, R.J. and Marians, K.J.** (1988) Identification of a potent decatenating enzyme from *Escherichia coli*. *Journal of Biological Chemistry*, **263**, 13366–13373.
- Doetsch, P.W., Zastawny, T.H., Martin, A.M. and Dizdaroglu, M.** (1995) Monomeric Base Damage Products from Guanine, Adenine, and Thymine Induced by Exposure of DNA to Ultraviolet Radiation. *Biochemistry*, **34**, 737–742.
- Doherty, K.M., Sommers, J.A., Gray, M.D., Lee, J.W., Kobbe, C. von, Thoma, N.H., Kureekattil, R.P., Kenny, M.K. and Brosh, R.M.** (2005) Physical and functional

- mapping of the replication protein a interaction domain of the werner and bloom syndrome helicases. *J Biol Chem*, **280**, 29494–29505.
- Dominguez, E., Cuartero, J. and Fernández-Muñoz, R.** (2002) Reduced Container Volume Increases Tomato Pollen Fertility at Low Ambient Temperatures. *Journal of the American Society for Horticultural Science. American Society for Horticultural Science*, **127**.
- Dorn, A. and Puchta, H.** (2019) DNA Helicases as Safekeepers of Genome Stability in Plants. *Genes (Basel)*, **10**, E1028.
- Dorn, A., Röhrig, S., Papp, K., Schröpfer, S., Hartung, F., Knoll, A. and Puchta, H.** (2018) The topoisomerase 3 $\alpha$  zinc-finger domain T1 of *Arabidopsis thaliana* is required for targeting the enzyme activity to Holliday junction-like DNA repair intermediates. *PLOS Genetics*, **14**, e1007674.
- Douki, T. and Cadet, J.** (2001) Individual Determination of the Yield of the Main UV-Induced Dimeric Pyrimidine Photoproducts in DNA Suggests a High Mutagenicity of CC Photolesions. *Biochemistry*, **40**, 2495–2501.
- Douki, T. and Sage, E.** (2016) Dewar valence isomers, the third type of environmentally relevant DNA photoproducts induced by solar radiation. *Photochem. Photobiol. Sci.*, **15**, 24–30.
- Doutriaux, M.-P., Couteau, F., Bergounioux, C. and White, C.** (1998) Isolation and characterisation of the RAD51 and DMC1 homologs from *Arabidopsis thaliana*. *Mol Gen Genet*, **257**, 283–291.
- Elbakry, A. and Löbrich, M.** (2021) Homologous Recombination Subpathways: A Tangle to Resolve. *Frontiers in genetics*, **12**, 723847.
- Ellis, N.A., Groden, J., Ye, T.-Z., Straughen, J., Lennon, D.J., Ciocci, S., Proytcheva, M. and German, J.** (1995) The Bloom's syndrome gene product is homologous to RecQ helicases. *Cell*, **83**, 655–666.
- Fausser, F., Schiml, S. and Puchta, H.** (2014) Both CRISPR/Cas-based nucleases and nickases can be used efficiently for genome engineering in *Arabidopsis thaliana*. *The Plant journal : for cell and molecular biology*, **79**, 348–359.
- Fernandes, J.B., Duhamel, M., Seguéla-Arnaud, M., et al.** (2018a) FIGL1 and its novel partner FLIP form a conserved complex that regulates homologous recombination. *PLoS Genet*, **14**, e1007317.
- Fernandes, J.B., Séguéla-Arnaud, M., Larchevêque, C., Lloyd, A.H. and Mercier, R.** (2018b) Unleashing meiotic crossovers in hybrid plants. *Proceedings of the National Academy of Sciences*, **115**, 2431–2436.
- Fernandez-Pozo, N., Menda, N., Edwards, J.D., et al.** (2015) The Sol Genomics Network (SGN)--from genotype to phenotype to breeding. *Nucleic Acids Res*, **43**, D1036-1041.

- Fidantsef, A.L. and Britt, A.B.** (2012) Preferential repair of the transcribed DNA strand in plants. *Front Plant Sci*, **2**, 105.
- Fillingham, J., Keogh, M.-C. and Krogan, N.J.** (2006) GammaH2AX and its role in DNA double-strand break repair. *Biochemistry and cell biology = Biochimie et biologie cellulaire*, **84**, 568–577.
- Flynn, R.L. and Zou, L.** (2010) Oligonucleotide/Oligosaccharide-Binding (OB) Fold Proteins: A Growing Family of Genome Guardians. *Crit Rev Biochem Mol Biol*, **45**, 266–275.
- Forterre, P. and Gadelle, D.** (2009) Phylogenomics of DNA topoisomerases: their origin and putative roles in the emergence of modern organisms. *Nucleic Acids Res*, **37**, 679–692.
- Fortini, P. and Dogliotti, E.** (2007) Base damage and single-strand break repair: Mechanisms and functional significance of short- and long-patch repair subpathways. *DNA Repair*, **6**, 398–409.
- Frosina, G., Fortini, P., Rossi, O., Carrozzino, F., Raspaglio, G., Cox, L.S., Lane, D.P., Abbondandolo, A. and Dogliotti, E.** (1996) Two pathways for base excision repair in mammalian cells. *J Biol Chem*, **271**, 9573–9578.
- Fujiwara, Y., Masutani, C., Mizukoshi, T., Kondo, J., Hanaoka, F. and Iwai, S.** (1999) Characterization of DNA recognition by the human UV-damaged DNA-binding protein. *J Biol Chem*, **274**, 20027–20033.
- Gangloff, S., Massy, B. de, Arthur, L., Rothstein, R. and Fabre, F.** (1999) The essential role of yeast topoisomerase III in meiosis depends on recombination. *EMBO J*, **18**, 1701–1711.
- Gangloff, S., McDonald, J.P., Bendixen, C., Arthur, L. and Rothstein, R.** (1994) The yeast type I topoisomerase Top3 interacts with Sgs1, a DNA helicase homolog: a potential eukaryotic reverse gyrase. *Mol Cell Biol*, **14**, 8391–8398.
- Gao, M.-J. and Murphy, T.M.** (2001) Alternative Forms of Formamidopyrimidine-DNA Glycosylase from *Arabidopsis thaliana*. *Photochemistry and Photobiology*, **73**, 128–134.
- Garcia, V., Bruchet, H., Camescasse, D., Granier, F., Bouchez, D. and Tissier, A.** (2003) AtATM is essential for meiosis and the somatic response to DNA damage in plants. *The Plant cell*, **15**, 119–132.
- García-Medel, P.L., Baruch-Torres, N., Peralta-Castro, A., Trasviña-Arenas, C.H., Torres-Larios, A. and Brieba, L.G.** (2019) Plant organellar DNA polymerases repair double-stranded breaks by microhomology-mediated end-joining. *Nucleic acids research*, **47**, 3028–3044.
- García-Ortiz, M.-V., Ariza, R.R. and Roldán-Arjona, T.** (2001) An OGG1 orthologue encoding a functional 8-oxoguanine DNA glycosylase/lyase in *Arabidopsis thaliana*. *Plant Molecular Biology*, **47**, 795–804.

- Georges, F. and Ray, H.** (2017) Genome editing of crops: A renewed opportunity for food security. *GM Crops & Food*, **8**, 1–12.
- German, J.** (1993) Bloom syndrome: a mendelian prototype of somatic mutational disease. *Medicine*, **72**, 393–406.
- Giannattasio, M., Zwicky, K., Follonier, C., Foiani, M., Lopes, M. and Branzei, D.** (2014) Visualization of recombination-mediated damage bypass by template switching. *Nature structural & molecular biology*, **21**, 884–892.
- Gillet, L.C.J. and Schärer, O.D.** (2006) Molecular Mechanisms of Mammalian Global Genome Nucleotide Excision Repair. *Chemical Reviews*, **106**, 253–276.
- Girard, C., Chelysheva, L., Choinard, S., Froger, N., Macaisne, N., Lemhemdi, A., Mazel, J., Crismani, W. and Mercier, R.** (2015) AAA-ATPase FIDGETIN-LIKE 1 and Helicase FANCM Antagonize Meiotic Crossovers by Distinct Mechanisms. *PLOS Genetics*, **11**, e1005369.
- Girard, C., Crismani, W., Froger, N., Mazel, J., Lemhemdi, A., Horlow, C. and Mercier, R.** (2014) FANCM-associated proteins MHF1 and MHF2, but not the other Fanconi anemia factors, limit meiotic crossovers. *NUCLEIC ACIDS RESEARCH*, **42**.
- Goff, S.A., Ricke, D., Lan, T.-H., et al.** (2002) A draft sequence of the rice genome (*Oryza sativa* L. ssp. japonica). *Science*, **296**, 92–100.
- Goodwin, A., Wang, S.W., Toda, T., Norbury, C. and Hickson, I.D.** (1999) Topoisomerase III is essential for accurate nuclear division in *Schizosaccharomyces pombe*. *Nucleic Acids Res*, **27**, 4050–4058.
- Gravel, S., Chapman, J.R., Magill, C. and Jackson, S.P.** (2008) DNA helicases Sgs1 and BLM promote DNA double-strand break resection. *Genes Dev.*, **22**, 2767–2772.
- Gray, S. and Cohen, P.E.** (2016) Control of Meiotic Crossovers: From Double-Strand Break Formation to Designation. *Annu Rev Genet*, **50**, 175–210.
- Guiraldelli, M.F., Eyster, C. and Pezza, R.J.** (2013) Genome instability and embryonic developmental defects in RMI1 deficient mice. *DNA Repair*, **12**, 835–843.
- Gutman, B.L. and Niyogi, K.K.** (2009) Evidence for base excision repair of oxidative DNA damage in chloroplasts of *Arabidopsis thaliana*. *J Biol Chem*, **284**, 17006–17012.
- Hanahan, D.** (1983) Studies on transformation of *Escherichia coli* with plasmids. *Journal of Molecular Biology*, **166**, 557–580.
- Harper, J.V., Anderson, J.A. and O'Neill, P.** (2010) Radiation induced DNA DSBs: Contribution from stalled replication forks? *DNA Repair*, **9**, 907–913.
- Hartung, F., Plchová, H. and Puchta, H.** (2000) Molecular characterisation of RecQ homologues in *Arabidopsis thaliana*. *Nucleic acids research*, **28**, 4275–4282.

- Hartung, F. and Puchta, H.** (2000) Molecular characterisation of two paralogous SPO11 homologues in *Arabidopsis thaliana*. *Nucleic Acids Res*, **28**, 1548–1554.
- Hartung, F. and Puchta, H.** (2001) Molecular characterization of homologues of both subunits A (SPO11) and B of the archaeobacterial topoisomerase 6 in plants. *Gene*, **271**, 81–86.
- Hartung, F. and Puchta, H.** (2006) The RecQ gene family in plants. *J Plant Physiol*, **163**, 287–296.
- Hartung, F., Suer, S., Knoll, A., Wurz-Wildersinn, R. and Puchta, H.** (2008) Topoisomerase 3alpha and RMI1 suppress somatic crossovers and are essential for resolution of meiotic recombination intermediates in *Arabidopsis thaliana*. *PLoS Genet*, **4**, e1000285.
- Hartung, F., Suer, S. and Puchta, H.** (2007a) Two closely related RecQ helicases have antagonistic roles in homologous recombination and DNA repair in *Arabidopsis thaliana*. *Proceedings of the National Academy of Sciences of the United States of America*, **104**, 18836–18841.
- Hartung, F., Wurz-Wildersinn, R., Fuchs, J., Schubert, I., Suer, S. and Puchta, H.** (2007b) The Catalytically Active Tyrosine Residues of Both SPO11-1 and SPO11-2 Are Required for Meiotic Double-Strand Break Induction in *Arabidopsis*. *The Plant Cell*, **19**, 3090–3099.
- Hays, J.B.** (2002) *Arabidopsis thaliana*, a versatile model system for study of eukaryotic genome-maintenance functions. *DNA Repair (Amst)*, **1**, 579–600.
- Hegde, M.L., Hazra, T.K. and Mitra, S.** (2008) Early steps in the DNA base excision/single-strand interruption repair pathway in mammalian cells. *Cell Research*, **18**, 27–47.
- Hendel, A., Krijger, P.H.L., Diamant, N., et al.** (2011) PCNA ubiquitination is important, but not essential for translesion DNA synthesis in mammalian cells. *PLoS genetics*, **7**, e1002262.
- Heslop-Harrison, J. and Heslop-Harrison, Y.** (1970) Evaluation of pollen viability by enzymatically induced fluorescence; intracellular hydrolysis of fluorescein diacetate. *Stain technology*, **45**, 115–120.
- Heyer, W.-D., Ehmsen, K.T. and Liu, J.** (2010) Regulation of homologous recombination in eukaryotes. *Annual review of genetics*, **44**, 113–139.
- Heyer, W.-D., Li, X., Rolfmeier, M. and Zhang, X.-P.** (2006) Rad54: the Swiss Army knife of homologous recombination? *Nucleic acids research*, **34**, 4115–4125.
- Hickson, I.D.** (2003) RecQ helicases: caretakers of the genome. *Nat Rev Cancer*, **3**, 169–178.
- Higgins, J.D., Buckling, E.F., Franklin, F.C.H. and Jones, G.H.** (2008) Expression and functional analysis of AtMUS81 in *Arabidopsis* meiosis reveals a role in the second pathway of crossing-over. *The Plant Journal*, **54**, 152–162.

- Higgins, J.D., Ferdous, M., Osman, K. and Franklin, F.C.H.** (2011) The RecQ helicase AtRECQ4A is required to remove inter-chromosomal telomeric connections that arise during meiotic recombination in Arabidopsis. *Plant J*, **65**, 492–502.
- Hill, J.T., Demarest, B.L., Bisgrove, B.W., Su, Y.-C., Smith, M. and Yost, H.J.** (2014) Poly peak parser: Method and software for identification of unknown indels using sanger sequencing of polymerase chain reaction products. *Developmental dynamics: an official publication of the American Association of Anatomists*, **243**, 1632–1636.
- Hoegel, C., Pfander, B., Moldovan, G.-L., Pyrowolakis, G. and Jentsch, S.** (2002) RAD6-dependent DNA repair is linked to modification of PCNA by ubiquitin and SUMO. *Nature*, **419**, 135–141.
- Hu, Q., Li, Y., Wang, H., Shen, Y., Zhang, C., Du, G., Tang, D. and Cheng, Z.** (2017) Meiotic Chromosome Association 1 Interacts with TOP3 $\alpha$  and Regulates Meiotic Recombination in Rice. *The Plant Cell*, **29**, 1697–1708.
- Huertas, P.** (2010) DNA resection in eukaryotes: deciding how to fix the break. *Nat Struct Mol Biol*, **17**, 11–16.
- Hustedt, N. and Durocher, D.** (2017) The control of DNA repair by the cell cycle. *Nat Cell Biol*, **19**, 1–9.
- Ishino, Y., Shinagawa, H., Makino, K., Amemura, M. and Nakata, A.** (1987) Nucleotide sequence of the iap gene, responsible for alkaline phosphatase isozyme conversion in Escherichia coli, and identification of the gene product. *J Bacteriol*, **169**, 5429–5433.
- Jaganathan, D., Ramasamy, K., Sellamuthu, G., Jayabalan, S. and Venkataraman, G.** (2018) CRISPR for Crop Improvement: An Update Review. *Frontiers in Plant Science*, **9**.
- Jennifer G. Peak and Meyrick J. Peak** (1990) Ultraviolet light induces double-strand breaks in DNA of cultured human P3 cells as measured by neutral filter elution. *Photochemistry and Photobiology*, **52**, 387–393.
- Jia, Q., Dulk-Ras, A. den, Shen, H., Hooykaas, P.J.J. and Pater, S.** (2013) Poly(ADP-ribose)polymerases are involved in microhomology mediated back-up non-homologous end joining in Arabidopsis thaliana. *Plant Molecular Biology*, **82**, 339–351.
- Jinek, M., Chylinski, K., Fonfara, I., Hauer, M., Doudna, J.A. and Charpentier, E.** (2012) A programmable dual-RNA-guided DNA endonuclease in adaptive bacterial immunity. *Science*, **337**, 816–821.
- Johnson, R.D. and Jasin, M.** (2000) Sister chromatid gene conversion is a prominent double-strand break repair pathway in mammalian cells. *The EMBO Journal*, **19**, 3398–3407.
- Kadyk, L.C. and Hartwell, L.H.** (1992) Sister chromatids are preferred over homologs as substrates for recombinational repair in Saccharomyces cerevisiae. *Genetics*, **132**, 387–402.

- Kannouche, P.L., Wing, J. and Lehmann, A.R.** (2004) Interaction of Human DNA Polymerase  $\eta$  with Monoubiquitinated PCNA: A Possible Mechanism for the Polymerase Switch in Response to DNA Damage. *Molecular Cell*, **14**, 491–500.
- Karmakar, P., Seki, M., Kanamori, M., et al.** (2006) BLM is an early responder to DNA double-strand breaks. *Biochemical and Biophysical Research Communications*, **348**, 62.
- Keeney, S., Giroux, C.N. and Kleckner, N.** (1997) Meiosis-Specific DNA Double-Strand Breaks Are Catalyzed by Spo11, a Member of a Widely Conserved Protein Family. *Cell*, **88**, 375–384.
- Kielbassa, C.** (1997) Wavelength dependence of oxidative DNA damage induced by UV and visible light. *Carcinogenesis*, **18**, 811–816.
- Kikuchi, K., Abdel-Aziz, H.I., Taniguchi, Y., Yamazoe, M., Takeda, S. and Hirota, K.** (2009) Bloom DNA Helicase Facilitates Homologous Recombination between Diverged Homologous Sequences. *J Biol Chem*, **284**, 26360–26367.
- Kim, Y.C., Lee, J. and Koo, H.S.** (2000) Functional characterization of *Caenorhabditis elegans* DNA topoisomerase IIIalpha. *Nucleic Acids Res*, **28**, 2012–2017.
- Kimura, S. and Sakaguchi, K.** (2006) DNA Repair in Plants. *Chemical Reviews*, **106**, 753–766.
- Kimura, S. and Sinha, N.** (2008) Tomato (*Solanum lycopersicum*): A Model Fruit-Bearing Crop. *Cold Spring Harb Protoc*, **2008**, pdb.emo105.
- Kirkegaard, K. and Wang, J.C.** (1985) Bacterial DNA topoisomerase I can relax positively supercoiled DNA containing a single-stranded loop. *J Mol Biol*, **185**, 625–637.
- Knoll, A. and Puchta, H.** (2011) The role of DNA helicases and their interaction partners in genome stability and meiotic recombination in plants. *Journal of Experimental Botany*, **62**, 1565–1579.
- Knoll, A., Schröpfer, S. and Puchta, H.** (2014) The RTR complex as caretaker of genome stability and its unique meiotic function in plants. *Front Plant Sci*, **5**, 33.
- Koga, A., Ishibashi, T., Kimura, S., Uchiyama, Y. and Sakaguchi, K.** (2006) Characterization of T-DNA Insertion Mutants and RNAi Silenced Plants of *Arabidopsis thaliana* UV-damaged DNA Binding Protein 2 (AtUV-DDB2). *Plant Molecular Biology*, **61**, 227–240.
- Kokic, G., Chernev, A., Tegunov, D., Dienemann, C., Urlaub, H. and Cramer, P.** (2019) Structural basis of TFIIF activation for nucleotide excision repair. *Nature Communications*, **10**, 2885.
- Koster, D.A., Croquette, V., Dekker, C., Shuman, S. and Dekker, N.H.** (2005) Friction and torque govern the relaxation of DNA supercoils by eukaryotic topoisomerase IB. *Nature*, **434**, 671–674.

- Krokan, H.E. and Bjørås, M.** (2013) Base excision repair. *Cold Spring Harbor Perspectives in Biology*, **5**, a012583.
- Kunkel, T.A. and Erie, D.A.** (2005) DNA mismatch repair. *Annual Review of Biochemistry*, **74**, 681–710.
- Kunz, B.A., Anderson, H.J., Osmond, M.J. and Vonarx, E.J.** (2005) Components of nucleotide excision repair and DNA damage tolerance in *Arabidopsis thaliana*. *Environmental and molecular mutagenesis*, **45**, 115–127.
- Kurzbauer, M.-T., Pradillo, M., Kerzendorfer, C., et al.** (2018) *Arabidopsis thaliana* FANCD2 Promotes Meiotic Crossover Formation. *Plant Cell*, **30**, 415–428.
- Kurzbauer, M.-T., Uanschou, C., Chen, D. and Schlögelhofer, P.** (2012) The Recombinases DMC1 and RAD51 Are Functionally and Spatially Separated during Meiosis in *Arabidopsis*. *The Plant Cell*, **24**, 2058–2070.
- Kusumoto, R., Dawut, L., Marchetti, C., Wan Lee, J., Vindigni, A., Ramsden, D. and Bohr, V.A.** (2008) Werner protein cooperates with the XRCC4-DNA ligase IV complex in end-processing. *Biochemistry*, **47**, 7548–7556.
- Kuzminov, A.** (2001) Single-strand interruptions in replicating chromosomes cause double-strand breaks. *Proceedings of the National Academy of Sciences of the United States of America*, **98**, 8241–8246.
- Lambing, C. and Heckmann, S.** (2018) Tackling Plant Meiosis: From Model Research to Crop Improvement. *Frontiers in Plant Science*, **9**.
- Lario, L.D., Botta, P., Casati, P. and Spampinato, C.P.** (2015) Role of AtMSH7 in UV-B-induced DNA damage recognition and recombination. *Journal of experimental botany*, **66**, 3019–3026.
- Lario, L.D., Ramirez-Parra, E., Gutierrez, C., Casati, P. and Spampinato, C.P.** (2011) Regulation of plant MSH2 and MSH6 genes in the UV-B-induced DNA damage response. *Journal of experimental botany*, **62**, 2925–2937.
- Leman, A.R. and Noguchi, E.** (2013) The Replication Fork: Understanding the Eukaryotic Replication Machinery and the Challenges to Genome Duplication. *Genes (Basel)*, **4**, 1–32.
- Letunic, I. and Bork, P.** (2019) Interactive Tree Of Life (iTOL) v4: recent updates and new developments. *Nucleic acids research*, **47**, W256–W259.
- Lhuissier, F.G.P., Offenberg, H.H., Wittich, P.E., Vischer, N.O.E. and Heyting, C.** (2007) The Mismatch Repair Protein MLH1 Marks a Subset of Strongly Interfering Crossovers in Tomato. *The Plant Cell*, **19**, 862–876.
- Li, B. and Comai, L.** (2000) Functional interaction between Ku and the werner syndrome protein in DNA end processing. *J Biol Chem*, **275**, 28349–28352.

- Li, B., Conway, N., Navarro, S., Comai, Luca and Comai, Lucio** (2005) A conserved and species-specific functional interaction between the Werner syndrome-like exonuclease atWEX and the Ku heterodimer in Arabidopsis. *Nucleic acids research*, **33**, 6861–6867.
- Li, F., Cheng, Y., Ma, L., Li, S. and Wang, J.** (2022) Identification of reference genes provides functional insights into meiotic recombination suppressors in *Gerbera hybrida*. *Horticultural Plant Journal*, **8**, 123–132.
- Li, W., Chen, C., Markmann-Mulisch, U., Timofejeva, L., Schmelzer, E., Ma, H. and Reiss, B.** (2004) The Arabidopsis AtRAD51 gene is dispensable for vegetative development but required for meiosis. *Proceedings of the National Academy of Sciences*, **101**, 10596–10601.
- Li, W. and Wang, J.C.** (1998) Mammalian DNA topoisomerase IIIalpha is essential in early embryogenesis. *Proc Natl Acad Sci U S A*, **95**, 1010–1013.
- Li, X., Yu, M., Bolaños-Villegas, P., Zhang, J., Ni, D., Ma, H. and Wang, Y.** (2021) Fanconi Anemia Ortholog FANCM Regulates Meiotic Crossover Distribution in Plants. *Plant physiology*.
- Lieber, M.R.** (2010) The mechanism of double-strand DNA break repair by the nonhomologous DNA end-joining pathway. *Annual Review of Biochemistry*, **79**, 181–211.
- Lindahl, T.** (1993) Instability and decay of the primary structure of DNA. *Nature*, **362**, 709–715.
- Lindstrom, E.W. and Koos, K.** (1931) Cyto-Genetic Investigations of a Haploid Tomato and Its Diploid and Tetraploid Progeny. *American Journal of Botany*, **18**, 398–410.
- Liu, S.J., Horlbeck, M.A., Cho, S.W., et al.** (2017) CRISPRi-based genome-scale identification of functional long noncoding RNA loci in human cells. *Science*, **355**, aah7111.
- Lobet, G., Pagès, L. and Draye, X.** (2011) A novel image-analysis toolbox enabling quantitative analysis of root system architecture. *Plant physiology*, **157**, 29–39.
- Löbrich, M., Shibata, A., Beucher, A., Fisher, A., Ensminger, M., Goodarzi, A.A., Barton, O. and Jeggo, P.A.** (2010) gammaH2AX foci analysis for monitoring DNA double-strand break repair: strengths, limitations and optimization. *Cell cycle (Georgetown, Tex.)*, **9**, 662–669.
- Mah, L.-J., El-Osta, A. and Karagiannis, T.C.** (2010) gammaH2AX: a sensitive molecular marker of DNA damage and repair. *Leukemia*, **24**, 679–686.
- Mannuss, A., Dukowic-Schulze, S., Suer, S., Hartung, F., Pacher, M. and Puchta, H.** (2010) RAD5A, RECQ4A, and MUS81 Have Specific Functions in Homologous Recombination and Define Different Pathways of DNA Repair in *Arabidopsis thaliana*. *The Plant Cell*, **22**, 3318–3330.

- Manova, V. and Gruszka, D.** (2015) DNA damage and repair in plants - from models to crops. *Front Plant Sci*, **6**, 885.
- Manthei, K.A. and Keck, J.L.** (2013) The BLM dissolvasome in DNA replication and repair. *Cell Mol Life Sci*, **70**, 4067–4084.
- Maréchal, A. and Zou, L.** (2013) DNA damage sensing by the ATM and ATR kinases. *Cold Spring Harbor Perspectives in Biology*, **5**.
- Martí, E., Gisbert, C., Bishop, G.J., Dixon, M.S. and García-Martínez, J.L.** (2006) Genetic and physiological characterization of tomato cv. Micro-Tom. *J Exp Bot*, **57**, 2037–2047.
- Martini, E., Diaz, R.L., Hunter, N. and Keeney, S.** (2006) Crossover homeostasis in yeast meiosis. *Cell*, **126**, 285–295.
- Massy, B. de** (2013) Initiation of Meiotic Recombination: How and Where? Conservation and Specificities Among Eukaryotes. *Annual Review of Genetics*, **47**, 563–599.
- Masutani, C., Sugasawa, K., Yanagisawa, J., et al.** (1994) Purification and cloning of a nucleotide excision repair complex involving the xeroderma pigmentosum group C protein and a human homologue of yeast RAD23. *The EMBO Journal*, **13**, 1831–1843.
- Matos, J. and West, S.C.** (2014) Holliday junction resolution: regulation in space and time. *DNA Repair*, **19**, 176–181.
- Mehta, A. and Haber, J.E.** (2014) Sources of DNA double-strand breaks and models of recombinational DNA repair. *Cold Spring Harbor Perspectives in Biology*, **6**, a016428.
- Meissner, R., Jacobson, Y., Melamed, S., Levyatuv, S., Shalev, G., Ashri, A., Elkind, Y. and Levy, A.** (1997) A new model system for tomato genetics. *The Plant journal : for cell and molecular biology*, **12**, 1465–1472.
- Mercier, R., Mézard, C., Jenczewski, E., Macaisne, N. and Grelon, M.** (2015) The Molecular Biology of Meiosis in Plants. *Annual Review of Plant Biology*, **66**, 297–327.
- Mieulet, D., Aubert, G., Bres, C., et al.** (2018) Unleashing meiotic crossovers in crops. *Nat Plants*, **4**, 1010–1016.
- Milligan, J.R., Ng, J.Y., Wu, C.C., Aguilera, J.A., Fahey, R.C. and Ward, J.F.** (1995) DNA repair by thiols in air shows two radicals make a double-strand break. *Radiation research*, **143**, 273–280.
- Mirkin Ekaterina V. and Mirkin Sergei M.** (2007) Replication Fork Stalling at Natural Impediments. *Microbiology and Molecular Biology Reviews*, **71**, 13–35.
- Mojica, F.J.M., Díez-Villaseñor, C., García-Martínez, J. and Soria, E.** (2005) Intervening sequences of regularly spaced prokaryotic repeats derive from foreign genetic elements. *J Mol Evol*, **60**, 174–182.

- Molinier, J., Lechner, E., Dumbliauskas, E. and Genschik, P.** (2008) Regulation and role of Arabidopsis CUL4-DDB1A-DDB2 in maintaining genome integrity upon UV stress. *PLoS genetics*, **4**, e1000093.
- Molinier, J., Ramos, C., Fritsch, O. and Hohn, B.** (2004) CENTRIN2 Modulates Homologous Recombination and Nucleotide Excision Repair in Arabidopsis[W]. *The Plant cell*, **16**, 1633–1643.
- Moynahan, M.E. and Jasin, M.** (1997) Loss of heterozygosity induced by a chromosomal double-strand break. *Proceedings of the National Academy of Sciences of the United States of America*, **94**, 8988–8993.
- Mullen, J.R., Nallaseth, F.S., Lan, Y.Q., Slagle, C.E. and Brill, S.J.** (2005) Yeast Rmi1/Nce4 Controls Genome Stability as a Subunit of the Sgs1-Top3 Complex. *Mol Cell Biol*, **25**, 4476–4487.
- Nakamura, K., Saredi, G., Becker, J.R., et al.** (2019) H4K20me0 recognition by BRCA1–BARD1 directs homologous recombination to sister chromatids. *Nat Cell Biol*, **21**, 311–318.
- Nakazawa, Y., Hara, Y., Oka, Y., et al.** (2020) Ubiquitination of DNA Damage-Stalled RNAPII Promotes Transcription-Coupled Repair. *Cell*, **180**, 1228-1244.e24.
- Nash, R.A., Caldecott, K.W., Barnes, D.E. and Lindahl, T.** (1997) XRCC1 Protein Interacts with One of Two Distinct Forms of DNA Ligase III. *Biochemistry*, **36**, 5207–5211.
- Neale, M.J., Pan, J. and Keeney, S.** (2006) Endonucleolytic processing of covalent protein-linked double-strand breaks. , 11.
- Nimonkar, A.V., Genschel, J., Kinoshita, E., Polaczek, P., Campbell, J.L., Wyman, C., Modrich, P. and Kowalczykowski, S.C.** (2011) BLM-DNA2-RPA-MRN and EXO1-BLM-RPA-MRN constitute two DNA end resection machineries for human DNA break repair. *Genes Dev*, **25**, 350–362.
- Nimonkar, A.V., Özsoy, A.Z., Genschel, J., Modrich, P. and Kowalczykowski, S.C.** (2008) Human exonuclease 1 and BLM helicase interact to resect DNA and initiate DNA repair. *Proc Natl Acad Sci U S A*, **105**, 16906–16911.
- Nishant, K.T., Chen, C., Shinohara, M., Shinohara, A. and Alani, E.** (2010) Genetic Analysis of Baker’s Yeast Msh4-Msh5 Reveals a Threshold Crossover Level for Meiotic Viability. *PLOS Genetics*, **6**, e1001083.
- NV, P., PA, V., Vemanna, R., MS, S. and Makarla, U.** (2017) Quantification of Membrane Damage/Cell Death Using Evan’s Blue Staining Technique. *BIO-PROTOCOL*, **7**.
- O’Brien, P.J. and Ellenberger, T.** (2004) Dissecting the broad substrate specificity of human 3-methyladenine-DNA glycosylase. *J Biol Chem*, **279**, 9750–9757.
- Ohtsubo, T., Matsuda, O., Iba, K., Terashima, I., Sekiguchi, M. and Nakabeppu, Y.** (1998) Molecular cloning of AtMMH, an Arabidopsis thaliana ortholog of the Escherichia coli

- mutM gene, and analysis of functional domains of its product. *Molecular and General Genetics MGG*, **259**, 577–590.
- Okuda, M., Nakazawa, Y., Guo, C., Ogi, T. and Nishimura, Y.** (2017) Common TFIIH recruitment mechanism in global genome and transcription-coupled repair subpathways. *Nucleic acids research*, **45**, 13043–13055.
- Onoda, F., Seki, M., Miyajima, A. and Enomoto, T.** (2000) Elevation of sister chromatid exchange in *Saccharomyces cerevisiae* sgs1 disruptants and the relevance of the disruptants as a system to evaluate mutations in Bloom's syndrome gene. *Mutation Research/DNA Repair*, **459**, 203–209.
- Osakabe, K., Osakabe, Y. and Toki, S.** (2010) Site-directed mutagenesis in *Arabidopsis* using custom-designed zinc finger nucleases. *Proceedings of the National Academy of Sciences of the United States of America*, **107**, 12034–12039.
- Oshima, J., Kato, H., Maezawa, Y. and Yokote, K.** (2018) RECQ helicase disease and related progeroid syndromes: RECQ2018 meeting. *Mech Ageing Dev*, **173**, 80–83.
- Osman, K., Higgins, J.D., Sanchez-Moran, E., Armstrong, S.J. and Franklin, F.C.H.** (2011) Pathways to meiotic recombination in *Arabidopsis thaliana*. *New Phytologist*, **190**, 523–544.
- Pâques, F. and Haber, J.E.** (1999) Multiple pathways of recombination induced by double-strand breaks in *Saccharomyces cerevisiae*. *Microbiology and molecular biology reviews : MMBR*, **63**, 349–404.
- Pećina-Šlaus, N., Kafka, A., Salamon, I. and Bukovac, A.** (2020) Mismatch Repair Pathway, Genome Stability and Cancer. *Frontiers in molecular biosciences*, **7**, 122.
- Pedroza-Garcia, J.-A., Veylder, L. and Raynaud, C.** (2019) Plant DNA Polymerases. *International journal of molecular sciences*, **20**.
- Pellegrino, S., Michelena, J., Teloni, F., Imhof, R. and Altmeyer, M.** (2017) Replication-Coupled Dilution of H4K20me2 Guides 53BP1 to Pre-replicative Chromatin. *Cell Reports*, **19**, 1819–1831.
- Peng, W. and Shaw, B.R.** (1996) Accelerated Deamination of Cytosine Residues in UV-Induced Cyclobutane Pyrimidine Dimers Leads to CC→TT Transitions. *Biochemistry*, **35**, 10172–10181.
- Plank, J.L., Chu, S.H., Pohlhaus, J.R., Wilson-Sali, T. and Hsieh, T.-S.** (2005) *Drosophila melanogaster* topoisomerase III $\alpha$  preferentially relaxes a positively or negatively supercoiled bubble substrate and is essential during development. *J Biol Chem*, **280**, 3564–3573.
- Podlutsky, A.Ja., Dianova, I.I., Podust, V.N., Bohr, V.A. and Dianov, G.L.** (2001) Human DNA polymerase  $\beta$  initiates DNA synthesis during long-patch repair of reduced AP sites in DNA. *The EMBO Journal*, **20**, 1477–1482.

- Pradillo, M., Varas, J., Oliver, C. and Santos, J.** (2014) On the role of AtDMC1, AtRAD51 and its paralogs during Arabidopsis meiosis. *Frontiers in Plant Science*, **5**.
- Provart, N.J., Alonso, J., Assmann, S.M., et al.** (2016) 50 years of Arabidopsis research: highlights and future directions. *New Phytol*, **209**, 921–944.
- Puchta, H.** (2004) The repair of double-strand breaks in plants: mechanisms and consequences for genome evolution. *Journal of experimental botany*, **56**, 1–14.
- Puchta, H. and Fauser, F.** (2014a) Synthetic nucleases for genome engineering in plants: prospects for a bright future. *The Plant journal : for cell and molecular biology*, **78**, 727–741.
- Puizina, J., Siroky, J., Mokros, P., Schweizer, D. and Riha, K.** (2004) Mre11 deficiency in Arabidopsis is associated with chromosomal instability in somatic cells and Spo11-dependent genome fragmentation during meiosis. *Plant Cell*, **16**, 1968–1978.
- Qin, Z., Bi, L., Hou, X.-M., et al.** (2020) Human RPA activates BLM's bidirectional DNA unwinding from a nick. *Elife*, **9**, e54098.
- Ramanna, M.S. and Prakken, R.** (1967) Structure of and homology between pachytene and somatic metaphase chromosomes of the tomato. *Genetica*, **38**, 115–133.
- Raynard, S., Bussen, W. and Sung, P.** (2006) A double Holliday junction dissolvasome comprising BLM, topoisomerase IIIalpha, and BLAP75. *J Biol Chem*, **281**, 13861–13864.
- Renty, C. de and Ellis, N.A.** (2017) Bloom's syndrome: Why not premature aging?: A comparison of the BLM and WRN helicases. *Ageing Res Rev*, **33**, 36–51.
- Rogers, C.M., Wang, J.C.-Y., Noguchi, H., Imasaki, T., Takagi, Y. and Bochman, M.L.** (2017) Yeast Hrq1 shares structural and functional homology with the disease-linked human RecQ4 helicase. *Nucleic Acids Res*, **45**, 5217–5230.
- Röhrig, S., Schröpfer, S., Knoll, A. and Puchta, H.** (2016) The RTR Complex Partner RMI2 and the DNA Helicase RTEL1 Are Both Independently Involved in Preserving the Stability of 45S rDNA Repeats in Arabidopsis thaliana. *PLoS genetics*, **12**, e1006394.
- Roldán-Arjona, T., Ariza, R.R. and Córdoba-Cañero, D.** (2019) DNA Base Excision Repair in Plants: An Unfolding Story With Familiar and Novel Characters. *Front Plant Sci*, **10**, 1055.
- Roser, M., Ritchie, H. and Ortiz-Ospina, E.** (2013) World Population Growth. *Our World in Data*. Available at: <https://ourworldindata.org/world-population-growth> [Accessed June 22, 2022].
- Ross, K.J., Fransz, P. and Jones, G.H.** (1996) A light microscopic atlas of meiosis in Arabidopsis thaliana. *Chromosome Res*, **4**, 507–516.
- Ruff, S.E., Logan, S.K., Garabedian, M.J. and Huang, T.T.** (2020) Roles for MDC1 in cancer development and treatment. *DNA Repair*, **95**, 102948.

- Sakamoto, A.N.** (2019) Translesion Synthesis in Plants: Ultraviolet Resistance and Beyond. *Front Plant Sci*, **10**.
- Sancar, A.** (2003) Structure and Function of DNA Photolyase and Cryptochrome Blue-Light Photoreceptors. *Chemical Reviews*, **103**, 2203–2238.
- Sancar, A., Lindsey-Boltz, L.A., Unsal-Kaçmaz, K. and Linn, S.** (2004) Molecular mechanisms of mammalian DNA repair and the DNA damage checkpoints. *Annual Review of Biochemistry*, **73**, 39–85.
- Saredi, G., Huang, H., Hammond, C.M., et al.** (2016) H4K20me0 marks post-replicative chromatin and recruits the TONSL–MMS22L DNA repair complex. *Nature*, **534**, 714–718.
- Sato, S., Tabata, S., Hirakawa, H., et al.** (2012) The tomato genome sequence provides insights into fleshy fruit evolution. *Nature*, **485**, 635–641.
- Schindele, A., Dorn, A. and Puchta, H.** (2020) CRISPR/Cas brings plant biology and breeding into the fast lane. *Curr Opin Biotechnol*, **61**, 7–14.
- Schmidt, C., Pacher, M. and Puchta, H.** (2019) DNA Break Repair in Plants and Its Application for Genome Engineering. In S. Kumar, P. Barone, and M. Smith, eds. *Transgenic Plants: Methods and Protocols*. Methods in Molecular Biology. New York, NY: Springer, pp. 237–266.
- Schröpfer, S., Kobbe, D., Hartung, F., Knoll, A. and Puchta, H.** (2014a) Defining the roles of the N-terminal region and the helicase activity of RECQ4A in DNA repair and homologous recombination in Arabidopsis. *Nucleic Acids Research*, **42**, 1684–1697.
- Séguéla-Arnaud, M., Choinard, S., Larchevêque, C., Girard, C., Froger, N., Crismani, W. and Mercier, R.** (2017) RMI1 and TOP3 $\alpha$  limit meiotic CO formation through their C-terminal domains. *Nucleic Acids Research*, **45**, 1860–1871.
- Séguéla-Arnaud, M., Crismani, W., Larchevêque, C., et al.** (2015) Multiple mechanisms limit meiotic crossovers: TOP3 $\alpha$  and two BLM homologs antagonize crossovers in parallel to FANCM. *Proc Natl Acad Sci U S A*, **112**, 4713–4718.
- Seol, Y. and Neuman, K.C.** (2016) The dynamic interplay between DNA topoisomerases and DNA topology. *Biophys Rev*, **8**, 101–111.
- Serra, H., Lambing, C., Griffin, C.H., et al.** (2018) Massive crossover elevation via combination of HEI10 and recq4a recq4b during Arabidopsis meiosis. *Proc Natl Acad Sci U S A*, **115**, 2437–2442.
- Sfeir, A. and Symington, L.S.** (2015) Microhomology-Mediated End Joining: A Back-up Survival Mechanism or Dedicated Pathway? *Trends in Biochemical Sciences*, **40**, 701–714.
- Shamanna, R.A., Lu, H., Freitas, J.K., Tian, J., Croteau, D.L. and Bohr, V.A.** (2016) WRN regulates pathway choice between classical and alternative non-homologous end joining. *Nat Commun*, **7**, 1–12.

- Sherman, J.D. and Stack, S.M.** (1995) Two-dimensional spreads of synaptonemal complexes from solanaceous plants. VI. High-resolution recombination nodule map for tomato (*Lycopersicon esculentum*). *Genetics*, **141**, 683–708.
- Shikata, M. and Ezura, H.** (2016) Micro-Tom Tomato as an Alternative Plant Model System: Mutant Collection and Efficient Transformation. In J. R. Botella and M. A. Botella, eds. *Plant Signal Transduction: Methods and Protocols*. Methods in Molecular Biology. New York, NY: Springer, pp. 47–55.
- Shinohara, A., Ogawa, H. and Ogawa, T.** (1992) Rad51 protein involved in repair and recombination in *S. cerevisiae* is a RecA-like protein. *Cell*, **69**, 457–470.
- Shrivastav, M., Haro, L.P. and Nickoloff, J.A.** (2008) Regulation of DNA double-strand break repair pathway choice. *Cell Research*, **18**, 134–147.
- Shuman, S., Kane, E.M. and Morham, S.G.** (1989) Mapping the active-site tyrosine of vaccinia virus DNA topoisomerase I. *Proc Natl Acad Sci U S A*, **86**, 9793–9797.
- Singh, D.K., Karmakar, P., Aamann, M., Schurman, S.H., May, A., Croteau, D.L., Burks, L., Plon, S.E. and Bohr, V.A.** (2010) The involvement of human RECQL4 in DNA double-strand break repair. *Aging Cell*, **9**, 358–371.
- Singh, T.R., Ali, A.M., Busygina, V., Raynard, S., Fan, Q., Du, C., Andreassen, P.R., Sung, P. and Meetei, A.R.** (2008) BLAP18/RMI2, a novel OB-fold-containing protein, is an essential component of the Bloom helicase-double Holliday junction dissolvosome. *Genes Dev*, **22**, 2856–2868.
- Snowden, T., Acharya, S., Butz, C., Berardini, M. and Fishel, R.** (2004) hMSH4-hMSH5 Recognizes Holliday Junctions and Forms a Meiosis-Specific Sliding Clamp that Embraces Homologous Chromosomes. *Molecular Cell*, **15**, 437–451.
- Soniat, M.M., Myler, L.R., Kuo, H.-C., Paull, T.T. and Finkelstein, I.J.** (2019) RPA phosphorylation inhibits DNA resection. *Mol Cell*, **75**, 145-153.e5.
- Soutoglou, E. and Misteli, T.** (2008) Activation of the cellular DNA damage response in the absence of DNA lesions. *Science (New York, N.Y.)*, **320**, 1507–1510.
- Spakman, D., Bakx, J.A.M., Biebricher, A.S., Peterman, E.J.G., Wuite, G.J.L. and King, G.A.** (2021) Unravelling the mechanisms of Type 1A topoisomerases using single-molecule approaches. *Nucleic Acids Research*, **49**, 5470–5492.
- Spampinato, C.P.** (2017) Protecting DNA from errors and damage: an overview of DNA repair mechanisms in plants compared to mammals. *Cell. Mol. Life Sci.*, **74**, 1693–1709.
- Srivastava, D.K., Berg, B.J., Prasad, R., Molina, J.T., Beard, W.A., Tomkinson, A.E. and Wilson, S.H.** (1998) Mammalian abasic site base excision repair. Identification of the reaction sequence and rate-determining steps. *J Biol Chem*, **273**, 21203–21209.
- Steinert, J., Schiml, S., Fauser, F. and Puchta, H.** (2015) Highly efficient heritable plant genome engineering using Cas9 orthologues from *Streptococcus thermophilus* and

- Staphylococcus aureus. *The Plant journal : for cell and molecular biology*, **84**, 1295–1305.
- Steinert, J., Schiml, S. and Puchta, H.** (2016) Homology-based double-strand break-induced genome engineering in plants. *Plant Cell Rep*, **35**, 1429–1438.
- Stelter, P. and Ulrich, H.D.** (2003) Control of spontaneous and damage-induced mutagenesis by SUMO and ubiquitin conjugation. *Nature*, **425**, 188–191.
- Stivers, J.T., Harris, T.K. and Mildvan, A.S.** (1997) Vaccinia DNA Topoisomerase I: Evidence Supporting a Free Rotation Mechanism for DNA Supercoil Relaxation. *Biochemistry*, **36**, 5212–5222.
- Stivers, J.T. and Jiang, Y.L.** (2003) A mechanistic perspective on the chemistry of DNA repair glycosylases. *Chemical Reviews*, **103**, 2729–2759.
- Strzalka, W., Bartnicki, F., Pels, K., Jakubowska, A., Tsurimoto, T. and Tanaka, K.** (2013) RAD5a ubiquitin ligase is involved in ubiquitination of Arabidopsis thaliana proliferating cell nuclear antigen. *Journal of experimental botany*, **64**, 859–869.
- Strzalka, W. and Ziemienowicz, A.** (2011) Proliferating cell nuclear antigen (PCNA): a key factor in DNA replication and cell cycle regulation. *Ann Bot*, **107**, 1127–1140.
- Sugasawa, K., Okamoto, T., Shimizu, Y., Masutani, C., Iwai, S. and Hanaoka, F.** (2001) A multistep damage recognition mechanism for global genomic nucleotide excision repair. *Genes Dev*, **15**, 507–521.
- Sugasawa, K., Shimizu, Y., Iwai, S. and Hanaoka, F.** (2002) A molecular mechanism for DNA damage recognition by the xeroderma pigmentosum group C protein complex. *DNA Repair*, **1**, 95–107.
- Sun, Y., McCorvie, T.J., Yates, L.A. and Zhang, X.** (2020) Structural basis of homologous recombination. *Cell. Mol. Life Sci.*, **77**, 3–18.
- Symington, L.S.** (2014) End resection at double-strand breaks: mechanism and regulation. *Cold Spring Harbor Perspectives in Biology*, **6**.
- Tamura, K., Adachi, Y., Chiba, K., Oguchi, K. and Takahashi, H.** (2002) Identification of Ku70 and Ku80 homologues in Arabidopsis thaliana: evidence for a role in the repair of DNA double-strand breaks. *The Plant journal : for cell and molecular biology*, **29**, 771–781.
- Taneja, B., Schnurr, B., Slesarev, A., Marko, J.F. and Mondragón, A.** (2007) Topoisomerase V relaxes supercoiled DNA by a constrained swiveling mechanism. *Proceedings of the National Academy of Sciences*, **104**, 14670–14675.
- Terekhova, K., Marko, J.F. and Mondragón, A.** (2014) Single-molecule analysis uncovers the difference between the kinetics of DNA decatenation by bacterial topoisomerases I and III. *Nucleic Acids Res*, **42**, 11657–11667.

- The Arabidopsis Genome Initiative** (2000) Analysis of the genome sequence of the flowering plant *Arabidopsis thaliana*. *Nature*, **408**, 796–815.
- Thompson, L.H.** (2012) Recognition, signaling, and repair of DNA double-strand breaks produced by ionizing radiation in mammalian cells: the molecular choreography. *Mutation research*, **751**, 158–246.
- Tourrière, H. and Pasero, P.** (2007) Maintenance of fork integrity at damaged DNA and natural pause sites. *DNA Repair*, **6**, 900–913.
- Trenner, A. and Sartori, A.A.** (2019) Harnessing DNA Double-Strand Break Repair for Cancer Treatment. *Frontiers in oncology*, **9**, 1388.
- Uanschou, C., Ronceret, A., Von Harder, M., et al.** (2013) Sufficient Amounts of Functional HOP2/MND1 Complex Promote Interhomolog DNA Repair but Are Dispensable for Intersister DNA Repair during Meiosis in Arabidopsis[W]. *Plant Cell*, **25**, 4924–4940.
- Uanschou, C., Siwec, T., Pedrosa-Harand, A., et al.** (2007) A novel plant gene essential for meiosis is related to the human CtIP and the yeast COM1/SAE2 gene. *EMBO J*, **26**, 5061–5070.
- Uchiyama, Y., Kimura, S., Yamamoto, T., Ishibashi, T. and Sakaguchi, K.** (2004) Plant DNA polymerase  $\lambda$ , a DNA repair enzyme that functions in plant meristematic and meiotic tissues. *European Journal of Biochemistry*, **271**, 2799–2807.
- Urban, V., Dobrovolna, J. and Janscak, P.** (2017) Distinct functions of human RecQ helicases during DNA replication. *Biophysical Chemistry*, **225**, 20–26.
- Vaisman, A. and Woodgate, R.** (2017) Translesion DNA polymerases in eukaryotes: what makes them tick? *Critical Reviews in Biochemistry and Molecular Biology*, **52**, 274–303.
- Valdiglesias, V., Giunta, S., Fenech, M., Neri, M. and Bonassi, S.** (2013)  $\gamma$ H2AX as a marker of DNA double strand breaks and genomic instability in human population studies. *Mutation research*, **753**, 24–40.
- Velkova, M., Silva, N., Stritto, M.R.D., Schleiffer, A., Barraud, P., Hartl, M. and Jantsch, V.** (2021) *Caenorhabditis elegans* RMI2 functional homolog-2 (RMIF-2) and RMI1 (RMH-1) have both overlapping and distinct meiotic functions within the BTR complex. *PLOS Genetics*, **17**, e1009663.
- Vrielynck, N., Chambon, A., Vezon, D., Pereira, L., Chelysheva, L., De Muyt, A., Mézard, C., Mayer, C. and Grelon, M.** (2016) A DNA topoisomerase VI-like complex initiates meiotic recombination. *Science*, **351**, 939–943.
- Walker, J.R., Corpina, R.A. and Goldberg, J.** (2001) Structure of the Ku heterodimer bound to DNA and its implications for double-strand break repair. *Nature*, **412**, 607–614.
- Wang, F., Yang, Y., Singh, T.R., et al.** (2010) Crystal Structures of RMI1 and RMI2, Two OB-fold Regulatory Subunits of the BLM Complex. *Structure*, **18**, 1159–1170.

- Wang, H., Di Gate, R.J. and Seeman, N.C.** (1996) An RNA topoisomerase. *Proceedings of the National Academy of Sciences*, **93**, 9477–9482.
- Wang, H. and Xu, X.** (2017) Microhomology-mediated end joining: new players join the team. *Cell & Bioscience*, **7**, 6.
- Wang, Q., Goldstein, M., Alexander, P., Wakeman, T.P., Sun, T., Feng, J., Lou, Z., Kastan, M.B. and Wang, X.-F.** (2014) Rad17 recruits the MRE11-RAD50-NBS1 complex to regulate the cellular response to DNA double-strand breaks. *The EMBO Journal*, **33**, 862–877.
- Wang, S., Wen, R., Shi, X., Lambrecht, A., Wang, H. and Xiao, W.** (2011) RAD5a and REV3 function in two alternative pathways of DNA-damage tolerance in Arabidopsis. *DNA Repair*, **10**, 620–628.
- Wang, Y., Rengs, W.M.J. van, Zaidan, M.W.A.M. and Underwood, C.J.** (2021) Meiosis in crops: from genes to genomes. *J Exp Bot*, **72**, 6091–6109.
- Ward, J.F.** (1994) The complexity of DNA damage: relevance to biological consequences. *International journal of radiation biology*, **66**, 427–432.
- Waterworth, W.M., Kozak, J., Provost, C.M., Bray, C.M., Angelis, K.J. and West, C.E.** (2009) DNA ligase 1 deficient plants display severe growth defects and delayed repair of both DNA single and double strand breaks. *BMC Plant Biol*, **9**, 1–12.
- Watt, P.M., Hickson, I.D., Borts, R.H. and Louis, E.J.** (1996) Sgs1, a Homologue of the Bloom's and Werner's Syndrome Genes, Is Required for Maintenance of Genome Stability in *Saccharomyces Cerevisiae*. *Genetics*, **144**, 935–945.
- Wechsler, T., Newman, S. and West, S.C.** (2011) Aberrant chromosome morphology in human cells defective for Holliday junction resolution. *Nature*, **471**, 642–646.
- West, C.E., Waterworth, W.M., Jiang, Q. and Bray, C.M.** (2000) Arabidopsis DNA ligase IV is induced by gamma-irradiation and interacts with an Arabidopsis homologue of the double strand break repair protein XRCC4. *The Plant journal : for cell and molecular biology*, **24**, 67–78.
- West, C.E., Waterworth, W.M., Story, G.W., Sunderland, P.A., Jiang, Q. and Bray, C.M.** (2002) Disruption of the Arabidopsis AtKu80 gene demonstrates an essential role for AtKu80 protein in efficient repair of DNA double-strand breaks in vivo. *The Plant journal : for cell and molecular biology*, **31**, 517–528.
- West, S.C.** (2003) Molecular views of recombination proteins and their control. *Nat Rev Mol Cell Biol*, **4**, 435–445.
- Whitbread, A.L., Dorn, A., Röhrig, S. and Puchta, H.** (2021) Different functional roles of RTR complex factors in DNA repair and meiosis in Arabidopsis and tomato. *The Plant Journal*, **106**, 965–977.
- Wicky Collaud, C., Alpi, A., Passannante, M., Rose, A., Gartner, A. and Mueller, F.** (2004) Multiple Genetic Pathways Involving the *Caenorhabditis elegans* Bloom's Syndrome

- Genes *him-6*, *rad-51*, and *top-3* Are Needed To Maintain Genome Stability in the Germ Line. *Molecular and cellular biology*, **24**, 5016–27.
- Wu, L., Bachrati, C.Z., Ou, J., et al.** (2006) BLAP75/RMI1 promotes the BLM-dependent dissolution of homologous recombination intermediates. *Proc Natl Acad Sci U S A*, **103**, 4068–4073.
- Wu, L., Davies, S.L., Levitt, N.C. and Hickson, I.D.** (2001) Potential role for the BLM helicase in recombinational repair via a conserved interaction with RAD51. *J Biol Chem*, **276**, 19375–19381.
- Wu, L. and Hickson, I.D.** (2003) The Bloom's syndrome helicase suppresses crossing over during homologous recombination. *Nature*, **426**, 870–874.
- Wu, S.-Y., Culligan, K., Lamers, M. and Hays, J.** (2003) Dissimilar mispair-recognition spectra of Arabidopsis DNA-mismatch-repair proteins MSH2\*MSH6 (MutSalpha) and MSH2\*MSH7 (MutSgamma). *Nucleic acids research*, **31**, 6027–6034.
- Wu, Z., Jianhui, J., Tang, D., et al.** (2015) OsSDS is essential for DSB formation in rice meiosis. *Frontiers in Plant Science*, **6**.
- Wyatt, H.D.M. and West, S.C.** (2014) Holliday junction resolvases. *Cold Spring Harbor Perspectives in Biology*, **6**, a023192.
- Xu, C., Fang, L., Kong, Y., Xiao, C., Yang, M., Du, L.-Q. and Liu, Q.** (2017) Knockdown of RMI1 impairs DNA repair under DNA replication stress. *Biochemical and Biophysical Research Communications*, **494**, 158–164.
- Xu, D., Guo, R., Sobock, A., et al.** (2008) RMI, a new OB-fold complex essential for Bloom syndrome protein to maintain genome stability. *Genes Dev*, **22**, 2843–2855.
- Xu, D., Shen, W., Guo, R., et al.** (2013) Top3 $\beta$  is an RNA topoisomerase that works with fragile X syndrome protein to promote synapse formation. *Nat Neurosci*, **16**, 1238–1247.
- Xu, J., Lahiri, I., Wang, W., et al.** (2017) Structural basis for the initiation of eukaryotic transcription-coupled DNA repair. *Nature*, **551**, 653–657.
- Xue, C., Daley, J.M., Xue, X., Steinfeld, J., Kwon, Y., Sung, P. and Greene, E.C.** (2019) Single-molecule visualization of human BLM helicase as it acts upon double- and single-stranded DNA substrates. *Nucleic Acids Res*, **47**, 11225–11237.
- Yang, J., Bachrati, C.Z., Ou, J., Hickson, I.D. and Brown, G.W.** (2010) Human topoisomerase IIIalpha is a single-stranded DNA decatenase that is stimulated by BLM and RMI1. *J Biol Chem*, **285**, 21426–21436.
- Yang, S., Zhang, C., Cao, Y., Du, G., Tang, D., Li, Y., Shen, Y., Yu, H. and Cheng, Z.** (2022) FIGNL1 Inhibits Non-homologous Chromosome Association and Crossover Formation. *Front Plant Sci*, **13**, 945893.

- Ye, J., Coulouris, G., Zaretskaya, I., Cutcutache, I., Rozen, S. and Madden, T.L.** (2012) Primer-BLAST: A tool to design target-specific primers for polymerase chain reaction. *BMC Bioinformatics*, **13**, 134.
- Yeh, C.D., Richardson, C.D. and Corn, J.E.** (2019) Advances in genome editing through control of DNA repair pathways. *Nat Cell Biol*, **21**, 1468–1478.
- Yin, J., Sobeck, A., Xu, C., Meetei, A.R., Hoatlin, M., Li, L. and Wang, W.** (2005) BLAP75, an essential component of Bloom’s syndrome protein complexes that maintain genome integrity. *EMBO J*, **24**, 1465–1476.
- Yokoi, M., Masutani, C., Maekawa, T., Sugasawa, K., Ohkuma, Y. and Hanaoka, F.** (2000) The xeroderma pigmentosum group C protein complex XPC-HR23B plays an important role in the recruitment of transcription factor IIIH to damaged DNA. *J Biol Chem*, **275**, 9870–9875.
- Zaidi, S.S.-A., Vanderschuren, H., Qaim, M., Mahfouz, M.M., Kohli, A., Mansoor, S. and Tester, M.** (2019) New plant breeding technologies for food security. *Science*, **363**, 1390–1391.
- Zhu, H., Li, C. and Gao, C.** (2020) Applications of CRISPR-Cas in agriculture and plant biotechnology. *Nat Rev Mol Cell Biol*, **21**, 661–677.

## 7. Supplementary

### 7.1 Oligonucleotide and primer combinations

**Table 7.1.** Oligonucleotides and sequences used for amplification of *TOP3α* and *RMI1* genomic DNA (gDNA) and copy DNA (cDNA) within the genome of *Solanum lycopersicum*, and the *ACTIN* gene as a control.

| Target         | Name          | Internal Primer ID/Name | Sequence (5' – 3')        | Use  |
|----------------|---------------|-------------------------|---------------------------|--|
| <i>SITOP3α</i> | TOP3α-gDNA-FW | AW87                    | AGTGAGCACGGCTGTAAGGC      | Amplification of Cas9 target loci within <i>SITOP3α</i> gDNA |
|                | TOP3α-gDNA-RV | AW90                    | CGAAGATCTATCTCCTCAGGGACAA |  |
|                | TOP3α-cDNA-FW | AW284                   | ATTCCGGCAACCGTTTCGT       | Amplification of Cas9 target loci within <i>SITOP3α</i> cDNA |
|                | TOP3α-cDNA-RV | AW285                   | GGCAGGGACCATAGCTCAAG      |  |
| <i>SIRMII</i>  | RMI1-gDNA-FW  | AW65                    | TCCGACGAAGAAGACGACGG      | Amplification of Cas9 target loci within <i>SIRMII</i> gDNA  |
|                | RMI1-gDNA-RV  | AW66                    | CCCACCTCATCGCCGGTAAA      |  |
|                | RMI1-cDNA-FW  | AW282                   | CTCCGACGAAGAAGACGACGG     | Amplification of Cas9 target loci within <i>SIRMII</i> cDNA  |
|                | RMI1-cDNA-RV  | AW283                   | GCCTGTACTCCATCCCAAACA     |  |
| <i>SIACTIN</i> | Actin-gDNA-FW | Actin_Fwd               | CCACTGGTTCGTACTIONGGCT    | Amplification of a loci within <i>SIACTIN</i> gDNA           |
|                | Actin-gDNA-RV | Actin_Rev               | TCTGGGCAACGGAACCTCTC      |  |
|                | Actin-cDNA-FW | AW259                   | TGTTGCTATCCAGGCTGTGCT     | Amplification of a loci within <i>SIACTIN</i> cDNA           |
|                | Actin-cDNA-RV | AW260                   | TCACACTGTCCCTATCTATGAAGGT |  |

**Table 7.2.** Oligonucleotides used for analysis of loci targeted during Cas9-mediated mutagenesis, via Sanger sequencing.

| Target         | Name     | Internal Primer ID | Sequence (5' – 3')        | Use  |
|----------------|----------|--------------------|---------------------------|--|
| <i>SITOP3α</i> | TOP3α-FW | AW87               | AGTGAGCACGGCTGTAAGGC      | Sequencing of Cas9 target loci within <i>SITOP3α</i> gDNA from PCR product using AW87/90 primers.            |
| <i>SIRMI1</i>  | RMI1-FW  | AW65               | TCCGACGAAGAAGACGACGG      | Sequencing of Cas9 target loci within <i>SITOP3α</i> gDNA using PCR product amplified using AW65/66 primers. |
|                | RMI1-SEQ | AW269              | AGGGCTAAGATTGCGGAGGGAATGG |  |

**Table 7.3.** Oligonucleotides used for *High Resolution Melting* (HRM) analysis.

| Target         | Name         | Internal Primer ID | Sequence (5' – 3')        | Use  |
|----------------|--------------|--------------------|---------------------------|--|
| <i>SITOP3α</i> | TOP3α-HRM-FW | SIT3ASa2_HRM1_Fwd  | AGAGACGGACGTTCCAGGTACAAC  | Amplification of Cas9 target loci within <i>SITOP3α</i> gDNA for HRM analysis. |
|                | TOP3α-HRM-RV | SIT3ASa2_HRM1_Rev  | GCGGGTCACACGAGTGCCAT      |  |
| <i>SIRMI1</i>  | RMI1-HRM-FW  | SIRmi1Sa2_HRM1_Fwd | TCTACTAACTTCCAATCAGTTACCC | Amplification of Cas9 target loci within <i>SIRMI1</i> gDNA for HRM analysis.  |
|                | RMI1-HRM-RV  | SIRmi1Sa2_HRM1_Rev | GCCCTAAATTTCCAATACCCGAC   |  |

**Table 7.4.** Oligonucleotides used for cloning the CRISPR/Cas9 constructs used for Cas9-mediated mutagenesis of both *TOP3α* and *RMI1* in tomato.

| Target         | Name                 | Internal Primer ID  | Sequence (5' – 3')       | Use   |
|----------------|----------------------|---------------------|--------------------------|---|
| <i>SITOP3α</i> | TOP3α-Protospacer-FW | T3a_py1_fw (AW123)  | GATGCTGTTACATCTGTCA      | Targeted mutagenesis of <i>SITOP3α</i> using CRISPR/Cas9.   |
|                | TOP3α-Protospacer-RV | T3a_py1_rv (AW124)  | AAACTGACAGATGTGAACAGCATC |   |
| <i>SIRMI1</i>  | RMI1-Protospacer-FW  | RMI1_py1_fw (AW131) | TTCGGATTGTGGTATTGGTC     | Targeted mutagenesis of <i>SIRMI1</i> using CRISPR/Cas9.  |
|                | RMI1-Protospacer-RV  | RMI1_py1_rv (AW132) | AAACGACCAATACCACAATCCGAA |   |
|                | SS129                |                     | CACAGGAAACAGCTATGAC      | Reverse primer for colony PCR to ensure integration of protospacer sequences into the pEn-Chimera CRISPR construct. |
|                | SS42                 |                     | TCCAGGATTAGAATGATTAGG    | Sequencing primer to ensure protospacer sequence integrated correctly into pEn-Chimera.                             |
|                | SS102                |                     | CACCATGTTATCACATCAATCC   | Reverse primer for colony PCR to ensure successful gateway reaction during gateway cloning of CRISPR cloning.       |

## 7.2 Raw Data

### Statistical Significance

For statistical analysis of results obtained during this thesis, a T-test with unequal variance was used when comparing mutant lines with the respective wild-type control lines.

The P-Values were interpreted as follows:

P-Value  $\geq 0.05$  = not significant (ns)

$0.01 < \text{P-Value} < 0.05$  = significant (\*)

$0.001 < \text{P-Value} < 0.01$  = very significant (\*\*)

P-Value  $< 0.001$  = extremely significant (\*\*\*)

### 7.2.1 Raw data for the characterisation of *slrmil* mutant lines

**Table 7.5.** Number of seeds per fruit of *slrmil-1* and *slrmil-2* homozygous mutant plant lines compared to wild type (WT), for four independent assays. The average number of seeds per fruit is shown as a boxplot in Figure 3.4.

| Line          | Average number of seeds per fruit. |         |         |         | Average | St-Dev | t-test    |
|---------------|------------------------------------|---------|---------|---------|---------|--------|-----------|
|               | Assay 1                            | Assay 2 | Assay 3 | Assay 4 |         |        |           |
| WT            | 6.7                                | 3.5     | 10.85   | 18.03   | 9.77    | 6.27   |           |
| <i>rmil-1</i> | 4.04                               | 0.69    | 13      | 12.81   | 7.64    | 6.24   | 0.65 (ns) |
| <i>rmil-2</i> | 4.31                               | 0.80    | 15.12   | 15.16   | 8.85    | 7.41   | 0.86 (ns) |

**Table 7.6.** Percentage of viable pollen for both *slrmil-1* and *slrmil-2* homozygous mutant plants compared to wild type (WT), for three independent assays. The average percentage of viable pollen is shown as a bar chart in Figure 3.5.

| Line          | Average percentage of viable pollen (%). |         |         | Average | St-Dev | t-test    |
|---------------|--|---------|---------|---------|--------|-----------|
|               | Assay 1                                  | Assay 2 | Assay 3 |         |        |           |
| WT            | 38.29                                    | 78.93   | 65.89   | 61.04   | 20.75  |           |
| <i>rmil-1</i> | 30.22                                    | 67.44   | 65.32   | 54.32   | 20.90  | 0.71 (ns) |
| <i>rmil-2</i> | 87.76                                    | 73.61   | 90.67   | 84.01   | 9.13   | 0.19 (ns) |

**Table 7.7.** Raw data for the genotoxin sensitivity analysis of *slrmi1-1* and *slrmi1-2* homozygous mutant lines compared to wild type (WT), with the genotoxic agent *cis*-Platin. Fresh weights (mg) at each concentration, for each line shown, for three independent assays. The average fresh weight relative to WT is shown as a bar chart in Figure 3.7.A.

|                                  |             |             |           |            |                                  |             |             |           |            |
|----------------------------------|-------------|-------------|-----------|------------|----------------------------------|-------------|-------------|-----------|------------|
| <b>Wild type</b>                 |             |             |           |            | <b>Wild type</b>                 |             |             |           |            |
| <i>cis</i> -Platin concentration | 1.5 $\mu$ M | 2.5 $\mu$ M | 5 $\mu$ M | 10 $\mu$ M | <i>cis</i> -Platin concentration | 1.5 $\mu$ M | 2.5 $\mu$ M | 5 $\mu$ M | 10 $\mu$ M |
| Assay 1                          | 67.12       | 49.54       | 36.45     | 28.48      | Average                          | 70.76       | 53.81       | 43.74     | 35.20      |
| Assay 2                          | 71.81       | 57.09       | 50.15     | 39.85      | St-Dev                           | 3.24        | 3.87        | 6.89      | 5.96       |
| Assay 3                          | 73.35       | 54.78       | 44.61     | 39.85      |                                  |             |             |           |            |
| <b><i>rmi1-1</i></b>             |             |             |           |            | <b><i>rmi1-1</i></b>             |             |             |           |            |
| <i>cis</i> -Platin concentration | 1.5 $\mu$ M | 2.5 $\mu$ M | 5 $\mu$ M | 10 $\mu$ M | <i>cis</i> -Platin concentration | 1.5 $\mu$ M | 2.5 $\mu$ M | 5 $\mu$ M | 10 $\mu$ M |
| Assay 1                          | 78.43       | 60.74       | 41.69     | 40.13      | Average                          | 70.00       | 53.55       | 40.30     | 37.62      |
| Assay 2                          | 59.41       | 47.34       | 39.36     | 36.25      | St-Dev                           | 9.69        | 6.75        | 1.23      | 2.18       |
| Assay 3                          | 72.14       | 52.58       | 39.84     | 36.47      |                                  |             |             |           |            |
| <b><i>rmi1-2</i></b>             |             |             |           |            | <b><i>rmi1-2</i></b>             |             |             |           |            |
| <i>cis</i> -Platin concentration | 1.5 $\mu$ M | 2.5 $\mu$ M | 5 $\mu$ M | 10 $\mu$ M | <i>cis</i> -Platin concentration | 1.5 $\mu$ M | 2.5 $\mu$ M | 5 $\mu$ M | 10 $\mu$ M |
| Assay 1                          | 70.02       | 59.47       | 46.09     | 33.95      | Average                          | 71.18       | 51.55       | 52.71     | 40.04      |
| Assay 2                          | 64.80       | 54.63       | 54.53     | 47.72      | St-Dev                           | 7.03        | 9.82        | 5.92      | 7.02       |
| Assay 3                          | 78.72       | 40.56       | 57.50     | 38.44      |                                  |             |             |           |            |
|                                  |             |             |           |            | <b><i>t</i>-test</b>             |             |             |           |            |
|                                  |             |             |           |            | <i>cis</i> -Platin concentration | 1.5 $\mu$ M | 2.5 $\mu$ M | 5 $\mu$ M | 10 $\mu$ M |
|                                  |             |             |           |            | <i>rmi1-1</i>                    | 0.91        | 0.96        | 0.48      | 0.57       |
|                                  |             |             |           |            | <i>rmi1-2</i>                    | 0.93        | 0.74        | 0.16      | 0.42       |

**Table 7.8.** Raw data for the genotoxin sensitivity analysis of *slrmi1-1* and *slrmi1-2* homozygous mutant lines compared to wild type (WT), with the genotoxic agent CPT. Fresh weights (mg) at each concentration, for each line shown, for four independent assays. The average fresh weight relative to WT is shown as a bar chart in Figure 3.7.B.

|                      |          |           |           |           |                      |          |           |           |           |
|----------------------|----------|-----------|-----------|-----------|----------------------|----------|-----------|-----------|-----------|
| <b>Wild type</b>     |          |           |           |           | <b>Wild type</b>     |          |           |           |           |
| CPT concentration    | 50<br>μM | 100<br>μM | 150<br>μM | 300<br>μM | CPT concentration    | 50<br>μM | 100<br>μM | 150<br>μM | 300<br>μM |
| Assay 1              | 66.22    | 68.33     | 55.43     | 36.37     | Average              | 64.76    | 60.70     | 52.65     | 45.78     |
| Assay 2              | 54.32    | 54.58     | 47.53     | 46.49     | St-Dev               | 8.68     | 5.80      | 3.67      | 5.52      |
| Assay 3              | 63.14    | 58.53     | 52.48     | 38.44     |                      |          |           |           |           |
| Assay 4              | 75.35    | 61.38     | 55.17     | 51.38     |                      |          |           |           |           |
| <b><i>rmi1-1</i></b> |          |           |           |           | <b><i>rmi1-1</i></b> |          |           |           |           |
| CPT concentration    | 50<br>μM | 100<br>μM | 150<br>μM | 300<br>μM | CPT concentration    | 50<br>μM | 100<br>μM | 150<br>μM | 300<br>μM |
| Assay 1              | 75.96    | 72.14     | 50.81     | 42.49     | Average              | 69.70    | 60.85     | 54.71     | 50.91     |
| Assay 2              | 58.87    | 55.92     | 58.91     | 49.66     | St-Dev               | 7.68     | 7.58      | 3.42      | 6.71      |
| Assay 3              | 69.74    | 58.07     | 53.51     | 58.56     |                      |          |           |           |           |
| Assay 4              | 74.21    | 57.28     | 55.62     | 52.93     |                      |          |           |           |           |
| <b><i>rmi1-2</i></b> |          |           |           |           | <b><i>rmi1-2</i></b> |          |           |           |           |
| CPT concentration    | 50<br>μM | 100<br>μM | 150<br>μM | 300<br>μM | CPT concentration    | 50<br>μM | 100<br>μM | 150<br>μM | 300<br>μM |
| Assay 1              | 80.20    | 67.24     | 65.60     | 42.49     | Average              | 70.48    | 60.35     | 59.34     | 44.59     |
| Assay 2              | 69.01    | 59.11     | 61.53     | 40.63     | St-Dev               | 8.95     | 4.84      | 6.64      | 3.67      |
| Assay 3              | 73.76    | 55.91     | 60.23     | 46.69     |                      |          |           |           |           |
| Assay 4              | 58.96    | 59.13     | 49.99     | 48.56     |                      |          |           |           |           |
|                      |          |           |           |           | <b><i>t-test</i></b> |          |           |           |           |
|                      |          |           |           |           | CPT concentration    | 50<br>μM | 100<br>μM | 150<br>μM | 300<br>μM |
|                      |          |           |           |           | <b><i>rmi1-1</i></b> | 0.43     | 0.98      | 0.44      | 0.28      |
|                      |          |           |           |           | <b><i>rmi1-2</i></b> | 0.39     | 0.93      | 0.14      | 0.73      |

**Table 7.9.** Raw data for the genotoxin sensitivity analysis of *slrmi1-1* and *slrmi1-2* homozygous mutant lines compared to wild type (WT), with the genotoxic agent MMS. Fresh weights (mg) at each concentration, for each line shown, for three independent assays. The average fresh weight relative to WT is shown as a bar chart in Figure 3.8.A.

| <b>Wild type</b>     |        |        |        |         | <b>Wild type</b>     |        |        |        |         |
|----------------------|--------|--------|--------|---------|----------------------|--------|--------|--------|---------|
| MMS concentration    | 25 ppm | 40 ppm | 60 ppm | 100 ppm | MMS concentration    | 25 ppm | 40 ppm | 60 ppm | 100 ppm |
| Assay 1              | 47.87  | 49.54  | 39.74  | 30.44   | Average              | 65.90  | 56.05  | 39.86  | 36.42   |
| Assay 2              | 83.62  | 50.66  | 32.16  | 38.92   | St-Dev               | 17.88  | 10.33  | 7.76   | 5.20    |
| Assay 3              | 66.20  | 67.96  | 47.68  | 39.91   |                      |        |        |        |         |
| <b><i>rmi1-1</i></b> |        |        |        |         | <b><i>rmi1-1</i></b> |        |        |        |         |
| MMS concentration    | 25 ppm | 40 ppm | 60 ppm | 100 ppm | MMS concentration    | 25 ppm | 40 ppm | 60 ppm | 100 ppm |
| Assay 1              | 78.16  | 40.51  | 38.59  | 33.81   | Average              | 81.33  | 49.08  | 41.01  | 35.59   |
| Assay 2              | 76.46  | 61.76  | 46.25  | 43.24   | St-Dev               | 7.02   | 11.21  | 4.54   | 6.94    |
| Assay 3              | 89.38  | 44.96  | 38.19  | 29.71   |                      |        |        |        |         |
| <b><i>rmi1-2</i></b> |        |        |        |         | <b><i>rmi1-2</i></b> |        |        |        |         |
| MMS concentration    | 25 ppm | 40 ppm | 60 ppm | 100 ppm | MMS concentration    | 25 ppm | 40 ppm | 60 ppm | 100 ppm |
| Assay 1              | 82.34  | 45.85  | 39.55  | 34.03   | Average              | 81.99  | 48.60  | 40.77  | 33.08   |
| Assay 2              | 82.75  | 54.92  | 37.47  | 31.04   | St-Dev               | 0.98   | 5.49   | 4.04   | 1.77    |
| Assay 3              | 80.88  | 45.02  | 45.27  | 34.17   |                      |        |        |        |         |
|                      |        |        |        |         | <b><i>t</i>-test</b> |        |        |        |         |
|                      |        |        |        |         | MMS concentration    | 25 ppm | 40 ppm | 60 ppm | 100 ppm |
|                      |        |        |        |         | <i>rmi1-1</i>        | 0.27   | 0.47   | 0.84   | 0.88    |
|                      |        |        |        |         | <i>rmi1-2</i>        | 0.26   | 0.35   | 0.87   | 0.38    |

**Table 7.10.** Raw data for the genotoxin sensitivity analysis of *slrmil-1* and *slrmil-2* homozygous mutant lines compared to wild type (WT), with the genotoxic agent MMC. Fresh weights (mg) at each concentration, for each line shown, for three independent assays. The average fresh weight relative to WT is shown as a bar chart in Figure 3.8.B.

|                      |             |             |             |             |                      |             |             |             |             |
|----------------------|-------------|-------------|-------------|-------------|----------------------|-------------|-------------|-------------|-------------|
| <b>Wild type</b>     |             |             |             |             | <b>Wild type</b>     |             |             |             |             |
| MMC concentration    | 10<br>µg/ml | 20<br>µg/ml | 30<br>µg/ml | 35<br>µg/ml | MMC concentration    | 10<br>µg/ml | 20<br>µg/ml | 30<br>µg/ml | 35<br>µg/ml |
| Assay 1              | 53.25       | 42.23       | 39.06       | 40.62       | Average              | 52.29       | 46.73       | 45.42       | 44.35       |
| Assay 2              | 41.53       | 50.80       | 52.85       | 45.66       | St-Dev               | 10.31       | 4.30        | 6.95        | 3.28        |
| Assay 3              | 62.09       | 47.16       | 44.34       | 46.77       |                      |             |             |             |             |
| <b><i>rmi1-1</i></b> |             |             |             |             | <b><i>rmi1-1</i></b> |             |             |             |             |
| MMC concentration    | 10<br>µg/ml | 20<br>µg/ml | 30<br>µg/ml | 35<br>µg/ml | MMC concentration    | 10<br>µg/ml | 20<br>µg/ml | 30<br>µg/ml | 35<br>µg/ml |
| Assay 1              | 44.97       | 51.97       | 56.76       | 51.91       | Average              | 46.01       | 50.88       | 47.08       | 42.39       |
| Assay 2              | 35.75       | 46.44       | 33.86       | 30.45       | St-Dev               | 10.82       | 4.01        | 11.85       | 10.93       |
| Assay 3              | 57.32       | 54.24       | 50.62       | 44.80       |                      |             |             |             |             |
| <b><i>rmi1-2</i></b> |             |             |             |             | <b><i>rmi1-2</i></b> |             |             |             |             |
| MMC concentration    | 10<br>µg/ml | 20<br>µg/ml | 30<br>µg/ml | 35<br>µg/ml | MMC concentration    | 10<br>µg/ml | 20<br>µg/ml | 30<br>µg/ml | 35<br>µg/ml |
| Assay 1              | 41.51       | 30.84       | 34.36       | 38.28       | Average              | 48.84       | 42.92       | 41.78       | 43.97       |
| Assay 2              | 54.68       | 57.60       | 52.91       | 56.92       | St-Dev               | 6.71        | 13.57       | 9.82        | 11.25       |
| Assay 3              | 50.33       | 40.31       | 38.09       | 36.70       |                      |             |             |             |             |
|                      |             |             |             |             | <b><i>t</i>-test</b> |             |             |             |             |
|                      |             |             |             |             | MMC concentration    | 10<br>µg/ml | 20<br>µg/ml | 30<br>µg/ml | 35<br>µg/ml |
|                      |             |             |             |             | <b><i>rmi1-1</i></b> | 0.51        | 0.29        | 0.85        | 0.79        |
|                      |             |             |             |             | <b><i>rmi1-2</i></b> | 0.66        | 0.68        | 0.63        | 0.96        |

**Table 7.11.** Average root lengths of *slrmil-1* and *slrmil-2* homozygous mutant plant lines compared to wild type (WT), for three independent assays. The average number of seeds per fruit is shown as a bar chart in Figure 3.9.

| Line          | Average root length (cm) |         |         |         | St-Dev | t-test    |
|---------------|--------------------------|---------|---------|---------|--------|-----------|
|               | Assay 1                  | Assay 2 | Assay 3 | Average |        |           |
| WT            | 9.59                     | 12.06   | 11.60   | 11.08   | 1.32   |           |
| <i>rmil-1</i> | 7.70                     | 9.50    | 10.10   | 9.10    | 1.25   | 0.13 (ns) |
| <i>rmil-2</i> | 1.04                     | 0.83    | 0.81    | 0.90    | 0.13   | 0.23 (ns) |

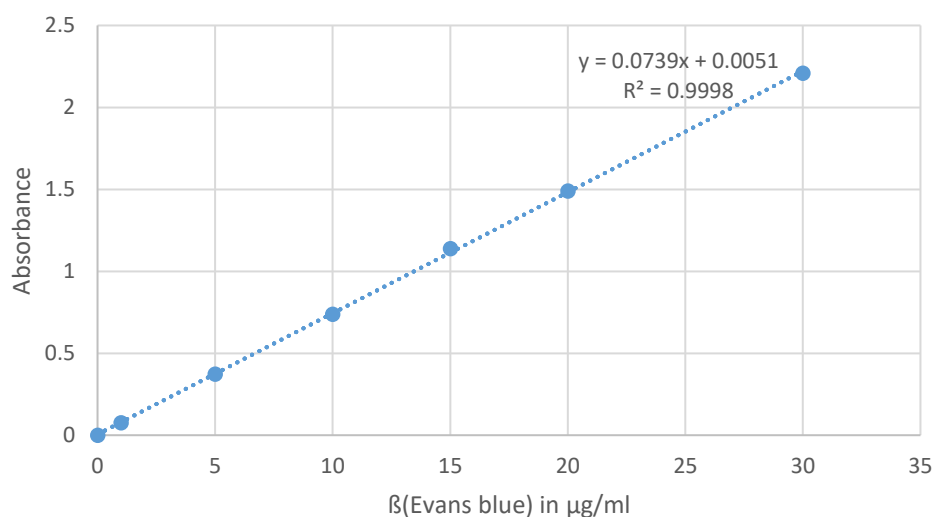


**Figure 7.1.** Standard curve for the calibration of the absorbance and the uptake of Evan's blue dye in µg/ml, at various concentrations for calculating the uptake by the roots in the cell viability analysis (Table 7.12).

**Table 7.12** Raw data for the meristematic root cell viability analysis in *rmil* tomato mutant lines. The mean measurement of Evan's blue dye uptake (µg/ml) from three roots of nine-day-old plantlets for *slrmil-1* and *slrmil-2* mutant lines, compared with WT. Mean measurements were calculated from three independent assays, and shown as a bar chart in Figure 3.10.

| Line          | β(Evans Blue) in µg/ml. |         |         |                  | Average | St-Dev | t-test    |
|---------------|-------------------------|---------|---------|------------------|---------|--------|-----------|
|               | Assay 1                 | Assay 2 | Assay 3 | Positive Control |         |        |           |
| WT            | 2.94                    | 3.14    | 2.98    | 6.93             | 3.02    | 0.11   |           |
| <i>rmil-1</i> | 3.54                    | 2.99    | 4.46    |                  | 3.66    | 0.74   | 0.27 (ns) |
| <i>rmil-2</i> | 3.26                    | 2.34    | 3.42    |                  | 3.01    | 0.58   | 0.98 (ns) |

## 7.2.2 Raw data for the characterisation of *stop3α* mutant lines

**Table 7.13.** Raw data for the fruit diameter and seed counts of both the regular (> 1 mm) seed number from *stop3α-1* and *stop3α-2* heterozygous mutant plants compared to wild type (WT). Data is shown in bar charts in Figure 3.14 for the fruit diameter, and in Figure 3.17 for the seed count analysis. Data for the seed count analysis was used to conduct a chi-squared ( $\chi^2$ ) test, as shown in Table 3.2.

| Line                            | Assay                   | Average fruit diameter (cm) | Total number of small seeds (< 1 mm) | Total number of regular seeds ( $\geq 1$ mm) | Total number of seeds | Percentage of small seeds (< 1 mm) (%) | Percentage of regular seeds ( $\geq 1$ mm) (%) |
|---------------------------------|-------------------------|-----------------------------|--------------------------------------|--|-----------------------|--|--|
| WT                              | 1                       | 1.51                        | 1116                                 | 529  | 1645                  | 67.84                                  | 32.16  |
|                                 | 2                       | 1.47                        | 1296                                 | 760  | 2056                  | 63.04                                  | 36.96  |
|                                 | 3                       | 1.37                        | 549                                  | 481  | 1030                  | 53.30                                  | 46.70  |
|                                 | Average                 | 1.45                        | 987                                  | 590  | 1577                  | 61.39                                  | 38.61  |
|                                 | St-Dev                  | 0.07                        | 389.85                               | 149.17                                       | 516.37                | 7.41                                   |  |
| <i>top3α-1</i><br>(+/-)         | 1                       | 1.44                        | 942                                  | 346  | 1288                  | 73.14                                  | 26.86  |
|                                 | 2                       | 1.53                        | 1327                                 | 516  | 1843                  | 72                                     | 28   |
|                                 | 3                       | 1.48                        | 1456                                 | 635  | 2091                  | 69.63                                  | 30.37  |
|                                 | Average                 | 1.48                        | 1241.67                              | 499  | 1740.67               | 71.59                                  | 28.40  |
|                                 | St-Dev                  | 0.04                        | 267.41                               | 145.25                                       | 411.16                | 1.79                                   |  |
|                                 | <i>t</i> -test          | 0.61 (ns)                   |                                      |  |                       |  |  |
|                                 | Relative to WT (WT = 1) |                             |                                      |  |                       | 1.18                                   | 0.75   |
| <i>t</i> -test (relative to WT) |                         |                             |                                      |  |                       | 0.04 (*)                               |  |
| <i>top3α-2</i><br>(+/-)         | 1                       | 1.52                        | 1052                                 | 373  | 1425                  | 73.82                                  | 26.18  |
|                                 | 2                       | 1.56                        | 1552                                 | 497  | 2049                  | 75.74                                  | 24.26  |
|                                 | 3                       | 1.44                        | 868                                  | 497  | 1365                  | 63.59                                  | 36.41  |
|                                 | Average                 | 1.51                        | 1156.33                              | 455.67                                       | 1613                  | 71.05                                  | 28.95  |
|                                 | St-Dev                  | 0.06                        | 353.96                               | 71.59  | 378.78                | 6.53                                   |  |
|                                 | <i>t</i> -test          | 0.36 (ns)                   |                                      |  |                       |  |  |
|                                 | Relative to WT (WT = 1) |                             |                                      |  |                       | 1.16                                   | 0.75   |
| <i>t</i> -test (relative to WT) |                         |                             |                                      |  |                       | 0.03 (*)                               |  |

**Table 7.14.** Raw data for the average percentage of viable pollen for both *sttop3α-1* and *sttop3α-2* heterozygous mutant plants compared to wild type (WT). Data is shown in Figure. 3.16.

| Line                    | Average % of viable pollen | St-Dev | t-test    |
|-------------------------|----------------------------|--------|-----------|
| WT                      | 63.54                      | 7.93   |           |
| <i>top3α-1</i><br>(+/-) | 62.70                      | 22.02  | 0.96 (ns) |
| <i>top3α-2</i><br>(+/-) | 83.84                      | 13.37  | 0.10 (ns) |

### 7.2.3 Bioinformatic analysis of MEICA1 orthologues in plants

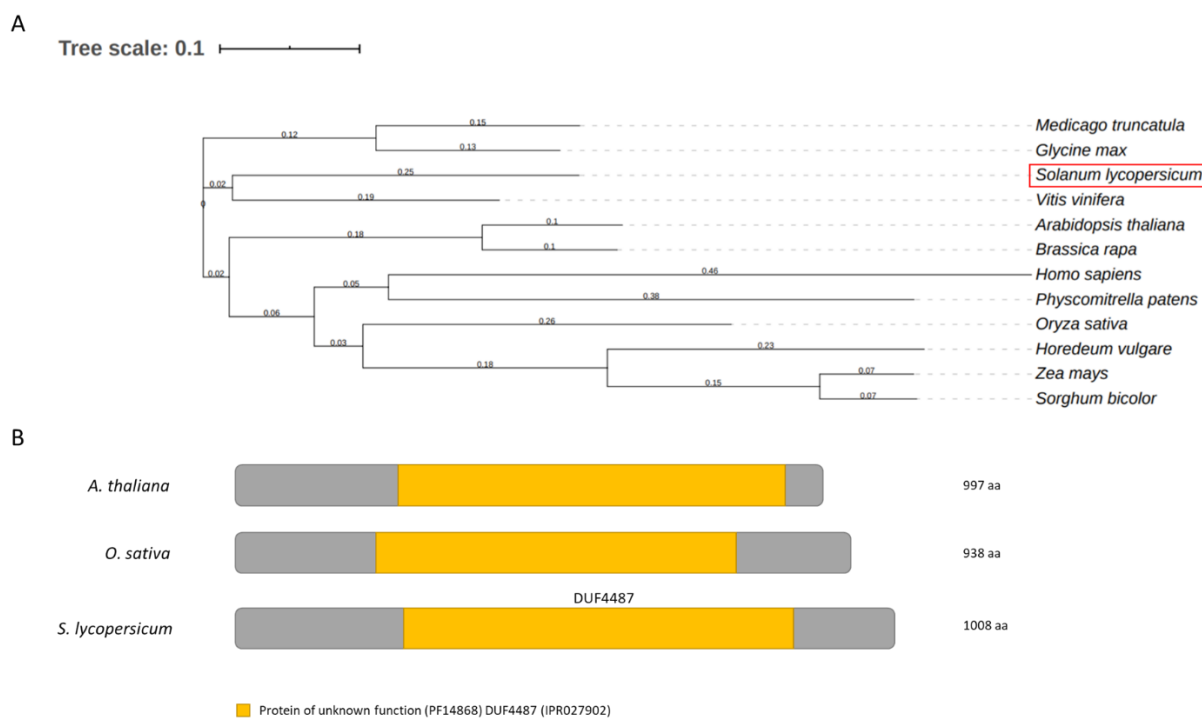


**Figure 7.2. OsMEICA1/AtFLIP phylogenetic analysis and domain structure comparison.**

A) Phylogenetic tree constructed using the amino acid sequences of various DUF4487 containing orthologues in a number of plant species and *Homo sapiens*. Scale of the tree is 0.1 substitutions. Phylogenetic tree constructed using iTOL v5 (Letunic and Bork, 2019).

B) Schematic diagram illustrating the DUF4487 domains within AtFLIP (Fernandes *et al.*, 2018a), OsMEICA1 (Hu *et al.*, 2017), and the homologue of both of these identified in *Solanum lycopersicum*

#### 7.2.4 Sequence Data

Sequence data from this thesis can be found with the following locus identifiers within the current Tomato Genome version SL4.0 available from The Sol Genomics Network (SGN): *SITOP3a*, *Solyc05g014720.3*; *SIRMI1*, *Solyc12g005900.2*; *SIRMI2*, *Solyc11g066690.2*; and *SIMEICA1*, *Solyc09g091370.3* (Fernandez-Pozo *et al.*, 2015), MEICA1/FLIP orthologue data can be found using the following identifiers: *Medicago truncatula*, XP\_003591635.2; *Glycine max*, XP\_014627763.1; *Vitis vinifera*, XP\_019075832.1; *Arabidopsis thaliana*, AT1G04650; *Brassica rapa*, XP\_009111092.1; *Homo sapiens* NP\_060656.2; *Physcomitrella patens*, XP\_001766106.1; *Zea mays*, XP\_008650960.1; *Sorghum bicolor*, XP\_002465870.1; *Hordeum vulgare*, KAE8799555.1.

## Curriculum vitae

### Amy Leanne Whitbread

Born 27.03.1992 in Stafford, UK

Nationality: British

- 10/2014 – 12/2022      **Doctorate at the chair for Molecular and Biochemistry of plants,**  
Botanical Institute, Karlsruhe Institute for Technology (KIT)  
Supervisor: Prof. Dr. Holger Puchta
- 10/2014 – 10/2017      **Early-Stage Researcher (ESR) within The COMREC Network**  
Marie Curie Initial Training Network FP7 Grant agreement no. 606956  
Hosted at at the chair for Molecular and Biochemistry of Plants,  
Botanical Institute, Karlsruhe Institute for Technology (KIT)  
Supervisor: Prof. Dr. Holger Puchta
- 09/2013 – 09/2014      **Master of Research in Molecular and Cellular Biology**  
University of Birmingham, UK  
Supervisors: Prof. Dr. Chris Franklin & Dr. Juliet Coates  
Qualification: *Master of Research (M. Res.)*
- 09/2010 – 07/2013      **Bachelor of Science in Biology**  
University of Worcester, UK  
Supervisor: Dr. Mike Wheeler  
Qualification: *Bachelor of Science with Honours, First Class*  
(*B. Sc. with Hons*)  
- received an Academic Achievement Scholarship Award in 2011
- 09/2008 – 07/2010      **GCE Advanced Levels**
- 09/2003 – 07/2008      **High School**

## **Affidavit**

The experimental part of the present work was carried out at the Botanical Institute, Chair of Molecular Biology and Biochemistry, Karlsruhe Institute of Technology (KIT) in the period from October 2014 to March 2020.

I hereby assure that I have prepared the present work independently and have not used any sources and aids other than those indicated. I have identified the literal or substantive passages as such. The rules for safeguarding good scientific practice of the Karlsruhe Institute of Technology in the valid version of 24th May 2018 have been observed. The electronic version of the present work is consistent with the written work. Furthermore, the submission and archiving of the primary data is ensured in accordance with paragraph 1 § 3 of the Rules for Safeguarding Good Scientific Practice of the Karlsruhe Institute of Technology at the Institute.

---

Place, Date

---

Amy Leanne Whitbread